STRATEGIES FOR NON-LINEAR SYSTEM IDENTIFICATION

A thesis submitted for the degree of

Doctor of Philosophy

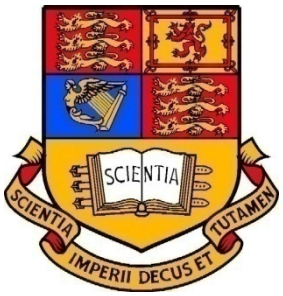

By

Aditya Chandrashekhar Gondhalekar

Department of Mechanical Engineering

Imperial College London/ University of London

October, 2009

Abstract

The thesis presents different strategies to detect, characterize, and identify localized and distributed non-linearities in practical engineering structures. The formulations presented in the thesis work in the frequency domain and based on first-order describing functions to express the non-linearities.

The novel idea of 'non-linear force footprints' is proposed to characterize the type of non-linearity. A library containing footprints of different non-linearities like cubic stiffness, clearance, and friction is compiled. This library can be used as a look-up chart to subjectively identify the type of non-linearity in a structure. A shape-matching algorithm is proposed to numerically compare the extracted non-linear restoring force with the footprints from the library. This provides an automatic identification of the non-linearity type.

Three different methods are proposed for the parametric identification of non-linear systems. All these methods extract the non-linear restoring force, identify the location of non-linearity, and finally estimate the non-linear parameters via a genetic algorithm optimization. The first method uses an FE model of the underlying linear system; while the second and the third methods use a modal model and a response model of the underlying linear system respectively. The performance of the three methods for a range of criteria is evaluated on common ground by using simulated data for a representative engineering structure with localized non-linearities.

An experimental study is undertaken on the so-called MACE structure sub-assembly with the aim to identify non-linearities in an actual industrial structure. Different methods proposed in this thesis, and also from the literature, are used to detect the presence of non-linearity, and identify its type. The response of the structure at different excitation amplitudes is measured using step-sine excitation with constant force. An attempt is made to estimate the non-linear parameters using the methods proposed in the thesis. It has been found that the methods accurately detect, locate and characterize the non-linearities.

A three-stage strategy is presented for the identification of non-linear parameters, for base-excited structures. The method is illustrated on a pyramid-like structure by using simulated measurement data. It has been found that if the non-linearities in the system are independent of the mass matrix; the non-linear parameters can be accurately identified using the proposed method.

Acknowledgements

I would like to express my sincere gratitude to my supervisors, Professor Mehmet Imregun and Dr Evgeny Petrov, for their guidance, encouragement and support throughout the research. It was a great honour and privilege to work with you both.

I am indebted to the Department of Mechanical Engineering for providing me the opportunity to work in a world class research environment, and for funding my studies. I would also like to thank the *Higher Education Funding Council for England* (HEFCE) for partially contributing towards my tuition fees during the study.

Special thanks to Ms Vernette Rice for helping me in administrative matters during my stay. Her politeness and understanding nature is worthy of an ovation.

I would like to show appreciation to Mr D. Robb and Dr Christoph Schwingshackl for their constructive comments and suggestions during the experimental work.

I would like to acknowledge the *Atomic Weapons Establishment* (AWE) UK, for providing a realistic non-linear structure for the research. I would like to thank Dr Philip Ind, Mr Tony Moulder, Mr Alex Humber, and others who were involved in the collaboration.

I wish to say a word of thanks to my colleagues and friends of Dynamics Section and VUTC for making my stay at Imperial College a memorable experience. I would particularly like to thank Dr Luca de Mare, Dr Mehdi Vahdati, Mr Armel De Montgros, and Mr Yum Ji Chan. Big thanks to Mr Sanjay Mata and Mr Davendu Kulkarni, who were always ready for a cup of coffee. The long discussions we had around the coffee table acted as a stress-buster in many cases. Thanks to the system administrators, Dr Sridhar Dhandapani and Dr Zachariadis Zacharias-Ioannisthe, for promptly solving any computer related issues. I appreciate the help of Ms Nina Hancock and Mr Peter Higgs in administrative issues within the centre.

A special word of thanks to the *'94 Ellington road'* bunch, Mr Aditya Karnik, Mr Sandeep Saha, and Mr Srikrishna Sahu. The time spent with you all, is surely amongst the best in my life.

Finally, words would never be enough to thank my beloved wife, Kanchan, for her un-conditional love, encouragement, and support through thick and thin of my research.

To my Parents,
with love and admiration

Nomenclature

Latin symbols

a_i	Binary multiplier corresponding to the i^{th} non-linearity
c	Artificial noise percentage in data
[C]	Viscous damping matrix
[D]	Proportional damping matrix
{F}	Excitation force vector
{F^d}	Excitation force vector for base-excited systems
$\{g\}$	Non-linear restoring force vector in time-domain
g^{cub}	Non-linear force related to cubic stiffness non-linearity
g^{cle}	Non-linear force related to clearance non-linearity
g^{fri}	Non-linear force corresponding to friction non-linearity
{G}	Non-linear restoring force vector in frequency-domain
[K]	Stiffness matrix
K_d	Tangential stiffness for stick friction
K_z	Clearance stiffness
m	Number of measured degrees of freedom
[M]	Mass matrix
n_p	Number of non-linear parameters
n_f	Number of frequency lines in measurement
N	Total number of degrees of freedom
N_r	Reduced number of degrees of freedom
{P^d}	Pseudo excitation force vector
r	Index representing mode number
R	Residual quantity to be minimized in optimization
$\left\{\widetilde{R}^{es}\right\}$	Vector containing non-linear residual
t	Time
u	Number of un-measured degrees of freedom
{U}	Vector of relative displacement amplitude
Y^B	Y-coordinate of benchmark curve
Y^E	Y-coordinate of extracted non-linear force curve
{y}	Displacement vector in time-domain
y_c	Clearance gap distance
{Y}	Displacement amplitude vector

Greek letters

$[\alpha]$	Receptance matrix
$[Z]$	Dynamic stiffness matrix
β	Coefficient for cubic stiffness non-linearity
ε	Error in estimation
η	Modal damping ratio
$[\lambda]$	Complex eigenvalues matrix
μ	Coefficient of friction
ϕ_i	Vector containing i^{th} column from mode shape matrix
$[\Phi]$	Mode shape matrix
ω	Excitation Frequency
ω_r	Resonance frequency of the r^{th} mode
$\{\chi\}$	Non-linear modal vector

Subscripts

c	Index representing the measurement location close to non-linear degree of freedom.
e	Index representing excitation degree of freedom
m	Index representing measured degrees of freedom
max	Index representing the maximum value of a variable
M_r	Index representing the identified modes
nl	Index representing non-linear degree of freedom
u	Index representing un-measured degrees of freedom
U_r	Index representing the un-identified modes

Superscripts

T	Transpose of a matrix
-1	Inverse of a square matrix
+	Pseudo-inverse of a rectangular matrix

Abbreviations

1D, 2D,..	One dimensional, two dimensional,...
CFD	Computational fluid dynamics
DOF	Degree of freedom
DFM	Describing function method
FEA	Finite element analysis
FEM	Finite element method
FFT	Fast Fourier transform
FRF	Frequency response function
GA	Genetic algorithm
HBM	Harmonic balance method
HMT	Hybrid modal technique
I-HMT	Improved hybrid modal technique
LMA	Linear modal analysis
MDOFs	Multi-degrees of freedom
NMG	Non-linear modal grade
NMV	Non-linear modal vector
POD	Proper orthogonal decomposition
SDOF	Single-degree of freedom
SSD	Sum of squared distance

Contents

Abstract 2

Acknowledgements 3

Nomenclature 5

Abbreviations 7

List of Figures 12

List of Tables 16

Chapter 1 18

Introduction 18

1.1 Background of the problem 18

1.2 Non-linear system identification 19

1.3 The describing function method 20

1.4 Objectives of the thesis 21

1.5 Organization of the thesis 22

Chapter 2 24

Literature Survey 24

2.1 Introduction 24

2.2 Non-linear system identification 25

2.2.1 Non-linearity detection 27

2.2.2 Non-linearity characterization 28

2.2.3 Non-linear parameter extraction: Spatial methods 29

2.2.4 Non-linear parameters extraction: Modal methods 31

2.2.4 Model updating for non-linear systems 33

2.3 Non-linear response prediction 35

2.4 Non-linear structural dynamics: Real life structures 39

2.5 Summary of the literature review 41

Chapter 3 43

Non-linearity type identification using a 'footprint library' 43

3.1 Introduction 43

3.2 Generation of non-linear force curves 44

3.3 Footprints of different non-linearities 46

3.3.1 Cubic stiffness non-linearity 47

3.3.2 Clearance non-linearity 48

3.3.3 Friction non-linearity 49

3.3.4 Combination of different non-linearities 50
3.4 Quantitative comparison using shape-matching algorithm 55
3.4.1 Generation of footprint curves 55
3.4.2 Shape-matching algorithm 57
3.4.3 Universal applicability of the footprint comparison 59
3.4.4 Numerical examples 64
3.5 Concluding remarks 68
Chapter 4 71
Spatial method for non-linear parameter identification 71
4.1 Introduction 71
4.2 Theoretical formulation 72
4.2.1 Non-linearity detection and characterization 73
4.2.2 Formulation of the optimization problem 73
4.2.3 Search for the non-linear parameters using a genetic algorithm 75
4.2.4 Use of binary multipliers to improve the efficiency 77
4.2.5 Non-linear parameter identification without full measurement set at non-linear DOFs 78
4.3 Numerical examples 79
4.3.1 Effect of the number of measurements on parameter estimation 80
4.3.2 Effect of measurement noise on parameter estimation 83
4.3.3 Effect of binary multipliers on computational efficiency 85
4.3.4 Effect of the error in the FE model on parameter estimation 87
4.3.5 Non-linear parameter identification in absence of measurements at non-linear DOFs 89
4.4 Concluding remarks 90
Chapter 5 92
Non-linear identification using modal models and response models 92
5.1 Introduction 92
5.2 Improved hybrid modal technique (I-HMT) 93
5.2.1 Theoretical formulation 93
5.2.2 Quantification of the level of non-linearity 96
5.2.3 Decoupling the non-linear modal vector 97
5.2.4 Comments on the non-linear residual 99
5.2.5 Numerical validation of I-HMT method 102
5.3 FRF-based method 107

5.3.1 Theoretical formulation 107
5.3.2 Conditioning of the FRF matrix 109
5.3.3 Numerical validation of the FRF based method 111
5.4 Concluding remarks 115
5.4.1 Comments on the I-HMT method 115
5.4.2 Comments on the FRF-based method 115
Chapter 6 117
Comparison of non-linear parameter identification methods 117
6.1 Introduction 117
6.2 Test cases for the comparison 119
6.3 Pre-processing of the input data 120
6.3.1 Non-linear displacement measurements on the structure 120
6.3.2 Input models for different methods 122
6.4 Results of non-linear parameter identification for Case A 123
6.4 Results of non-linear parameter identification for Case B 128
6.5 Discussion and concluding remarks 134
Chapter 7 137
Experimental investigation of non-linearities in MACE structure 137
7.1 Introduction 137
7.1.1 Choice of the structure 137
7.1.2 Description of joints in Sub-assembly 3 138
7.1.3 Objectives of the exercise 139
7.2 Validation of the FE models 140
7.3 Detection of non-linear behaviour 144
7.3.1 Problem of force-drop near resonance 144
7.3.2 Non-linearity detection with constant-force step-sine tests 147
7.4 Characterization of the non-linearity 150
7.4.1 Identifying the location non-linearity 151
7.4.2 Identifying the type of non-linearity 152
7.4.3 Estimation of non-linear parameters 156
7.5 Concluding remarks 160
Chapter 8 161
Non-linear parameter identification for base-excited structures 161
8.1 Introduction 161

8.2 Theoretical formulation 162
8.3 Implementation of the method 164
8.4 Illustration of the method 165
8.4.1 Stage 1: Extraction of pseudo excitation force vector (P^d) 166
8.4.2 Stage 2: Obtaining the non-linear restoring force 168
8.4.3 Stage 3: Estimation of the non-linear parameters 168
8.4.4 Performance in the presence of experimental noise 170
8.5 Concluding remarks 170
Chapter 9 172
Conclusions and future work 172
9.1 Conclusions of the research work 172
9.1.1 Type characterization using footprints 172
9.1.2 Genetic algorithm optimization 173
9.1.3 On the choice of the model for the underlying linear system 173
9.1.4 Experimental investigation of non-linear behaviour 174
9.1.5 Identification method for base-excited structures 175
9.3 Contributions and publications of the thesis 176
9.4 Suggestions for future work 176
References 178
Appendix A 185
System used for the generation of footprint library 185
Appendix B 186
Structures used for the validation 186
Validation Structure-1: Cantilever beam 186
Validation Structure-2 Cantilever plate 186
Validation Structure-3 Pyramid 188
Appendix C 190
Details of '1203 structure' 190
Appendix D 191
MACE structure details and repeatability test results 191
D.1. Material properties and the FE model mesh information 191
D.2. Repeatability tests for non-linear measurements 191

List of Figures

1.1	Difference between linear and non-linear systems	20
1.2	Single HBM approximation of clearance non-linearity	21
1.3	Thesis contents	22
2.1	Research in non-linear structural dynamics	25
2.2	Benchmark structures for European COST F3	39
2.3	Experimental setup used by Ferreira and Elizalde	40
3.1	The two DOF system used to generate footprint library	45
3.2	A typical frequency response curve for a non-linear system	46
3.3	Non-linear force: Cubic stiffness non-linearity (hardening)	47
3.4	Non-linear force: Cubic stiffness non-linearity (softening)	47
3.5	Non-linear force: Clearance non-linearity	48
3.6	Comparison of cubic stiffness and clearance non-linearity	48
3.7	Non-linear force: Friction with pure slip	49
3.8	Non-linear force: Friction with pure stick	49
3.9	Non-linear force: Friction with stick and slip	50
3.10	Non-linear force: cubic stiffness and clearance	51
3.11	Non-linear force: Cubic stiffness and friction	51
3.12	Non-linear force: Clearance and friction	51
3.13	Non-linear force: Cubic stiffness, clearance and friction	52
3.14	Footprint library: magnitude plots for non-linear force	53
3.15	Footprint library: Nyquist plots for non-linear force	54
3.16	Normalized footprint for cubic stiffness	55
3.17	Library of normalized footprints for quantitative comparison	57
3.18	Comparison steps for shape-matching	58
3.19	Flowchart for shape-matching algorithm	59
3.20	Numerical experiments: cubic stiffness non-linearity	60
3.21	Numerical experiments: clearance non-linearity	60
3.22	Numerical experiments: friction	61

3.23	Numerical experiments: clearance and friction	62
3.24	Comparison with finer footprints for cubic stiffness and friction	63
3.25	Non-linear force for case 1 (cubic stiffness)	65
3.26	Quantitative comparison for Case 1	65
3.27	Non-linear force for Case 2 (friction)	66
3.28	Quantitative comparison for Case 2	66
3.29	Non-linear force for Case 3 (cubic stiffness + friction)	67
3.30	Quantitative comparison for Case 3	67
3.31	Quantitative comparison for Case 3 with 7.5% noise	69
4.1	Flowchart of the genetic algorithm optimization	77
4.2	Comparison of linear and non-linear responses	80
4.3	Identification of non-linearity location (Case A)	81
4.4	Non-linearity characterization (Case A)	82
4.5	Displacement response with 5% random noise	84
4.6	Comparison of the extracted and regenerated non-linear force	85
4.7	Performance of binary multipliers: fittest string fitness	86
4.8	Performance of binary multipliers: Average fitness	87
4.9	Accumulated non-linear force plot	88
4.10	Non-linear force at un-measured DOFs	89
5.1	Half power method to calculate the average NMV	97
5.2	Flow chart for the improved hybrid modal method	100
5.3	Comparison of linear and non-linear residual for a typical case	101
5.4	Non-linear residuals with different number of modes in the range	101
5.5	Comparison of linear and non-linear response for clearance non-linearity	102
5.6	Details of the measured locations	103
5.7	Extracted non-linear modal vector for the first mode	104
5.8	Zoomed-in view of NMV near the first resonance	105
5.9	Non-linear modal grades for the modes in the measurement range	105
5.10	Variation of the condition number of the FRF matrix	110
5.11	Effect of measurement locations on the condition number	110
5.12	Linear and non-linear response at the excitation DOF	111
5.13	Details of the measurement locations for three cases	112
5.14	Non-linear force for Cases A and B	112
5.15	Extraction of the non-linear force for Case C	113
5.16	Comparison of the accurate response and the regenerated	114

	response for the FRF-based method predictions	
6.1	CAD and FE models '1203 structure'	119
6.2	Depiction of two test cases used for comparison study	120
6.3	Measurement locations on the 1203 structure	121
6.4	Non-linear response for Case A (cubic stiffness non-linearity)	121
6.5	Non-linear response for Case B (clearance non-linearity)	122
6.6	Identification of the location of non-linearity for Case A	124
6.7	Non-linear force at the non-linear DOF for Case A	124
6.8	Non-linear modal vector plotted for Case A	125
6.9	Non-linear modal grade (NMG) plot for Case A	125
6.10	Non-linear force plot with 5% measurement noise for Case A	126
6.11	NMV for the 2nd mode plotted for Case A with noise	127
6.12	Accumulated non-linear force at measured DOFs for Case B	129
6.13	Accumulated non-linear force mapped on measurement locations	130
6.14	NMV and NMG plots for Case B	130
6.15	Comparison of non-linear force for Method 1	131
6.16	Comparison of non-linear force for Method 3	132
6.17	Depiction of calculation of errors for Case B	133
7.1	Computer-generated drawing of the MACE structure	138
7.2	Schematic of Sub-assembly 3	139
7.3	FE models of the individual components	140
7.4	Mode shapes of the assembled structure via FEA	142
7.5a	Point FRF plot for the assembled structure (hammer tests)	142
7.5b	Overlaid FRFs for the EMA on the assembled structure	143
7.6	Force drop near resonance for the MACE sub-assembly	145
7.7	Overlaid FRFs at different excitation levels without force-control	145
7.8	Flow chart for the force-control algorithm	146
7.9	Experimental setup for non-linear step-sine testing	147
7.10	Overlaid accelerance at different excitation levels with force-control	148
7.11	Nyquist plots for accelerance at different excitation levels	148
7.12	Presence of higher-harmonics in the response at 10N force level	149
7.13	Contribution of the higher harmonics at different excitation levels	150
7.14	Measurement locations on the MACE sub-assembly	151
7.15	Accumulated non-linear force at the measurement locations	151
7.16	Variation of the resonance amplitude for the first mode	152

7.17	Variation of the resonance frequency of the first mode	153
7.18	Inverse FRF plots at excitation force level = 5N	153
7.19	Non-linear force at locations A1 and A4	154
7.20	Non-linear force at A4 against displacement at A4	155
7.21	Comparison of non-linear force extracted using different methods	155
7.22	Comparison of the extracted non-linear force with footprint library	156
7.23	Regenerated non-linear forces with parametric and non-parametric models	158
7.24	Regeneration of response using non-parametric model	158
7.25	Regeneration of response using parametric model	159
8.1	Flowchart of the proposed method	165
8.2	Schematic of Validation structure-3	166
8.3	Overlaid FRFs of the underlying linear structure	167
8.4	Pseudo excitation force at measured DOFs	167
8.5	Comparison of linear and non-linear responses at low and high acceleration input	168
8.6	Identification of non-linearity location	169
8.7	Non-linear force at the non-linear DOF	169
A1	2 DOF system used to generate footprint library	185
B1	Validation structure- 1: Cantilever beam	186
B2	Validation structure- 2: Cantilever plate	187
B3	Mode shapes for validation structure-2	188
B4	Engineering drawing of validation structure-3	189
C1	Engineering drawing of 1203 structure	190
D1	Repeatability test results at force level 0.5N	192
D2	Repeatability test results at force level 3N	192
D3	Repeatability test results at force level 5N	192

List of Tables

3.1	Expressions for non-linear restoring force	56
3.2	Summary of non-linear parameters used for validation	64
3.3	Summary of the quantitative comparison	68
3.4	Summary of the quantitative comparison with noise	69
4.1	Description of measured DOFs	81
4.2	Parameters used in the GA	82
4.3	Summary of results for parameter estimation	83
4.4	Results of parameter estimation in presence of noise	84
4.5	Performance of binary multipliers	86
4.6	Effects of the erroneous FE model	88
4.7	Case description for non-linear parameter identification in absence of the measurement at non-linear DOFs	89
5.1	Results of parameter estimation for different cases using I-HMT method	106
5.2	Summary of the parameter identification results using FRF-based method	113
6.1	Details of the three methods compared	118
6.2	Summary of non-linear parameters used for the two cases	120
6.3	Results of parameter estimation for clean measurement data with accurate input models	126
6.4	Estimated non-linear parameter with noise for Case A	127
6.5	Estimated non-linear parameter with erroneous input models for Case A	128
6.6	Estimated parameters with accurate input models and without measurement noise for Case B	131
6.7	Summary of estimated non-linear parameters for cases of noisy data and erroneous input models for Case B	132
6.8	Summary of errors in resonance response and resonance frequency	133
6.9	Quantitative comparison of the three methods	136
7.1	Description of joints in Sub-assembly 3	139

7.2	Correlation of modal properties for individual components	141
7.3	Comparison of the modal properties of the assembled structure	143
7.4	Estimated non-linear parameters with parametric and non-parametric models	157
7.5	Comparison of errors in the regenerated response	159
8.1	Estimated parameters with and without noise	170
A1	Non-linear parameters for different non-linearities	185
B1	Linear natural frequencies for validation structure-2	187
B2	Material properties for beams in validation structure-3	188
C1	Natural frequencies of the underlying linear structure	190
D1	Details of material properties and FE model mesh	191

Chapter 1

Introduction

This chapter presents a brief introduction to the subject of non-linear structural dynamics. The importance of the research in this area and its relevance to industry are stated. The terminologies specific to non-linear structural dynamics, which are frequently used in the thesis, are discussed to facilitate the reading of the thesis. The statement of the problem, as addressed in this thesis, is presented. In the last section, the structure of the thesis and the relationships between different chapters are presented in order to give an overview of the thesis.

1.1 Background of the problem

In recent years, continuous attempts have been made to shorten the product design cycle. To survive in a competitive market, it is of paramount interest to manufacturers to reduce the cost and the time associated with the experimental validation of prototypes. This need, coupled with the availability of computational resources and numerical tools like FEA and CFD, has increased the use of computer simulations to predict structural behaviour. For linear systems, the dynamic behaviour of a system can be accurately predicted using numerical tools like FEA. But in the real world, non-linearity is omnipresent and linear behaviour is the exception. As engineers are seeking to design lighter, flexible, faster, and more efficient products, the designs are shifting more in the non-linear regime. On the other hand, there are very few established and validated methods for predicting the response of non-linear systems.

What is non-linearity?

Non-linearity is quite a broad term which may possess different meanings in contexts of different engineering disciplines. From structural dynamicist's perspective, non-linearity is something which causes the system to violate the principle of homogeneity. Mathematically, non-linear systems can be represented by

a set of differential equations with non-linear terms. The resonance frequencies and mode shapes of such systems are functions of the operating conditions [1].

Various domains of engineering, like aerospace, automobile, machine tool industry, spacecraft technology, civil and structural engineering, encounter non-linear systems in one form or the other. Some common occurrences of non-linearities in engineering are: (i) friction induced non-linearities in bolted joints, (ii) backlash and clearance non-linearities in control surfaces of aero-structures, (iii) polynomial stiffness non-linearities observed in the engine-wing connection of an airplane, (iv) non-linearities demonstrated by engineering materials like composites, plastics, and viscoelastic materials.

As discussed in [2], non-linearities arising from various sources can easily invalidate the results of simulations based on linearity. It has been shown in [3-5], either experimentally or through simulations, that the dynamic behaviour of strongly non-linear systems can be significantly different than that of their linear counterparts. Thus, it has become important to accurately predict the behaviour of non-linear systems.

To predict the behaviour of non-linear systems, it is necessary to include the corresponding non-linear elements into the numerical/mathematical models which describe those systems. The parameters of such non-linear elements are case specific, and must usually be identified through experimental route for the case of interest. The process of identifying the parameters of the mathematical model of a system is known as *system identification*

1.2 Non-linear system identification

Linear system identification, which attempts to determine mathematical models of linear dynamic systems from vibration measurements, is an established area of study. The tools like modal testing and analysis [6, 7] are available off-the-shelf for linear system identification. For linear systems, the transfer function, relating the input of the system to its output, remains constant at all excitation levels. Thus, the mathematic model obtained through the identification at one operating point can later be used for prediction at some other operating point. For non-linear systems, it is difficult to obtain a universal mathematical model of the system by performing the system identification only at a single excitation level. A model obtained at a given operating condition can, at best, provide the equivalent linear system at that point. Figure 1.1 depicts the difference between linear and non-linear systems seen from a

system identification perspective. It can be seen from the figure that for non-linear systems, the transfer function is not independent of the input.

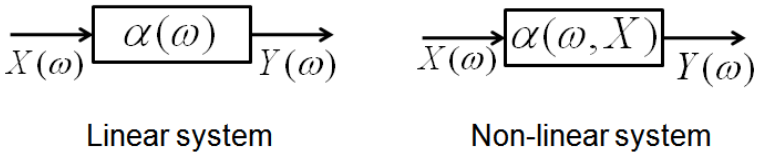

Figure 1.1 Difference between linear and non-linear systems

Thus, the identification of non-linear systems differs from the conventional linear system identification. The scope of non-linear system identification in this thesis is confined to detecting the non-linear behaviour, identifying its location and type, and estimating its parameters as inputs to the models which describe the non-linear system.

1.3 The describing function method

The describing function method (DFM), which finds its origin in control systems engineering [8], is a very popular method to predict the response of non-linear systems. The method seeks to find an input-output relationship for non-linear systems by assuming approximate functions, called *describing functions*, to describe the behaviour of non-linear elements in the system. The coefficients of these describing functions are obtained by matching the restoring force in the system.

For systems with sinusoidal input, the coefficients of describing functions can be derived by using a method which is popularly known as the *harmonic balance method* (HBM). In this case, the non-linear part of the restoring force is assumed to be periodic, so that it can be expressed as a Fourier series. The Fourier series may be truncated to include only the fundamental harmonics, leading to a technique called single-harmonic balance method. As the number of harmonics in the analysis is increased, a better approximation can be achieved. In the harmonic balance method, the Fourier coefficients are obtained by computing the area under the non-linear force curve for one complete cycle. Figure 1.2 shows, for clearance non-linearity, a comparison of actual non-linear force and the approximated non-linear force with single harmonic balance method.

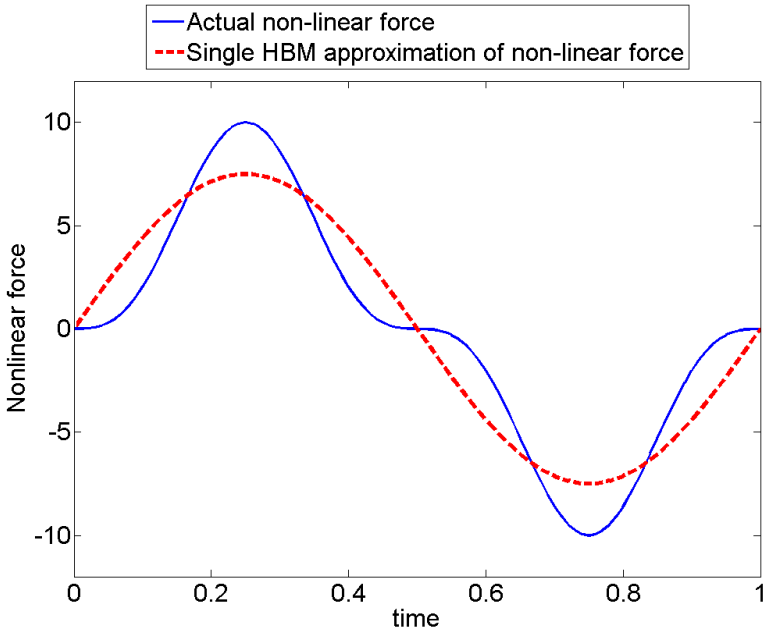

Figure 1.2 Single HBM approximation of clearance non-linearity

The describing function method, or the harmonic balance method, provides a fast and efficient way to calculate the response of a non-linear system under harmonic excitation. The HBM with fundamental harmonics only, fails to predict complex phenomena like internal resonances, sub-harmonic and super-harmonic components in the response. These phenomena are typical of non-linear systems. Another reason for the popularity of this method amongst structural dynamists is because it mimics step-sine vibration tests performed with conventional spectral analysers. The describing functions for different non-linearities encountered in engineering structures, can be found in [2, 9].

The research in this thesis uses the describing function method as the basic engine. All identification methods presented in this thesis essentially use the describing functions for different non-linearities. The simulated data used to illustrate the identification methods are generated using single-harmonic balance method.

1.4 Objectives of the thesis

Non-linear structural dynamics is a wide area of research which includes, predicting the behaviour of non-linear systems, non-linear system identification, stability studies for non-linear system etc. The scope of the research presented in this thesis is restricted to the area of non-linear system identification. The entire work in the

thesis is based on the already established theory of describing functions (DFM). The statement of the problem, which is attempted in this thesis, is given as follows:

"To propose and illustrate different strategies for non-linear system identification which suit complex and realistic engineering systems. The realm of non-linear system identification would encompass different sub-activities like detection of non-linearities in the system, identification of the type of non-linearity, and estimation of the non-linear parameters."

1.5 Organization of the thesis

The chart shown in Figure 1.3 summarizes the contents of the thesis.

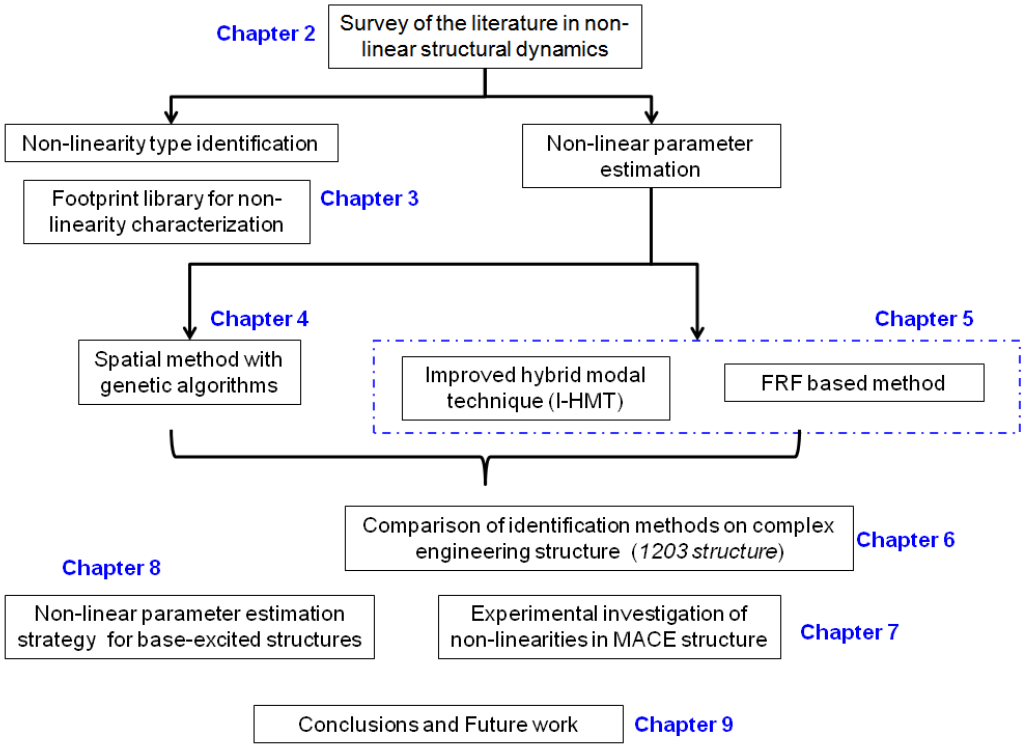

Figure 1.3 Thesis contents

The material in the thesis is arranged logically, starting with a survey of the literature in the area of non-linear structural dynamics, which is presented in Chapter 2.

A novel method for the identification of non-linearity type, based on footprints of non-linear restoring force, is proposed in Chapter 3. A footprint library, consisting non-linear restoring forces for different types of non-linearities commonly encountered in engineering structures, is presented. A method based on shape-

matching algorithm for quantitative matching of non-linear force curves is also presented.

After the non-linearity type identification, the next stage is the non-linear parameter estimation. A method for non-linear parameter estimation, which uses the FE model of the underlying linear structure, is proposed in Chapter 4. The method extracts the non-linear parameters via genetic algorithm optimization. The method is illustrated on a simple cantilever beam case.

An accurate FE model might not be available in some practical cases. The methods which bypass the requirement of the updated FE model are presented in Chapter 5. Two proposed methods use the modal model and the response model of the underlying linear structure respectively. The methods are exemplified using simulated data for a cantilever plate.

The methods presented in earlier chapters have their own advantages and disadvantages. These are compared on common ground by using simulated data for a relatively complex and realistic engineering structure, the so-called 1203 structure. The results of the comparison are presented in Chapter 6.

Chapter 7 presents an experimental investigation of non-linearities in the so-called MACE structure, the structure with different joints and connections contributing towards non-linear behaviour. A complete process of non-linear identification is attempted on this structure with experimental data.

Many times, for large structures, vibration tests are performed with the structure mounted on a shaker table, and controlling the acceleration input to the structure. Since the force input is not measured in such cases, conventional non-linearity identification methods cannot be applied. Chapter 8 presents a novel strategy of non-linear parameter estimation for the case of base-excited structures.

In the last chapter of the thesis, Chapter 9, the main contributions of the research are summarized. Some concluding remarks on the research and suggestions for future work on this topic are presented.

Chapter 2

Literature Survey

This chapter presents a survey of the literature in the area of non-linear structural dynamics. The survey presented is not all-encompassing but more specific to the topics related to the thesis. The literature which helped the author to define the research problem, and which is closely related to the research presented in the thesis is dealt with in detail. For an exhaustive survey of the literature, the reader is directed to the excellent review articles [10-13] published on this topic. For an introduction to non-linear structural dynamics in general, the books by Nayfeh and Mook [14] and Worden and Tomlinson [2] serve as a good starting point. The review in this chapter is organized methodologically, and within the methodologies, the work is arranged in chronological order.

2.1 Introduction

From a structural dynamicist's perspective, non-linearity can be defined as the deviation of a structure from linear behaviour. The non-linearity is manifested in the form of amplitude-dependent vibration properties, complex phenomena like mode localization, bifurcations, internal resonances, presence of sub-harmonic and super-harmonic components in the response, jump phenomenon etc.

The research in the area of non-linear structural dynamics started more than four decades ago. The research later gained the popularity and wide acceptance when it was understood that all engineering structures are non-linear to some extent. The research progressed in two fundamental branches: (i) non-linear system identification and, (ii) prediction of non-linear response under different operating conditions. Different methodologies emerged within these two fundamental branches. A chart showing the span of the research in this area is presented in Figure 2.1. The different methods proposed for identification and modelling of non-

linearities are presented in separate sections. The last section presents the literature on application of these methods to complex engineering structures.

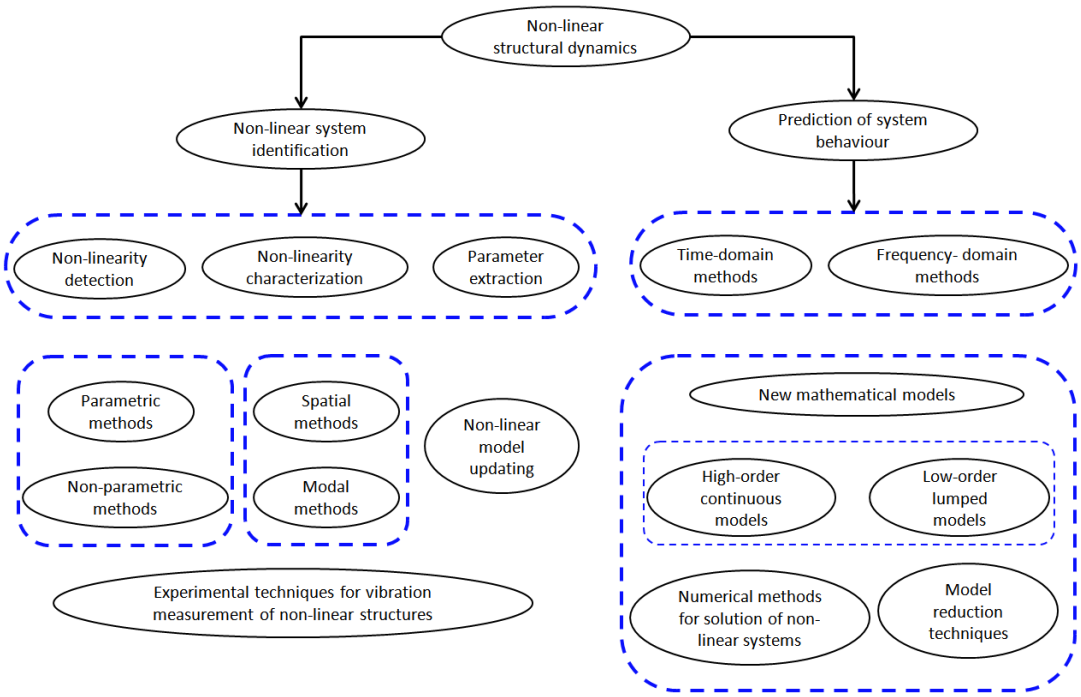

Figure 2.1 Research in non-linear structural dynamics

2.2 Non-linear system identification

The main goal of any system identification method is to find parameters of a mathematical model representing a physical system, by making use of the input and output data describing the excitation and response of the system. For linear structural dynamics, there are three popular representations to describe the physical system: (i) the spatial model, (ii) the modal model, and (iii) the response model. The modal model is the most compact form which is easily obtainable through experimental route [6]. Thus, most of the linear system identification methods extract the parameters of the modal model of the system, a process which is popularly known as linear modal analysis (LMA).

For a non-linear system, the properties like linear modal superposition, reciprocity, homogeneity which form the back-bone of LMA theory are not valid. Thus, non-linear system identification is more involved than just to extract the parameters for the modal model of the system. Some basic treatment and practical

advice on handling the non-linear system is presented in a primer on modal analysis published by Dynamic Testing Agency [15].

There are three stages of non-linear system identification, (i) Non-linearity detection, (ii) Non-linearity characterization, and (iii) Non-linear parameter extraction. In the first stage, the presence of the non-linearity is detected from the experimental measurements. In the second stage, the type and form of non-linearity is identified and in the last stage, the corresponding non-linear parameters are identified [11].

There are several ways to classify the literature on non-linear system identification. One way of classification is based on how the non-linear system identification problem is perceived. It can be perceived merely as a parameter estimation problem in which the non-linear parameters are extracted making use of the model of the underlying linear system[1]. It can also be perceived as non-linear modal analysis problem in which the linear modal analysis theory is extended to the non-linear systems. In this approach, the non-linearities are either described in modal coordinates, or they are presented as a variation in modal properties like natural frequency, mode shapes, and damping. Another way of perceiving non-linear system identification is as a problem of model updating. In this approach, the linear model of the structure is refined/ corrected in order to match the experimental measurements. This is achieved either by modifying the system properties or by adding some special elements which may or may not have physical significance.

Another classification of the parameter estimation methods is based on the nature of model that is fitted in the data. The methods can be classified into: (i) parametric and (ii) non-parametric methods. In parametric methods, the model has some physical meaning. For example, to describe a clearance non-linearity, the parameters identified are the clearance distance and the normal stiffness. Naturally, the parametric methods give insight into the nature and the physics of non-linear behaviour, but the highly individualistic nature of non-linearities makes it difficult to find a parametric model to suit different non-linearities observed in engineering structures. In non-parametric identification, the extracted parameters do not necessarily have any physical meaning.

It is relatively easy to extract a non-parametric model to fit into the data, but the extrapolation capacity of non-parametric models cannot be guaranteed. The non-parametric models, being non-physical, are not universal. In many cases they yield poor predictions when stretched outside their working range. Black box

[1] Most of the times, for practical structures, it's the FE model

methods form a significant group in non-parametric methods. These methods sometimes use non-conventional techniques like neural networks, fuzzy logic etc. to model the input-output relationship for the non-linear systems. It is not intended to discuss these methods, and a detailed review of black box methods can be found in [16, 17].

The literature associated with non-linearity detection, characterization and different approaches for non-linear parameter estimation is presented separately in the following sections.

2.2.1 Non-linearity detection

The first stage in non-linear system identification is to detect if there is any non-linearity in the system. Non-linearity detection is a mature area of research with many established methods available in the literature. A summary of non-linearity detection techniques and their comparison is presented in [12, 18, 19]. The methods are compared on the basis of different criteria like measurement time, computation time, range of application, subjectivity involved etc.

Mostly, the presence of non-linearity is detected by verifying the fundamental principles of linear systems like linear superposition or reciprocity. The distortion of Nyquist plot and frequency response functions (FRFs) also indicate the presence of non-linearity as explained in [2, 6]. The first-order FRFs obtained using the conventional vibration testing are primarily used to validate these properties.

He and Ewins [20] suggested the use of inverse FRF to detect the presence of non-linearity. For a non-linear system, real and imaginary parts of FRF, plotted against frequency-squared and frequency respectively, deviate from a straight line indicating the presence of non-linearity. A similar method based on mapping of stiffness and damping at each frequency value is suggested by Mertens et al. [21]. This method, which is limited to single degree of freedom (SDOF) systems, detects the presence of non-linearity in the system if any variation in stiffness or damping is observed. Tomlinson [22] proposed the use of Hilbert transform to detect the non-linearity. Hilbert transform of a complex FRF of a linear system is same as the original FRF. For non-linear system the transform deviates from the original FRF, the deviation being utilized to detect the presence of non-linearity.

For linear systems with single harmonic excitation, the response is harmonic with the same frequency. For non-linear systems, the response is expected to contain higher harmonics. The higher harmonics in the response can be used to detect the non-linearity. Wyckaert [23] proposed a term called harmonic detection

function (HDF) to quantify the presence of higher harmonics at each frequency. The HDF is defined as the ratio of the energy associated with higher harmonics at a frequency to the total energy in the response at that frequency. Chong and Imregun [24] showed that a lack of orthogonality between the mode shape vectors and the reciprocal modal vectors (RMV), obtained from measured frequency response functions, can also indicate the non-linear behaviour.

To decide on whether to use a linearized model or to build a non-linear model of a system, it is essential to know the extent of non-linearity in the system. Though the above methods work well to detect the presence of non-linearity, they provide little information about the extent of non-linearity. Surprisingly, there are very few attempts to quantify the level of non-linearity in the structure.

Kim and Park [25] proposed a term called 'non-casual power ratio' (NPR) to gauge the extent of non-linear contamination. They used inverse Fourier transform on the FRF to get a time-domain signal. NPR is defined as the ratio of non-casual power to the total power in the signal. It is claimed that as the non-linear effects dominate, the non-causal power in the signal increases. NPR varies from 0 to 1 with increasing non-linear contribution.

Elizalde [26] coined a term called non-linear modal grade to quantify the non-linear contamination of each mode. He used thresholds based on engineering judgments to define 3 ranges: weakly non-linear, moderately non-linear and strongly non-linear for each mode. Depending on the non-linear grade for a mode, it can be decided whether to include that mode in non-linear analysis.

2.2.2 Non-linearity characterization

Non-linearity characterization, as defined in [11], is to find the location, the type, and the functional form of all non-linearities in the system. Non-linearity characterization is an important step in a bigger goal of non-linear system identification. Many non-linear parameter extraction methods in the literature assume that the characterization is completed in advance.

For simple structures with few joints and connections, the spatial location of non-linearity can be guessed merely by looking at the structure. For complex structures with many connections, it becomes necessary to locate the connections which are contributing towards the non-linear behaviour of the structure. Al-Hadid and Wright [27] proposed a method based on force-state mapping to locate the non-linear DOF. The method is developed for lumped-parameter system and it is difficult to implement for a continuous system. Elizalde [26] and Ozer et al. [28] used non-

linear restoring force at each DOF as an indication of non-linearity. A non-zero value of non-linear restoring force at any DOF signifies the non-linearity at that DOF. The methods are potentially applicable for engineering structures and work well with FE models.

Some of the methods stated for non-linearity detection in the earlier section can be extended to find the type of non-linearity. The inverse FRF method proposed by He and Ewins [20] classifies the non-linearity broadly into stiffness type and damping type. A deviation of Hilbert transform of an FRF from the original FRF is characteristic of the type of non-linearity as shown by Tomlinson [22]. He presented Hilbert transform of simulated FRFs for different types on non-linearities. A restoring force surface technique (RFS), proposed by Masri and Caughey [29] can be used to characterize the non-linearity type. In this method, the restoring force due to stiffness and damping is plotted against the system variables to form a surface. The restoring surface thus formed is unique to the type of non-linearity in the system.

The subjective observation of the distortions in FRF is often used to characterize the type of non-linearity. Adams and Allemang [30] proposed a method for characterization based on the distortions in the FRF. They modelled the non-linear system as a closed loop linear system with non-linear elements providing internal feedback. The modulation of the FRF due to this feedback is used to characterize the non-linearity type. Tanrikulu and Ozguven [31] used the non-linearity matrix to characterize the type of non-linearity. The non-linear restoring force is separated into a matrix and a non-linear response vector. The matrix contains non-linearities in the form of describing functions. Later, a similar approach is implemented by Elizalde [26].

Even though the non-linearity characterization forms an important and sometimes rather essential step in non-linear system identification, there is lack of well established methods to handle complex engineering structures. Still, most of the times, a subjective judgment is made about the location and type of non-linearity.

2.2.3 Non-linear parameter extraction: Spatial methods

Non-linear system modelling techniques use mathematical models to describe the physical phenomena. Non-linear parameter extraction methods essentially extract the values of the parameters used in these models using experimental measurements.

Amongst the non-parametric spatial methods, which are mostly in time-domain, a pioneering work is done by Marsi and Caughey [29]. They proposed a method called restoring force surface (RFS) in which the restoring force is plotted against instantaneous values of displacement and velocity in phase plane. The surface is then approximated by the double Chebyshev polynomials to identify the non-linear parameters. The original method, which was developed for an SDOF system, was later extended by different researchers to suit the multi degrees of freedom (MDOFs) systems [11]. Leontaritis and Billings [32] proposed another method in time domain non-parametric class called non-linear auto regressive moving average with exogenous inputs (NARMAX). This is an extension of ARMAX method [33] used in the linear system identification. The method is versatile in its use, but for complex engineering structures, the computational burden of the method can be significant.

In frequency domain, most of the methods use first-order frequency response functions. There are some methods as listed in [11] which make use of higher order FRFs and Volterra series, but their use is restricted due to difficulties in measuring the higher order FRFs for engineering structures. The use of harmonic balance method [34, 35] and describing functions is popular for parametric description of non-linearities. The basic assumption in this approach is that for harmonic excitation, the non-linear restoring force is periodic, and it can be represented as a summation of different harmonics. Single and multi-harmonic describing functions for different non-linearities can be formulated and parametric identification can be performed by fitting the extracted non-linear restoring force in the describing functions. A list of describing functions for common structural non-linear elements is presented by Tomlinson and Worden [2]. A more specific list for the non-linear elements relevant to aerospace industry is published by Goge et al. in [9].

Tanrikulu and Ozguven [31] proposed a method which separates the non-linear restoring force into a non-linear response vector and a non-linearity matrix. This non-linearity matrix is formulated using the describing functions. The method, originally restricted to grounded non-linearities, is extended for more general use by Ozer et al. [28]. A similar approach is followed by Elizalde [36] to propose a method called *explicit formulation* (EF). The method, which is originally developed for non-linear response prediction, can be used in reverse path for non-linear identification. The method is tested on simulated data for a plate with cubic stiffness non-linearities at multiple locations.

The above methods make use of an accurate underlying linear spatial model, which is not easy to obtain for a complex engineering structure. Elizalde [26] addressed this difficulty partially by proposing a hybrid method for identification called *reverse hybrid modal technique* (R-HMT). This method uses the modal description for the underlying linear structure and spatial description for the non-linear elements.

Amongst the other frequency domain methods, Richard and Singh [37] proposed a method for non-linear identification based on first order FRFs. The method is called *conditioned reverse path* (CRP) with a central theme to separate the non-linear distortions from the measured FRFs using spectral conditioning. The underlying linear model and non-linearities are then identified independently. The method has a potential to identify complex MDOFs systems excited using Gaussian random excitations. The method assumes that the location and the type of non-linearity are known a priori, and measurements are available at all non-linear DOFs This puts considerable limitation on its use for real-life engineering structures. Another frequency domain method, similar to CRP is *non-linear identification through feedback of the output* (NIFO) proposed by Adams and Allemang [38]. The identification for underlying linear system and non-linear components is carried out simultaneously. In this method, non-linear forces are modelled as an internal feedback into a closed loop linear system. This method does not guarantee conditioning as CRP, but its compact formulation makes it simpler to implement.

Most of the parametric methods in spatial domain suffer from some common limitations like: the need to measure the response at all non-linear DOFs and the need to know in advance the location and the types of non-linearities present in the structure. The modal approach, which is discussed in next section, can sometimes be used to overcome these limitations.

2.2.4 Non-linear parameters extraction: Modal methods

For a linear system, a modal model is very compact way of representing a system for accurate response predictions. The fundamental properties like natural frequencies, damping ratios, and mode shapes, for linear systems, are independent of the excitation amplitude. The modal model is easily obtainable through experimental route using modal testing and modal analysis [6, 7] which is an established area of study.

Rosenberg [39] in 1960s proposed a concept of normal modes for non-linear systems. He defined non-linear normal modes (NNMs) as a motion in which all

points of the system vibrate with same phase. This is purely an extension of the definition of normal modes used for linear system. There was not much research in this area until Vakakis [40, 41], Shaw and Pierre [42, 43] independently started to work on it. Shaw and Pierre generalized Rosenberg's definition by proposing a concept of invariant manifold. They represented NNMs as surfaces in a phase plane. NNMs theory is based on a thorough mathematical framework and it successfully explains distinctive non-linear phenomena like internal resonance, localization of mode shapes, mode bifurcations, frequency-energy dependence etc. The very mathematics that enables the theory to describe all complex physics makes it difficult to use in everyday engineering applications. Recently, Gilbert [44] proposed a method to synthesize measured non-linear FRFs using a concept of non-linear normal modes. Peeters et al. [45, 46] proposed numerical techniques for computation of NNMs based on continuation of periodic solutions. The method makes use of system matrices to obtain NNMs for the system and it is potentially suitable for complex engineering structures. It would be interesting to see if the NNMs theory establishes itself a place in practical engineering applications in the near future.

Without sticking strictly to the NNMs, many researchers attempted to express non-linear identification problem in modal domain. He and Ewins [20, 47] proposed a method based on inverse receptance to find the variation of natural frequency[2] and damping factor for each mode. The method is based on SDOF assumption and neglects the contribution from the other modes. The method also assumes that mode shapes of non-linear system are same as the mode shapes of the underlying linear system.

For free vibration response, Feldman [48] developed a method called FREEVIB based on Hilbert transform in time domain to obtain the variation of natural frequency and damping with respect to the amplitude of vibration. He observed that the dissipative (damping) and elastic (stiffness) non-linearities have an effect on the instantaneous natural frequency and damping parameters. From the free vibration response for different non-linearities, he obtained variation of natural frequencies and damping with amplitude of vibration. He proposed another method, FORCEVIB [49] based on similar principle to analyze the systems with forced vibrations under narrow and wide band random excitations and slow and fast sweep sine tests.

[2] Or shall we say the resonance frequency

Setio et al. [50] proposed a method to extract the non-linear modal parameters from frequency response tests. They further used the extracted modal parameters to predict the response of the system at different force levels using non-linear modal superposition. Chong and Imregun [51] extended the work of Setio et al. to large MDOF systems. They considered the amplitude dependence of mode shapes which some of the other researchers had neglected in the past. The method was checked for the robustness by evaluating the effect of measurement noise and the sensitivity of the method to inaccurate underlying linear model. In the second part of the paper [52], they successfully implemented the technique on experimental data obtained for a laboratory structure with polynomial stiffness characteristics.

Platten et al. [53, 54] proposed the *non-linear resonant decay method* (NL-RDM) to identify the non-linearities in modal domain. The method represents system equations in modal coordinates with the non-linear modal force to incorporate non-linearities. The force appropriation technique with burst sine excitation is used to excite a single mode at a time. The extracted non-linear modal force at each mode is plotted against modal displacement and modal velocity for form a non-linear restoring surface in modal domain. The surface is fitted to polynomial to identify the coefficients of the polynomial.

Ozge and Ozguven [55] presented a method to find the variation of modal properties of non-linear system. They proposed an equivalent linearization of the system by keeping a constant value of response at the non-linear DOF. A series of such constant-amplitude tests yields variation of modal properties as a function of displacement amplitude.

Recently, Elizalde et al. [56] presented a semi-analytical and approximate approach to determine the variation in modal parameters (natural frequencies and mode shapes) of a large MDOF system. They used an iterative procedure to extract the non-linear modal parameters, using the modal model for the underlying linear system as an initial guess.

2.2.4 Model updating for non-linear systems

The main theme of model updating is to compare the measured and predicted data for a system, and to refine the model of the system in order to obtain a better agreement between the two sets of data. Model updating for linear systems received a good deal of attention for more than last three decades. Different techniques emerged essentially to update the FE model of the system in light of the experimental measurements. The reviews of different techniques on this topic can

be found in [57, 58]. Friswell and Mottershead [59] wrote a book dedicated to finite element model updating.

For linear systems, the results from numerical models deviate from the experimental results mainly because of the uncertainties in boundary conditions, material properties, and to some extent, the physical dimensions. These parameters are generally chosen for updating the numerical model. As a basis of comparison, different quantities can be used. The most popular are either the modal properties like natural frequencies and mode shapes, or the response of the system either in frequency domain (FRFs) or time domain.

For a non-linear system, modal properties are not constant. The resonance frequencies and mode shapes are dependent on the response amplitude at non-linear DOFs, and, indirectly on the excitation level. If the modal properties determined at some excitation level are used as a basis of comparison in model updating; then the updated model would result in a linearized model of the system at that excitation level. This model can seldom be used to accurately predict the response of the system at some other excitation level. If the type of the excitation and its range remains more or less constant for the application, the linearized updated model can be sufficient.

The linearized updated model is popular for connections and joints as it gives fairly accurate and compact description of the joints. Mottershead et al. [60] used a sensitivity based method to update the model for welded joint. They chose the physical parameters like offset distances and joint mass as the updating parameters. Moon et al. [61] proposed an analytical joint modelling strategy for automobile joints. They used sensitivity based method to later update the parameters of the joints. Ratcliffe and Lieven [62] presented a method to update the properties of joints in a structure. They used an FRF based comparison to find the stiffness, mass and damping matrix for a lap joint element. Ahmadian et al. [63] used the natural frequencies and mode shapes as a basis for comparison to get an updated model for the MACE structure containing large surface-to-surface joints. They used a thin layer of connection elements to depict the joint, and updated the properties of these elements to obtain a linearized model for the structure. Palmonella et al. [64] reviewed the updating strategies for spot welds. They compared six different models and investigated the effectiveness of the models from model updating perspective.

The literature discussed earlier used the modal properties as a basis of comparison for updating. Schmidt [65] used time series based correlation to update FE models with localized non-linearities like friction, gap and local plasticity. He

used the concept of ‘state observers’ from control theory to compare the time histories. This method is closer to the traditional non-linear identification methods described in previous section.

Hemez and Doebling [66] assessed different available model updating methods from the non-linearity perspective. They presented different test-beds, some numerical and the others experimental to compare these methods. After studying their performance, they argued that the conventional modal-based updating techniques update the model of a non-linear structure by alterations, which sometimes can be non-physical. Alternatively, the use of time series as a basis for comparison results in the updated model with some physical interpretation. Schultze et al. [67] proposed a feature-based iterative method to update the parameters of so-called *meta models*. A *feature* can be anything that describes the output state of the system. For example, for conventional modal-based methods, the eigen values can qualify as one of the features. The objective function for the optimization problem is defined as the difference between experimentally observed features and numerically predicted features.

Lenaerts et al. [68, 69] used proper orthogonal decomposition (POD) to update the non-linear system. They used an optimization routine with an objective function defined as the difference between POD matrices for the experimental and numerical time series data. The use of POD essentially reduces the size of the model while retaining the required accuracy. In this particular case, they included the proper orthogonal modes (POMs) contributing towards 90% of the system’s energy for the analysis.

As discussed above, the conventional modal-based updating methods yield a linearized updated model, which is generally not useful for strong non-linear systems. The time-series based methods are better suitable for the strong non-linear system. The research in this area sometimes tends to overlap with the research in conventional non-linear identification described in earlier sections.

2.3 Non-linear response prediction

Predicting the system behaviour is the ultimate goal for which the system identification acts as the first step. Because of the cost and time associated with the experiments, coupled with the availability of relatively inexpensive computational power, the route of computer simulations to predict the system behaviour has gained popularity. The results from computer simulations are widely used in the design and performance optimization of systems.

From structural dynamicist's view point, the prediction of system behaviour essentially translates to predicting the response of a system at different excitation levels. For a linear system, the commercially available FE codes can predict the response with good accuracy but for non-linear systems, such predictions are still a research area. For non-linear systems, the values of parameters used in the models are extracted from experimental measurements. There is always a natural variation in the extracted values, and the non-linear model should be robust enough to compensate for these variations. Thus, it is necessary to find the sensitivity of the solution to the uncertainly in the input parameters [70]. A review of the literature on uncertainties in bolted and other fasteners is presented by Ibrahim and Pettit [71]. In the current review, only the methods using a deterministic approach are considered.

The research in this topic deals with: (i) mathematical models which can describe different phenomenon like friction, clearance, impact, plasticity, geometric non-linearity etc., (ii) numerical methods to solve the non-linear system, and (iii) the approaches like model reduction, domain-decomposition, sub-structuring to reduce the problem size.

Amongst the common types of non-linearities observed in the engineering structures, geometric non-linearities can generally be expressed in polynomial form as is shown for a clamped beam in [2]. Material non-linearity arises when the material disobeys the Hook's law. It can either be plasticity, creep, or viscoelastic/ viscoplastic behaviour of the material. The literature on material non-linearity is not discussed here and basic treatment on this topic can be found in a text book on by Zienkiewicz and Taylor [72]. The widely used mathematical models for clearance, bi-linear stiffness, saturation type non-linearity etc are given by Tomlinson and Worden in [2].

Friction constitutes a major phenomenon in non-linear structural dynamics. Friction modelling is a separate research area in itself. Berger [73] wrote a review on the use of different friction models for dynamic simulation. He broadly classified the models into high-order continuous models and low-order lumped models. He argued that the high-order models are accurate and physically more appealing, but the low-order models are often used in structural dynamic simulations, as they are computationally less expensive and easy to implement numerically.

Iwan [74] suggested lumped models to represent 1D micro-slip and macro-slip phenomenon. These models are found very effective for dynamic studies, and are now popularly known as Iwan models. Menq and Griffin [75] incorporated similar models in frequency domain using a single harmonic balance method to predict the forced response of frictionally damped structures. Menq et al. [76] extended the

earlier method for 2D friction contact. Sanliturk and Ewins [77] proposed a 2D macro slip model using single harmonic balance method. Sanliturk et al. [78] later used macro and micro slip models to predict the forced response of 3D idealized turbine blade with multiple friction dampers. All the above methods assume a constant value for contact force in the normal direction, which may not be the case in real contacts.

Petrov and Ewins [79, 80] proposed an analytical frequency domain formulation for multi-harmonic analysis of frictional contacts. They derived analytical expressions for contact force vectors and stiffness matrix taking into account the influence of variable normal loads including the extreme case of separation. The analytical formulation provides an accurate and computationally inexpensive means to obtain the forced response in the presence of frictional contact. A time domain version of generic friction models is proposed in [81]. These models take into account the time variations of friction contact parameters (coefficient of friction and contact stiffness coefficient) and arbitrary variation in normal force.

The joints and fasteners are of common occurrence in engineering structures. Many researchers attempted to model the frictional contact at a joint. Gaul and Lenz [82] studied an isolated bolted lap joint for two of its vibration modes (longitudinal and torsional). A lumped parameter model is proposed to simulate macro and micro-slip behaviour. The Valanis model known from plasticity is fitted into the experimentally obtained hysteresis loop to identify its parameters. A simplified 2D space structure with 15 such joints is modelled in FE code to verify the method. Oldfield et al. [83] used a similar approach to isolate a bolted joint and extract the lumped parameter model for the joint. They generated the hysteresis loop using a detailed FE model of the joint and used this to identify the parameters of Jenkins model[3] and Bouc-Wen model. They compared the results from the two models and found that the Jenkins model is effective when the hysteresis loop is bi-linear. Genzo et al. [84] investigated the performance of a 1D friction model to predict the forced response of an assembled structure with several bolts. They compared the numerical results with the experiments and found a good correlation in frequency space for the first two modes.

Coming to the numerical solution of non-linear systems, the time-domain methods using numerical integration algorithms are direct and more accurate. These methods are well suited for the transient solution of non-linear systems. For frequency response calculations, where a steady-state solution is sought at each

[3] similar to Iwan parallel-series models [77]

frequency step within a wide frequency range, the time-domain methods become computationally very expensive. The frequency-domain methods using harmonic balance technique are widely used for steady-state frequency response prediction of non-linear systems. Sanliturk et al. [78] implemented the single harmonic balance method for friction problems. Petrov and Ewins [79, 80, 85, 86] proposed analytically derived friction elements using multi-harmonic balance method for fast and accurate prediction of turbine blade friction dampers. Budak and Ozguven [87, 88] proposed an iterative receptance method based on first order describing functions to predict the response of multi DOFs system with symmetric non-linearities. This was the first of its kind effort where they used the receptance matrix of the underlying linear system combined with the non-linearity matrix to obtain a quasi-linear receptance matrix for the non-linear system. Singh et al. [89, 90] used the multi-harmonic balance method for clearance/backlash non-linearities observed in gearing problems. A summary of describing functions for different non-linear elements frequently encountered in aerospace industry is given by Goge et al. [9].

Another way of reducing the computational effort is via model reduction. For linear systems, model reduction is straight-forward and different static and dynamic spatial model reduction techniques are already established [91-93]. In addition, the use of modal models [6, 7] presents another way of having an accurate reduced-order model. For non-linear systems, the modal model in its conventional sense does not exist. To obtain a spatial reduced-order model, it is necessary to include all non-linear DOFs as master coordinates in the model reduction.

Kerschen et al. [94] presented an overview of the use of POD as a technique for model order reduction for non-linear systems. Segalman [95] proposed a technique for development of reduced-order models for localized non-linear systems. He used a combination of the conventional basis functions with the functions possessing local discontinuity at the joint for model reduction. Petrov [86] used FRF matrices of underlying linear structures to exclude linear DOFs from the set of equations to be solved iteratively. This reduces the size of the problem to the number of non-linear DOFs without forfeiting the accuracy. The method is effective in case of localized non-linearities. Avitabile and O'Callahan [96] presented three methods for efficient calculation of frequency response for the linear structures connected with discrete non-linear elements using the reduced order models. They compared *effective reduced model technique* (ERMT), *modal modification response technique* (MMRT), and *component element method* (CEM). It is claimed that the methods require 2-3 orders of magnitude less computation than the full models.

2.4 Non-linear structural dynamics: Real life structures

There are numerous methods for the identification and modelling of non-linear systems, some of those are mentioned in earlier sections. Most of the methods are tested with simulated data for lumped mass systems with few DOFs or simple continuous systems like cantilever beam. These academic structures act as a good starting point to evaluate newly proposed methods, but the current need is to go beyond this and apply the methods to complex engineering structures. This section reviews the literature in which the identification or modelling methods are applied to the relatively complex structures of industrial interest.

There are different groups working independently or in collaboration towards achieving this goal. The AWE (UK) started a modal coupling research program to study the non-linear behaviour of mechanical couplings. They designed a benchmark structure called MACE [97] for the study. In another program called 'European COST F3' researchers studied the behaviour of structures exhibiting localized non-linearity. Two test structures, as shown in Figure 2.2 were proposed as the benchmark structures. The VTT benchmark is a helical wire rope isolator exhibiting unknown type of non-linearity. The ECL benchmark is a beam with a very thin section attached at one end exhibiting geometric non-linearity. Golinval et al. [3] discussed the outcome of the exercise comparing the results when using different methods for identification. Kerschen et al. [98] used the measurements on VTT benchmark to compare the results for a time domain method (CRP) and a frequency domain method (restoring force surface).

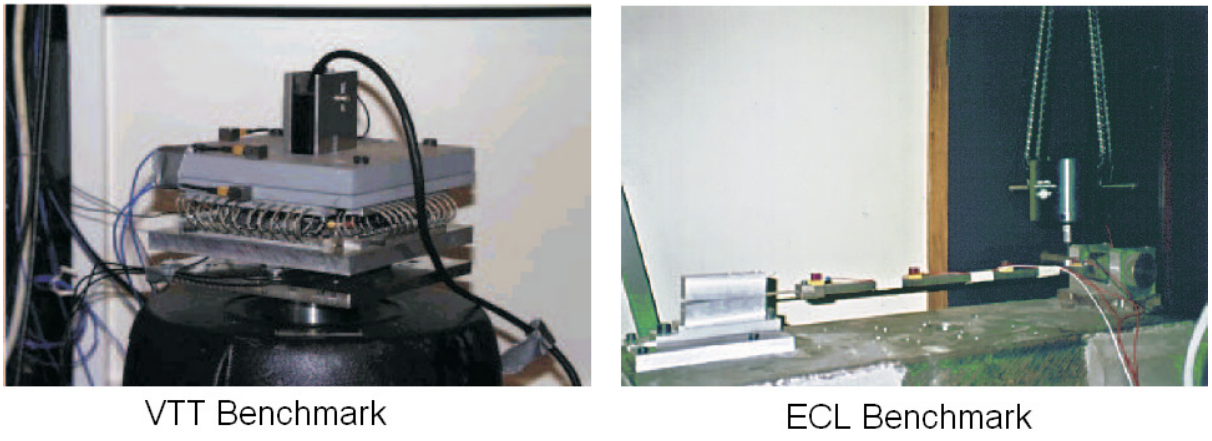

Figure 2.2 Benchmark structures for European COST F3 [3]

A group from Sandia National Laboratories is working towards the development of methodologies for joint modelling. Dohner in the report [99] summarized the work

carried out in this program. They proposed 3 test-beds consisting of different joints to carry out the benchmark experiments. Segalman et al. [100] reviewed the status of joint modelling and proposed an integrated roadmap for the future research.

Ferreira [101] during his PhD work built a laboratory structure with 3 beams to exhibit polynomial stiffness non-linearity. Chong and Imregun [52, 102, 102] used experimental results obtained using the same structure to test the variable modal parameter identification method. Elizalde [26] again used the structure to verify the explicit formulation method for prediction of non-linear response in frequency domain. The experimental setup used for the exercise is shown in Figure 2.3.

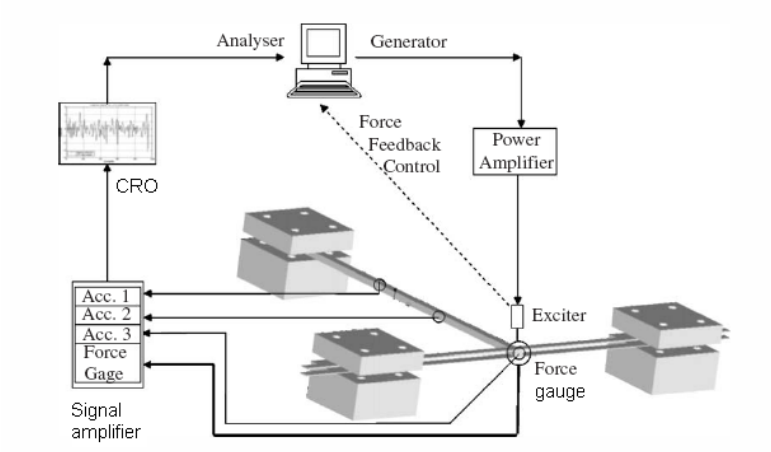

Figure 2.3 Experimental setup used by Ferreira [101] and Elizalde [26]

Platten et al. [53] experimentally verified the non-linear resonant decay method (NL-RDM) on a fully clamped plate with integral edges exhibiting geometric non-linearity. Platten et al. [54], in another study, implemented the NL-RDM on a laboratory structure depicting a 'wing-store' model. They excited the first four modes with increasing level of excitation force to extract the variation of natural frequency and modal damping. Later each mode is identified separately by plotting the restoring modal force surface for each mode.

Adams et al. [103, 104] used the *restoring force method* (RFS) and NIFO method to characterize the non-linearities and identify the non-linear parameters in a tire-vehicle suspension system in absence of input measurement. Worden et al. [105] attempted the identification of non-linearity in an automobile damper using three different methods available in the literature. They used both time domain approach (restoring force surface, and neural network) and frequency domain approach (NIFO method) for identification. Garibaldi et al. [106] successfully used NIFO method to extract the non-linearities from the experimental data for a scaled model of a building.

Aerospace industry is a challenging sector from non-linear structural dynamics perspective. There are various attempts to analyze the non-linear aero structures. Perinpanayagam et al. [107] performed controlled level vibration tests on an aero-engine casing to detect the non-linear behaviour of the structure. They extracted the variable modal parameters for the first bending mode of the structure using SDOF non-linear method. Gloth and Sinapius [108] proposed a method to extract the amplitude dependency of the modal parameters using sweep sine tests. The method is implemented on large aircraft structure. Kerschen and Golinval [109] used a plane-like laboratory structure with non-linear components for the study. They employed the CRP method in the first stage to extract the underlying linear model of the structure and the non-linear components. In the second stage, the underlying linear model obtained from the experiments is used to update the FE model of the structure. Da Silva and Voroto [110] designed and fabricated a scaled model of a wing-engine assembly to study the parametrically excited internal resonance, a phenomenon specific to non-linear structures. Goege [5] proposed a two-stage methodology to characterize and identify the non-linearity in a ground vibration test for an aircraft. In the first stage he used different methods to quickly detect the non-linear modes. In the second stage, he used modal restoring force surface method to identify the non-linear parameters for each mode. The method is applied to an actual aircraft in a ground vibration test.

2.5 Summary of the literature review

Non-linear structural dynamics has been of interest to the researchers for more than four decades. There is an increasing need for accurate prediction methods in order to reduce the time and the cost involved with the experimentation. This need coupled with easy availability of computational power acted as a stimulus to the research in this area.

The ultimate aim of the research in this area is to predict the dynamic behaviour of a system under different excitation conditions using a computer-based model of the system. The research progressed in two fundamental branches. The first branch deals with proposing mathematical models to explain the non-linear phenomenon. The second branch deals with the identification of the parameters used in the non-linear models.

The non-linear identification is an inverse problem. It attempts to identify the system in its mathematical form. The non-linear identification has three steps viz. non-linearity detection, non-linearity characterization and non-linear parameter

extraction. The methods for non-linearity detection are well established and are widely used in the aerospace and automobile industries. The methods for the characterization of non-linearity types are still not industrially usable. An experience based subjective judgement is widely used in the industry for non-linearity characterization. Extraction of non-linear parameters poses even bigger challenge. Most of the methods available in the literature are presented for few DOF lumped-mass systems or simple continuous systems of academic interest. There are some potential issues when applying these methods to real-life engineering structures. Recently some attempts have been made to use the identification methods on complex engineering structures.

Because of the individualistic nature of non-linearities, it is difficult to propose a universal method for identification to suit all cases. The methods discussed in the literature have their application region within which they succeed. Even today, the industry is waiting for a method for non-linear identification which can be used alongside the main-stream tools like linear modal analysis and FEA and which is applicable to complex real-life structures.

Chapter 3

Non-linearity type identification using a ‘footprint library’

This chapter presents the concept of a ‘footprint library’ to identify the type of non-linearity in the system. It is observed that the shape of non-linear restoring force curve is unique to the type of non-linearity. A library of non-linear restoring force curves, generated using a simple 2-DOF system with different types of non-linearities is presented. Two methods are proposed for non-linearity type characterization. In the first method, the footprint library is used as a look-up chart to identify the type of non-linearity in the system by visual comparison. In the second method, a shape-matching algorithm is proposed to quantify the match between the shape of a non-linear restoring force curve obtained for any non-linear structure and the shape of the curves from the footprint library. The methods are validated on simulated data for a cantilever beam with different non-linearities.

3.1 Introduction

Non-linearity characterization is an important step in non-linear system identification. It encompasses the task of locating non-linear DOFs and of finding the type and the form of non-linearities in the system. After non-linearities are characterized successfully, the non-linear parameters are identified by posing non-linear parameter extraction as an optimization problem, which is solved by using the available methods for optimization. Different methods for non-linearity characterization are proposed in the literature [9, 20, 22, 29, 30, 111]. Almost all of these methods are based on some subjective judgement.

Elizalde [26] observed that the variation of non-linear restoring force with excitation frequency produces a unique ‘footprint’ for each type of non-linearity. This idea is extended in the current research to present a collection of footprints for

different non-linearities. For a better comparison, the non-linear restoring force is represented in different formats like Bode plot, Nyquist plot etc.

For a multi degrees of freedom (MDOFs) non-linear system, undergoing harmonic excitation, the equation of motion can be written as:

$$[M]\{\ddot{y}\}+[C]\{\dot{y}\}+[K]\{y\}+\{g(y,\dot{y})\}=\{F\}\sin(\omega t) \tag{3.1}$$

where, [*M*], [*C*], and [*K*] are mass, damping, and stiffness matrices, $\{F\}$ is the excitation force vector, and $\{g(y,\dot{y})\}$ is the non-linear restoring force. Equation (3.1) can be converted into frequency domain by considering only the first harmonic, and can be written in a compressed form as:

$$\underbrace{[\Lambda]\{Y\}}_{\text{Linear restoring and inertia force}} + \underbrace{\{G\}}_{\text{Non-linear restoring force}} = \underbrace{\{F\}}_{\text{Excitation force}} \tag{3.2}$$

where $[\Lambda]$ is the dynamic stiffness matrix of the underlying linear system, $\{Y\}$ is the displacement amplitude vector, and $\{G\}$ is the vector containing the non-linear restoring force. The non-linear restoring force at the non-linear DOF can be extracted using (3.2) if the mathematical model for the underlying linear system is known[4]. In the thesis, the terms 'non-linear restoring force' and 'non-linear force' are used interchangeably.

As stated in [26, 28, 31], the extracted non-linear force is a function of the type of non-linearity and the non-linear parameters. The magnitude of the non-linear force varies with the values of non-linear parameters, dynamic properties of the system and the excitation force, but the shape of the non-linear force curve is observed to be independent of all these parameters [26]. Thus, a set of non-linear force curves obtained for any simplified system with arbitrary non-linear parameters can be used as a universal look-up library to identify the type of non-linearity in engineering structures.

3.2 Generation of non-linear force curves

The 2-DOF system, shown in Figure 3.1, was used as a benchmark system to generate the library of non-linear restoring force curves. As seen in the figure, a grounded non-linear element is attached to the DOF-1. A detailed description of the system is given in Appendix A. The type of non-linearity was varied to simulate

[4] More on this in Chapter 4

several types of non-linear systems commonly encountered in engineering structures. Different non-linearities like cubic stiffness (softening and hardening), clearance, friction and a combination of all these types are considered for the footprint library.

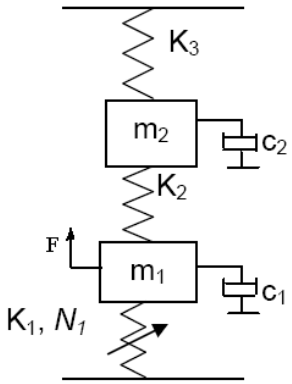

Figure 3.1 The two DOF system used to generate footprint library

The displacement response for the system was captured using an in-house harmonic-balance code, *FORSE* [4]. The code uses the single-harmonic-balance method to generate displacement responses, which simulates experimental measurements of a first-order frequency response on a structure.

The numerically-predicted response can be multi-valued for some frequency range, which is typical of some non-linearities. Figure 3.2 shows one of such frequency response showing both the stable and the unstable branches. In experimental measurements, it is only possible to realize the stable branches of the curve. For example, with an increasing frequency step sine test, the response corresponding to stable branch 1 is realizable. Alternatively, with a decreasing frequency step sine test, the response corresponding to stable branch 2 can be realized. For generating the footprint library, the response corresponding to the increasing step sine test was used for all non-linearities except the softening cubic stiffness non-linearity. For softening cubic stiffness non-linearity, the response corresponding to the decreasing step-sine test was used.

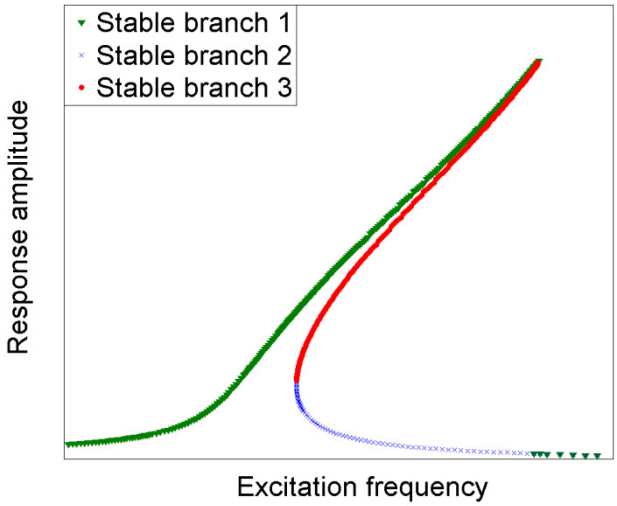

Figure 3.2 A typical frequency response curve for cubic stiffness non-linearity

3.3 Footprints of different non-linearities

A total of ten different types of non-linear forces are included in the footprint library. The cases considered are as follows:

(1) Cubic stiffness with hardening behaviour
(2) Cubic stiffness with softening behaviour
(3) Clearance
(4) Friction dominated with stick phenomenon
(5) Friction dominated with slip phenomenon
(6) Stick-slip type friction
(7) Combined cubic stiffness and clearance
(8) Combined cubic stiffness and friction
(9) Combined clearance and friction
(10) Combined cubic stiffness, clearance, and friction.

The following section presents the plots of non-linear force for all ten cases. The non-linear force is plotted in the vicinity of the first resonance of the system. For each figure, the plot on the left shows the magnitude of non-linear force plotted against the frequency and the plot on the right is a Nyquist plot. Since only the shape of the plot is of primary importance, the scale is not shown on the plot axes.

3.3.1 Cubic stiffness non-linearity

Figures 3.3 and 3.4 show the non-linear force for the cubic stiffness non-linearity with hardening and softening behaviour respectively. For hardening type non-linearity, the non-linear force increases continuously till the resonance frequency, and then drops suddenly to a lower value. This drop is corresponding to the jump in the frequency response. In the Nyquist plot, it traces an arc in the forth quadrant.

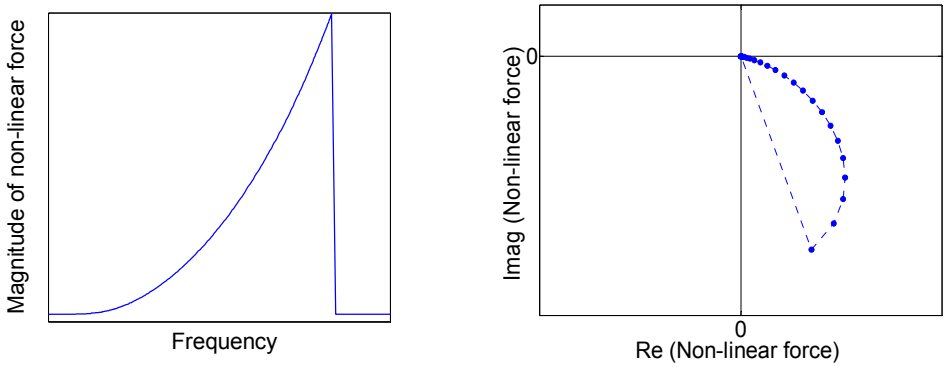

(a) (b)

Figure 3.3 Non-linear force: Cubic stiffness non-linearity (hardening)

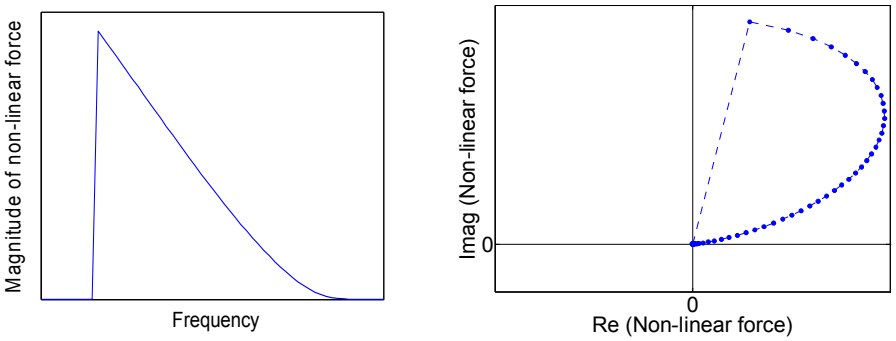

(a) (b)

Figure 3.4 Non-linear force: Cubic stiffness non-linearity (softening)

For the softening cubic stiffness non-linearity, the non-linear force jumps to a higher value at the resonance frequency, and then gradually reduces to zero as the system moves away from the resonance. The Nyquist plot traces an arc in the positive Y-axis region. This observation is justified by the fact that the non-linear force for the softening cubic stiffness non-linearity is 180 degrees out of phase with the displacement.

3.3.2 Clearance non-linearity

The clearance non-linearity was modelled using a bi-linear stiffness spring with the clearance gap (y_c) and the clearance stiffness (K_z) as the non-linear parameters. Once the clearance gap is closed, an additional stiffness is coupled to the system. Figure 3.5 shows the variation of the non-linear force for clearance non-linearity.

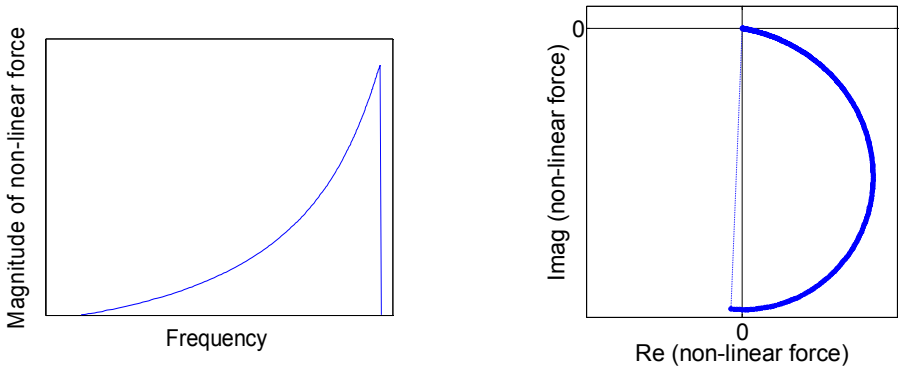

(a) (b)

Figure 3.5 Non-linear force: Clearance non-linearity

At first sight, the shape of the plots looks similar to that of the hardening type cubic stiffness non-linearity. But the close observation of the plots in the region away from the resonance shows that the non-linear force for clearance non-linearity is zero until the displacement at the non-linear DOF exceeds the gap distance, and increases sharply after the gap closure. For the cubic stiffness non-linearity, the non-linear force shows a steady increment. An enlarged view of the comparison of the two plots is shown in Figure 3.6.

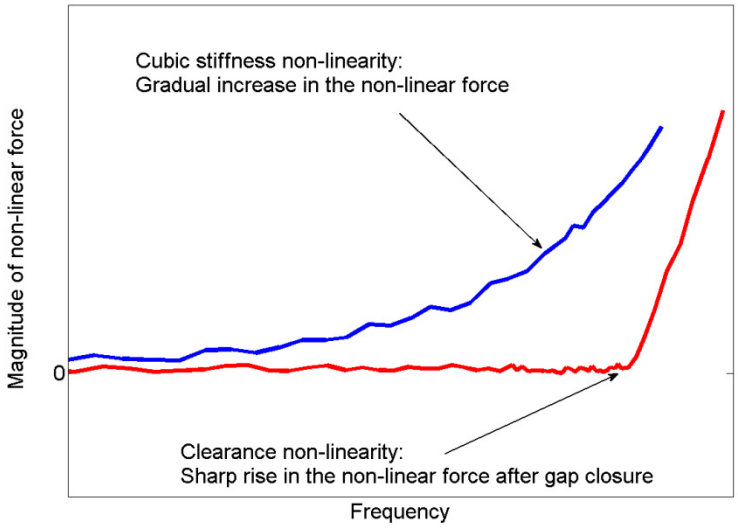

Figure 3.6 Comparison of cubic stiffness and clearance non-linearity

3.3.3 Friction non-linearity

The friction non-linearity was modelled using a micro-slip element with tangential stiffness (K_d), coefficient of friction (μ) and normal reaction (N) as the non-linear parameters. Three cases are considered based on the occurrence of stick and slip phenomenon. In the first case, the non-linear parameters were chosen such that the damper is mostly in the slip region. Figure 3.7 shows the plot of non-linear force for this case. In the magnitude plot, it can be seen that the magnitude of non-linear force remains almost constant at a value close to the value of the limiting friction force used in the simulation. In the Nyquist plot, it traces a distinctive shape covering the first, second and third quadrant.

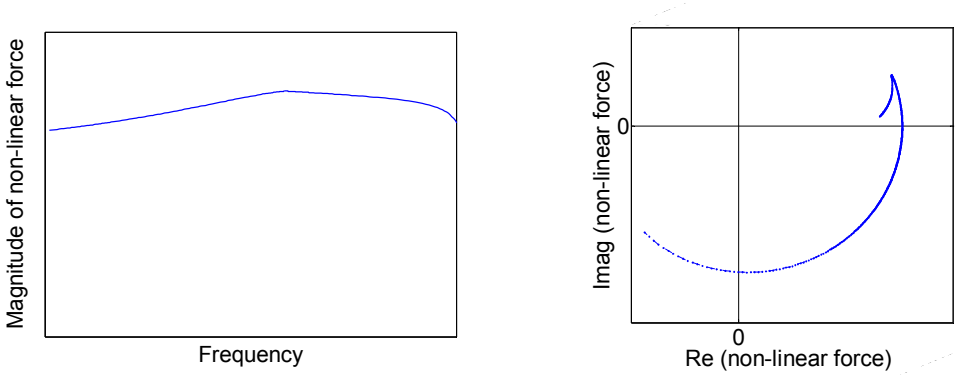

(a) (b)

Figure 3.7 Non-linear force: Friction with pure slip

In the second case, the non-linear parameters were selected such that the damper is always stuck. Figure 3.8 shows the non-linear force plot for this case. From Figure 3.8(a), it can be seen that the magnitude of the non-linear force increases steadily until the resonance, after which it drops steadily. In the Nyquist plot, it traces an arc in the negative Y-axis region, indicating that the non-linear force is in-phase with the displacement.

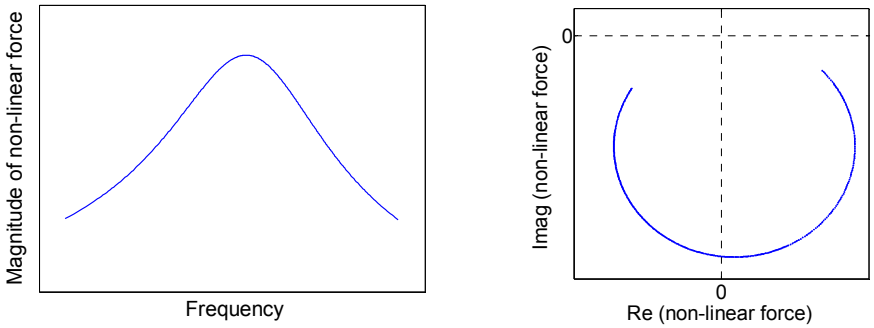

(a) (b)

Figure 3.8 Non-linear force: Friction with pure stick

In the third case, the parameters were chosen such that the damper experiences a stick-slip condition in the frequency range considered. Figure 3.9 shows the plot for the non-linear force for this case. From the magnitude plot, the regions of stick and slip can easily be identified. The non-linear force increases steadily till the damper starts slipping. In the slip region, the force remains nearly constant. In the Nyquist plot, two arcs of different radii, corresponding to stick and slip, can be identified.

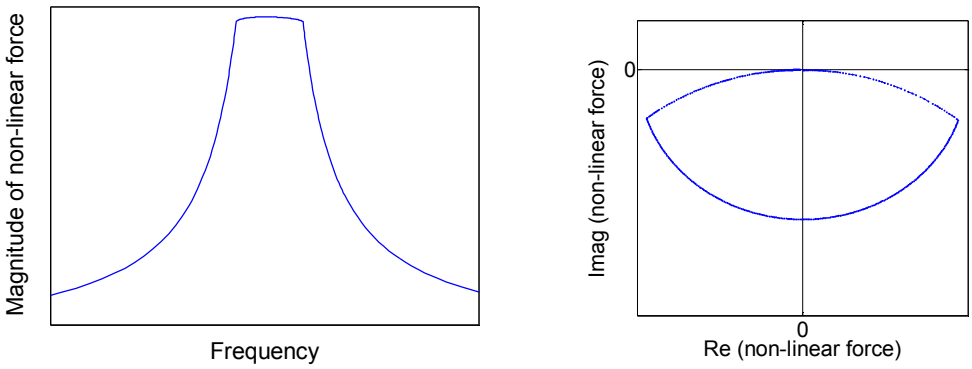

(a) (b)

Figure 3.9 Non-linear force: Friction with stick and slip

3.3.4 Combination of different non-linearities

In many practical cases, two or more types of non-linearities may co-exist in the system. If any one type is overpowering the others, then the shape of the non-linear force curve remains similar to the footprint of the dominant non-linearity type. If two or more non-linearities are contributing in equal percentage towards the non-linear force, the resultant non-linear force curve can take a completely different shape. To identify the type of non-linearity in such cases, the footprint library is extended to include some combined non-linearity types. While generating the footprints of combined non-linearities, the non-linear parameters were selected such that each non-linearity type contributes in equal percentage in the total non-linear restoring force, when summed over the frequency range.

Figure 3.10 shows the footprint for combined cubic stiffness and clearance non-linearity. The shape of the footprint is very much similar to the individual clearance footprint as shown in Figure 3.5.

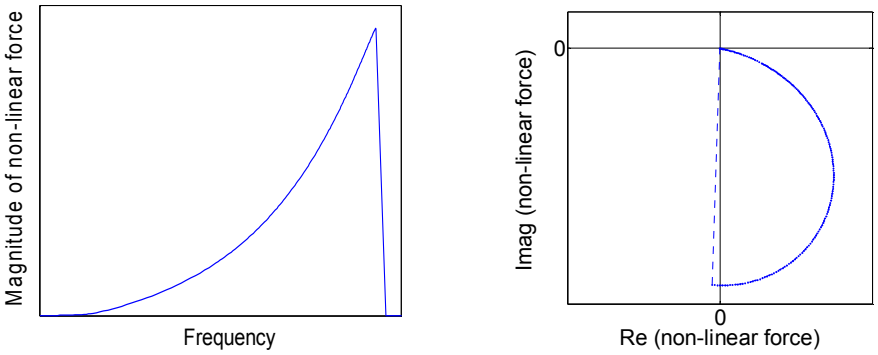

(a) (b)

Figure 3.10 Non-linear force: cubic stiffness and clearance

Figure 3.11 shows the footprint for combined cubic stiffness and friction non-linearity. Figure 3.12 shows the footprint for combined clearance and friction non-linearity. The shape of both footprints looks distinct and can be used to identify the non-linearity type.

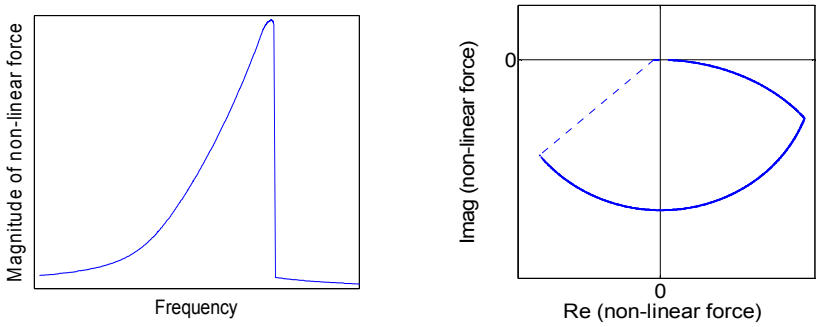

(a) (b)

Figure 3.11 Non-linear force: Cubic stiffness and friction

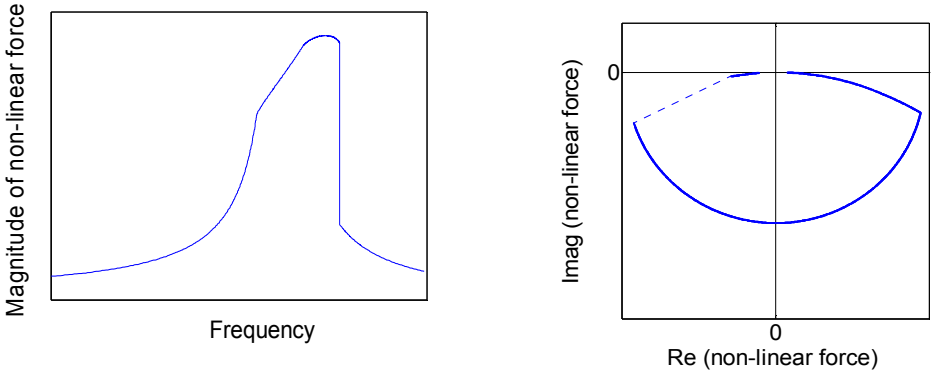

(a) (b)

Figure 3.12 Non-linear force: Clearance and friction

Figure 3.13 shows the footprint for combined cubic stiffness, clearance, and friction non-linearity. From the magnitude plot, it is difficult to identify the type of non-linearity. The Nyquist plot also looks similar to the footprint in Figure 3.11.

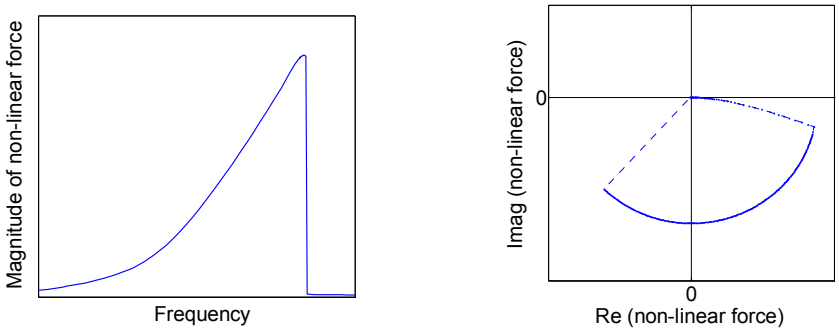

(a) (b)

Figure 3.13 Non-linear force: Cubic stiffness, clearance and friction

The footprints of different non-linearities, as presented above, can be collected to form a library of curves. The library can be used as a look-up chart to qualitatively comment on the type of non-linearity in the structure. A combined chart with all types is shown in Figures 3.14 and 3.15.

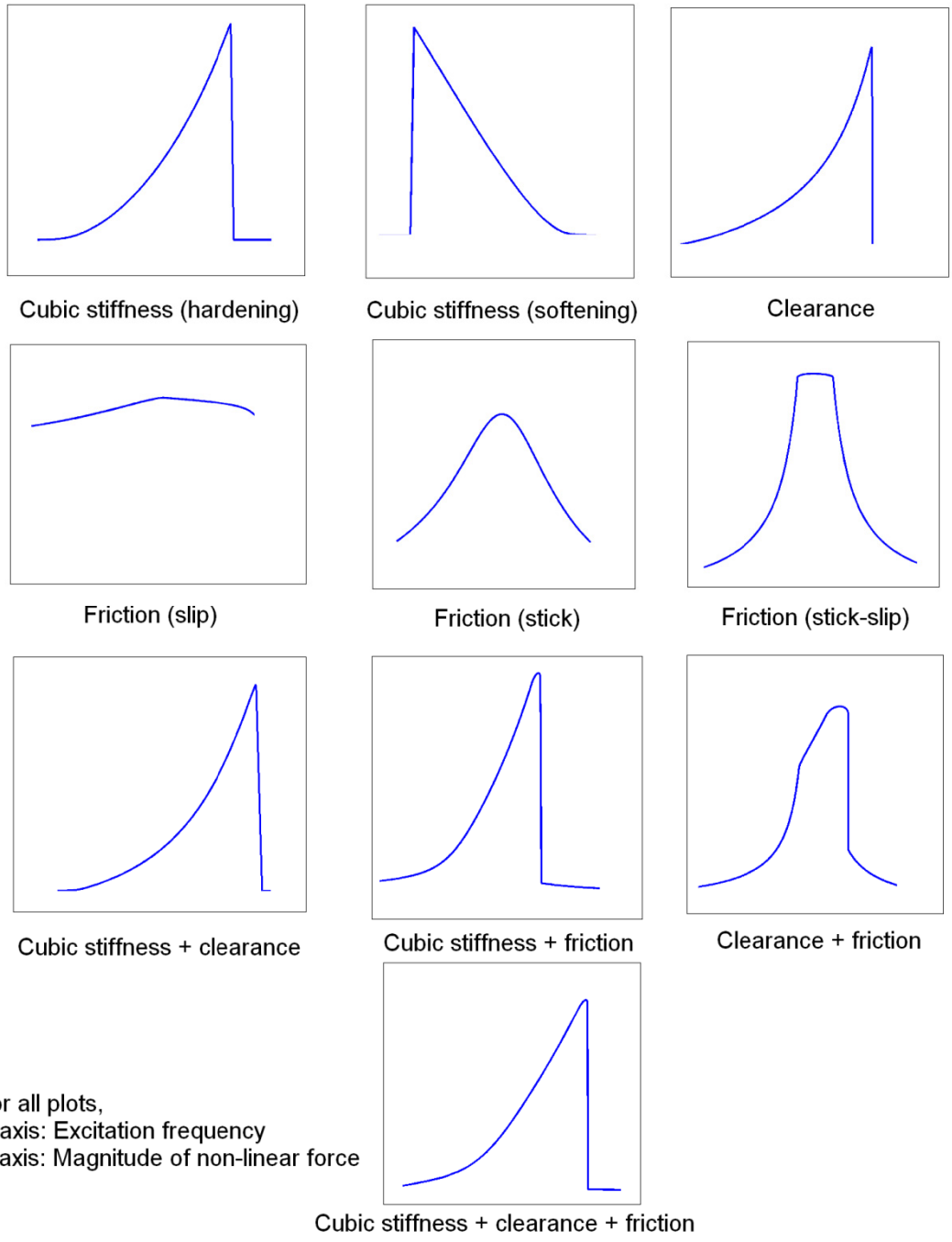

Figure 3.14 Footprint library: magnitude plots for non-linear force

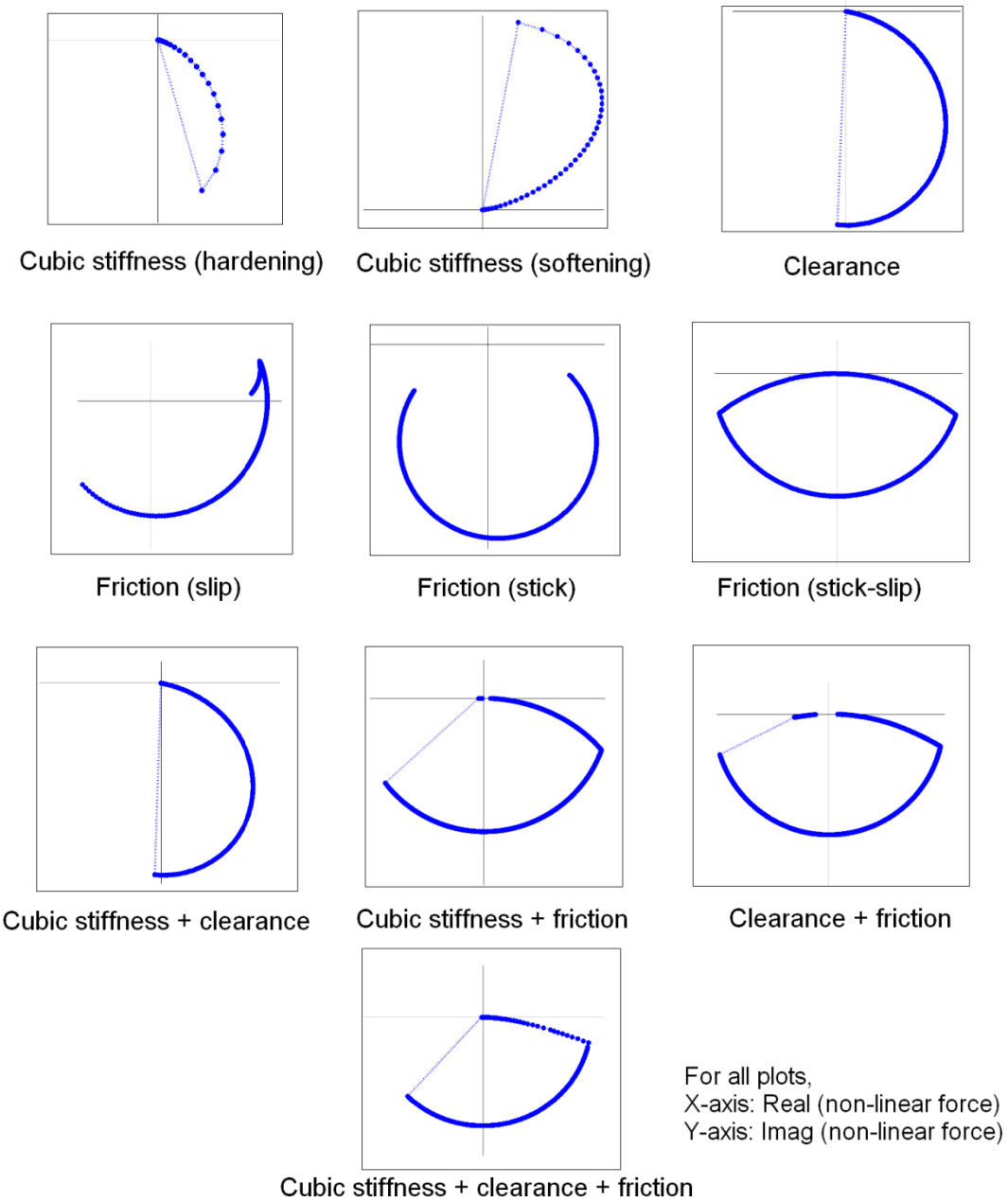

Figure 3.15 Footprint library: Nyquist plots for non-linear force

The library can be extended further to accommodate other types of non-linearities commonly occurring in engineering structures. It can be seen that some types like friction are clearly distinguishable whereas the others are more difficult to identify.

3.4 Quantitative comparison using shape-matching algorithm

The footprint library presented in the section 3.3 uses a subjective judgement to identify the type of non-linearity. It is observed that some non-linearities are difficult to distinguish using just the visual comparison. This section presents an objective way of identifying the type of non-linearity. A shape-matching algorithm is proposed to measure the closeness of the shape of the extracted non-linear force curve to the shape of different curves in the footprint library.

The plots in the footprint library presented in the earlier section are not suitable to use for a quantitative comparison as the frequency axis is difficult to normalize. For a better quantitative comparison, the non-linear force is plotted against the magnitude of relative displacement between the non-linear DOFs. As the plot of the non-linear force is used only to identify the non-linearity type, and not the strength of the non-linearity or the non-linear parameters at this stage, it is possible to normalize both axes to unity.

A sample plot showing the non-linear force for cubic stiffness non-linearity is presented in Figure 3.16. Since the non-linear force is expressed directly as a function of relative displacement, it completely eliminates the dependence of the shape of the curve on the system under consideration.

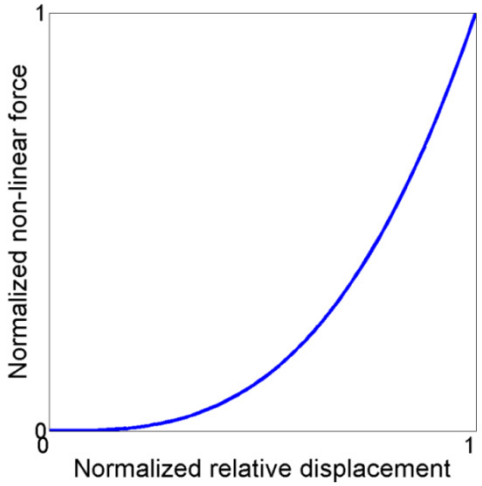

Figure 3.16 Normalized footprint for cubic stiffness

3.4.1 Generation of footprint curves

Since this representation of non-linear force does not depend on the system, the footprints can be generated using the mathematical expressions for the non-linearities. The expressions based on the harmonic balance method were used to generate the footprints. The non-linear force was calculated using the expressions

shown in Table 3.1 assuming a grounded non-linearity. The relative displacement amplitude, (Y_i - Y_j), at the non-linear DOF was varied from 0 to 1 uniformly. Later, the non-linear force was normalized to unity to have a library of footprints with normalized X and Y axes. Similar to the earlier footprints for combined non-linearities, the parameters were chosen such that each non-linearity contributes equally towards the non-linear force. The library of footprints is shown in Figure 3.17.

Table 3.1 Expressions for non-linear restoring force [2, 75]

Type of non-linearity	**Magnitude of non-linear force**
Cubic stiffness	$$g^{cub} = \frac{3}{4}\beta(Y_i - Y_j)^3$$ where β is the coefficient of cubic stiffness non-linearity, Y_i and Yj are the amplitudes of displacement at i^{th} and j^{th} DOF respectively.
Clearance	$$g^{cle} = \frac{K_z * (Y_i - Y_j)}{2\pi}\left[\pi - 2\theta_c + \sin(2\theta_c) - \frac{4y_c}{(Y_i - Y_j)}\cos\theta_c\right]$$ $$\theta_c = \sin^{-1}\left(\frac{y_c}{(Y_i - Y_j)}\right)$$ where, K_z is the additional stiffness after the clearance gap is closed, y_c is the gap distance.
Friction	Stick region: $g^{fri} = \frac{K_d(Y_i - Y_j)}{\pi}\left(\theta_l - \sin\theta_l\cos\theta_l\right)$ Slip region: $g^{fri} = \frac{-4\mu N}{\pi}\left(1 - \frac{\mu N}{K_d(Y_i - Y_j)}\right)$ $$\theta_l = \cos^{-1}\left(1 - \frac{2\mu N}{K_d(Y_i - Y_j)}\right)$$ Where, K_d is the tangential stiffness in stick region, N is the normal reaction, and μ is the coefficient of friction.

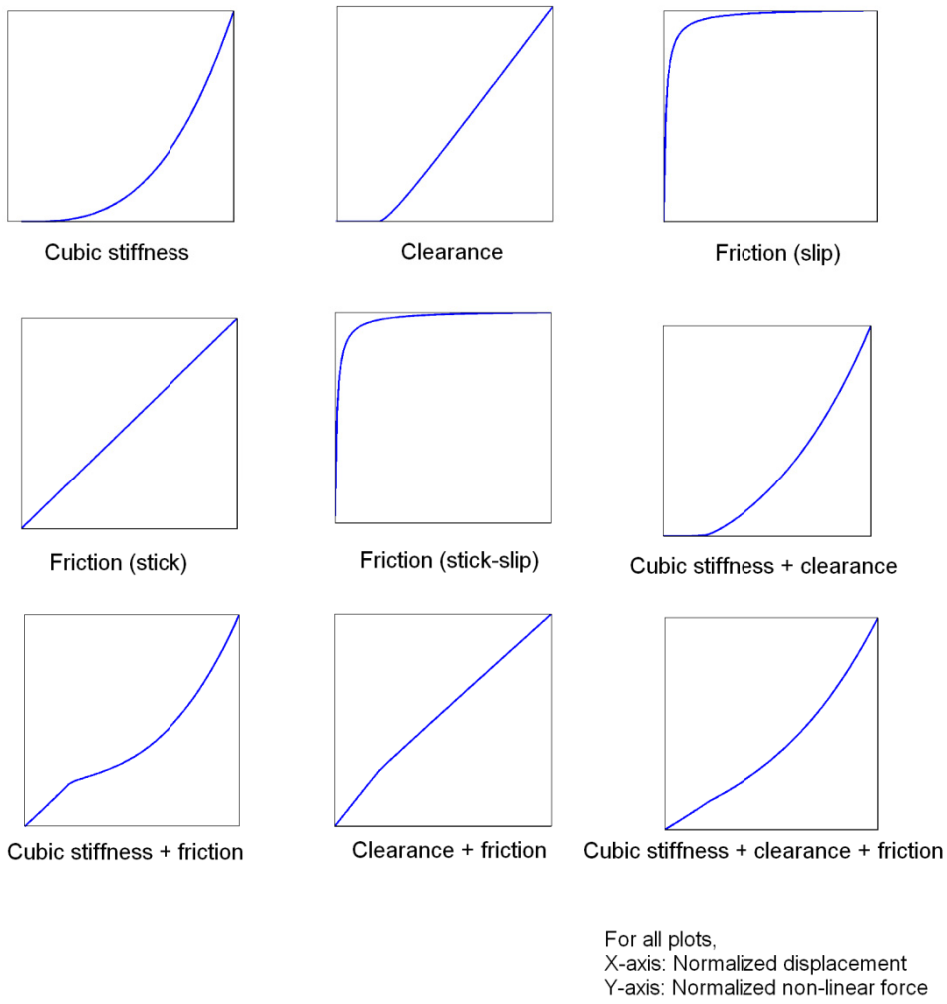

Figure 3.17 Library of normalized footprints for quantitative comparison

3.4.2 Shape-matching algorithm

An algorithm is proposed to numerically compare the shape of the non-linear force curve extracted for any structure with the shape of different curves in the footprint library. The 'match' between two curves is examined to identify the type of non-linearity in the structure. If any two curves are normalized on both axes, then the average distance between the two curves can be treated as a measure of closeness. A numerical quantity called 'sum of squared distance' (SSD) is used to evaluate the Euclidian distance between the two curves. If the SSD value for two curves is significantly lower, the curves can be said to have a good match.

Since the numerical value of the extracted non-linear force is a function of non-linear parameters in the system, the curves must be normalized before the comparison. Four operations of linear transformation viz. translation to origin, X-axis scaling, Y-axis scaling and rotation about Z-axis are performed on the extracted

non-linear force curve before the comparison. Figure 3.18 depicts the four steps on a typical non-linear force curve. The blue curve is for clearance non-linearity from the footprint library and the red curve is the extracted non-linear force curve.

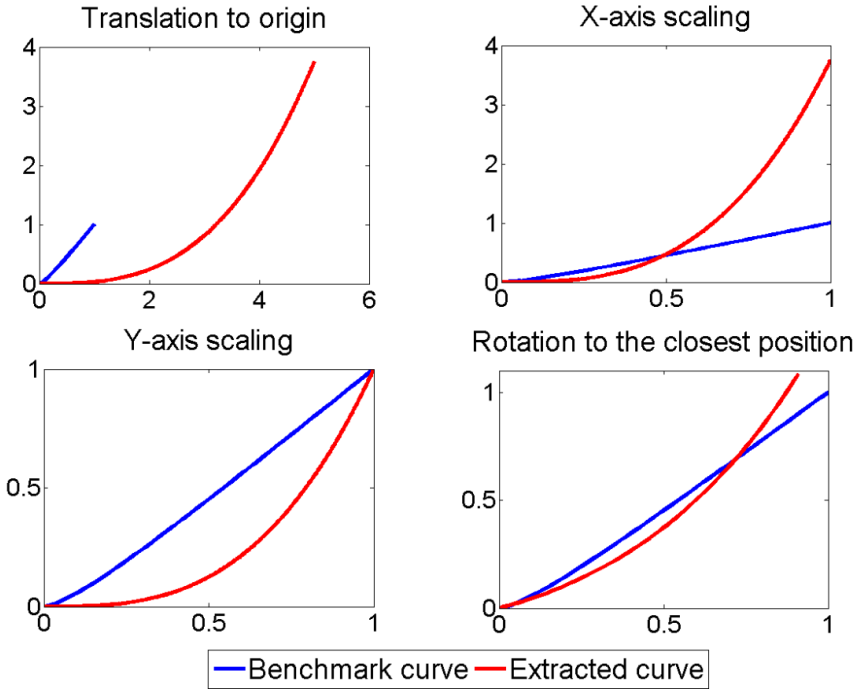

Figure 3.18 Comparison steps for shape-matching

Once the extracted non-linear force curve and the curve from the footprint library are aligned properly for comparison, the Euclidian distance between the two curves, represented by the SSD, is calculated as:

$$SSD = \sum_{i=1}^{N} \left(Y^E - Y^B \right)_i^2 \tag{3.3}$$

where, Y^E is the Y coordinate of extracted non-linear force curve and Y^B is the Y coordinate of the benchmark curve. The curves for which the SSD value is the least are said to be in a close match, hence identifying the type of non-linearity for the extracted curve. Figure 3.19 show the flowchart for the shape-matching algorithm.

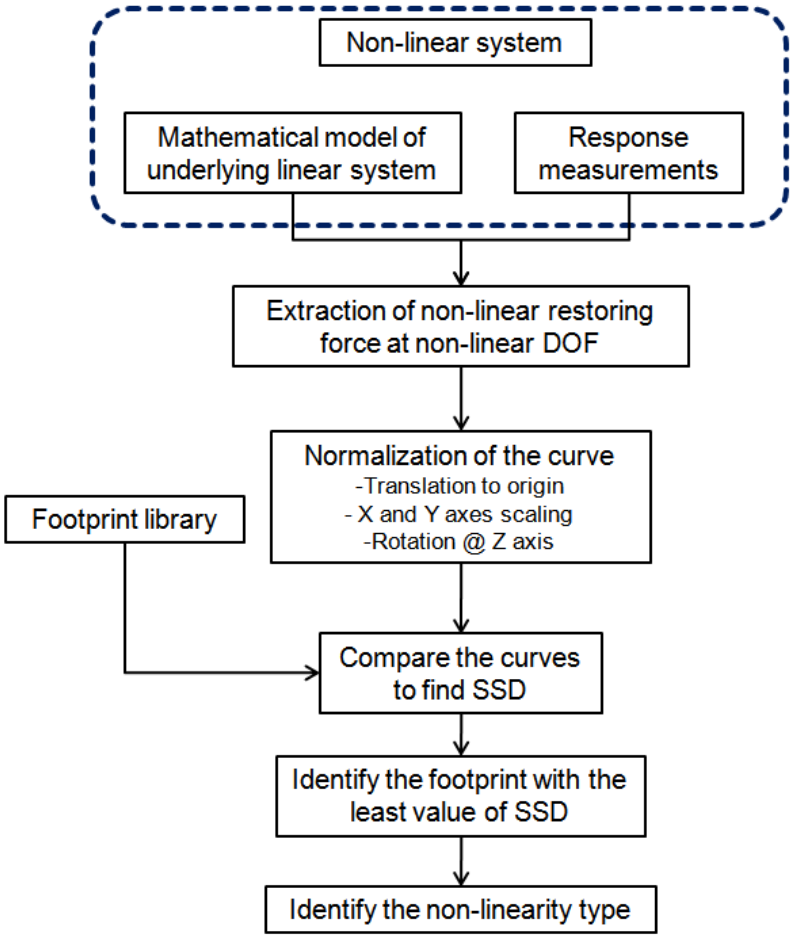

Figure 3.19 Flowchart for shape-matching algorithm

3.4.3 Universal applicability of the footprint comparison

To validate the suitability of the parameter, SSD, as a comparison criterion, and to check its universal applicability, a numerical experiment was undertaken. For the same 2-DOF system configuration shown in Figure 3.1, the parameters, both linear and non-linear were varied randomly to form 1000 different systems. The non-linear force was extracted for each system and it was compared with the footprints from the library to calculate an SSD value for each case. Figures 3.20-3.22 show the results of numerical experiments for the systems with cubic stiffness, clearance and friction non-linearities respectively.

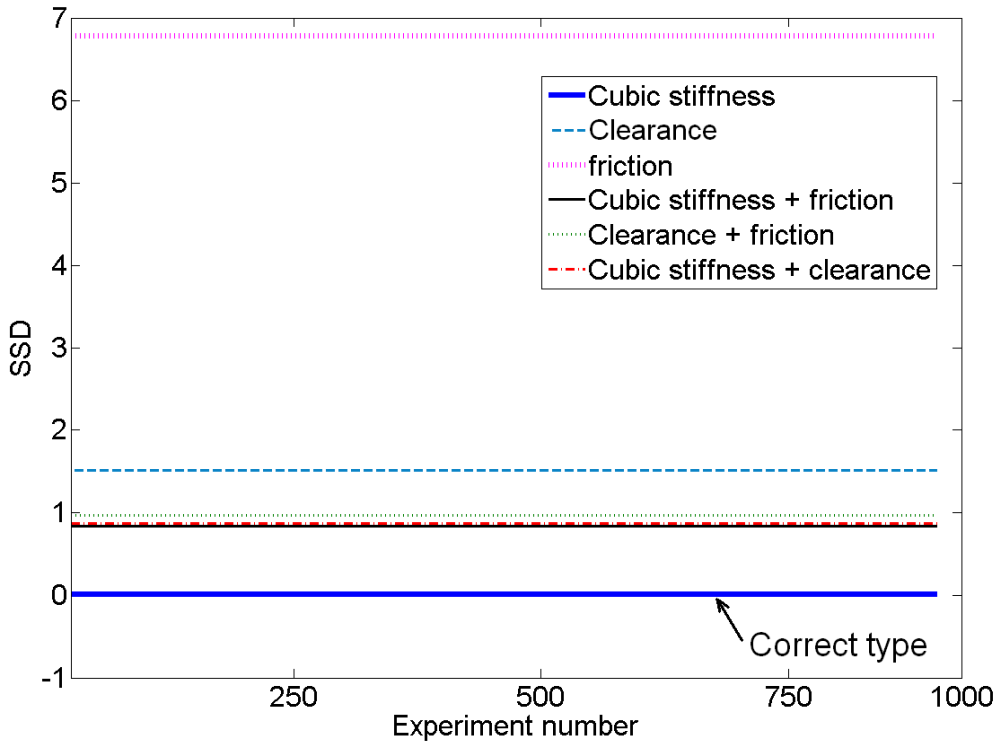

Figure 3.20 Numerical experiments: cubic stiffness non-linearity

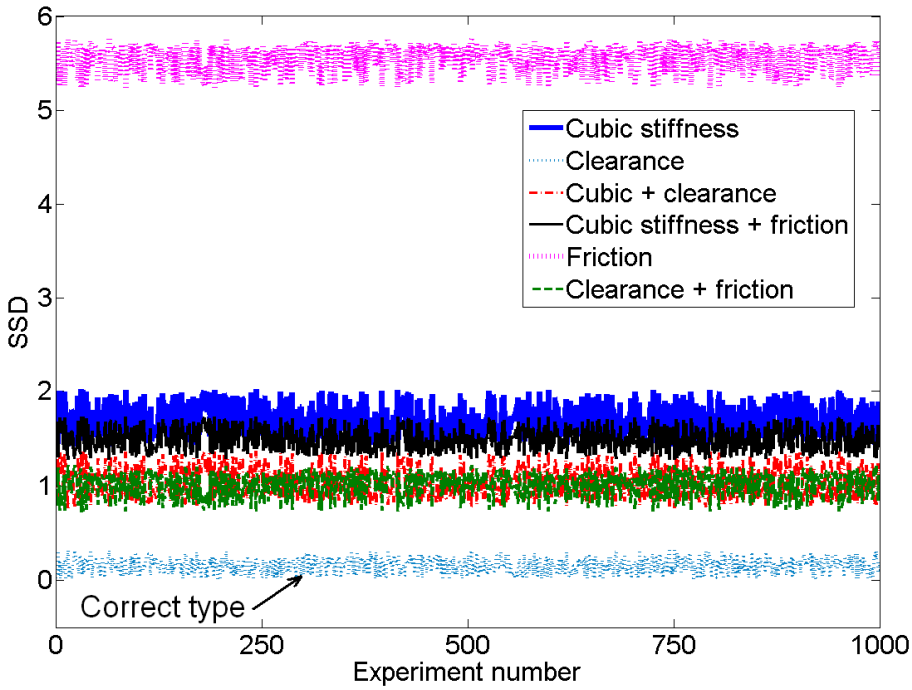

Figure 3.21 Numerical experiments: clearance non-linearity

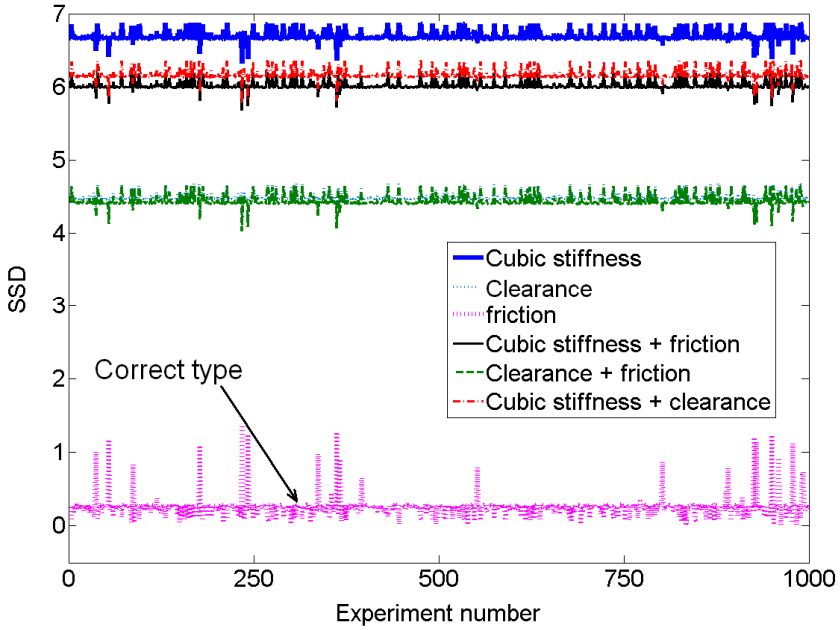

Figure 3.22 Numerical experiments: friction

It can be seen that for all three cases, when the non-linearity type is matched correctly, the SSD value is the smallest irrespective of the system parameters. For cubic stiffness non-linearity, the SSD value is zero throughout the experiments when compared with the cubic stiffness non-linearity footprint. This suggests that after the linear transformations, the two curves lie exactly on top of each other. For other two non-linearities, the SSD value is not zero when compared with the corresponding footprint, but still it is significantly lower than the other SSD values so as to identify the correct non-linearity type.

For combined non-linearities, the footprints in the library are generated based on an assumption of equal contribution by each non-linearity. The contribution of each non-linearity in the total non-linear force is calculated over the entire frequency range considered

$$C^i = \sum_{\omega=\omega_s}^{\omega_f} \frac{G^i(\omega)}{G^{tot}(\omega)} \tag{3.4}$$

Where, C^i is the contribution of ith type of non-linearity, G^i is the non-linear force due to ith non-linearity type, G^{tot} is the total non-linear force, ω_s and ω_f are the start and end frequencies in the considered frequency range. In the numerical experiments, the equal contribution constraint was not incorporated. Thus, the systems with randomly generated parameters had unequal contribution of different non-linearities. Figure 3.23 shows the results of numerical experiments for combined clearance and friction non-linearity.

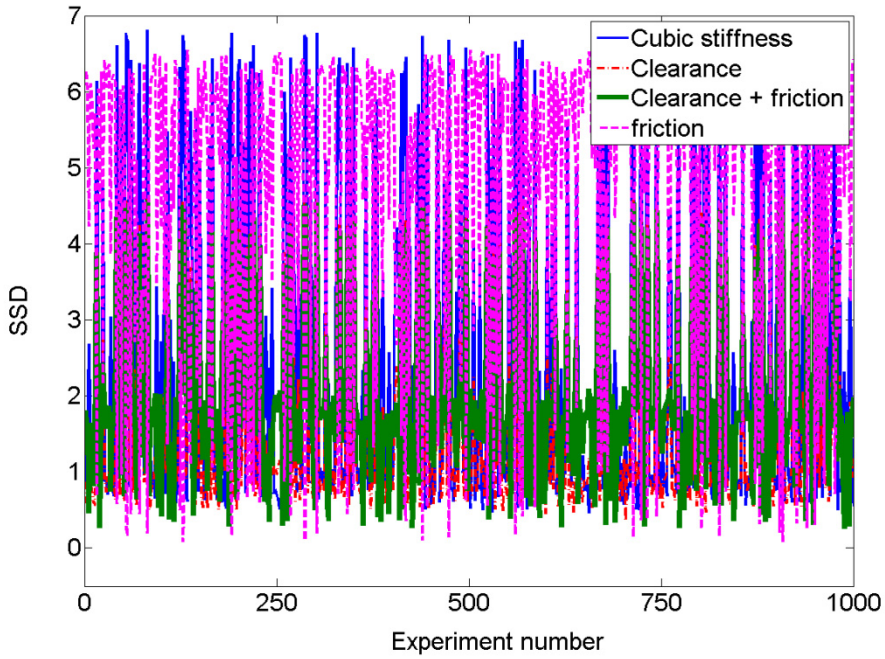

Figure 3.23 Numerical experiments: clearance and friction

From the figure, it is observed that the SSD's for different footprints are overlapping and it is difficult to clearly identify the type of non-linearity based on the SSD criterion. This is because the shape of non-linear force changes significantly with the contribution of non-linearity type. In practical structures, it is a rare situation when two or more non-linearities contribute equally. Thus, the footprints for combined non-linearities which are generated assuming an equal contribution have a limited application in identifying the non-linearity type in practical structures.

However, if more footprints of combined non-linearities with varied contribution are included in the library, then the SSD parameter might be used for conclusive determination of non-linearity type. The idea of such fine division in the footprints of combined non-linearities was validated with a numerical study. Three footprints with combined cubic stiffness and friction non-linearity were generated with varied contribution from each type. The contribution of each non-linearity type was evaluated by integrating the non-linear force versus displacement curve for individual non-linearities with selected non-linear parameters. In the current study, Footprint 1 was generated with 10% contribution of cubic stiffness non-linearity and 90% contribution of friction non-linearity. Footprint 2 was generated with 40% contribution of cubic stiffness and 60% contribution of friction non-linearity and finally Footprint 3 was generated with 90% contribution of cubic stiffness and 10% contribution of friction non-linearity.

The footprints were compared with a set of non-linear force curves for 2-DOF system with the combined cubic stiffness and friction non-linearity, and randomly chosen linear and non-linear parameters. Figure 3.24 shows the results of the numerical study. Each dot in the figure represents a 2-DOF system. The X axis shows the contribution of cubic stiffness non-linearity in the system, and the Y axis shows the SSD value which is normalized to the maximum SSD value obtained in the set.

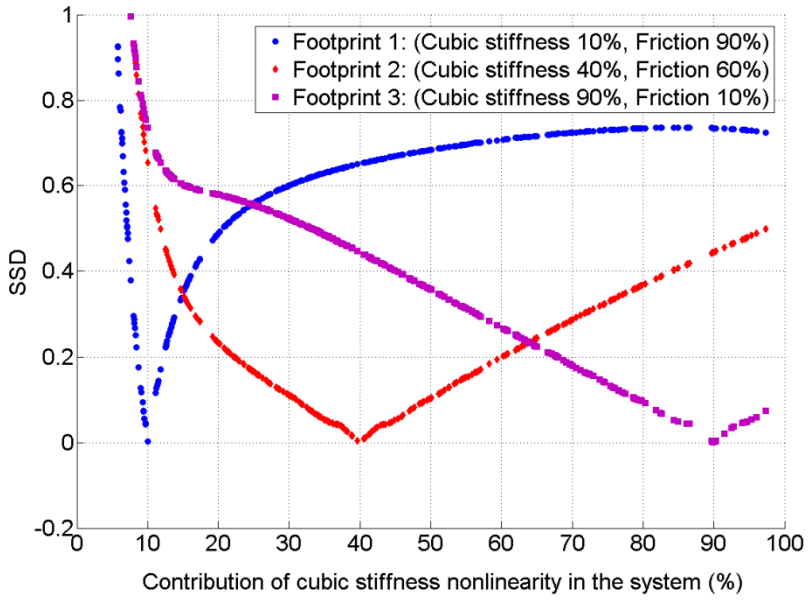

Figure 3.24 Comparison with finer footprints for cubic stiffness and friction

It can be observed from the figure that the SSD for all three footprints vary as the contribution of the cubic stiffness non-linearity in the system changes. The SSD for a footprint is the smallest when the contribution of non-linearities in the system matches with the contribution of non-linearities in the footprint. For example, for Footprint 1, with 10% cubic stiffness non-linearity and 90% friction non-linearity, the SSD value is the smallest, when the contribution of cubic stiffness non-linearity in the system is around 10%. Similar trend is observed for the other two cases.

Thus, if the footprint library is expanded to include the footprints of combined non-linearities with un-equal contribution, then it would be, in principle, possible to correctly identify the type of non-linearities in the system along with the percentage contribution of each non-linearity.

3.4.4 Numerical examples

The two methods for non-linearity characterization presented in the chapter are exemplified using numerically synthesized data for Validation structure-1, a cantilever beam with non-linearity at the free end. The details of the beam are presented in Appendix B. The study considers three cases with different non-linearities, and the details of the type of non-linearity and the non-linear parameters used in the study are presented in Table 3.2.

Table 3.2 Summary of non-linear parameters used for validation

Case	Type of non-linearity	Non-linear parameters
1	Cubic stiffness	β =5e3 Nm^{-3}
2	Friction	K_d = 50 N/m; μN = 1e-3 N
3	Cubic stiffness + friction	β =5e8 Nm^{-3} K_d = 10 N/m; μN = 3e-3 N

The synthesized non-linear response data for the beam was generated using the in-house code *FORSE* [4]. The non-linear restoring force at the non-linear DOF is extracted using the spatial method described in Chapter 4 of the thesis[5]. The extracted non-linear force for all three cases was used for visual comparison with the footprint library presented in Section 3.2. For validation of the second method, the non-linear restoring force for all three cases was numerically compared with different footprints to evaluate the SSD value for each footprint. The SSD values for all cases are summarized in Table 3.3.

Figure 3.25 shows a plot of non-linear restoring force at the non-linear DOF for case 1. The shape of the plot resembles both the cubic stiffness footprint and the clearance footprint. Figure 3.26 shows the non-linear force for Case 1 overlaid on top of the footprints of different non-linearities. From the figure, it can be seen that the extracted non-linear force curve clearly matches with the cubic stiffness non-linearity footprint. This observation is strengthened by the least SSD value for the cubic stiffness footprint shown in Table 3.3, identifying the type of non-linearity correctly.

[5] Extracting the non-linear restoring force for a MDOF system is a challenge in itself. The different methods for extraction of non-linear restoring force are presented in subsequent chapters of the thesis

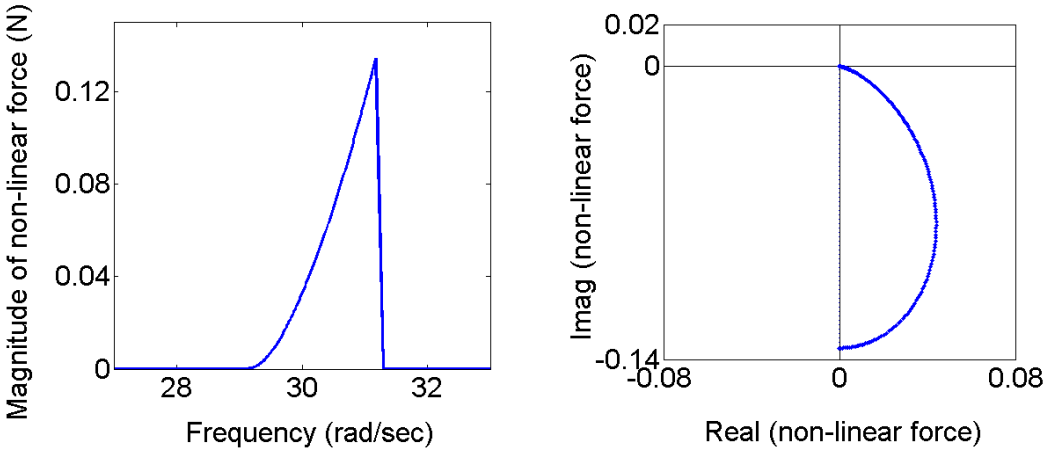

Figure 3.25 Non-linear force for case 1 (cubic stiffness)

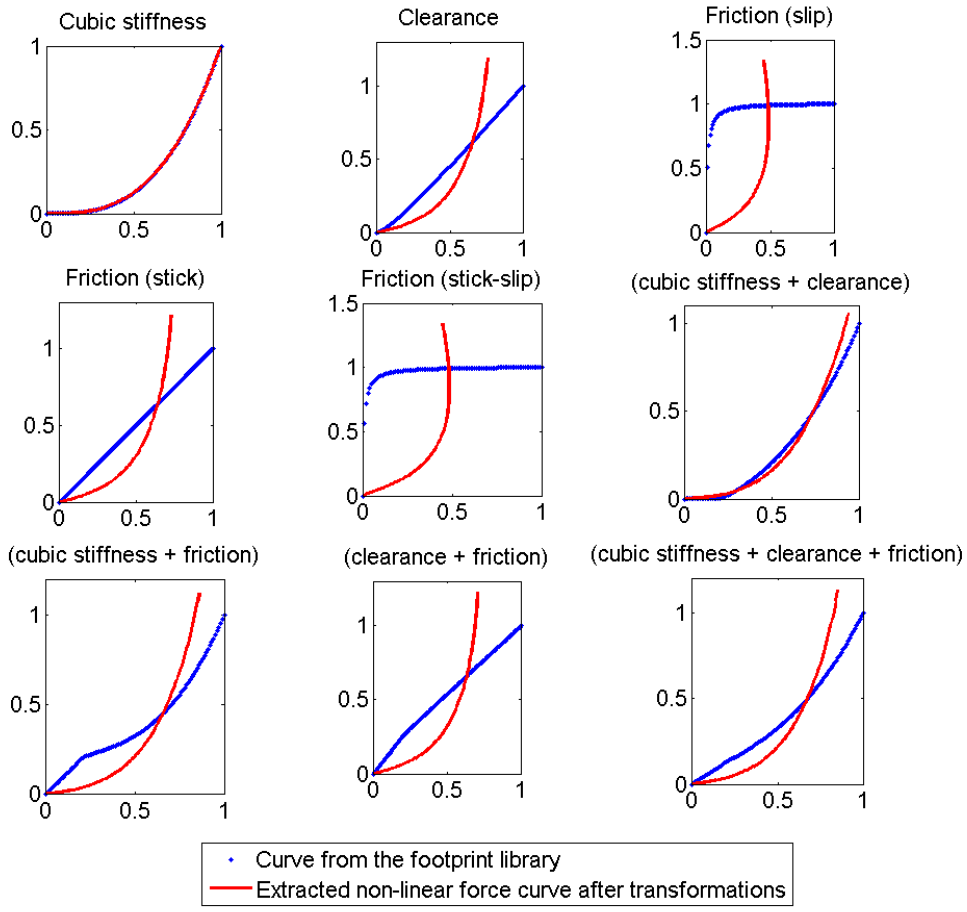

Figure 3.26 Quantitative comparison for Case 1

Figure 3.27 shows the plot of the non-linear force for case 2, with friction non-linearity. From the visual comparison of the shape of this curve with the footprints, it is difficult to reach any conclusion. When the non-linear force is compared with the footprints to find the SSD value, the slip-dominated friction non-

linearity is identified as the one with the least SSD value. Figure 3.28 shows the quantitative comparison with the footprints for Case 2.

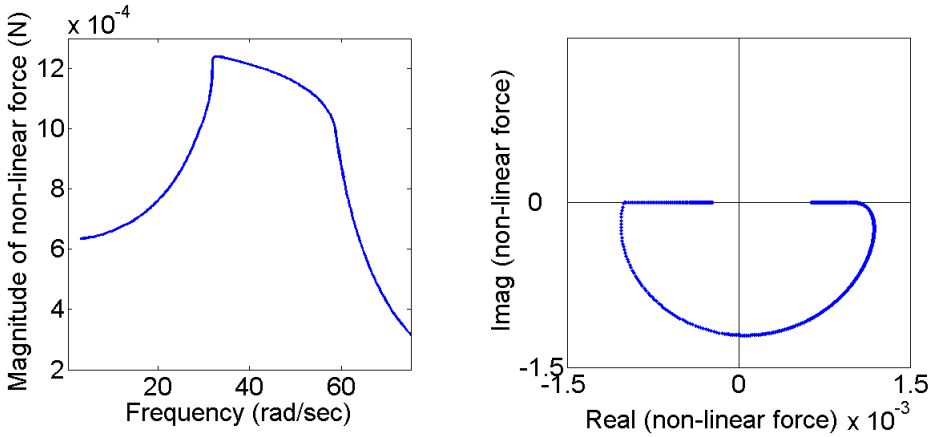

Figure 3.27 Non-linear force for Case 2 (friction)

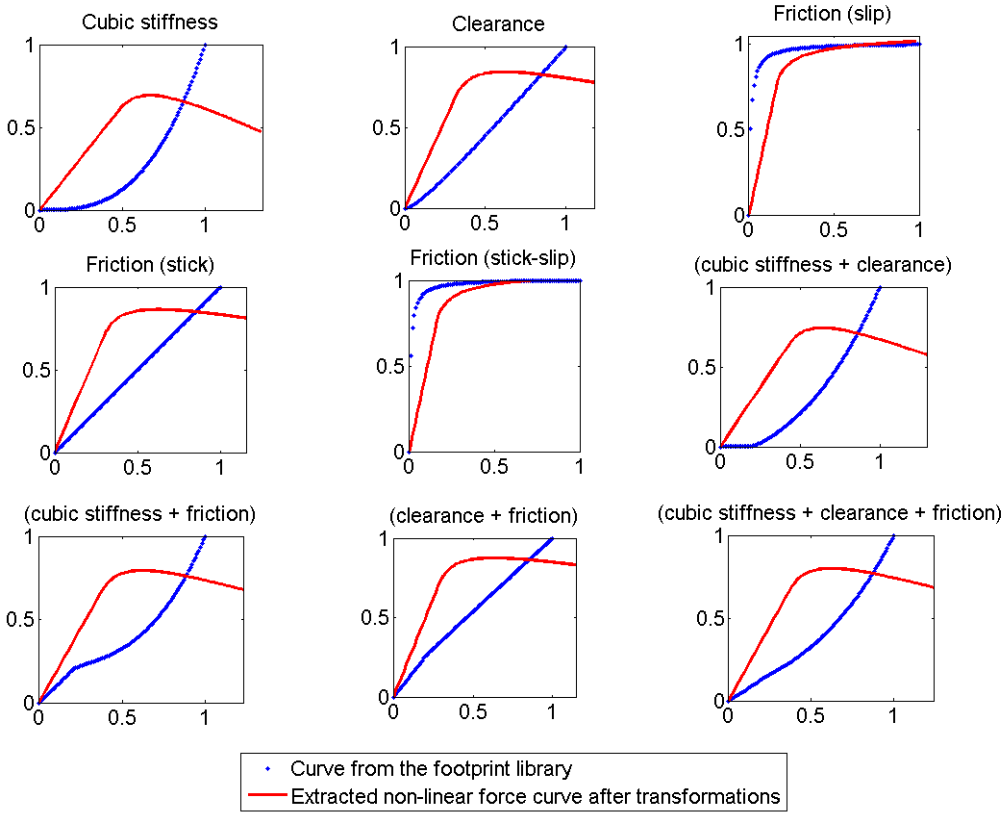

Figure 3.28 Quantitative comparison for Case 2

In Case 3, a combined cubic stiffness and friction non-linearity was used. For the system with selected non-linear parameters, the cubic stiffness non-linearity contributes 84% towards the non-linear force. In Figure 3.29, the shape of magnitude versus frequency plot resembles the cubic stiffness non-linearity footprint

but the Nyquist plot shows a different shape. The SSD value for combined cubic stiffness and clearance non-linearity is found to be the least. The SSD value for the cubic stiffness non-linearity is the next lowest. Figure 3.30 shows the result of the shape-matching algorithm for Case 3.

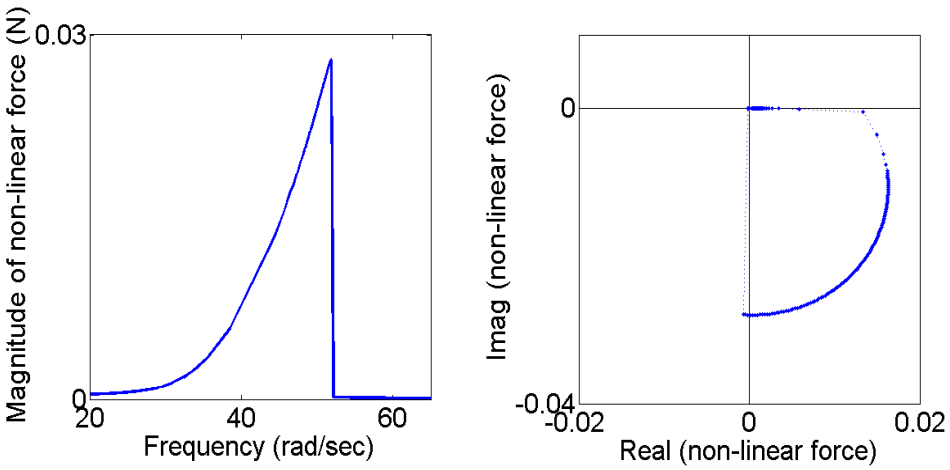

Figure 3.29 Non-linear force for Case 3 (cubic stiffness + friction)

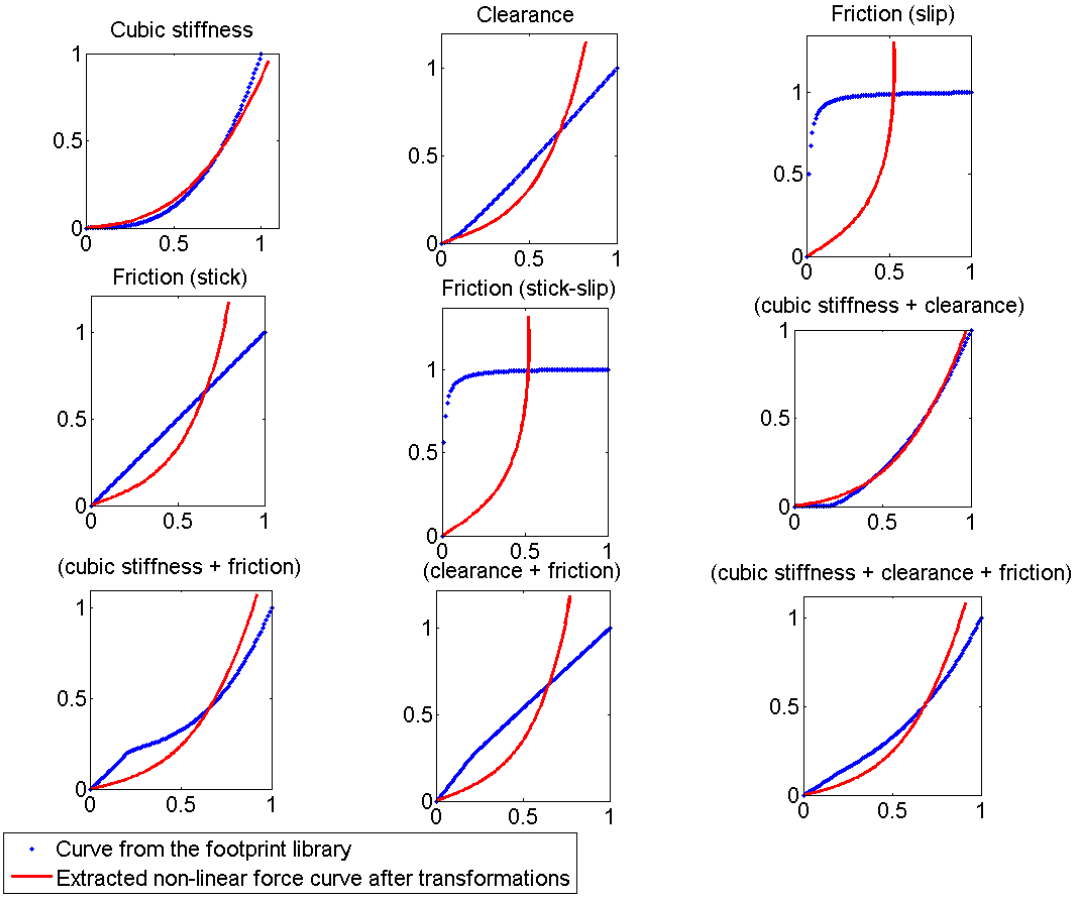

Figure 3.30 Quantitative comparison for Case 3

Table 3.3 Summary of the quantitative comparison

Footprint type	Sum of squared distance (SSD)		
	Case 1	Case 2	Case 3
Cubic stiffness	**9.8×10^{-4}**	5.59	**0.33**
Clearance	1.50	3.41	1.23
Friction (slip)	6.60	**2.06**	6.36
Friction (stick)	2.09	3.70	1.76
Friction (stick-slip)	6.67	2.15	6.42
Cubic stiffness + clearance	0.45	5.32	**0.29**
Cubic stiffness + friction	1.26	4.41	0.97
Clearance + friction	2.37	3.41	2.04
Cubic stiffness + clearance + friction	1.13	4.57	0.81

To evaluate the effect of noise on the quantitative method of non-linearity characterization, data for the same three cases was polluted with 7.5% random noise. The non-linear force was extracted for noisy measurements, and it was compared with the footprints from the library. Figure 3.30 shows the comparison of the extracted non-linear force with the footprint library for Case 3, combined cubic stiffness and friction non-linearity. Table 3.4 shows presents the detailed results for all three cases with noise. It can be observed that owing to noisy measurements, the SSD values are a bit higher than the corresponding values for clean data. Still, the correct type of non-linearity can be identified for Case 1 and 2.

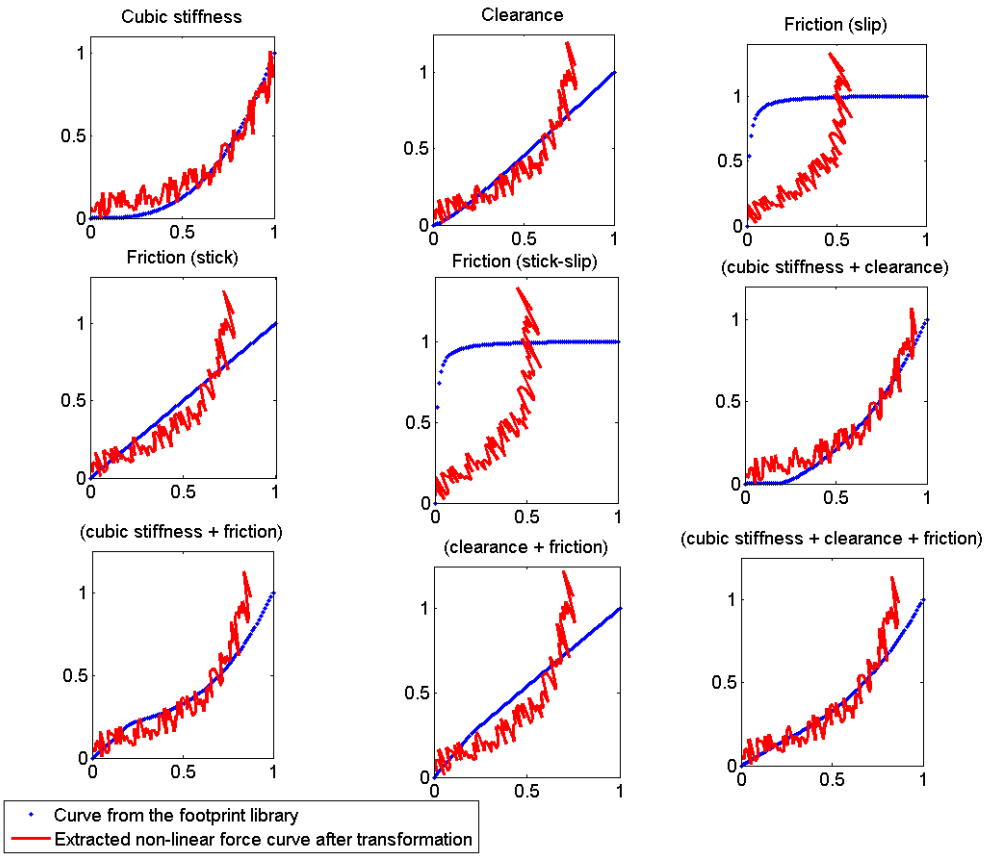

Figure 3.31 Quantitative comparison for Case 3 with 7.5% noise

Table 3.4 Summary of the quantitative comparison with noise

Footprint type	**Sum of squared distance (SSD)**		
	Case 1	Case 2	Case 3
Cubic stiffness	**0.153**	6.21	**0.84**
Clearance	1.62	3.67	1.53
Friction (slip)	5.94	**2.31**	5.81
Friction (stick)	1.89	3.77	1.75
Friction (stick-slip)	5.99	2.53	5.87
Cubic stiffness + clearance	0.45	5.71	0.87
Cubic stiffness + friction	1.13	4.44	0.94
Clearance + friction	2.12	3.15	1.96
Cubic stiffness + clearance + friction	1.02	4.63	0.96

3.5 Concluding remarks

A novel idea of collecting the non-linear restoring force curves for different non-linearities to form a 'footprint library' has been proposed in the chapter. This footprint library can be used for non-linearity characterization, which forms an important step in non-linear system identification. The shape of the non-linear restoring force curves was found to be unique to the type of non-linearity and independent of the system. The main developments of this chapter can be listed as follows:

- A library of non-linear force footprints for different non-linearities including the cubic stiffness, clearance, friction, and combination of all three has been generated using a 2-DOF benchmark system. The library consists of magnitude versus frequency plots and Nyquist plots for the non-linearities. The library can be used as a look-up chart for making a judgement on the type of non-linearity in the system.
- A shape-matching algorithm has been proposed to quantify the match between the shape of the extracted non-linear force curve and the footprints. The term SSD indicating the Euclidian distance between the two curves is used as a measure of closeness of the shape of the curves.
- The proposed methods have been tested on simulated response data for a cantilever beam with different non-linearities. The methods worked well for the individual non-linearities.
- For combined non-linearities, the shape of the non-linear force curve was observed to be dependent on the contribution of each type of non-linearity. With the current footprint library, it was found difficult to correctly identify the combined non-linearity type. An idea of including more footprints in the library with varying contribution of two or more non-linearities has been suggested as a possible solution to this problem.
- The quantitative comparison has been tested for measurement data with noise. It has been observed that the type characterization is accurate even for data with 7.5 percent random noise.

Chapter 4

Spatial method for non-linear parameter identification

This chapter presents a frequency-domain method for a parametric identification of non-linear systems. The method uses the finite element (FE) model of the underlying linear system to extract the non-linear restoring force. The magnitude of the non-linear restoring force at each DOF is used to find the location of the non-linearity. A genetic algorithm based optimization method is proposed to extract the non-linear parameters using the non-linear restoring force at the identified non-linear DOFs. The method allows successful extraction of non-linear parameter values even when the type of non-linearity is unknown. The method is illustrated on simulated data for a cantilever beam with cubic stiffness non-linearity. The robustness of the method in the presence of measurement noise is checked by artificially polluting the response data with random noise.

4.1 Introduction

Non-linear system identification is an important stage in structural analysis. Once the non-linear parameters are known as a function of displacement, velocity etc, the information can be used to predict the response at different operating conditions [4, 79]. Non-linear system identification consists of three stages, namely the detection of non-linearity, the type characterization, and the non-linear parameter extraction. Once the non-linearity is detected and characterized, the parameter extraction can be posed as an optimization problem. In most of the methods, the success of non-linear parameter extraction depends on the success of the earlier stages of non-linearity detection and characterization.

The method proposed in this chapter is based on the reverse explicit formulation proposed by Elizalde [26, 36]. The basic theme of the method is to recover the non-linear restoring force for a non-linear system by making use of the

FE model of the underlying linear system and the measured responses of the system. In the current research, a genetic algorithm (GA) based optimization method is used to identify the non-linear parameters. The use of such a method allows identifying simultaneously several non-linearities of unknown type. The method has a potential to identify large non-linear structures, which is the prime advantage. The theoretical formulation of the method is presented in the next section.

4.2 Theoretical formulation

For a multi DOF system, undergoing harmonic excitation, the equations of motion can be written as:

$$[M]\{\ddot{y}\}+[C]\{\dot{y}\}+[K]\{y\}+\{g(y)\}=\{F\}\sin(\omega t) \tag{4.1}$$

where, $[M],[C]$,and$[K]$ are mass, viscous damping, and stiffness matrices, $\{F\}$ is the amplitude of excitation force, and $\{g(y)\}$ is the non-linear restoring force as a function of displacement.

The solution to (4.1) is multi-harmonic, with significant contributions from higher order harmonics as shown in [79]. With single-harmonic limitation, assuming that the response to a harmonic force is also harmonic at the same frequency, and neglecting the higher order harmonics in the response, (4.1) can be converted into frequency domain:

$$\left(-\omega^2[M]+i\omega[C]+[K]\right)\{Y\}+\{G(Y,\omega)\}=\{F\} \tag{4.2}$$

where, $G(Y,\omega)$ is the non-linear restoring force as a function of the non-linear response and excitation frequency. The non-linear restoring force vector can be written as:

$$\{G(Y,\omega)\}=\{F\}-[Z]\{Y\} \tag{4.3}$$

where, the linear dynamic stiffness matrix, $[Z]$, can be expressed as:

$$[Z]=\left(-\omega^2[M]+i\omega[C]+[K]\right) \tag{4.4}$$

If the measured and un-measured DOFs are indicated by subscripts *m* and *u* respectively, (4.3) can be expanded as follows:

$$\begin{Bmatrix} G_m \\ G_u \end{Bmatrix} = \begin{Bmatrix} F_m \\ F_u \end{Bmatrix} - \begin{bmatrix} Z_{mm} & Z_{mu} \\ Z_{um} & Z_{uu} \end{bmatrix} \begin{Bmatrix} Y_m \\ Y_u \end{Bmatrix} \tag{4.5}$$

If it is assumed that the non-linearity is confined to the measured zone, vector G_u becomes zero, and the un-measured responses can be expressed in terms of known quantities as:

$$\{Y_u\} = [Z_{uu}]^{-1}(\{F_u\} - [Z_{um}]\{Y_m\}) \tag{4.6}$$

Substituting $\{Y_u\}$ in (4.5), $\{G_m\}$ can be expressed in terms of the measured responses as:

$$\{G_m\} = \{F_m\} - [Z_{mu}]([Z_{uu}]^{-1}(\{F_u\} - [Z_{um}]\{Y_m\})) - [Z_{mm}]\{Y_m\} \tag{4.7}$$

The non-linear restoring force vector of (4.7) can be extracted if the excitation force vector and the underlying FE model are known, and if the non-linearities are confined to the measured DOFs. This can be a serious limitation when applied to practical structures, where the measurement at non-linear DOF cannot be guaranteed. An approximated technique to overcome this limitation is presented in Section 4.2.5.

4.2.1 Non-linearity detection and characterization

The non-linear force vector for the measured DOFs is used for the detection and characterization of non-linearity. Assuming that all non-linearities are confined to the measured zone, a non-zero value in the non-linear restoring force vector detects the presence and location of non-linearity. The magnitude of the non-linear force at all measured DOFs is summed over the measured frequency range to get the accumulated force vector, $\{G_m^c\}$

$$\{G_m^c\} = \sum_{\omega=\omega_i}^{\omega_j} ABS(\{G(\omega)\}) \tag{4.8}$$

This vector is plotted for all measured DOFs to identify the location of non-linearity. A similar approach to locate the non-linear DOFs is presented in [26, 28].

Once the non-linear DOFs are identified, the shape of the non-linear restoring force at the non-linear DOFs can be compared with the footprint library presented in Chapter 3 to characterize the type of non-linearity.

4.2.2 Formulation of the optimization problem

Once the non-linear force at the non-linear DOFs is extracted, the non-linear parameters can be estimated by solving the optimization problem. This section presents the formulation of the optimization problem.

The non-linear force at the i^{th} DOF, and at a particular excitation frequency, can be written as a function of n_p non-linear parameters which are to be identified.

$$G_i = f(\overbrace{\beta, K_z, y_c, K_d, \mu N, ...}^{n_p}) \tag{4.9}$$

The above equation though formulated for cubic stiffness, clearance, and friction non-linearities at present, can be generalized to incorporate other types as well. The vibration measurements usually provide response amplitude values at a discrete set of frequency values. Let n_f be the number of frequency lines in the measurement range. As the non-linear parameters are assumed independent of frequency, one equation can be written per frequency line. Thus, there are a total of n_f equations with n_p unknowns. Generally, $n_f >> n_p$, thus a highly over determined system of equations is usually available.

In principle, all of the n_f equations can be solved by minimizing say the 2-norm of the error vector, but the response away from the resonance is generally small, the signal to noise ratio is generally low, and accuracy of modelling is less important for those frequencies. Thus, the data far away from the resonance can be ignored in most of the cases.

Thus n_s points out of total n_f available, can be chosen in the range where the non-linear force has significant magnitude. The number of points, n_s, should be higher than the number of unknown variables, n_p, and usually surpasses it significantly.

The identification problem can be posed as an optimization problem by formulating the residual at the i^{th} DOF, as:

$$R_i = (g^{cub} + g^{cle} + g^{fri})_i - G_i \tag{4.10}$$

where, G_i is the non-linear force at the i^{th} DOF obtained from (4.7), and g^{cub}, g^{cle}, and g^{fri} are the expressions based on the harmonic balance method for cubic stiffness, clearance and friction non-linearities, presented earlier in Table 3.1. This is a more general formulation considering the presence of different non-linearities at a particular DOF. This formulation potentially eliminates the need of accurate type characterization before this step.

Although, only cubic stiffness, clearance and friction non-linearities are considered in the formulation explicitly, the formulation can be extended to incorporate any other type of non-linearity. The total residual to be minimized for n_s selected points can be written as:

$$R = \frac{\left[\sum_{j=1}^{n_s} (R_i)_j^2\right]^{1/2}}{n_s} \tag{4.11}$$

The residual given in (4.11) can be minimized to find the optimized values for n_p non-linear parameters.

4.2.3 Search for the non-linear parameters using a genetic algorithm

The parameter identification problem for non-linear systems has been attempted by several researchers using evolutionary techniques. To point some of the work, Rodriguez et al [112] used Genetic programming to identify non-linear systems related to control theory. Hysteretic systems are identified using evolutionary optimization methods as found in [113] and [114].

In the current research, the optimization problem is solved by using a genetic algorithm. For the particular genetic algorithm used in the thesis, it is more convenient to express the problem as a maximization problem. Thus, the residual R can be converted into function R_m, to be maximized, as:

$$R_m = \frac{C}{C + R} \tag{4.12}$$

where, C is a real positive constant. This formulation makes R_m sensitive to the value of C. Thus, the value of C should be selected carefully depending on the case. In the current work, the value of C is taken as 100. If the case of R tending to 0 can be handled effectively, the simple formulation, $R_m = 1/R$, can also be used. R_m can be used as an objective function to be maximised via the genetic algorithm to obtain the optimized values of all non-linear parameters. The genetic algorithm from [115, 116] is used with some minor modifications. The variables in the optimization problem are converted into their binary equivalent for better manipulation.

In genetic algorithm terminology, a set of values of parameters to be optimised is called a *string*. A group of such sets spanning the feasible domain is called a *population*. The value of the objective function for a string is termed as the

fitness of the string. In the current formulation, the maximum fitness can reach unity. It can also be expressed as percentage value. The string with the highest objective function is called the *fittest string*. The three basic operators, namely: reproduction, cross-over, and mutation are used sequentially on the population. The reproduction operator aims at improving overall fitness of the population. The cross-over operator ensures a global search, whereas the mutation operator does a fine local search. These three operators constitute a *generation*. After the implementation of these three operators, an improved population emerges. The fitness of population and the number of generations are used as convergence criteria. In the current algorithm, the value of R_m tends to unity as the solution converges.

Initially, the upper and lower limits of all non-linear parameters are chosen based on the engineering judgement. After a predefined number of generations, called a *civilization*, the range of the non-linear parameters is refined by analysing the values taken by the fittest string in the population. With the new range and increased accuracy for these variables, another civilization is completed. This process is continued until the convergence criteria are satisfied. Figure 4.1 shows the flowchart showing one civilization of the GA used.

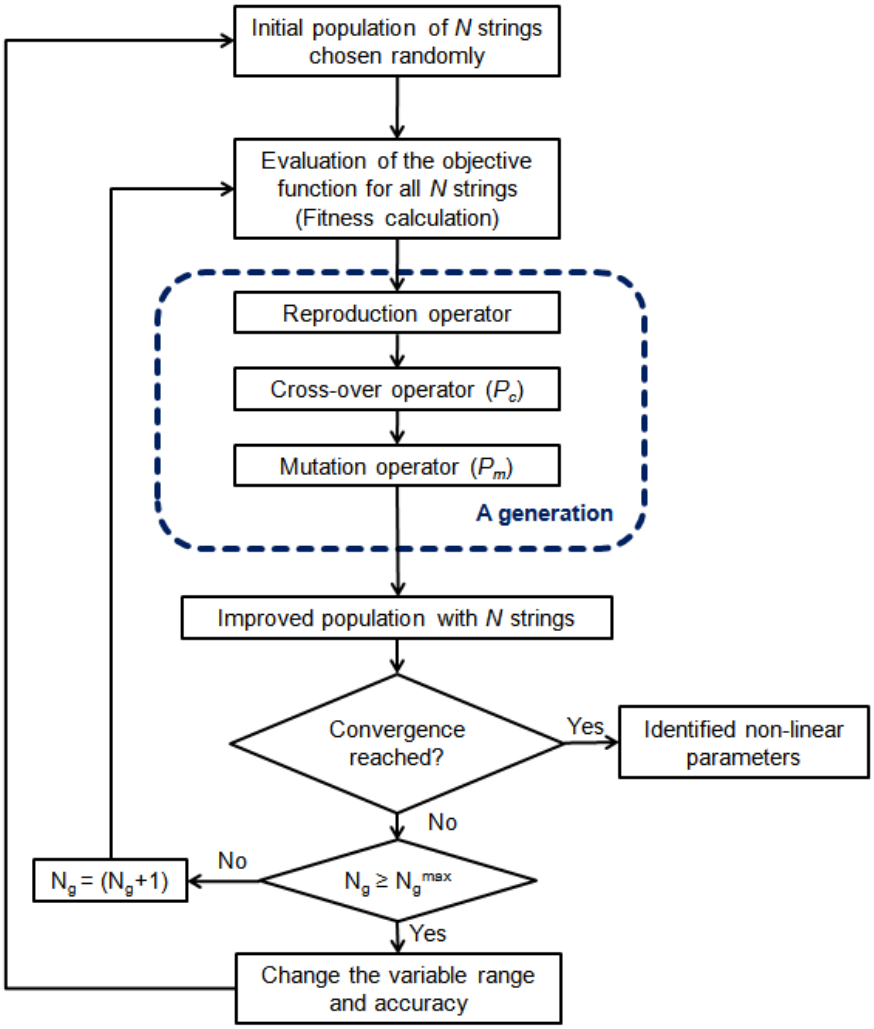

Figure 4.1 Flowchart of the genetic algorithm optimization

Since all possible non-linearities can be included in the formation[6], the global optimum solution would correspond to the accurate parameters of the non-linearities which are actually present in the system. For example, when only one type of non-linearity is present in the system, the converged solution will yield accurate parameter values for the correct type of non-linearity, and zero values for parameters corresponding to the other non-linearities. The genetic algorithm performs better at finding the global optimum, thus it is suitable for cases when the type of non-linearity is not known a priori.

4.2.4 Use of binary multipliers to improve the efficiency

When the type of non-linearity is known with certainty, or can be guessed with an associated probability, the method can be improved by taking into account this

[6] In this case, cubic stiffness, clearance and friction non-linearities are considered in the formation

information. This is achieved by introducing *binary multipliers*. In this approach, weighted residuals are formed for each non-linear force contribution. The residual non-linear force is written by modifying (4.10) as:

$$R_i = (a_1 g^{cub} + a_2 g^{cle} + a_3 g^{fri})_i - G_i \tag{4.13}$$

where all possible non-linear forces, g^{cub}, g^{cle} and g^{fri} are multiplied by weighing constants a_1, a_2, and a_3. If the type of non-linearity is successfully identified prior to this stage, then the constant corresponding to the identified type takes the value 1 and the other constants take the value 0 for the complete optimization.

If the type of non-linearity can be guessed with an associated probability, then during each generation of genetic algorithm, these constants take a value either 0 or 1, which is selected probabilistically. The probability of such value selection is provided by the user. If the probability of, say clearance non-linearity (g^{cle}) is the highest, then a_2 takes the value 1 more often than a_1 and a_3. Such a technique creates more instances in the population which are solved for the most probable non-linearity; ensuring a faster convergence. The rest of the procedure remains same with (4.12) giving the total residual to be maximised.

4.2.5 Non-linear parameter identification without full measurement set at non-linear DOFs

Most of the non-linear identification methods in the literature, including the methods proposed in [26, 37, 38], require the measurement at all non-linear DOFs. It is sometimes difficult to measure at all non-linear DOFs due to their inaccessible locations. A slight modification in the equations presented in Section 4.2, along with the use of spatial reduction methods, enables the extraction of the non-linear restoring force at the non-linear DOFs when measurements are not taken at these DOFs.

If it is ensured that the non-linear DOFs are restricted to the un-measured zone, the vector $\{G_m\}$ becomes zero, and using (4.5), the un-measured response vector can be represented in terms of known quantities as:

$$\{Y_u\} = [Z_{mu}]^{+} (\{F_m\} - [Z_{mm}]\{Y_m\}) \tag{4.14}$$

Equation (4.14) involves the inversion of a rectangular matrix, which puts the mathematical condition of $m \geq u$, to be satisfied. Generally, the number of un-measured DOFs is much higher than the number of measured DOFs ($u >> m$).

Thus, the condition required for the solution of (4.14) is seldom satisfied in practical cases.

The condition can be satisfied artificially, by reducing the system to N_r DOFs, such that $m \geq N_r/2$, while retaining all non-linear DOFs during the reduction. In the current research, the improved reduced system (IRS) method of [93] is used for the system reduction. This method is an extension of the Guyan reduction technique [91], with inclusion of an extra term to incorporate the inertial effects. The use of static reduction method results in system matrices which are independent of the frequency, thus saving a huge computational effort.

Once the reduced model for the system is achieved, (4.14) can be solved by calculating the pseudo inverse of $[Z_{mu}]$. The non-linear force vector, G_u, can be extracted by substituting (4.14) in (4.7):

$$\{G_u\} = -\left([Z_{um}]\{Y_m\} + [Z_{uu}]\left([Z_{mu}]^{+}\left(\{F_m\} - [Z_{mm}]\{Y_m\}\right)\right)\right) \quad (4.15)$$

Equation (4.15) gives the non-linear restoring force vector containing non-linear DOFs. The above technique can be used to extract the non-linear force at the non-linear DOFs when the location of the non-linearity is known, but no measurements could be taken at those locations.

The non-linear restoring force at the non-linear DOFs can be used to extract the non-linear parameters as explained in Sections 4.2.2 and 4.2.3.

4.3 Numerical examples

The proposed method was tested on 'Validation structure-1', a cantilever beam with cubic stiffness non-linearity at the free end. The details of the structure are shown in Appendix B. Numerically-synthesized data were used to validate the proposed method. A cubic stiffness non-linearity with non-linear coefficient, β = 5×10^6 Nm^{-3} was used for the validation. The response was predicted using the in-house code *FORSE* [4]. Figure 4.2 shows the comparison of linear and non-linear responses of the beam at the non-linear DOF. It is observed that the response is multi-valued in the frequency range of 32-55 rad/sec. The truncated response, corresponding to stable branch 1, as explained in Chapter 3 was used for the identification.

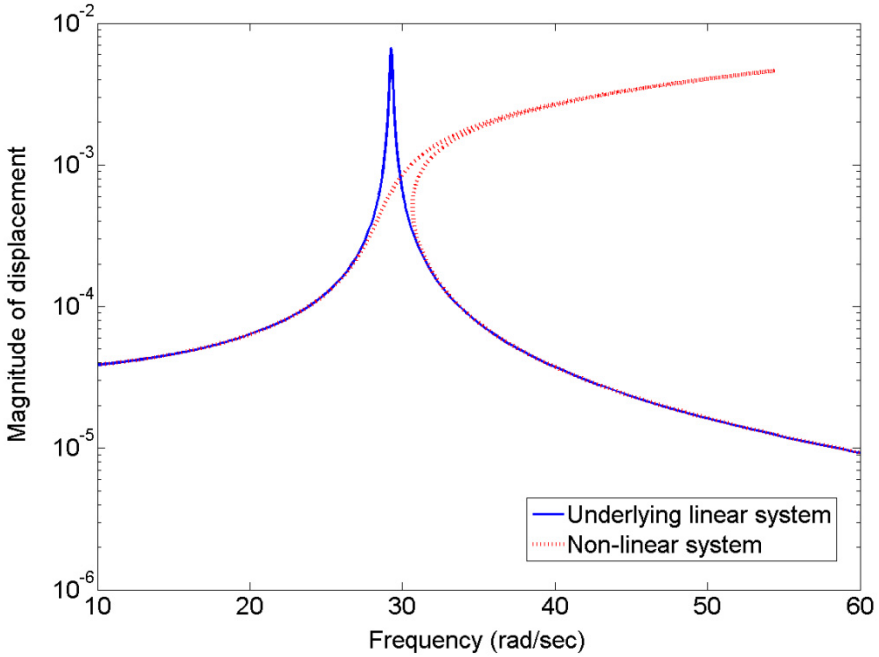

Figure 4.2 Comparison of linear and non-linear responses

4.3.1 Effect of the number of measurements on parameter estimation

For practical MDOF non-linear structures, it is not feasible to take measurements at all DOFs. Equation (4.7) gives the non-linear force vector at measured DOFs using an exact reduction of system equations. Thus, in principle, it is possible to extract the non-linear force vector using (4.7) if: (a) measurements are available at all non-linear DOFs, and (b) measurements are available at all excitation DOFs.

This section studies the effect of the number of measurements on the accuracy of parameter estimation. Three cases were considered for the analysis. In the first case (Case A), all DOFs of the FE model were assumed to be measured. In the second case (Case B), only the translational DOFs along Y-axis were assumed to be measured. In the last case (Case C), only the non-linear DOF and the excitation DOF were measured. This case satisfies only the minimum requirement for the use of (4.7). The summary of measured and un-measured DOFs, excitation force, and non-linear DOFs for all three cases is given in Table 4.1.

Table 4.1 Description of measured DOFs

Case	Measured DOFs	Un-measured DOFs	Excitation DOF	Non-linear DOF
A	{1, 2, 3, ...,20}	Nil		
B	{1, 3, 5, 7,....,19}	{2, 4, 6, 8, …., 20}	19	19
C	{19}	{1, 2, 3, 4,…,18 and 20}		

For all three cases, the non-linear force was extracted at all measured DOFs using (4.7). The accumulated non-linear force for the measured DOFs was used to identify the location of non-linearity. Figure 4.3 shows the plot of the accumulated non-linear force at measured DOFs for Case A. It can be seen that the accumulated non-linear force at DOF#19 is maximum. The non-linear force at other DOFs is close to zero. Thus, the location of non-linearity at DOF#19 is correctly identified.

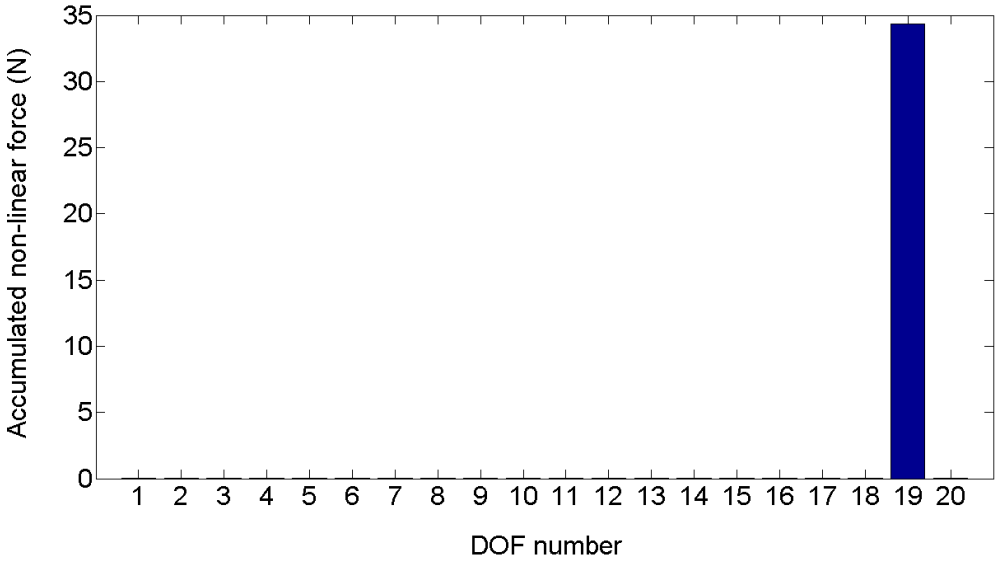

Figure 4.3 Identification of non-linearity location (Case A)

The non-linear force at the identified non-linear DOF, plotted against the frequency and as a Nyquist plot, was used for non-linearity characterization. Figure 4.4 shows the plot of non-linear force at DOF#19 for Case A. If the shape of the non-linear force is visually compared with the footprint library presented in Chapter 3, the cubic stiffness non-linearity can be deduced. This was confirmed when the non-linear force was numerically compared with the footprints to find the values of SSDs for different non-linearities. The SSD, when compared with cubic stiffness non-linearity, was found to have the least value (SSD=0.001), thus identifying the type of non-linearity.

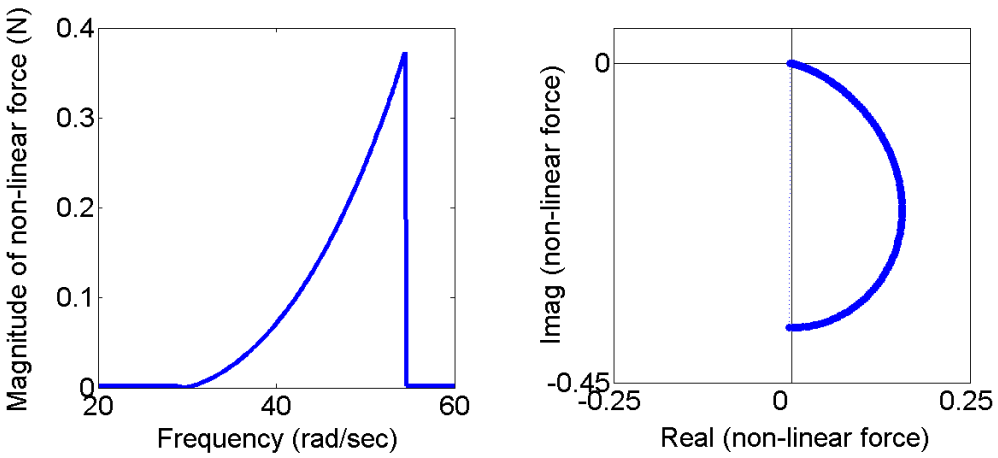

Figure 4.4 Non-linearity characterization (Case A)

In the next stage of non-linear parameter identification, the genetic algorithm (GA) presented earlier was used to extract the non-linear parameter values for all three cases. The parameters used in the GA are summarized in Table 4.2. In this case, since the type of non-linearity was correctly identified, the binary multipliers were used with a_1 = 1, and a_2 = a_3 = 0. The optimization problem was solved considering the presence of cubic stiffness non-linearity only in the objective function formulation.

Table 4.2 Parameters used in the GA

Parameter	Value
Probability of crossover operator (P_c)	0.8
Probability of mutation operator (P_m)	0.05
Population size (N)	700
Number of generations in a civilization	1000
Initial number of bits per variable	12

To keep a uniform basis for comparison, the initial range of the non-linear coefficient was kept the same (0-1×10^{10} Nm^{-3}) for all three cases. The identified parameters after the end of the first civilization are presented in Table 4.3.

Table 4.3 Summary of results for parameter estimation

Case	$(DOFs)_m$: $(DOFs)_u$	Identified β value ($N\text{-}m^{-3}$)	Fitness value (%)	Error in estimation (%)
A	20:0	4.9751×10^6	95.07	0.49
B	10:10	4.9735×10^6	94.93	0.53
C	1:19	4.9747×10^6	94.62	0.51

It can be seen that the error in the estimation of the non-linear parameter is almost constant at around 0.5%, which is within acceptable limits. Thus, it can be concluded that the estimation of non-linear parameters is not a function of the number of measurements. This is owing to the exact reduction of the system equations achieved in (4.7).

4.3.2 Effect of measurement noise on parameter estimation

This section checks the robustness of the method in presence of measurement noise. The simulated response data were polluted with white noise of varying strength. The response vector polluted with white noise was obtained using the following expression:

$$\{y(\omega)\}_p = \{y(\omega)\}_{up} + (rc/100) \times \{y_{\max}\}_{up} \tag{4.16}$$

where, $0 < \omega < \omega_{max}$

r is a random parameter ($-1 \le r \le 1$)

c is the maximum percentage of the noise to be added

$\{y(\omega)\}_p$ is the response vector polluted with noise

$\{y(\omega)\}_{up}$ is the un-polluted response vector

$\{y_{\max}\}_{up}$ is the vector containing peak response values

The identification was carried out with increasing level of noise, with the value of c ranging from 1.5 to 5. Figure 4.5 shows the distorted response at the non-linear DOF with 5% added noise. For Case A, the non-linear parameters could not be extracted because of the presence of unacceptable level of noise in the system. For the other two cases (Cases B and C) the non-linear parameters were successfully extracted. Table 4.4 summarizes the results of parameter estimation for the two cases in the presence of varying noise level.

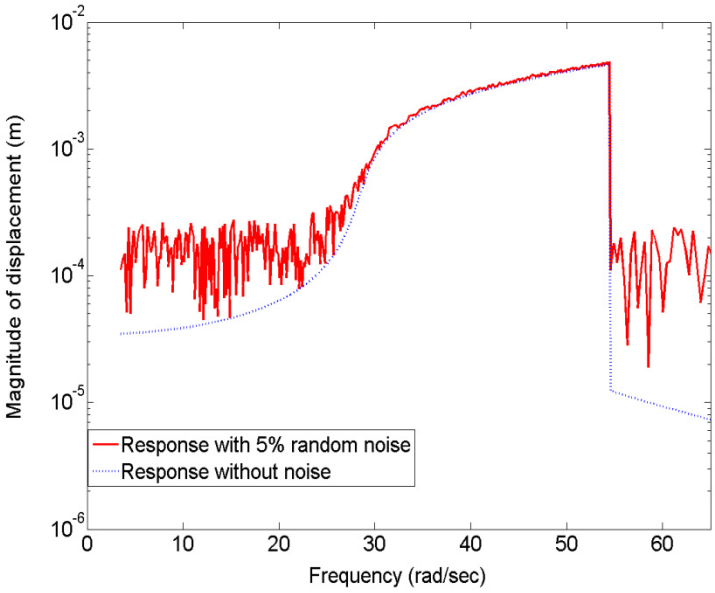

Figure 4.5 Displacement response with 5% random noise

Table 4.4 Results of parameter estimation in presence of noise

Case	Noise level	Identified β value ($N\text{-}m^{-3}$)	Error in estimation (%)	Fitness value (%)
B	*c = 1.5*	5.353×10^{6}	7.1	18.2
	c = 3	5.823×10^{6}	16.5	9.5
	c = 5	3.569×10^{6}	28.6	6.1
C	*c = 1.5*	4.888×10^{6}	2.2	92.7
	c = 3	4.805×10^{6}	3.9	91.1
	c = 5	4.725×10^{6}	5.5	85.9

It is seen for both cases that the error in parameter estimation increases with the increase in the noise level. The maximum error in parameter estimation is around 29% for Case B with 5% random noise. It is an interesting observation that the error is consistently higher in Case B, the case in which a higher number of measurements was available. This might look counter intuitive, but it is related to the fact that a highly over-deterministic system of equations is being solved in the optimization process, and each additional measurement is contributing towards additional noise in the system.

For Case B, with 1.5% noise, the accuracy of parameter estimation is better; but the fitness value of the fittest string obtained by the GA is quite low at 18.2%. This suggests that that there is a scatter in data points of the extracted non-linear

force. Figure 4.6 shows the comparison of the extracted and the regenerated non-linear force curve for this case.

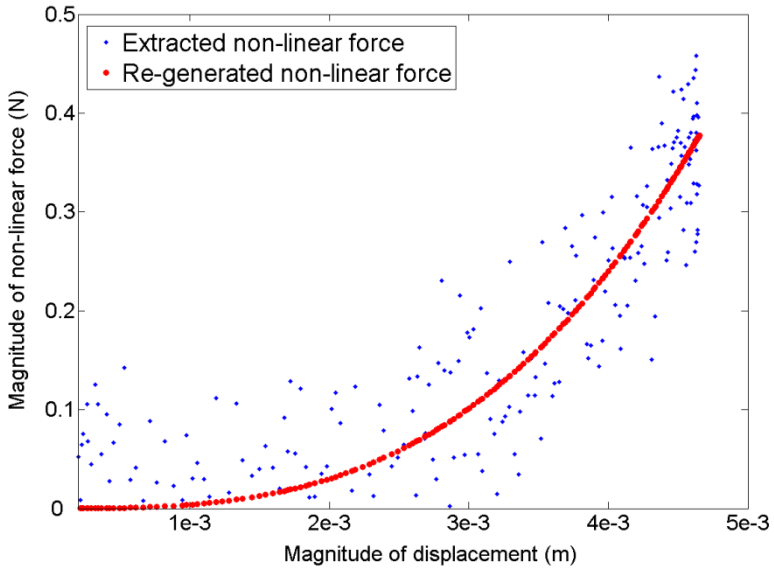

Figure 4.6 Comparison of the extracted and regenerated non-linear force

From the study of the effect of measurement noise on the parameter estimation, it is observed that the method is robust in the presence of measurement noise for Case B and Case C. The effect of noise becomes severe as the number of measurements in the analysis increases.

4.3.3 Effect of binary multipliers on computational efficiency

Binary multipliers are proposed to enhance the computational efficiency of the GA when the type of non-linearity can be guessed with some associative probability. This section studies the effect the use of binary multipliers in the GA.

A new set of three cases was considered for the study. In the first case, the binary multipliers were not used. In the second case, the binary multipliers were used with a high value of probability assigned to the correct type of non-linearity and a relatively low value of probability is assigned to the other types. In the third case, the binary multipliers were used with an equal value of probability assigned to all non-linearity types. This case corresponds to a situation when the type characterization fails, and the non-linearity type is not known in advance. The results for the three cases are compared with the benchmark case where only cubic stiffness non-linearity is included in the formulation of optimization problem.

The simulated data for the beam without any addition of noise was used for the analysis. The GA code was terminated after 5000 generations and the results were recorded. Table 4.5 summarizes the results for the exercise. In the table, P_{cub},

P_{cle}, and P_{fri} denote the probability of the presence of cubic stiffness, clearance and friction non-linearity. The values correlate to the probabilities with which the binary multipliers, a_1, a_2, and a_3 take the value of 1 in the simulation. G_{con} denotes the number of generations at which the fittest string was found. It is observed that the error in parameter estimation is the least when the binary multipliers are used with a high probability assigned to the correct non-linearity type. The error in the other two cases is comparable, but the use of the binary multipliers is found to speed-up the convergence.

Table 4.5 Performance of binary multipliers

Case	(P_{cub}, P_{cle}, P_{fri})	Identified β value (N-m^{-3})	Error (%)	G_{con}
Benchmark	-	4.9812×10^{6}	0.38	45
1	(1,1,1)	4.8818×10^{6}	2.36	2932
2	(0.9,0.2,0.2)	4.9781×10^{6}	0.44	96
3	(0.5,0.5,0.5)	4.8930×10^{6}	2.14	293

Figure 4.7 shows the plot of the fitness of the fittest string in the population at each generation for the first 500 generations. It is seen that in the absence of binary multipliers, the fitness of the fittest string in the population is lower than the fitness when the binary multipliers are used. The fluctuation in the fitness value is also more when the binary multipliers are not used.

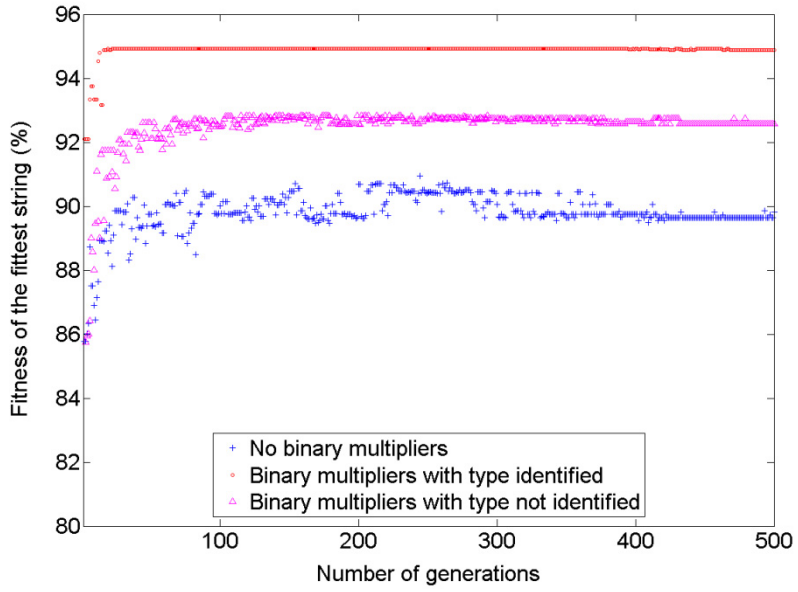

Figure 4.7 Performance of binary multipliers: fittest string fitness

Figure 4.8 shows the plot of the average fitness of the population for each generation. It is observed that the average fitness is consistently higher in the case when the binary multipliers are used with the correct type of non-linearity. The average fitness of the population is the least when binary multipliers are used with equal probability.

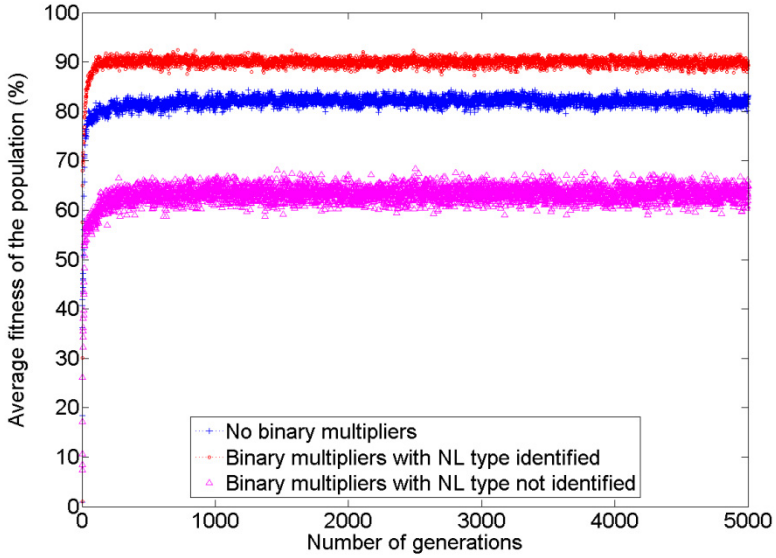

Figure 4.8 Performance of binary multipliers: Average fitness

4.3.4 Effect of the error in the FE model on parameter estimation

It is very difficult to obtain an accurate finite element model for practical structures, even in case of a linear structure. After correlating the model with the experimental data and updating it, the error in the FE model may be reduced. For a complex mechanical structure like the MACE structure, an error of around 5-7% in the natural frequencies of the first few modes is considered acceptable after the model updating [63]. The damping values inputted into the FE model are extracted using modal testing. This is another source of error in the underlying FE model. It is necessary to evaluate the sensitivity of the estimated non-linear parameters to the errors in the underlying FE model. This section studies the effect of the errors in the underlying FE model on the parameter estimation.

The physical properties of the beam were altered by a small amount so that the change is reflected in the natural frequencies of the beam. The damping ratio for the first mode was altered to evaluate the effect of the error in damping estimation. The non-linear identification was carried out with the erroneous FE model of the beam to extract the non-linear parameters. Table 4.6 shows a summary of the results. As the identification was carried out with the data covering only the first

mode of the beam, the deviation in the first natural frequency of the beam is recorded in the table. In the table, ω_{n1} denotes the first natural frequency and η_1 denotes the damping ratio for the first mode.

Table 4.6 Effects of the erroneous FE model

Error in the physical properties of the FE model			**Error in the damping estimate**		
Deviation in ω_{n1} (%)	Identified β (Nm^{-3})	Error (%)	Error in η_1 estimation (%)	Identified β (Nm^{-3})	Error (%)
-5	4.41×10^{6}	11.8	-10	4.98	0.4
-7	4.19×10^{6}	16.2	20	4.98	0.4
-10	3.87×10^{6}	22.6	50	5.07	1.4

It is seen that the effect of the error in damping estimation is negligible. Even with 50% error in the estimation of the damping ratio for the first mode, the error in the identified non-linear parameter is less than 2%. The effect of the deviation in natural frequencies on parameter estimation is seen to be significant. Figure 4.9 shows the plot of the accumulated non-linear force for all DOFs. It is observed that, with an increase in the error in the underlying FE model, the non-linear force contribution at the linear DOFs is increasing.

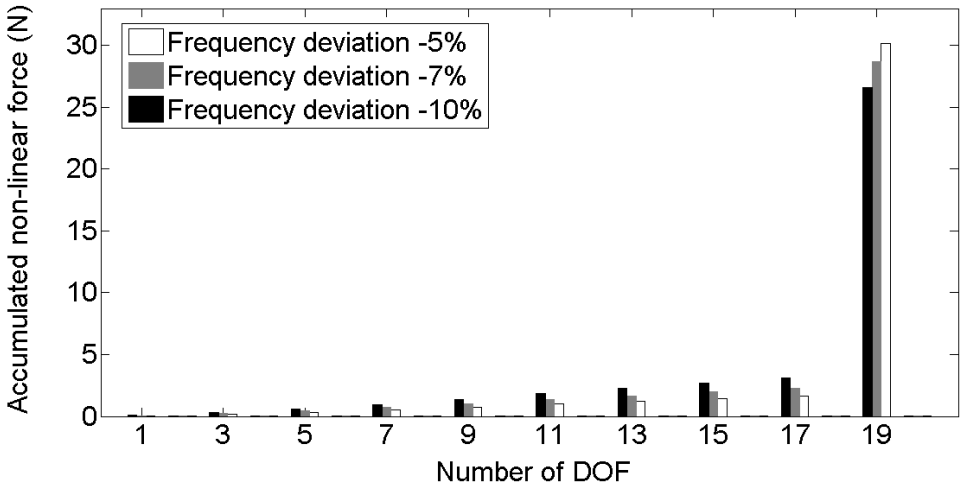

Figure 4.9 Accumulated non-linear force plot

For an erroneous FE model with 5-7% deviation in the first natural frequency value, which may be acceptable in some cases, the error in parameter estimation is more than 15%. Thus, it is necessary to obtain an accurate FE model of the structure before proceeding to the stage of non-linear parameter estimation.

4.3.5 Non-linear parameter identification in absence of measurements at non-linear DOFs

This section presents a numerical validation of the technique presented in Section 4.2.5 for non-linear identification in absence of the measurement at the non-linear DOFs. The details of the measured and un-measured DOFs are given in Table 4.7.

Table 4.7 Case description for non-linear parameter identification in absence of the measurement at non-linear DOFs

Measured region: $(DOFs)_m$	{3, 7, 9, 11, 13, 17}
Un-measured region: $(DOFs)_u$	{1, 5, 15, 19, and 2, 4, 6, ..18, 20}
Excitation DOF	{19}
Non-linear DOF	{19}

From the table, it is observed that the non-linear DOF, DOF#19, is in the un-measured region. The number of measured DOFs is, m = 6, and the number of un-measured DOFs is, u = 14. Since the number of measured DOFs is less than the number of un-measured DOFs, system reduction needs to be performed to satisfy the constraint, $m \geq u$.

The IRS technique was applied to perform a static reduction of system matrices removing all rotation DOFs. The non-linear DOFs, along with the other translational DOFs were retained during the reduction. For the reduced system, N_r = 10, and the condition, $m \geq N_r/2$ is satisfied. The non-linear force was extracted at the un-measured DOFs. Figure 4.10 shows a plot of non-linear force against frequency and the accumulated non-linear force at the un-measured DOFs.

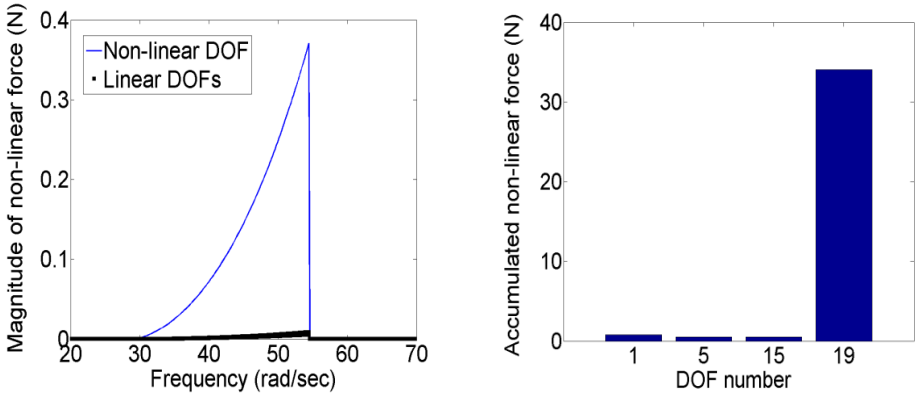

Figure 4.10 Non-linear force at un-measured DOFs

From the plot, it is observed that the non-linear force at the non-linear DOF is significantly higher in magnitude than that at the other DOFs. The non-linear force at

the non-linear DOF is used to extract the non-linear coefficient, β. The value of β is identified with less than 1% error ($\beta = 4.96\times10^{6}$ N-m^{-3}). Thus, the technique explained in Section 4.2.5 for the identification of non-linear parameters in the absence of the measurement at the non-linear DOF works well if the non-linearity location is correctly identified and retained as master coordinate during the process of model reduction.

4.4 Concluding remarks

A method for non-linearity detection and non-linear parameter identification has been proposed in the chapter. The method uses the FE model of the underlying linear system to extract the non-linear restoring force at non-linear DOFs. A genetic algorithm based optimization procedure is used to extract the non-linear parameters. The concept of binary multipliers is introduced to enhance the computational efficiency of the method. The method is validated on numerically simulated data for a cantilever beam. The proposed method has the potential to be used for practical engineering structures with localized non-linearities. The main developments of the chapter can be listed as follows:

- The proposed method recovers the non-linear restoring force. The accumulated value of the non-linear force at each DOF is used to locate the non-linearity. It has been seen that the magnitude of the non-linear force at the non-linear DOF is significantly higher than that at the linear DOFs.
- The variation of the non-linear force can be used to identify the type of non-linearity. It has been found that even if the non-linearity type is not known, the genetic algorithm based optimization accurately extracts the parameter corresponding to the correct non-linearity type.
- The concept of binary multipliers has been found to be effective in increasing the computational efficiency of the method if the type of non-linearity can be guessed with an associative probability.
- The performance of the method has been found satisfactory in the presence of measurement noise. It has been observed that, in the presence of noise, the parameter estimation is more accurate when fewer measurements are used.
- The effect of errors in the FE model on parameter estimation is studied. It has been seen that errors in the mass and stiffness matrices of the FE model has a significant effect on the accuracy of parameter estimation.

- A technique, which uses model reduction, is proposed to identify the non-linear parameters when the response at non-linear DOFs is not measured. The technique works accurately on the system when non-linear DOFs are retained during the model reduction.

Chapter 5

Non-linear identification using modal models and response models

This chapter presents two methods for non-linear parameter identification, with the distinctive feature that the methods do not use the FE model of the underlying linear system. The first method, called improved hybrid modal technique (I-HMT), uses a hybrid spatial-modal formulation. The non-linearities are described in spatial coordinates whereas the underlying linear system is represented using a *modal model*. The non-linear modal vector (NMV), containing the information about the non-linear restoring force, is extracted for the modes in the measured frequency range. Later, the NMV is used to extract non-linear parameters via a genetic algorithm optimization. The second method, called the FRF-based identification method, uses the *response model* of the underlying linear system to extract the non-linear restoring force vector. The response model is constructed using FRF measurements captured at low excitation amplitude. Once the non-linear restoring force is extracted, the non-linear parameters are identified using the genetic algorithm optimization of Chapter 4. The methods are illustrated with simulated response data for a cantilever plate with different localized non-linearities.

5.1 Introduction

The method presented in Chapter 4 for non-linear system identification requires an accurate FE model of the underlying linear system. The high sensitivity of the method to errors in the underlying FE model is seen as the major limitation when applied to practical structures. Moreover, during the product design stage, a full FE model of the product is seldom available. For complex structures like a gas turbine assembly, obtaining an accurate FE model even at later stages of design is a tough

task. Thus, there is a need for a method which can identify non-linear parameters without an FE model.

For a linear system, vibration measurement data can be arranged into an FRF matrix to constitute the *response model* of the system. This model can be used to predict the response of the system at different excitation levels. An even more compact description of the system can be found out via modal analysis [6, 7]. In modal analysis, the system is described using its dynamic properties viz. the natural frequencies, mode shapes and damping ratios. The mathematical model so obtained is called the *modal model* of the system.

For many non-linear systems (except friction and backlash), the system's behaviour is close to linear at a very low excitation force. If modal testing is carried out at such a low excitation force, the FRF matrix thus obtained would represent the FRF matrix of the underlying linear system. Similarly, the modal model obtained from the FRF matrix would represent the modal model of the underlying linear system. If these alternative models are used along with non-linear measurements for identifying the non-linear parameters, the approach presents two distinct advantages: (i) the need for an FE model is completely eliminated; (ii) the modal model and the response model are much more compact than the equivalent FE model, thus reducing the computational burden.

The following sections describe two identification methods based on the use of modal and response models of the underlying linear system respectively.

5.2 Improved hybrid modal technique (I-HMT)

Elizalde [26] proposed a method called hybrid modal technique (HMT), which describes the underlying linear system in modal domain, while keeping the non-linearities in spatial domain. The so-called non-linear modal vector is extracted as a result of the method. This vector contains the information about the non-linear parameters in an implicit form. In I-HMT, developed here, the non-linear modal vector is decoupled using genetic algorithm optimization to extract the non-linear parameters explicitly.

5.2.1 Theoretical formulation

This section presents the theoretical formulation of the improved hybrid modal technique (I-HMT). The detailed description of the hybrid modal technique (HMT), on which the method is based, is presented by Elizalde in [26]. The formulation presented in this chapter uses the same basic idea as the HMT, but the derivation

of the equations is novel and more concise. The extension of the HMT to decouple the non-linear modal vector using a GA optimization is the original contribution of the author.

For a harmonically-excited MDOF non-linear system with proportional structural damping, the system of equations can be written as:

$$[M]\{\ddot{y}\}+([K]+i[D])\{y\}+\{g(y,\dot{y})\}=\{F\}\sin(\omega t) \tag{5.1}$$

where, $[M],[K]$ and $[D]$ represent the mass, stiffness and damping matrices, $\{F\}$ is the excitation force vector, $\{y\}$ is the displacement vector, and $\{g\}$ is the non-linear restoring force vector. The proportional damping matrix can be written as:

$$[D]=\eta[K] \tag{5.2}$$

The above equation, though not used in the subsequent derivation, is used while generating simulated data. With the single harmonic assumption, the equation can be transformed into the frequency domain:

$$\left(-\omega^2[M]+[K]+i[D]\right)\{Y\}+\{G(\omega,Y)\}=\{F\} \tag{5.3}$$

Let $[\Phi]$ be the eigenvector matrix and $[\lambda^2]$ be a diagonal matrix containing the complex eigenvalues of the underlying linear system. Pre-multiplying (5.3) by $[\Phi]^T$ on both sides and inserting $[\Phi][\Phi]^{-1}$ on the left hand side we get

$$[\Phi]^T\left(-\omega^2[M]+[K]+i[D]\right)\left([\Phi][\Phi]^{-1}\right)\{Y\}=[\Phi]^T\left(\{F\}-\{G\}\right) \tag{5.4}$$

Recalling the orthogonal properties of a system [6] we can write,

$$[\Phi]^T[M][\Phi]=[I] \tag{5.5a}$$

$$[\Phi]^T([K]+i[D])[\Phi]=[\lambda^2] \tag{5.5b}$$

Substituting (5.5) into (5.4) we get:

$$\left[\lambda^2-\omega^2\right][\Phi]^{-1}\{Y\}=[\Phi]^T\left(\{F\}-\{G\}\right) \tag{5.6}$$

Re-arranging the terms in (5.6), the response vector can be written by as:

$$\{Y\}=[\Phi]\left[\lambda^2-\omega^2\right]^{-1}[\Phi]^T\left(\{F\}-\{G\}\right) \tag{5.7}$$

Alternatively, the non-linear modal vector can be extracted from (5.6)

$$\{\chi\} = [\Phi]^T \{G\} = [\Phi]^T \{F\} - \left[\lambda^2 - \omega^2\right][\Phi]^{-1}\{Y\} \tag{5.8}$$

Equation (5.8) presents the non-linear modal vector in terms of the modal model of the underlying linear system, and the non-linear response amplitude vector. Equation (5.8) can be used only when the full modal model, i.e. the responses at all DOFs and all modes, is available. For making use of (5.8) in practical cases, there are two major difficulties: (i) non-linear measurements at all DOFs are seldom available; (ii) the modal model obtained via an experimental route is not complete. It only contains the identified modes within the measured frequency range and the measured DOFs.

If the subscripts *m* and *u* represent the measured and un-measured DOFs, and subscripts M_r and U_r represent the identified and un-identified modes respectively, then (5.7) can be partitioned as:

$$\begin{Bmatrix} Y_m \\ Y_u \end{Bmatrix} = \begin{bmatrix} \Phi_{mM_r} & \Phi_{mU_r} \\ \Phi_{uM_r} & \Phi_{uU_r} \end{bmatrix} \begin{bmatrix} \left(\lambda^2 - \omega^2\right)_{M_r} & 0 \\ 0 & \left(\lambda^2 - \omega^2\right)_{U_r} \end{bmatrix}^{-1} \begin{bmatrix} \Phi_{M_r m} & \Phi_{M_r u} \\ \Phi_{U_r m} & \Phi_{U_r u} \end{bmatrix} \left(\begin{Bmatrix} F_m \\ F_u \end{Bmatrix} - \begin{Bmatrix} G_m \\ G_u \end{Bmatrix} \right) \tag{5.9}$$

Thus, the response at the measured DOFs can be written as:

$$\{Y_m\} = \underbrace{\left[\Phi_{mM_r}\right]\left[\lambda^2 - \omega^2\right]^{-1}_{M_r}\left[\Phi_{M_r m}\right]\{F_m - G_m\}}_{term\ A} + \underbrace{\left[\Phi_{mU_r}\right]\left[\lambda^2 - \omega^2\right]^{-1}_{U_r}\left[\Phi_{U_r m}\right]\{F_m - G_m\}}_{term\ B} \tag{5.10}$$

The second term in (5.10), *term B*, represents the contribution of the un-identified modes in the measured response. This is called the non-linear residual, represented by $\left\{\widetilde{R}^{es}\right\}_m$. Equation (5.10) can be expressed in a compact form

$$\{Y_m\} = \left[\Phi_{mM_r}\right]\left[\lambda^2 - \omega^2\right]^{-1}_{M_r}\left[\Phi_{M_r m}\right]\{F_m - G_m\} + \left\{\widetilde{R}^{es}\right\}_m \tag{5.11}$$

The non-linear modal vector for a system with *m* measured DOFs and M_r identified modes can be written as:

$$\{\chi\}_{M_r} = \left[\Phi_{M_r m}\right]\{F_m\} - \left[\lambda^2 - \omega^2\right]_{M_r}\left[\Phi_{mM_r}\right]^{-1}\left(\{Y_m\} - \left\{\widetilde{R}^{es}\right\}_m\right) \tag{5.12}$$

Equation (5.12) involves an inversion of a possible rectangular matrix; Φ_{mM_r}. A unique solution to (5.12) exists only when the mathematical condition, $m \geq M_r$, is met. This condition is easy to meet in practical cases where the number of

measured DOFs is generally greater than the number of identified modes. The non-linear modal vector can be extracted using (5.12) if the non-linearity is confined to the measured zone, and if the non-linear residual can be approximated. It is proposed in [26] that the non-linear residual can be approximated as the linear residual if the number of identified modes is sufficiently high. The different methods to express linear residual are given in [6, 7]. The study of the effects of such an approximation on the accuracy of the method is presented later in the chapter.

5.2.2 Quantification of the level of non-linearity

The effects of non-linearity are not the same in all modes of a structure. Some modes can be severely affected by non-linearity while the others can behave almost linearly. For a particular mode, the severity depends on the location of the non-linearity, the mode shape vector, and the resonance amplitude for the mode. Elizalde [26] proposed a term called 'non-linear modal grade' to quantify the level of non-linearity at a particular mode. The definition he proposed is based on the maximum value of non-linear modal vector in the vicinity of the resonance of the concerned mode. For example, the non-linear modal grade for the r^{th} mode is defined as $\left\{\Phi^T G\right\}_{\max} / \left\{\Phi^T F\right\}$, where $\left\{\Phi^T G\right\}_{\max}$ is the maximum value of $\left\{\Phi^T G\right\}$ in the vicinity of the r^{th} resonance.

It has been observed in Chapter 3 that the shape of the non-linear force vector *G* in the vicinity of a resonance is different for different non-linearities. For some non-linearities like friction, the non-linear force possesses the maximum magnitude for a wider frequency range. In another case, for clearance non-linearity, the non-linear force attains its highest magnitude at resonance and drops steeply thereafter. Thus, the use of the maximum non-linear force value only, to detect the level of non-linearity can be misleading. Instead, it is more appropriate to use the average value of non-linear modal force in the vicinity of the resonance while calculating the non-linear modal grade for the mode of interest.

An alternative definition of non-linear modal grade, proposed here, acknowledges the different shapes of non-linear force by calculating its average value over a frequency range. The frequency range is decided using the half power method as depicted in Figure 5.1.

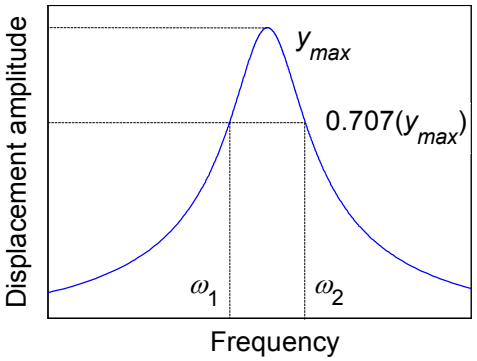

Figure 5.1 Half power method to calculate the average NMV

For the r^{th} mode, if there are n frequency lines between the frequencies ω_1 and ω_2, covering the half power region, the non-linear modal grade (NMG) for this mode is expressed as:

$$NMG_r = \frac{\sum_{\omega=\omega_1}^{\omega_2} \left\{\Phi^T G(\omega)\right\}_1 / \left\{\Phi^T F(\omega)\right\}_1}{n} \tag{5.13}$$

Theoretically, any row of $\left\{\Phi^T G\right\}$ can be used to evaluate the *NMG*. In the current definition, the first row, corresponding to the first mode is used to reduce the effects of the non-linear residual. The value of $\left\{\Phi^T F\right\}$ is independent of frequency, and it can be considered as the linear threshold as it gives the modal force for the underlying linear system. The modes for which the value of NMG is comparatively lower can be treated as linear modes and can be omitted from further analysis. The modes with higher values of NMG should be considered in further analysis for the extraction of non-linear parameters.

5.2.3 Decoupling the non-linear modal vector

The non-linear modal vector (NMV), presented in (5.12), holds the information about the non-linear restoring force at the measured DOFs in a coupled form. There are two approaches to extract the non-linear parameters from the NMV. In the first approach, the non-linear force vector $\{G_m\}$ can be recovered from the NMV, and then the method presented in Chapter 4 can be used to extract the non-linear parameters. This needs an inversion of a possible rectangular matrix, $\left[\Phi_{mM_r}\right]^T$, putting the mathematical condition of $m \leq M_r$ for the solution. This condition conflicts with the condition required for solving (5.12). The two conditions can be met

simultaneously only if the number of measurements is equal to the number of identified modes.

The current work follows the second approach, where the non-linear parameters are directly extracted from the NMV using an optimization technique. The extracted non-linear modal vector can be written in an expanded form as follows:

$$\{\chi\} = \{\Phi_{M_r m} G\} = \begin{Bmatrix} \phi_{11} G_1 + \phi_{21} G_2 + \cdots + \phi_{m1} G_m \\ \phi_{12} G_1 + \phi_{22} G_2 + \cdots + \phi_{m2} G_m \\ \vdots \\ \phi_{1M_r} G_1 + \phi_{2M_r} G_2 + \cdots + \phi_{mM_r} G_m \end{Bmatrix} \tag{5.14}$$

If the non-linearity is not located a-priori, which means it can be anywhere in the measured zone, there are m possible locations for it. At each location, if there are n_p non-linear parameters corresponding to different non-linearities, then the NMV can be written as a function of ($m \times n_p$) non-linear parameters.

$$\{\chi\} = f\overbrace{\left(\beta^1, K_z{}^1, y_c{}^1, K_d{}^1, \mu N^1 \ldots K_d{}^m, \mu N^m\right)}^{m \times n_p} \tag{5.15}$$

Since the non-linear parameters are independent of frequency, M_r independent equations are available at each frequency value. It has been observed that some modes in the analysis behave linearly, and the value of the NMV around such linearly-behaving modes is comparatively lower than that for the non-linear modes. The linearly behaving modes can be identified using the NLMG value and can be omitted from the analysis. Thus, n_s points in the vicinity of the resonance of the non-linear modes are chosen to form the system of equations. To obtain a unique solution to the system of equations, the minimum number of selected points must meet the following condition

$$n_s \geq m \times n_p \tag{5.16}$$

The error residual at any frequency value, ω_i, can be written using the describing functions for the different non-linearities previously explained in Chapter 3

$$R_i = \left\{\chi(g^{cub}, g^{cle}, g^{fri})\right\} - \{\chi_i\} \tag{5.17}$$

where, $\chi(g^{cub}, g^{cle}, g^{fri})$ represents the non-linear modal vector formed using describing functions, and $\{\chi_i\}$ represents the non-linear modal vector extracted

using (5.12). For n_s points, the total error residual to be minimized can be expressed as:

$$R = \frac{\left(\sum_{k=1}^{n_s} (R_i)_k^2 \right)^{1/2}}{n_s} \tag{5.18}$$

Since it is sometimes more suitable to solve a maximization problem using the genetic algorithm, the above quantity can be converted to an expression to be maximized as:

$$R_m = \frac{C}{C + R} \tag{5.19}$$

where C is a real positive number (C = 100).

The residual in (5.19) can be maximized using a genetic algorithm to find out the non-linear parameters at all measured locations. If the non-linearity location is identified prior to this stage, then the optimization problem can be formed using only the identified non-linear DOFs. This reduces the size of the problem by reducing the number of parameters to be optimized to n_p from (m× n_p). Figure 5.2 shows the flowchart for the proposed method.

5.2.4 Comments on the non-linear residual

Even for linear systems, practically it is not possible to obtain a complete modal model through an experimental route. We generally restrict the measured frequency range, depending on the application and some modes falling beyond this range remain un-identified. The contribution of these un-identified modes is represented by the residual term (linear residual). There are established approaches to take into account the effect of residuals, the details of which are given in [6]. An equivalent term for a non-linear system, which represents the contribution of the un-identified modes in the non-linear response, is called the non-linear residual.

This section studies the nature of the non-linear residual and how it differs from the linear residual. For an N-DOF non-linear system with M_r identified modes, using (5.10), the expression for non-linear residual at the i^{th} DOF can be written as:

$$\widetilde{R}_i^{es} = \sum_{r=M_r+1}^{N} \frac{\phi_{ir} \left[\left\{ \Phi^T F \right\}_r - \left\{ \Phi^T G \right\}_r \right]}{(\omega_r^2 - \omega^2) + i\eta_r \omega_r^2} \tag{5.20}$$

It can be seen that the value of the denominator of (5.20) is very high for the modes for which $\omega_r >> \omega$. The variation of numerator comes only from the non-linear restoring force vector G, which varies with frequency, while the excitation forces are assumed to be constant.

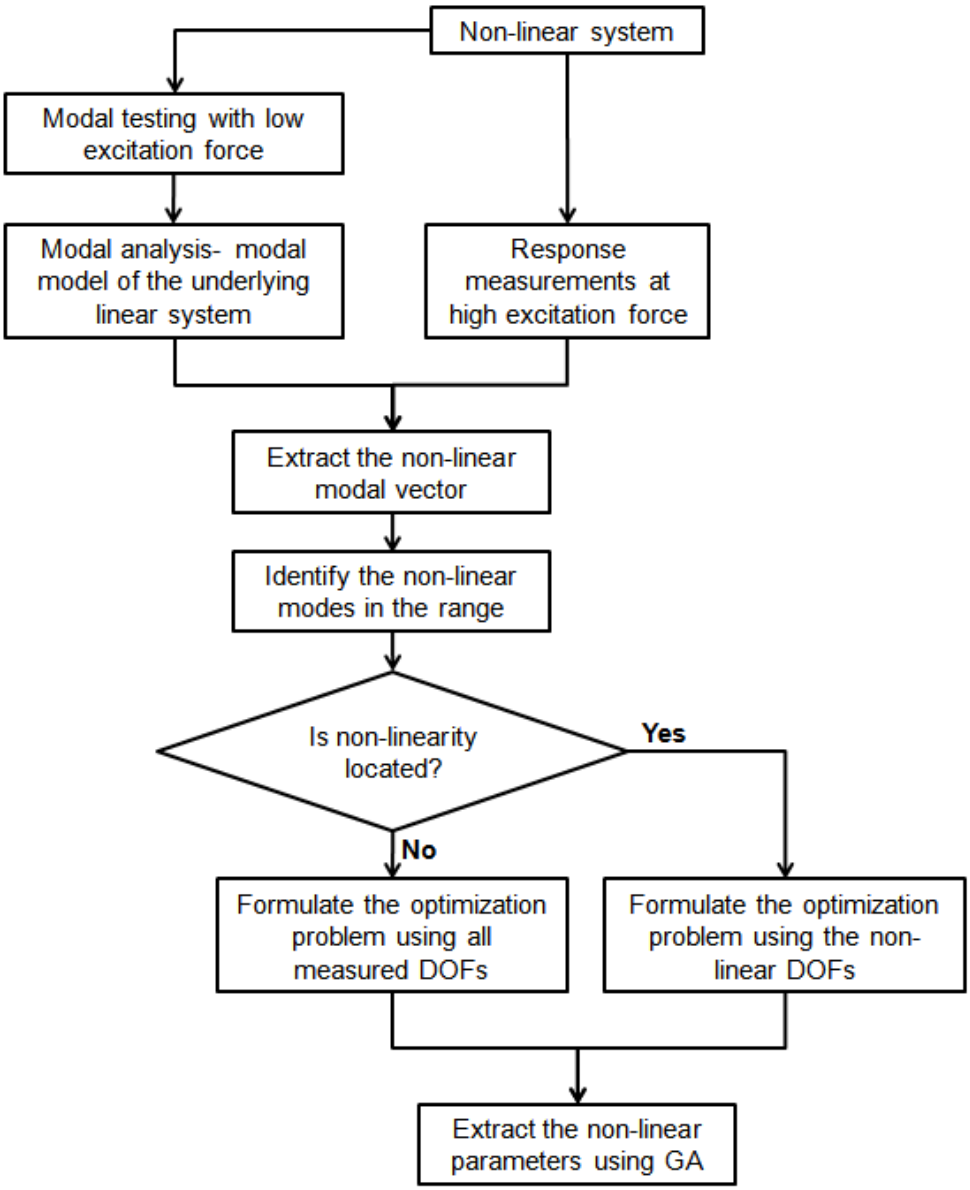

Figure 5.2 Flow chart for the improved hybrid modal method

The expression for linear residual can be obtained by putting $G = 0$ in (5.20). It has been observed in the earlier chapters that the non-linear force vector G, has an insignificant magnitude in the region away from the system's resonances. Thus, in these regions, $G \approx 0$, and the non-linear residual can be safely replaced by its linear counterpart without a significant loss of accuracy. In the region in the vicinity of any system resonance, the magnitude of the non-linear restoring force is

significant, and hence the non-linear residual is expected to deviate from its linear counterpart. Figure 5.3 shows, for a typical case, the comparison of linear and non-linear residuals. For the case considered, the non-linear resonance frequency of the first mode of the system is at 30.7 rad/sec.

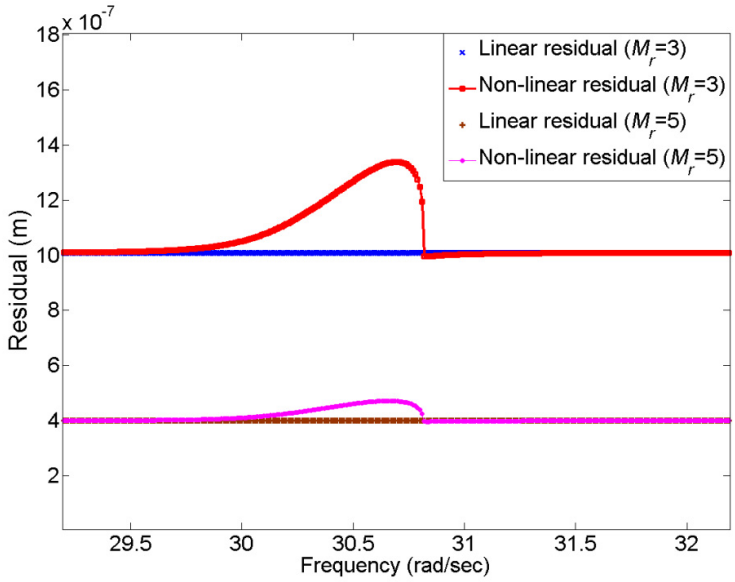

Figure 5.3 Comparison of linear and non-linear residual for a typical case

It is observed from Figure 5.3 that in the vicinity of the first resonance, there is a significant difference between the linear and non-linear residuals. The magnitude of the residual is higher when the number of modes identified in the modal analysis, M_r, is low. Figure 5.4 shows the variation of the non-linear residual with the number of identified modes.

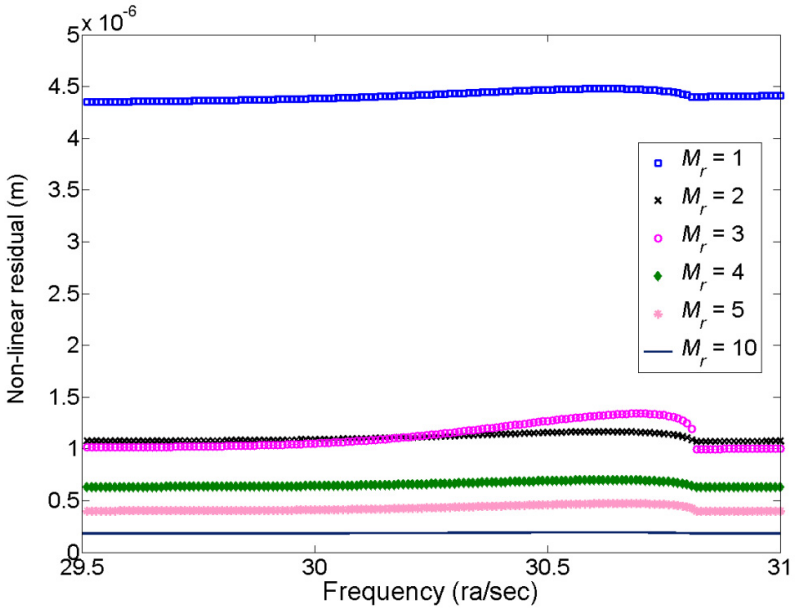

Figure 5.4 Non-linear residuals with different number of modes in the range

With an assumption that the non-linear residual behaves in a similar way to the linear residual, the value of the non-linear residual is expected to decrease with the number of modes identified. This assumption is found valid in the region away from the resonance. An interesting anomaly is observed in the vicinity of the resonance. The magnitude of non-linear residual for the case, M_r = 3, is found higher than the magnitude for the case, M_r = 2. Though the observation may be specific to this case, and cannot be generalized, care should be taken while neglecting the effect of non-linear residuals in the identification process.

It is also observed that if a sufficient number of modes is considered in the analysis, (M_r = 10), the magnitude of the non-linear residual is almost constant over the frequency range, and the magnitude is same as for the linear residual. Thus if a sufficient number of modes are identified during the modal analysis, the non-linear residual can be safely replaced by the linear residual throughout the frequency range.

5.2.5 Numerical validation of I-HMT method

The method presented above is illustrated using simulated data for 'Validation Structure-2', a cantilever plate. The details of the plate are documented in Appendix B. An element with clearance non-linearity parameters, $y_c = 5\times10^{-5}$ m and k_z = 200 N/m was used for the validation analysis. The simulated non-linear response was obtained using the in-house code *FORSE* [4]. Figure 5.5 shows a comparison of the linear and non-linear response at the non-linear DOF.

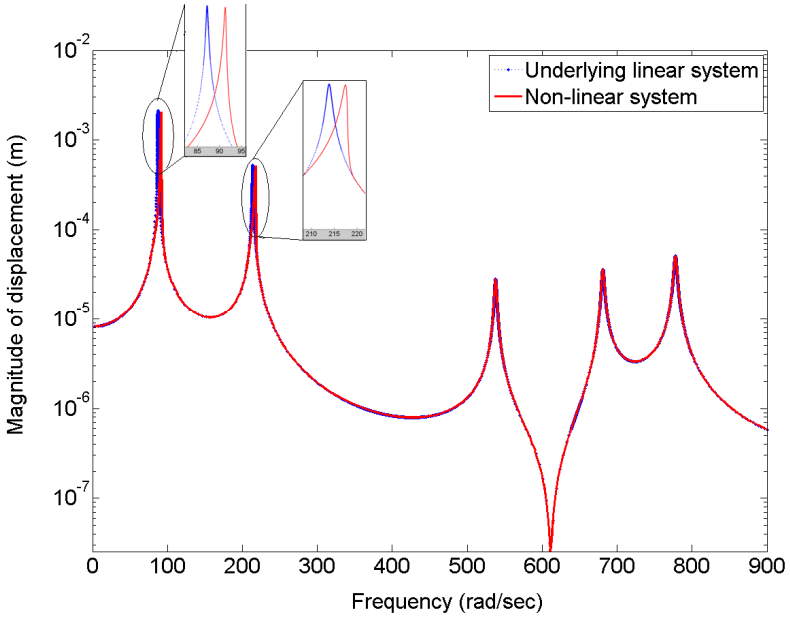

Figure 5.5 Comparison of linear and non-linear response for clearance non-linearity

It is seen from Figure 5.5 that the first two modes are affected most by the non-linearity and the rest of the modes behave almost linearly.

Pre-processing stage

The underlying linear modal model was obtained by performing modal analysis on the structure to extract the modal properties for the first nine modes (M_r = 9). The displacement responses were captured at 16 locations uniformly distributed over the plate (m = 16). As it is difficult to measure the rotational DOFs in practical cases, all 16 responses are the translational displacements along Z axis. The details of the available modal model and the non-linear response measurements are given below. The numbers below indicate the node number followed by a letter indicating the DOF at the node, X for the rotation about X axis, Y for the rotation about Y axis and Z for the translation along Z axis. The information is also depicted in Figure 5.6 for a better illustration of the process.

Measured DOFs (Z translational): {1, 3, 5, 7, 11, 13, 15, 17, 21, 23, 25, 27, 29, 32, 37, 42}

Un-measured DOFs: {1X-42X; 1Y-42Y; 2Z, 4Z, 6Z, 8Z-10Z, 12Z, 14Z, 16Z, 18Z-20Z, 22Z, 24Z, 26Z, 28Z, 30Z, 31Z, 33Z-36Z, 38Z-41Z}

Excitation force applied at: {37Z} **Excitation force amplitude** = 0.01N

Non-linear element incorporated at: {42Z}

Identified modes from linear modal analysis: {1, 2, 3..., 9}

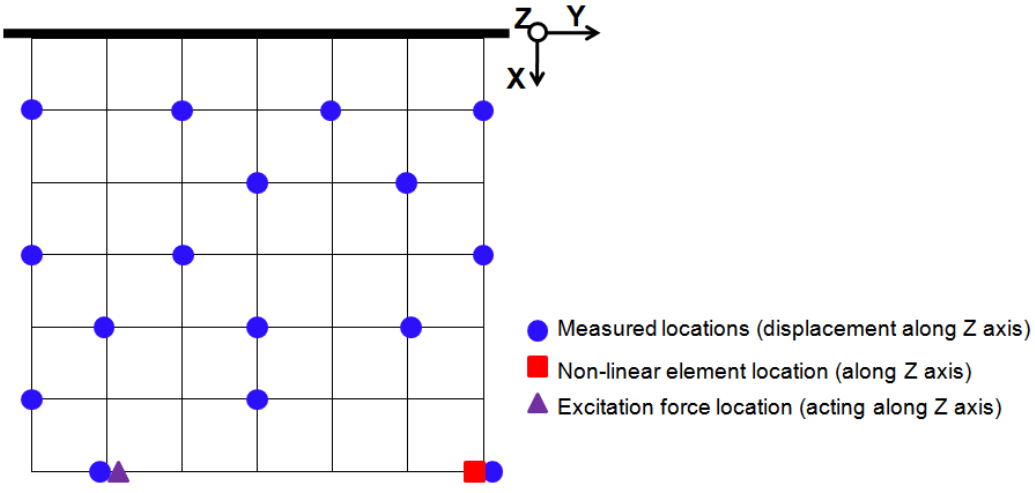

Figure 5.6 Details of the measured locations

Extraction of the non-linear modal vector (NMV)

The non-linear modal vector was extracted using (5.12). Out of the first nine modes which were identified in the modal analysis, only the first two modes behave non-linearly. Owing to this, the non-linear residual value around the non-linear resonances was assumed to be small. Thus the non-linear residual was replaced by the linear residual. Figure 5.7 shows the plot of the amplitude of non-linear modal vector for the first mode. The top part of the figure shows the non-linear response at the non-linear DOF, and the bottom part of the figure shows the amplitude of non-liner modal vector for the first mode plotted in the same frequency range as the non-linear response. The dashed line in the bottom plot shows the linear threshold for the first mode. It can be observed from the plot that the NMV crosses the linear threshold for the first two resonances. Figure 5.8 shows a zoomed-in view of the NMV in the vicinity of the first resonance.

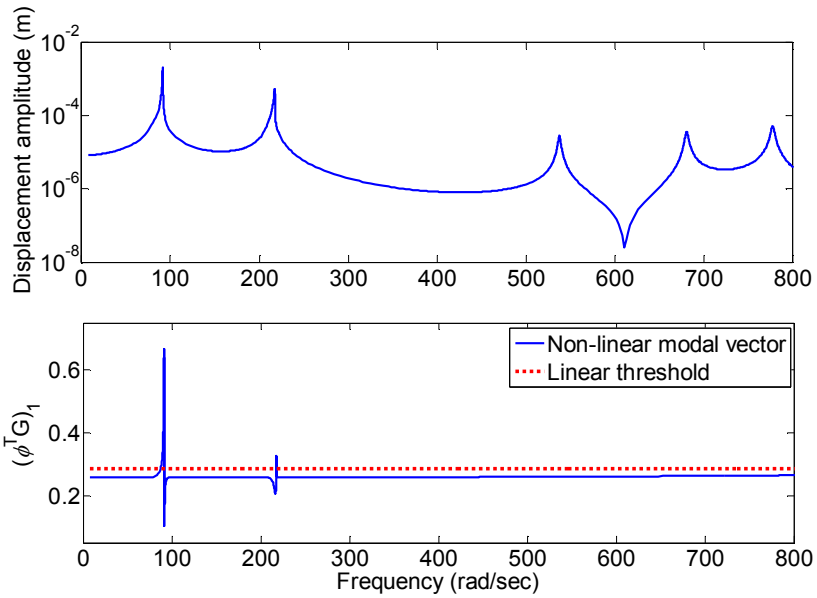

Figure 5.7 Extracted non-linear modal vector for the first mode

Once the NMVs were extracted for the identified modes, the non-linear modal grade (NMG) was calculated for each mode using (5.13) to decide on the modes to be retained in further analysis. Figure 5.9 shows a bar chart for NMGs for the first five modes. It is seen that the NMGs for the first two modes are greater than that for the other modes. Thus, the first two modes are classified as the non-linear modes, and the points in the vicinity of the first two resonances are selected while formulating the optimization problem.

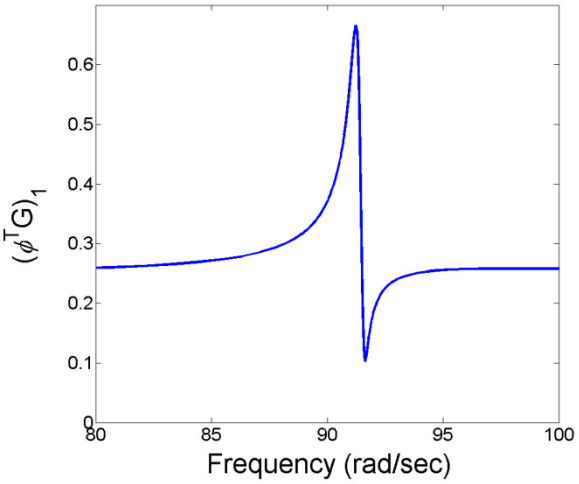

Figure 5.8 Zoomed-in view of NMV near the first resonance

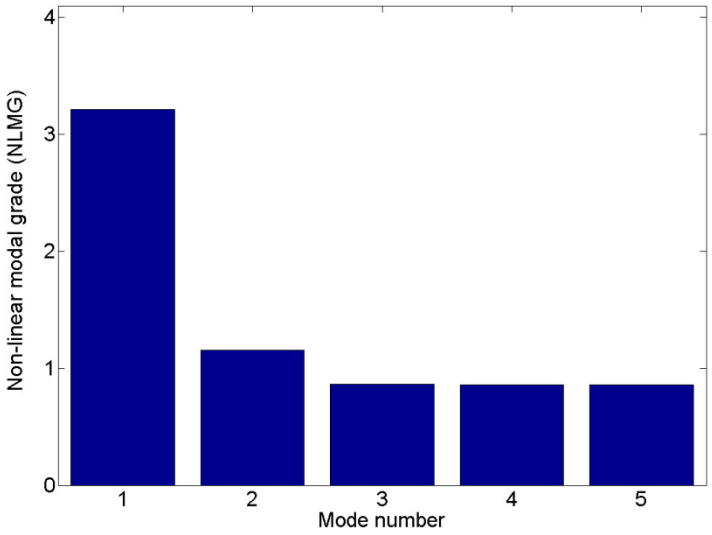

Figure 5.9 Non-linear modal grades for the modes in the measurement range

Estimation of the non-linear parameters

The optimization problem was solved using a GA to extract the non-linear parameters. The values of the control parameters, like the population size, the number of generations, and the probability of cross-over operator were kept same as those in Table 4.1. The range for the non-linear parameters used in the first civilization is as follows:

Gap distance, y_c,: $(1\times10^{-7}\text{-}1\times10^{-4})$ m.

Clearance stiffness, K_z: (0-400) N/m

Initially (Case A), the optimization problem was formulated with all measured DOFs, simulating the case where the non-linear location is not identified a-priori. The total number of non-linear parameters to be identified is 80. For this case, the

algorithm did not converge, and the location of non-linearity and the correct values of the non-linear parameters could not be identified.

In the second case (Case B), probability-based binary multipliers[7] were used. More weight was given to the correct location of the non-linearity (p = 0.9) and lesser weight to the other locations (p = 0.5). For Case B, the solution converged to reasonably accurate values of non-linear parameters at the non-linear DOF, but a spurious non-linearity at DOF#1Z was also identified. Since this node is very close to the fixed edge of the plate, the displacement amplitude at this DOF is expected to be low. Thus, the non-linear element wrongly put at this location would not contribute much to the non-linear response prediction.

In the third case (Case C), the location of the non-linearity was assumed to be known, and the optimization problem was formulated with only the non-linear DOF, reducing the number parameters to be optimized to n_p = 5. The solution converged giving accurate values for the non-linear parameters.

The effect of the deviation of non-linear residual from its linear counterpart on the estimated parameters is examined by reducing the number of identified modes in the analysis. It is observed that the estimated parameters are fairly accurate even with only the first mode included in the analysis. Table 5.1 summarizes the results of the numerical study.

Table 5.1 Results of parameter estimation for different cases using I-HMT method

Case	M_r	Location of non-linearity	Estimated parameters {K_z (N/m), y_c (m)}	$(\text{Fitness})_{\max}$
A	9		Algorithm did not converge	
B	9	1Z	$\{2.34\times10^{-6}, 50\}$	7.91
		42Z	$\{7.18\times10^{-5}, 200\}$	
C	9	42Z	$\{5.21\times10^{-5}, 200\}$	35.31
	5		$\{4.91\times10^{-5}, 200\}$	35.30
	3		$\{4.82\times10^{-5}, 200\}$	35.30
	1		$\{5.61\times10^{-5}, 200\}$	34.48

[7] Similar to the binary multipliers described in Chapter 4

5.3 FRF-based method

The I-HMT method presented in Section 5.2 uses the modal model of the underlying linear system, which can be obtained by performing modal analysis on the raw FRF measurements. There are two limitations of the I-HMT method:

(i) The non-linearity must be correctly located and the non-linear DOF must be measured for efficient working of the optimization algorithm.

(ii) The modal analysis of measured data can introduce additional errors if it is not performed carefully.

The method proposed in this section uses the raw FRF measurements directly to extract the non-linear restoring force. On the one hand, if the non-linear DOFs are located and measured, the method extracts the non-linear force at these non-linear DOFs. On the other hand, if there is a localized non-linearity at a single point, which is located but not measured, the method uses a technique to approximate the non-linear restoring force at the non-linear DOF.

As the FRF matrix for a linear system is symmetric, it is not necessary to obtain the complete FRF matrix through experiments, thus reducing the costs related to the experimentation. The method completely relies on measured data, making it useful when the accurate FE model and sophisticated modal analysis tools are not available.

5.3.1 Theoretical formulation

In the frequency domain, the equations of motion for an MDOF non-linear system under harmonic excitation are written as:

$$\left(-\omega^2[M]+[K]+i[D]\right)\{Y\}+\{G(\omega,Y)\}=\{F\} \tag{5.21}$$

The quantity inside the curved brackets on the left-hand side of (5.21) is defined as the dynamic stiffness matrix of the system, denoted by $[Z]$. The FRF matrix for a system, $[\alpha]$, is defined as the inverse of the dynamic stiffness matrix. Pre-multiplying (5.21) by the FRF matrix we get

$$\{Y\}+[\alpha]\{G\}=[\alpha]\{F\} \tag{5.22}$$

If subscript *m* denotes the measured DOFs and subscript *u* denotes the un-measured DOFs of the system, (5.22) can be partitioned as:

$$\begin{Bmatrix} Y_m \\ Y_u \end{Bmatrix} + \begin{bmatrix} \alpha_{mm} & \alpha_{mu} \\ \alpha_{um} & \alpha_{uu} \end{bmatrix} \begin{Bmatrix} G_m \\ G_u \end{Bmatrix} = \begin{bmatrix} \alpha_{mm} & \alpha_{mu} \\ \alpha_{um} & \alpha_{uu} \end{bmatrix} \begin{Bmatrix} F_m \\ F_u \end{Bmatrix} \tag{5.23}$$

If the displacements at the measured DOFs are considered, the system of equations can be written as:

$$\{Y_m\} + [\alpha_{mm}]\{G_m\} + [\alpha_{mu}]\{G_u\} = [\alpha_{mm}]\{F_m\} + [\alpha_{mu}]\{F_u\} \tag{5.24}$$

If it is assumed that all excitation DOFs are measured, a condition which can be easily achieved during controlled experimentation, the vector $\{F_u\}$ becomes zero. Substituting $\{F_u\} = 0$ in (5.24), and multiplying by $[\alpha_{mm}]^{-1}$,

$$\{G_m\} = \underbrace{\{F_m\} - [\alpha_{mm}]^{-1}\{Y_m\}}_{\{G^0\}} - [\alpha_{mm}]^{-1}([\alpha_{mu}]\{G_u\}) \tag{5.25}$$

Rearranging (5.25) we get

$$\{G^0\} = \{G_m\} + [\alpha_{mm}]^{-1}([\alpha_{mu}]\{G_u\}) \tag{5.26}$$

where, $\{G^0\}$ denotes the term in (5.25) which can be extracted using available measurements. In a special case where all non-linear DOFs are measured, $\{G_u\} = 0$, and $\{G^0\}$ gives the non-linear restoring force vector at the measured DOFs:

$$\{G^0\} = \{G_m\} = \{F_m\} - [\alpha_{mm}]^{-1}\{Y_m\} \tag{5.27}$$

Equation (5.27) gives the expression for the non-linear restoring force at the measured DOFs when all excitation DOFs and all non-linear DOFs are measured. This is an exact equation with no approximations or truncations if it is used within the above constraints.

In many practical cases, the location of non-linearity is physically inaccessible, and a measurement cannot be made at that location. However, if there is a location close to the non-linearity location where the measurement can be taken, the non-linear restoring force at the non-linear DOF can be extracted indirectly. Let subscript *c* denotes the location close to the non-linear DOF at which the measurement is taken, subscript *e* denotes the excitation DOF, and subscript *nl* denotes the non-linear DOF, which is not measured. If all measured

DOF are linear, $\{G_m\} = 0$. If the FRF matrix is constructed using the excitation DOF and the DOF close to the non-linearity location only, (5.26) can be expanded as:

$$\{G^0\} = \begin{bmatrix} \alpha_{cc} & \alpha_{ce} \\ \alpha_{ec} & \alpha_{ee} \end{bmatrix}^{-1} \left([\alpha_{mu}] \{G_u\} \right) \tag{5.28}$$

For a localized non-linearity at the *nl* th DOF, only the corresponding value in the vector $\{G_u\}$ would be non-zero. Thus, rewriting (5.28)

$$\{G^0\} = \begin{bmatrix} \alpha_{cc} & \alpha_{ce} \\ \alpha_{ec} & \alpha_{ee} \end{bmatrix}^{-1} \begin{Bmatrix} \alpha_{cnl} G_{nl} \\ \alpha_{enl} G_{nl} \end{Bmatrix} \tag{5.29}$$

The two entries in vector G^0 can be explicitly written as:

$$G_1^0 = \left(\frac{\alpha_{ee}\alpha_{cnl} - \alpha_{ce}\alpha_{enl}}{\alpha_{ee}\alpha_{cc} - \alpha_{ec}\alpha_{ce}} \right) G_{nl} \tag{5.30a}$$

$$G_2^0 = \left(\frac{\alpha_{cc}\alpha_{enl} - \alpha_{ec}\alpha_{cnl}}{\alpha_{ee}\alpha_{cc} - \alpha_{ec}\alpha_{ce}} \right) G_{nl} \tag{5.30b}$$

If the measured location *c* is sufficiently close to the non-linear location, then for lower modes where the structural deformation is not localized, location *c* can be replaced by the non-linear location *nl* in the FRF matrix. Thus, replacing α_{enl} by α_{ec} , and α_{cnl} by α_{cc} in (5.30a) and (5.30b) and adding the two equations we get:

$$G_{nl} \approx \left(G_1^0 + G_2^0 \right) \tag{5.31}$$

Thus, an approximate expression for the non-linear force at the non-linear DOF can be obtained using the measurement closest to the non-linearity location. This expression is only valid in the case of single point excitation and a single localized non-linearity in the system.

5.3.2 Conditioning of the FRF matrix

The condition number of a matrix is mathematically expressed as the ratio of its largest singular value to its smallest non-zero singular value [7]. A high value of the condition number represents an ill-conditioned matrix. The inversion of an ill-conditioned matrix can be inaccurate, thus it should be avoided.

The expression for the non-linear force vector in (5.25) involves an inversion of the part of the FRF matrix containing the measured DOFs. The value of condition number of the FRF matrix is a function of different parameters like the excitation frequency, damping in the system, the number of measurements, and locations of measurements. Figure 5.10 shows the variation of the condition number of an FRF matrix in a typical case. It is observed that the condition number varies with the

excitation frequency, and attains a maximum value near the resonance frequency of the system. The maximum value of the condition number is higher for lightly damped systems. The maximum value also increases with the size of the FRF matrix.

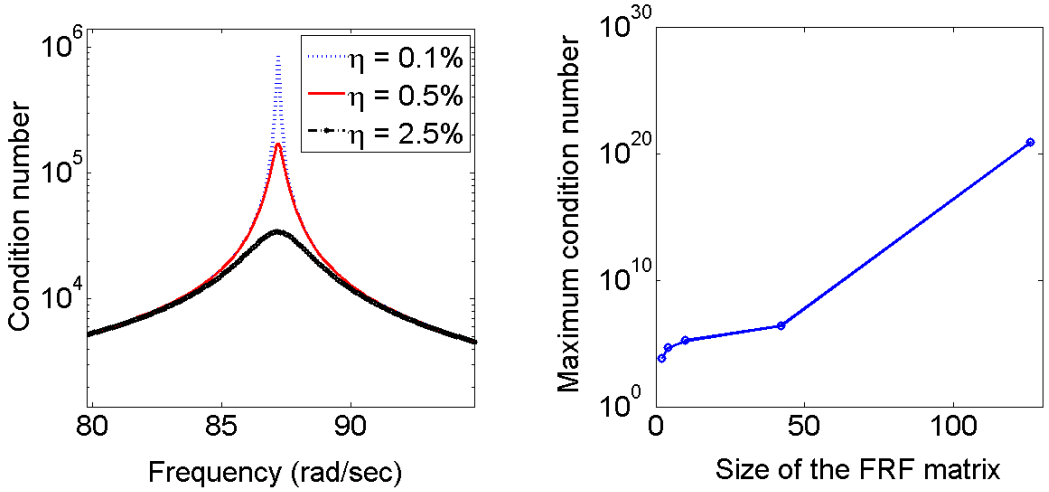

Figure 5.10 Variation of the condition number of the FRF matrix

The condition number of the FRF matrix is also dependent on the selection of the measured DOFs. For a fixed number of measurements, it is observed that if only the translational measurements are distributed uniformly over the structure, the condition number is the lowest. On the other side if the translational and rotational DOFs are combined in the FRF matrix, the condition number is highest. Figure 5.11 shows the effect of the location of the measurements on the condition number of the FRF matrix.

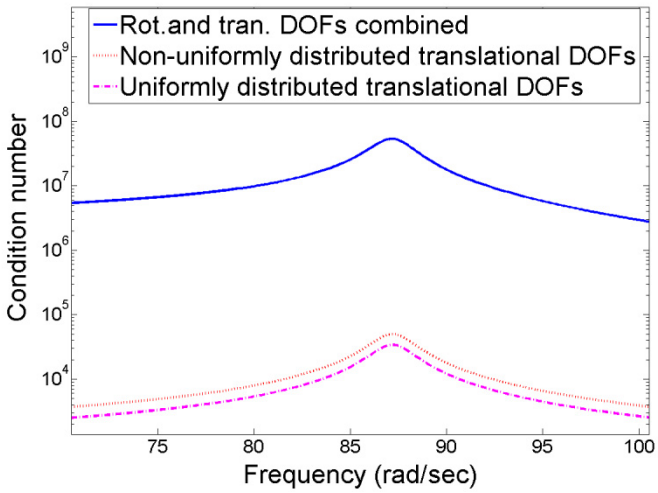

Figure 5.11 Effect of measurement locations on the condition number

Thus, for an accurate extraction of the non-linear force vector using (5.25), it is advisable to keep the number of measurements to the minimum required, distribute the measurements uniformly over the structure, and avoid combining the measurements in different directions which are of different orders of magnitude. In cases where it is required to use measurements which differ by orders of magnitude, the inverse of the matrix can be calculated by special techniques like SVD as explained in [7].

5.3.3 Numerical validation of the FRF based method

The method presented in Section 5.3.1 is illustrated using simulated data for Validation Structure-2, a cantilever plate. A case with combined cubic stiffness and clearance non-linearity was used for the validation. The non-linear parameters used in the simulation are as follows:

- For cubic stiffness non-linearity, the non-linear coefficient, $\beta = 1\times10^{8}$ N-m^{-3}.
- For clearance non-linearity, the gap distance, $y_c = 5\times10^{-5}$ m, and clearance stiffness, $K_z = 200$ N/m.

The non-linear response of the structure was obtained using the in-house code *FORSE* [4]. Figure 5.12 compares the displacement responses for the non-linear and the underlying linear system for the first two modes.

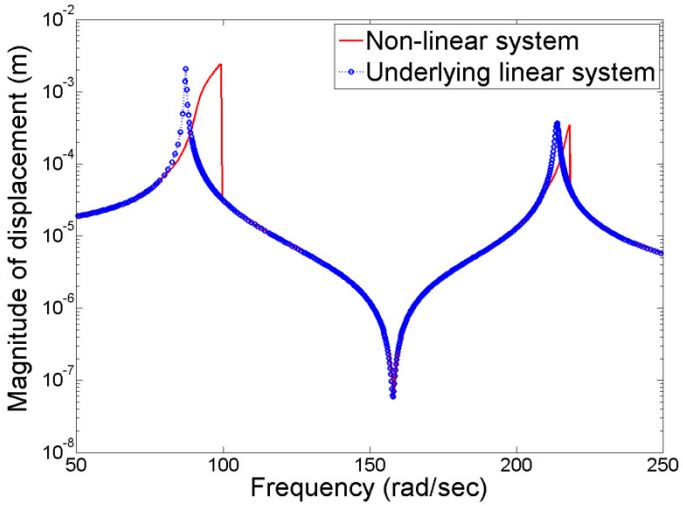

Figure 5.12 Linear and non-linear response at the excitation DOF

Pre-processing stage

To ensure a low condition number for the FRF matrix, the measurements were distributed uniformly over the plate. Only the translational DOFs along the Z axis were included. Three cases were considered for the validation of the method. In the first case, Case A, a total of 10 measurements, including the measurement at the

non-linear DOF were used. In the second case, Case B, only the measurements at the excitation DOF and the non-linear DOF were used. In the third case, Case C, to verify the technique in the absence of measurement at the non-linear DOF, the measurements at the excitation DOF and at a DOF close to the non-linearity location were used. The details for all three cases are given below, and the measurement locations are also depicted Figure 5.13.

Excitation force location: {37Z} **Excitation force amplitude** = 0.01N

Non-linear element location: {42Z}

Measured DOFs

Case A: {1Z, 6Z, 10Z, 16Z, 20Z, 25Z, 33Z, 37Z, 41Z, 42Z}

Case B: {37Z, 42Z}

Case C: {37Z, 41Z}

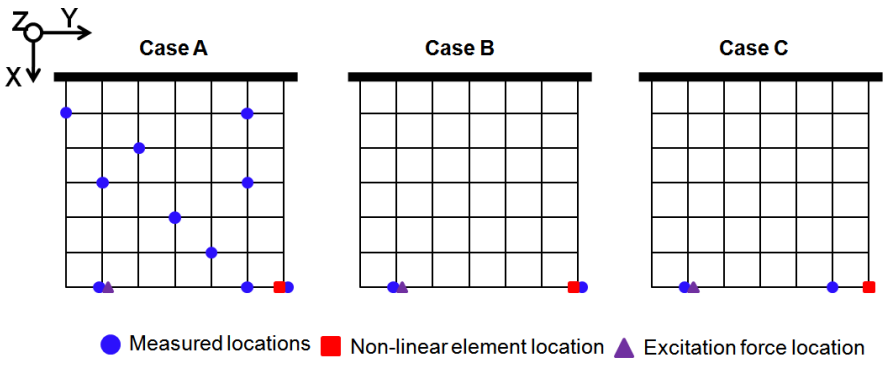

Figure 5.13 Details of the measurement locations for three cases

For Cases A and B, where the measurement at the non-linear DOF was available, the non-linear restoring force at the non-linear DOF was extracted using (5.27). Figure 5.14 shows the non-linear force for both cases plotted on a logarithmic scale. It is seen that the extracted non-linear forces are very similar for both cases.

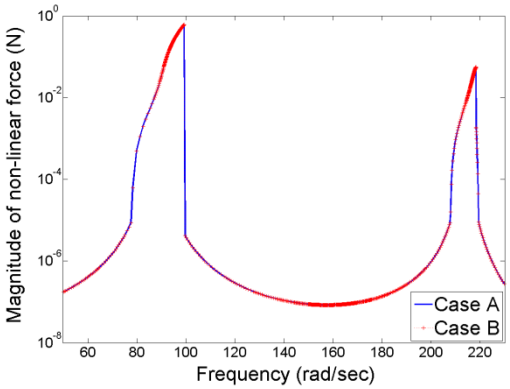

Figure 5.14 Non-linear force for Cases A and B

For Case C, since the non-linear DOF was not measured, (5.30) was used to extract the non-linear force components, G^0_1 and G^0_2, at the measured DOFs. Finally the two components were summed up to find the approximate value of non-linear force at the non-linear DOF. In Figure 5.15, the plot on the left shows the non-linear forces at the measured DOFs, and the plot on the right compares the summed non-linear force with the non-linear force for Case A. It is seen that approximated non-linear force for Case C is in close agreement with the actual non-linear force.

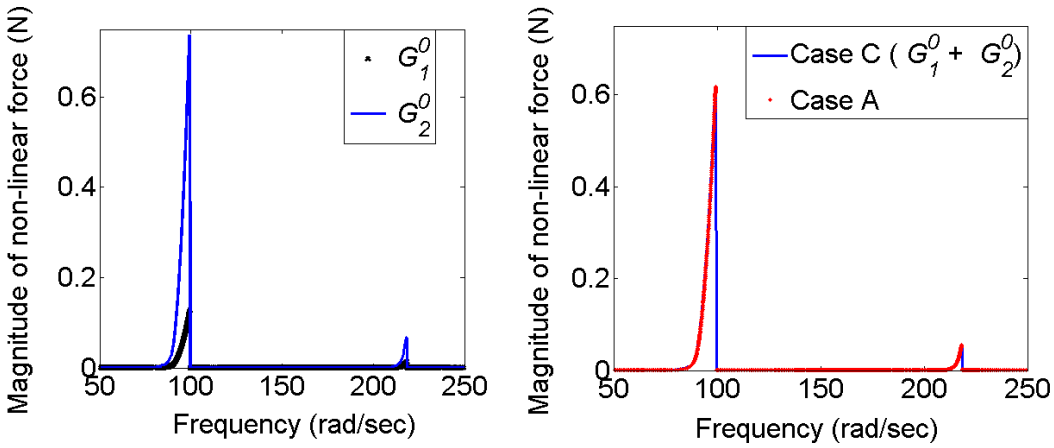

Figure 5.15 Extraction of the non-linear force for Case C

For Cases A and B, the extracted non-linear force was expressed as a function of the displacement at the non-linear DOF. For Case C, the approximated non-linear force was expressed as a function of the displacement at the DOF close to the non-linear DOF. The non-linear parameters were identified using the genetic algorithm optimization presented in Chapter 4. For the initial civilization, the range for β was kept as (0-1×10^{10}) Nm^{-3}, for y_c, was kept as (0-5×10^{-4}) m and for K_z, was kept as (0-800) N/m. Later, the range was narrowed down to increase the accuracy of parameter estimation. The final values of the estimated non-linear parameters are summarised in Table 5.2.

Table 5.2 Summary of the parameter identification results using FRF-based method

Case	Max. Cond. number	Identified parameters {β (Nm^{-3}), y_c (m), K_z (N/m)}	Error (%) {ε_β, ε_{yc}, ε_{kz}}	Fitness
A	2.78×10^5	{1.002×10^8, 5.36×10^{-5}, 200}	{0.2, 7.2, 0}	99.36
B	550.7	{1.003×10^8, 5.23×10^{-5}, 200}	{0.3, 4.6, 0}	98.73
C	841.6	{7.212×10^7, 9.62×10^{-5}, 225}	{27.9, 92.4, 12.5}	95.31

It is observed that the maximum error in parameter estimation for Cases A and B is less than 8%. For Case C, where the non-linear parameters are identified in absence of the measurement at non-linear location, the error is high. It can be also observed that for Case A, though the condition number is in the order of 10^5, the parameters are accurately identified. Figure 5.16 shows the regenerated response at the excitation DOF with the identified parameters for all three cases. It is seen that even for Case C, where the average error in the estimation of parameters is more than 40%, the deviations in resonance frequency and resonance response are around 4-5%. It suggests that the response difference has different sensitivities for non-linear parameters.

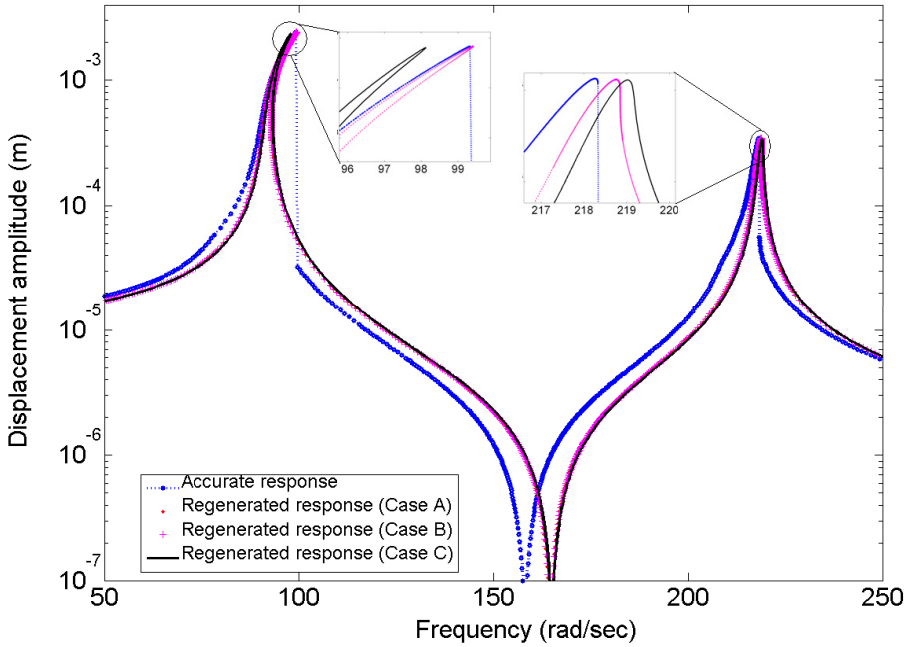

Figure 5.16 Comparison of the accurate response and the regenerated response for the FRF-based method predictions

5.4 Concluding remarks

Two non-linear identification methods which do not require an FE model of the underlying linear system have been presented. The methods use the modal model and the response model of the underlying linear system respectively. The methods have been tested on simulated data for a cantilever plate with localized non-linearities. The observations and comments on both methods are listed below.

5.4.1 Comments on the I-HMT method

The method uses the modal model of the underlying linear system to extract the non-linear modal vector (NMV) which contains the non-linear restoring force in a coupled form. The extracted NMV is de-coupled using the GA optimization to identify the non-linear parameters. The method has been successfully implemented on simulated data for a cantilever plate with localized clearance non-linearity. Some remarks on the usefulness of the method are listed below:

- The method provides a useful alternative to the spatial method non-linear identification method in the absence of an underlying FE model of the system.
- If a sufficient number of modes are identified through the linear modal analysis, the non-linear residual, which is difficult to obtain otherwise, can be replaced by the linear residual.
- The newly-introduced term “non-linear modal grade” acknowledges the difference in the shapes of the non-linear restoring force for different non-linearities. The proposed definition is more general than the earlier definition but it needs to be validated on different engineering structures.
- Though theoretically it is possible to obtain a unique solution to the optimization problem when the non-linearity is not located a priori, it has been observed that the solution takes a very long time to converge, and may not even converge in some cases. If the non-linearity is located, or the location is guessed with an associative probability, the algorithm has been found to be reasonably stable and accurate.

5.4.2 Comments on the FRF-based method

The method uses the FRF matrix (response model) of the underlying linear structure to extract the non-linear restoring force at the measured DOFs. The non-linear restoring force at the non-linear DOF is then used to extract the non-linear parameters via genetic algorithm optimization.

- It has been observed that the measurements at the non-linear DOFs and the excitation DOF are sufficient to accurately identify the non-linear parameters. This significantly reduces the size of the problem for practical cases.
- If the response at the non-linear DOF is not available, a technique has been presented to approximate the non-linear restoring force at the non-linear DOF using the measurement at a location close to the non-linearity location. This technique has reduced accuracy in comparison to the original technique.

The method has been successfully validated on simulated data for a cantilever plate with combined cubic stiffness and clearance non-linearity.

Chapter 6

Comparison of non-linear parameter identification methods

This chapter presents a comparative study of three methods for non-linear system identification, presented in Chapters 4 and 5. The study is carried out on the so-called '1203 structure', which can be considered as a representative engineering structure. Simulated non-linear response data and numerical models of the underlying linear structure are used as input to the parameter identification. Two cases of increasing complexity are considered: (i) an idealized cubic stiffness non-linearity and (ii) a realistic clearance non-linearity. The methods are compared on the basis of different evaluation criteria like: accuracy of parameter estimation, sensitivity to measurement noise, sensitivity to errors in the input model, ability to locate the non-linearity, performance with partial measurement set, and computational efficiency.

6.1 Introduction

The methods presented in Chapters 4 and 5, for non-linear system identification, can potentially be used to tackle large multi-degrees of freedom (MDOFs) systems of practical interest. Each method requires different input, and it has its own advantages and limitations. Table 6.1 gives the summary of input requirements for the three methods. The methods have been illustrated on simple structures before, but it is necessary to compare their performance on common grounds, using data obtained for a representative engineering structure.

Table 6.1 Details of the three methods compared

Method name	Method number	Input requirement
Spatial method	1	Updated FE model of the underlying linear system
Improved hybrid modal technique (I-HMT)	2	Modal model of the underlying linear system
FRF-based method	3	Response model of the underlying linear system

It can be argued that actual experimental data obtained for a practical non-linear structure should be used for comparing the identification methods. However, in case of non-linear structures, the use of experimental data poses many additional difficulties, some of which are as follows:

(i) Obtaining consistent and repeatable vibration measurements on a non-linear structure is a challenging task.

(ii) In practical non-linear structures, the non-linearities may not behave as per their idealized mathematical formulation.

(iii) The actual values of the non-linear parameters are unknown in practical cases, making the comparison of different methods difficult because of a lack of reference data.

The methods presented in the earlier chapters work within certain assumptions like the idealized mathematical formulation for different non-linear elements, the use of first-order describing functions to represent the non-linear force etc. The objective of the work presented in this chapter is to compare the three identification methods based on their accuracy and robustness within these assumptions. Thus, it is more appropriate to use simulated data for the comparison.

The so-called ‘1203 structure’ is used for the comparison. This structure, based on the outer cover geometry of an electrical component, was used as the benchmark structure for validating linear modal analysis algorithms in the MODENT software in ICATS [117]. The same structure, with some alterations to the dimensions, is used. The detailed engineering drawings of the 1203 structure, as used in this study, are given in Appendix C.

The underlying linear structure was modelled in ANSYS using shell elements (SHELL63) to mesh the surfaces and 3D beam elements (BEAM4) to mesh the two stiffening beams. All elements used possess 6 DOFs per node. The structure was

assumed to be bolted to a fairly rigid structure, which could be treated as ground, at the locations of two holes. The excitation force of amplitude 0.1N was applied at one corner of the structure acting in positive X direction. Figure 6.1 shows the computer model, and the meshed model with boundary conditions for the structure.

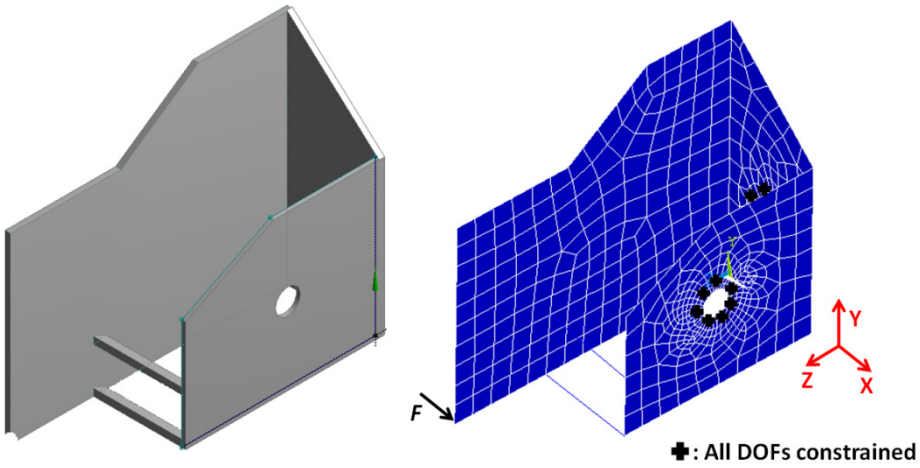

Figure 6.1 CAD and FE models '1203 structure'

6.2 Test cases for the comparison

Two test cases of increasing complexity are considered in this chapter for the comparison of the methods. The first case, Case A, uses a grounded cubic stiffness non-linearity at one end of the lower beam. This is an idealized case used to evaluate the performance of the methods with a complex structure. The second case, Case B, implements a realistic clearance non-linearity. A rubber block, 4×4 cm in cross-section and 5cm thick, is placed adjacent to the structure with a small clearance between the block and the structure. During the vibration of the structure, the structure will hit the rubber block, thus producing clearance non-linearity. In the simulation, this condition was approximated by using four clearance elements distributed over the patch spanning the rubber block. Figure 6.2 shows, in front view, the location of non-linearities in both cases. The details of non-linearity locations and the parameters used to simulate the non-linearities are given in Table 6.2.

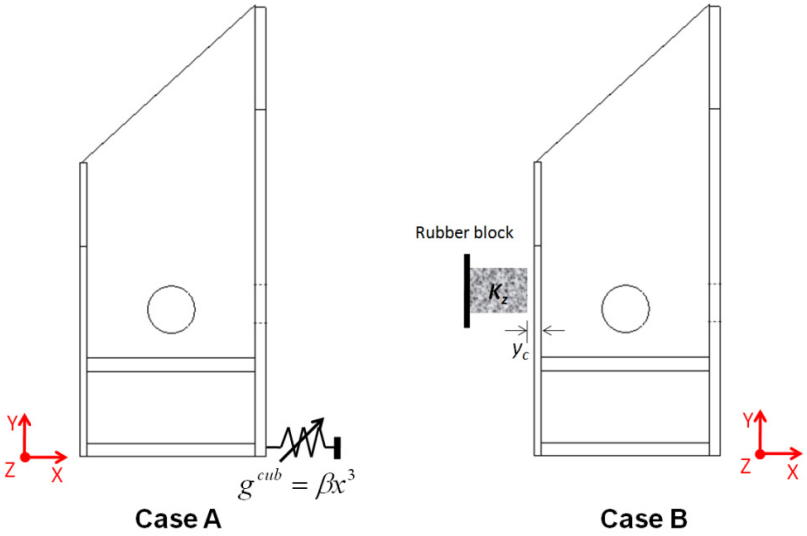

Figure 6.2 Depiction of two test cases used for comparison study

Table 6.2 Summary of non-linear parameters used for the two cases

Case	Non-linearity location	Non-linear parameters
A	473X-grounded	$\beta = 5\times10^{10}$ Nm^{-3}
B	255X-grounded 260X-grounded 264X-grounded 273X-grounded	K_z = 20 KN/m y_c = 0.4mm

6.3 Pre-processing of the input data

Before presenting the results for the comparison, the input requirements for the methods are discussed. All three methods essentially use two inputs: (i) non-linear displacement measurements at various locations on the structure, (ii) a numerical model of the underlying linear structure.

6.3.1 Non-linear displacement measurements on the structure

Simulated response data for the two cases, described in Section 6.2, were obtained using an in-house non-linear response prediction code, *FORSE* [4]. The displacement responses were captured at 14 locations, uniformly distributed over the structure. The frequency range was selected to be 0-200Hz which covers the first 10 natural frequencies of the underlying linear structure. A constant, frequency

independent modal damping of 1% (η = 0.01) was used for simulations. Figure 6.3 shows the locations of displacement measurements, the location of the excitation force, and the corresponding node numbers used in the FE model. The translational displacements were captured at these locations in the X direction.

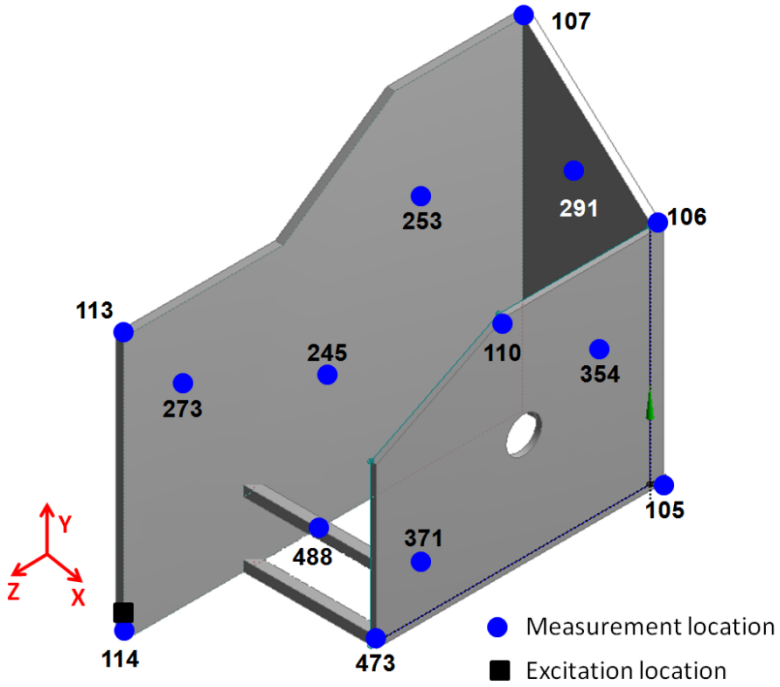

Figure 6.3 Measurement locations on the 1203 structure

The displacement responses at the excitation DOF, in the captured frequency range, for Cases A and B, are shown in Figures 6.4 and 6.5 respectively. It can be observed that, for both cases, the effects of the non-linearity are insignificant after the first 3 modes.

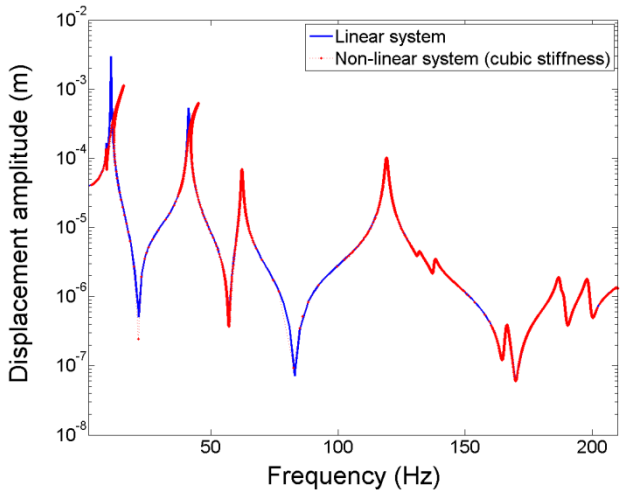

Figure 6.4 Non-linear response for Case A (cubic stiffness non-linearity)

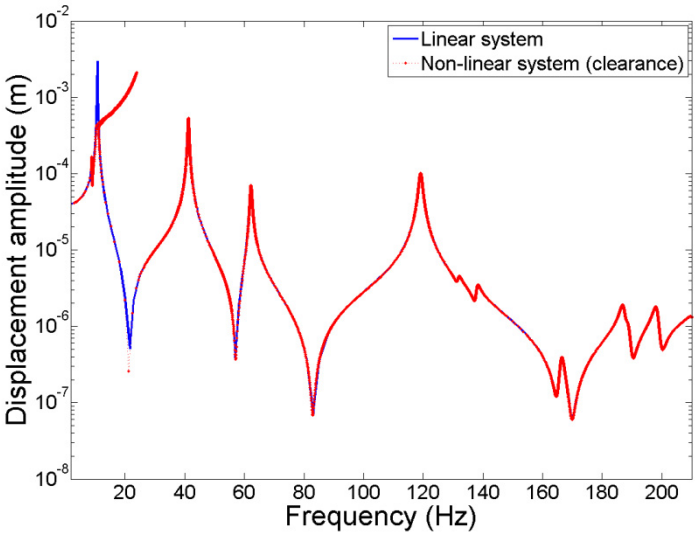

Figure 6.5 Non-linear response for Case B (clearance non-linearity)

Later in the analysis, to evaluate the effects of measurement noise on the accuracy of parameter estimation, the responses were polluted with 5% random noise using (4.15) from Chapter 4.

6.3.2 Input models for different methods

The three methods which are compared in this chapter require a numerical model of the underlying linear structure in different forms. The extent of possible errors in the input models of these methods may also differ in practice. For example, an FE model which is used in one method may be more prone to errors than a response model which is required for the other method. The following section discusses different numerical models which are used as the input for the three methods. It also states the sources and the extent of errors in these models. The levels of errors, at which the methods are to be tested, are decided based on the engineering judgement so as to make a fair comparison.

The spatial method for non-linear parameter identification, presented in Chapter 4, is referred to as 'Method 1' in further discussion for the purpose of brevity. The finite element matrices of the underlying linear structure are used as the input to this method. The errors in FE models can come from the uncertainties in material properties and joint stiffness, or the tolerances on physical dimensions. To evaluate the effect of errors in the input data, it was decided to change the material properties. The Young's modulus of elasticity and the density of the material in the FE model were increased by 4.5% and 3.5% respectively. This resulted in

approximately 1-2% change in the first few natural frequencies. This level of accuracy in FE models can arguably be attained in the updated FE models.

The improved hybrid modal technique (I-HMT), presented in Chapter 5, is referred to as 'Method 2' in further discussion. The modal model of the underlying linear structure serves as the input model for this method. Modal models, which are extracted via an experimental route, are usually incomplete. For the current study, a modal model with the first ten modes (M_r = 10), and measurements at 14 locations on the structure (m = 14) was used. The condition, $m \geq M_r$, required for extracting the non-linear modal vector was met while selecting the modal model. Though the modal analysis tools are well established, only the first few modes are generally identified with good accuracy. Thus, errors in a modal model may arise from the errors in the estimation of modal properties of higher modes of the system. To study the effects of errors in the input model, the natural frequencies and mode shape vectors for identified modes were polluted with a random error of up to 3%. The lower modes, which are generally identified with good accuracy, were polluted with less error.

The FRF based method, presented in Chapter 5, is referred to as 'Method 3' in further discussion. The measured FRF matrix of the underlying linear structure is used as the input to this method. To evaluate the effects of errors in the input model on parameter estimation, the FRF measurements were polluted with 5% random noise. The polluted FRF matrix at each frequency line was calculated using (6.1)

$$\alpha_{ij}{}^{p}(\omega) = (1 \pm cr/100) \times \alpha_{ij}(\omega) \tag{6.1}$$

where, r is a random number ($0 \leq r \leq 1$),

c is the maximum level of noise in percentage,

$\alpha_{ij}{}^{p}$ and α_{ij} are the components of FRF matrix with and without noise respectively.

6.4 Results of non-linear parameter identification for Case A

The three methods were used successively to identify the non-linear parameters for Case A, with cubic stiffness non-linearity. As, the response beyond 50Hz was consistently linear, the frequency range was restricted to 50Hz. Firstly, a clean non-linear displacement response and accurate input models for the three methods were used to identify the non-linear parameters. Methods 1 and 3 were used extract the non-linear force vector, which helps to identify the location of the non-linearity.

Method 2 was used to extract the values of non-linear parameters directly. For Methods 1 and 3, the accumulated non-linear force at the measured DOFs was calculated to locate the non-linearity.

Figure 6.6 shows a plot of the accumulated non-linear force. It is observed that the non-linearity location is correctly identified at node#473 using both methods. Figure 6.7 shows the comparison of the magnitude of non-linear force at the non-linear DOF for Methods 1 and 3.

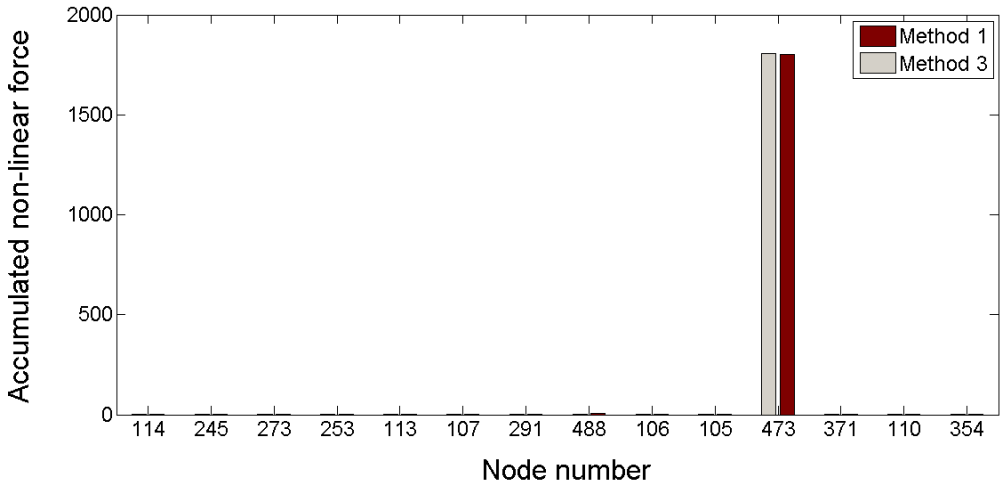

Figure 6.6 Identification of the location of non-linearity for Case A

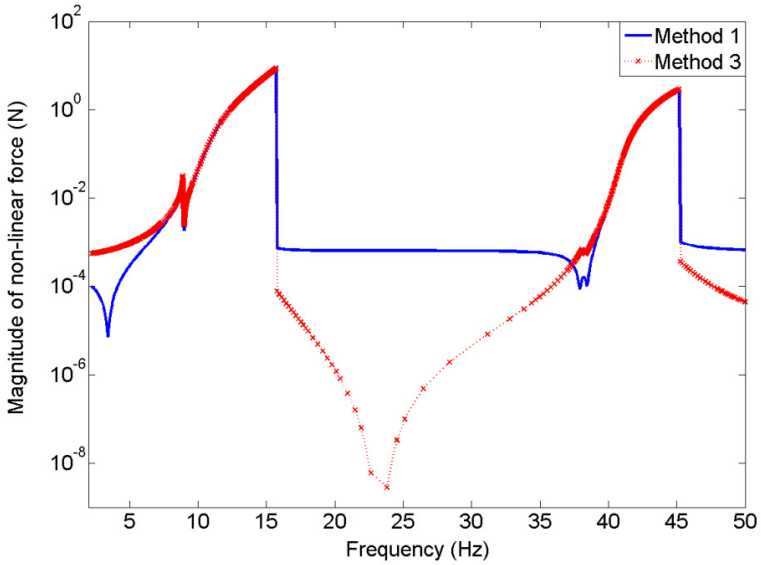

Figure 6.7 Non-linear force at the non-linear DOF for Case A

It can be observed that the values of non-linear force extracted using the two methods differ significantly at the anti-resonances. The values match closely in the vicinity of the resonances. As explained in Chapters 4 and 5, the points in the

vicinity of resonances are to be selected to form the optimization problem. Thus, the difference in the values at anti-resonances will not affect the identification results.

For Method 2, the non-linear modal vector was extracted for the measured modes. This vector implicitly stores the information about non-linear parameters. Figure 6.8 shows the plot of non-linear modal vector for the second mode and the corresponding linear-threshold.

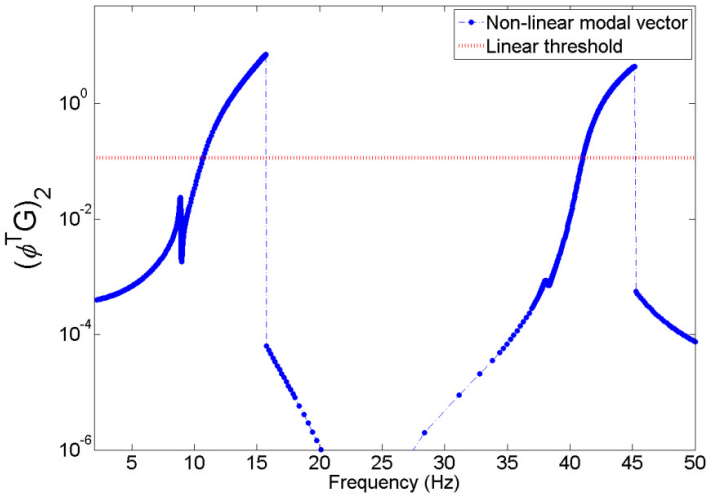

Figure 6.8 Non-linear modal vector plotted for Case A

It is observed that, in the vicinity of the second and the third resonances, the NMV exceeds the linear threshold value. In the vicinity of the first mode, the NMV is consistently below the linear threshold. This indicates that the first mode is behaving linearly while the effect of non-linearity is dominant in the second and the third modes.

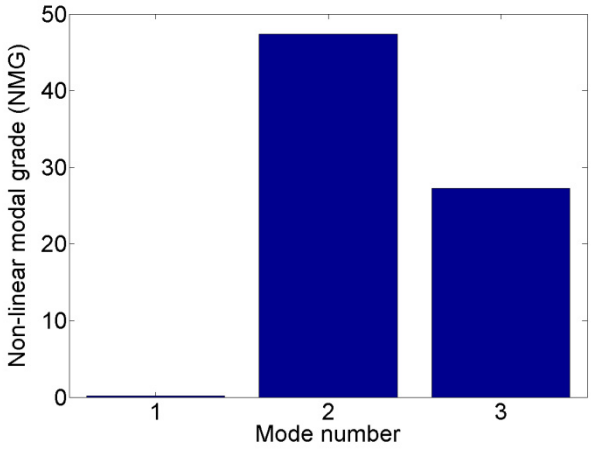

Figure 6.9 Non-linear modal grade (NMG) plot for Case A

This is confirmed by the non-linear modal grade (NMG) plotted in Figure 6.9 for the first three modes. It is observed that Mode 2 is the strongest non-linear mode for this case.

The non-linear parameters were identified using a genetic algorithm optimization. The initial range for the non-linear coefficient, β, was selected to be (0-5×10^{12}) Nm^{-3}, and it was kept the same for all three methods. Table 6.3 shows the summary of the results for clean data and accurate input model.

Table 6.3 Results of parameter estimation for clean measurement data with accurate input models

Method	Identified value of β (Nm^{-3})	Error (%)	Fitness value (%)	Computation time (min)
1	4.986×10^{10}	0.28	98.3	540
2	5.30×10^{10}	6.0	64.6	2.5
3	4.986×10^{10}	0.28	98.3	17

It is observed that the non-linear coefficient is identified very accurately using Methods 1 and 3. For Method 2, the error is the highest at 6%. The computation time required for Method 2 is the lowest amongst the three methods.

To evaluate the sensitivity of the methods to measurement noise, the non-linear response data were polluted with 5% random noise. The identification was performed with noisy data using the three methods. Figure 6.10 shows the extracted non-linear force at the non-linear DOF for Methods 1 and 3.

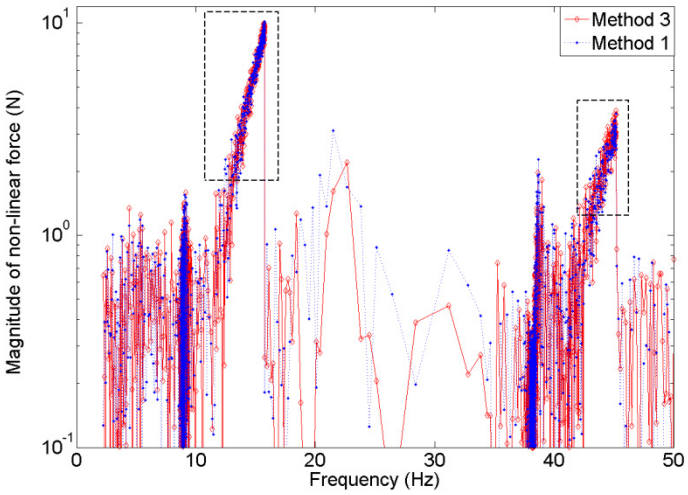

Figure 6.10 Non-linear force plot with 5% measurement noise for Case A

It can be observed that the extracted non-linear force plot is extremely noisy in the region away from the resonances. The non-linear force values in the vicinity of resonances, indicated by the rectangular boxes in Figure 6.10, were used to identify the non-linear parameters. The non-linear modal vector (NMV) was extracted using Method 2. Figure 6.11 shows the plot of the NMV for the 2nd mode in the vicinity of the 2nd resonance. The summary of parameter estimation is given in Table 6.4.

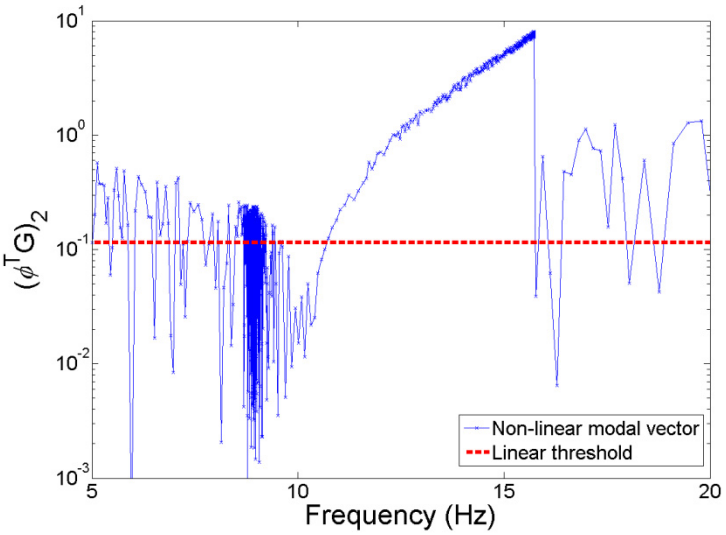

Figure 6.11 NMV for the 2nd mode plotted for Case A with noise

Table 6.4 Estimated non-linear parameter with noise for Case A

Method	Identified value of β (Nm^{-3})	Error (%)	Fitness value (%)
1	5.242×10^{10}	4.84	6.5
2	5.738×10^{10}	14.76	20.3
3	5.197×10^{10}	3.94	7.7

It is observed that the errors in the estimated parameter using Methods 1 and 3 are comparable, and are less than 5%. The error in the estimated parameter using Method 2 is the highest. The fitness value of the objective function used in the optimization process is consistently low for all three methods when compared to the fitness value in case of noise-free identification (Table 6.2). The low fitness value is consistent with the fact that the parameters are identified from noisy data.

To access the performance of the methods with erroneous input models, the corresponding input models for the three methods were polluted with artificial errors as explained in Section 6.3.2. The noise-free responses were used in this case.

Table 6.5 summarizes the estimated parameters for the case of erroneous input models.

Table 6.5 Estimated non-linear parameter with erroneous input models for Case A

Method	Identified value of β (Nm^{-3})	Error (%)	Fitness value (%)
1	5.195×10^{10}	3.90	83.9
2	4.353×10^{10}	12.93	55.6
3	4.819×10^{10}	3.62	7.8

It is observed that Methods 1 and 3 yield accurate values of non-linear parameter even with inaccurate input models. Method 2 identifies the non-linear parameter with around 13% error.

6.4 Results of non-linear parameter identification for Case B

In the second part of the comparison, a more practical case with distributed clearance non-linearity is considered. It is seen from Figure 6.5 that the non-linearity is affecting the response up to 50Hz only. Thus, the frequency range was restricted to 0-50 Hz, covering the first three modes, for the identification exercise.

The displacement response for this case was simulated using four clearance non-linearity elements distributed over the contact area. For the identification of non-linear parameters, the non-linear responses were captured at the same 14 locations as described in Section 6.3.1. It is interesting to note that the measurement was taken at only one out of the four nodes (Node 273), at which the non-linear elements were incorporated. Since all non-linear DOFs were not measured, it was not possible to identify the actual values of parameters which were used to simulate the displacement response. Instead, the equivalent non-linear parameters at the measured DOF were identified. This made it difficult to evaluate the accuracy of the methods, which was done earlier by direct comparison of the identified and actual non-linear parameters.

In this case, the accuracy of different methods was evaluated from the predicted non-linear displacement response using identified equivalent parameters. The error was specified in terms of deviation in the resonant response and the resonance frequency of the strongest non-linear mode.

Accurate input models and noise-free measurements were used firstly to identify the non-linear parameters. The non-linear restoring force vector was extracted independently using Methods 1 and 3. Figure 6.12 shows the accumulated non-linear forces at all measured DOFs. The values of the accumulated non-linear force are mapped on to the corresponding measurement locations on the structure, as shown in Figure 6.13. It is observed that, for the measurement locations which are close to the rubber block region, the values of the accumulated non-linear force are higher. The highest value of the non-linear force is observed at Node 273, one of the nodes at which clearance non-linear elements were placed while simulating the non-linear displacement response.

For Method 2, the non-linear modal vector was extracted for the modes within the measured frequency range. The level of non-linearity in each mode was calculated using the non-linear modal grade for the identified modes. Figure 6.14 shows the plot of the non-linear modal vector for the second mode, as well as the plot showing non-linear modal grades for the first four modes.

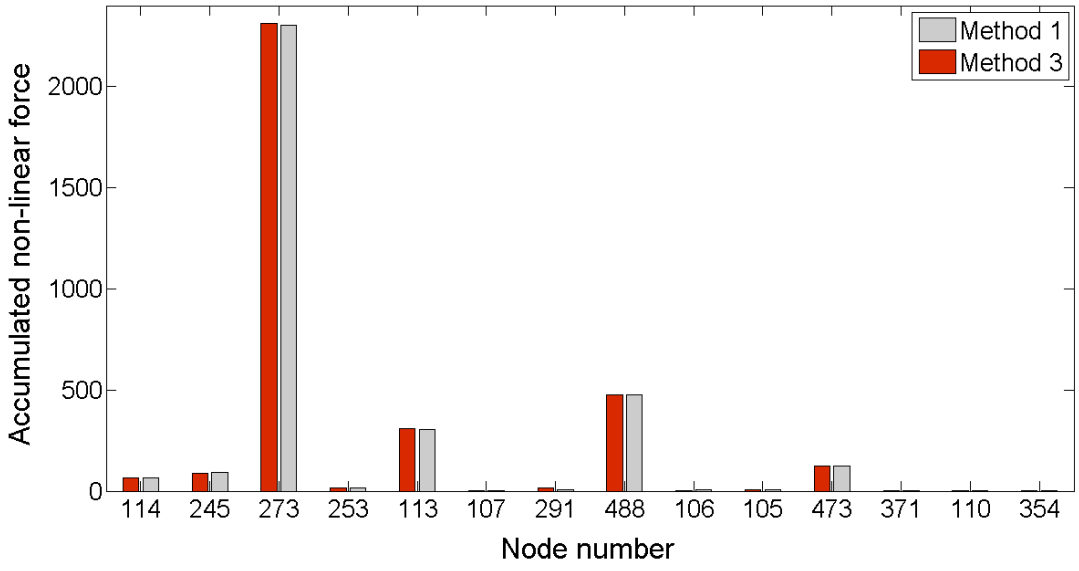

Figure 6.12 Accumulated non-linear force at measured DOFs for Case B

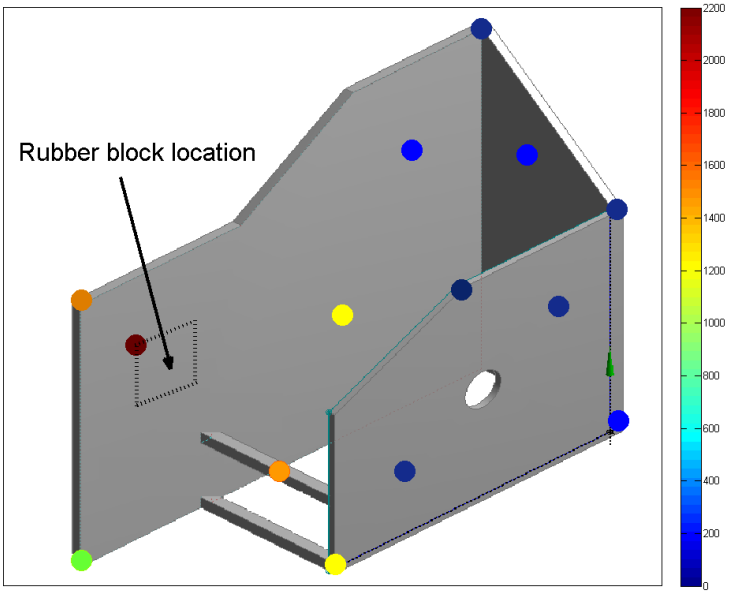

Figure 6.13 Accumulated non-linear force mapped on measurement locations

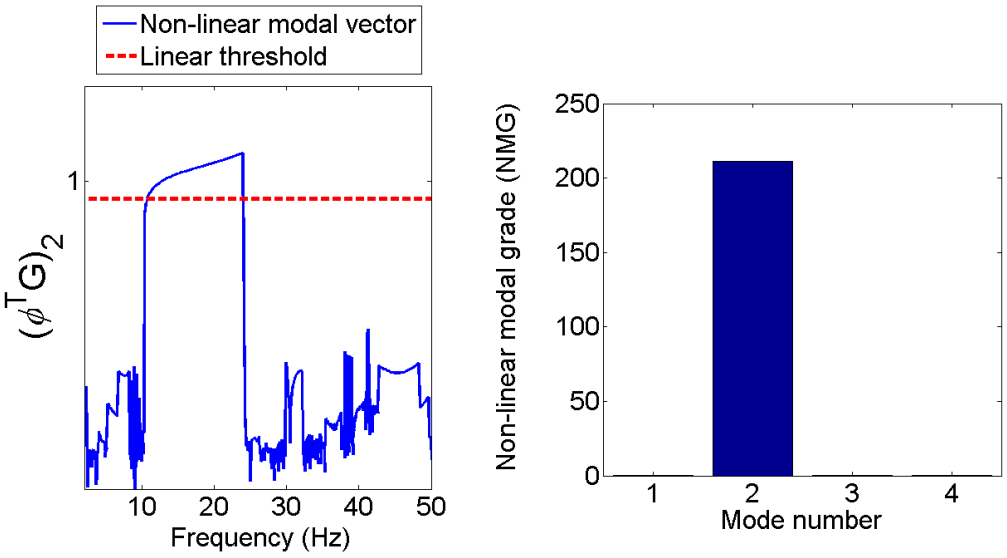

Figure 6.14 NMV and NMG plots for Case B

It is observed that the second mode is highly non-linear with NMG value reaching 200, whereas the other identified modes behave almost linearly. This information is useful while selecting the frequency lines to formulate the optimization problem in the later stage of the non-linear parameter identification process.

The non-linear parameters were identified using the non-linear force at the non-linear DOF for Methods 1 and 3, and using the non-linear modal vector for Method 2. The initial parameter ranges for the genetic algorithm were kept the same for all three methods. The initial range for the clearance gap was selected to be 0-1

mm, and it was selected to be 0-200 KN/m for the stiffness. Table 6.6 summarizes the results of the parameter estimation.

Table 6.6 Estimated parameters with accurate input models and without measurement noise for Case B

Method	Identified parameters		Fitness value (%)	Computation time (min)
	y_c (mm)	K_z (KN/m)		
1	0.4296	85.156	24.06	600
2	0.4531	103.52	54.50	5.5
3	0.4375	87.5	38.85	25

To evaluate the effects of noise in measurement data, the responses were polluted with 5% random noise. The identification was carried out in the presence of noisy data. Similarly, to evaluate the effects of erroneous input models, artificial deviations were introduced in the inputs models as described in Section 6.3.2. Figures 6.15 and 6.16 show the extracted non-linear force at Node 273 plotted against the displacement amplitude at the same node for Methods 1 and 3 respectively.

It is observed that, between the two methods, there is small difference in the values of extracted non-linear force. This difference will eventually lead to the differences in the identified non-linear parameters. It is noticeable in both figures that the values of non-linear force are close to zero until the amplitude of displacement reaches 0.4mm, identifying the value of clearance distance, y_c. Table 6.7 summarizes the estimated non-linear parameters for these cases for all three methods.

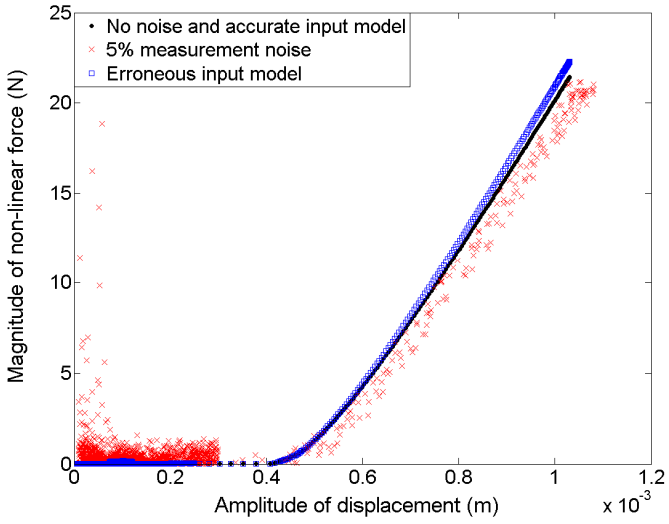

Figure 6.15 Comparison of non-linear force for Method 1

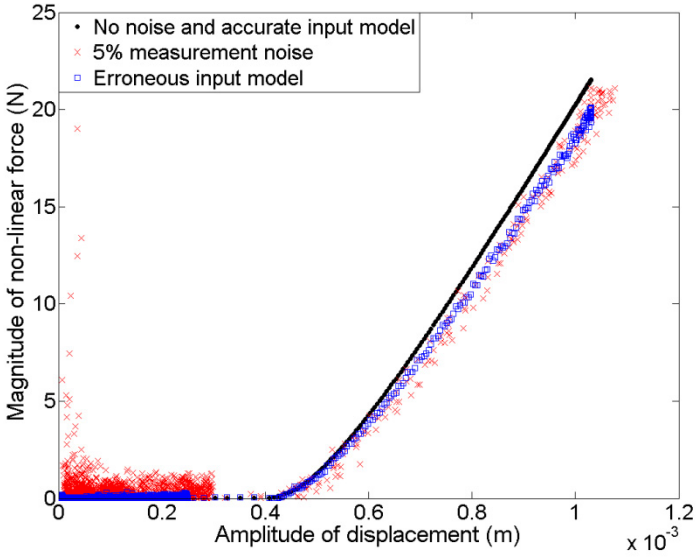

Figure 6.16 Comparison of non-linear force for Method 3

Table 6.7 Summary of estimated non-linear parameters for cases of noisy data and erroneous input models for Case B

Method	**Noise in measured data**	**Errors in input model**
	Estimated parameters $\{y_c$(mm), K_z (KN/m)$\}$	Estimated parameters $\{y_c$(mm), K_z (KN/m)$\}$
1	{0.414, 74.218}	{0.437, 90.625}
2	{0.453, 105.86}	{0.484, 100}
3	{0.469, 87.11}	{0.438, 79.69}

As discussed earlier, in this case of distributed clearance non-linearity, the values of the identified parameters for different cases give no conclusive information about the accuracy of parameter estimation. The accuracy of all three methods is to be evaluated by comparing the deviations in resonance frequency and resonance amplitude at a particular location on the structure, and for the strongest non-linear mode. The deviations were compared at Node 114 (the excitation location), and for the second mode, which is strongly non-linear. Figure 6.17 depicts the calculation of errors. The errors in prediction of resonance frequency and resonance amplitude are recorded in Table 6.8.

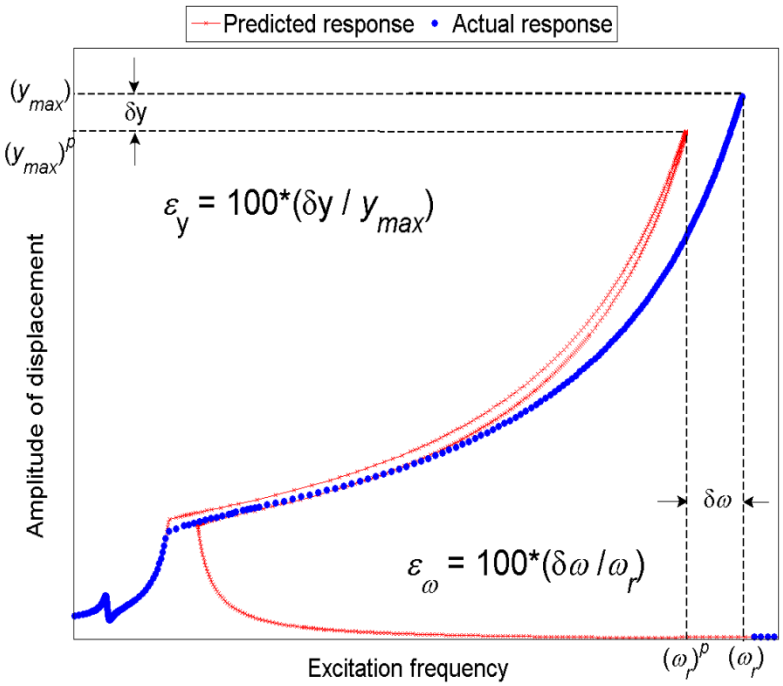

Figure 6.17 Depiction of calculation of errors for Case B

Table 6.8 Summary of errors in resonant response and resonance frequency

Method	No noise and accurate input models		Noise in displacement measurements		Errors in input models	
	ε_y (%)	ε_ω (%)	ε_y (%)	ε_ω (%)	ε_y (%)	ε_ω (%)
1	3.78	6.68	1.71	7.54	4.55	6.36
2	6.08	5.72	6.45	5.57	3.71	6.71
3	3.45	6.82	2.01	7.42	1.94	7.44

It is observed from Table 6.7 that there is no trend in the error propagation due to either noisy measurements or erroneous input model. The error in the prediction of response is consistently higher for Method 2. It is also observed that the resonance frequency is predicted less accurately than the resonance amplitude for this case. The average value of errors in resonance frequency and resonance amplitude are 3.7% and 6.7% respectively, which are within acceptable limits for practical cases.

6.5 Discussion and concluding remarks

The three methods for non-linear parameter identification, presented earlier in the thesis, have been compared on common ground using different criteria. Simulated data obtained for the '1203 structure', modelled using FEM with around two thousand DOFs are used. Two cases with increasing complexity have been used for the comparison. In the first case, an idealized grounded cubic stiffness non-linearity is used, while in the second case, a more realistic clearance non-linearity over an area of the structure is implemented. The identification of the non-linear parameters has been carried out for both cases using the three methods to compare the accuracy of parameter estimation. The conclusions of the comparison study are listed below:

- It has been observed that, for all three methods, errors in the estimated parameters are low when noise-free data along with an accurate input model of the underlying linear structure are used. The effects of measurement noise and erroneous input models are similar, to increase the error in parameter estimation. It has been observed that the error increases by 5-9% depending on the method.
- For all cases considered in this exercise, errors in the estimation of parameters using Method 2 are found to be higher than when using the other two methods. Method 1 has been found to identify the non-linear parameters accurately, even with an erroneous FE model. It should be noted though; that the amount of error in the underlying FE model, for which the method is tested, is very low. This can only be achieved after successfully updating the FE model.
- It has been observed that Methods 1 and 3 possess the ability to locate the non-linearity in the structure. Method 2 fails to locate the non-linearity, if the location is unknown beforehand. This can sometimes put limitations on the use of the method. On the positive side, Method 2 has successfully quantified the level of non-linearity in each mode within the measured frequency range. This information is useful at the later stage of parameter identification, for selecting frequency lines to form the optimization problem.
- The computation times taken by the three methods are an order of magnitude apart. Method 2 is the fastest of the three taking 2-orders of magnitude less time than Method 1. Method 1 involves the inversion of a matrix of the size of the number of un-measured DOFs, at each frequency line. For practical structures where only few percent of the total number of DOFs are measured, the matrix may become very large, making the computation inefficient. Method

3 consumes slightly more computation time than Method 2, but the order of magnitude is comparable. For Method 3, the computation time is directly proportional to the number of measured DOFs. Thus, the time can be reduced by using fewer measurements.

- It has been noted that the deviation in the predicted response, as a result of errors in non-linear parameters, is a function of the sensitivity of the structure to those errors. For a less sensitive or a more *robust* structure, large errors in non-linear parameters will probably yield a small deviation in the predicted response. Thus, the errors in the parameter estimation should be viewed keeping in perspective the robustness of the structure. Methods for calculating the sensitivity and robustness of forced response for non-linear structures are proposed in [118].

Based on the importance of different criteria for an engineer in his day to day applications, a weighing factor can be assigned for each criterion. For example, since having clean data and accurate input models may be a rare event in practice, it can be given less weighing factor as against the performance of the methods with noisy data and inaccurate input models. This approach of assigning the weighing factor for each comparison criteria is subjective, and depends on what user wants from the identification method.

A similar weighed evaluation is performed for the three methods to illustrate the process. Table 6.9 shows a summary of the performance of the methods quantified based on different evaluation criteria, weighing factor used for each criterion, and the total score for each method. Every method is scored on a scale of 0-3 for each criterion. With the weighing factors assigned in the current study, the FRF based method (Method 3) comes on top, providing the right mix of accuracy and computational efficiency. The method uses all raw inputs directly obtainable from vibration measurements. This eliminates the need of sophisticated tools like FEA and modal analysis at the stage of parameter identification.

Table 6.9 Quantitative comparison of the three methods

Criteria	Weighing factor	Method		
		Spatial method (Method 1)	Improved hybrid modal technique (Method 2)	FRF based method (Method 3)
Performance with clean data and accurate input models	0.05	3	2	3
Performance with clean data and erroneous input models	0.25	3	2	3
Performance with noisy data and accurate input models	0.25	3	2	3
Computation time	0.1	1	3	2
Ability to locate non-linearity	0.1	3	1	3
Ability to quantify non-linear modes	0.2	1	3	1
Ability to extract non-linear force explicitly	0.05	3	1	3
Total Score		2.4	2.15	2.5

Chapter 7

Experimental investigation of non-linearities in MACE structure

This chapter presents an experimental investigation of non-linearities in a complex mechanical structure. A sub-assembly of the so-called MACE structure is studied in detail. Different non-linearity detection techniques are used to detect the presence of non-linearity. The location and the type of non-linearity are identified using the non-linearity characterization techniques presented in the earlier chapters. Both parametric and non-parametric models are fitted into experimental data to describe the non-linear behaviour of the sub-assembly. The models are then used to predict the system response at different excitation levels.

7.1 Introduction

Different strategies for non-linear system identification have been proposed and compared in the earlier chapters of this thesis. The illustration of the methods and their comparison has been performed on simulated data. It has been mentioned in Chapter 6 that validating the proposed methods with experimental data on a realistic structure poses some additional challenges. This chapter attempts to tackle such challenges using experimentally measured vibration data. The main aim of this study is to improve the understanding of real-life non-linear structures and to gauge the scope and applicability of the proposed non-linear system identification strategies in such cases.

7.1.1 Choice of the structure

There are attempts in the literature to identify the non-linearities from vibration data measured on representative structures [3, 26, 101, 119]. The structures used in these exercises were intentionally designed to exhibit pure forms of non-linearities,

like polynomial stiffness, clearance etc. To meet the aim of the current study, it was decided to use a practical real-life structure, or at least a structure which employs joints and connections which are encountered in practice.

AWE-Aldermaston UK, in their modal coupling research program (MCRP), designed and used a structure called MACE. This structure has been specifically designed to contain different interfaces, connections and joints which are found in real engineering applications [97]. Figure 7.1 shows an annotated view of the MACE structure. Different research groups have collaboratively worked on model updating of this structure. Most studies have been restricted to small vibration amplitudes, treating the structure behaviour as linear [63].

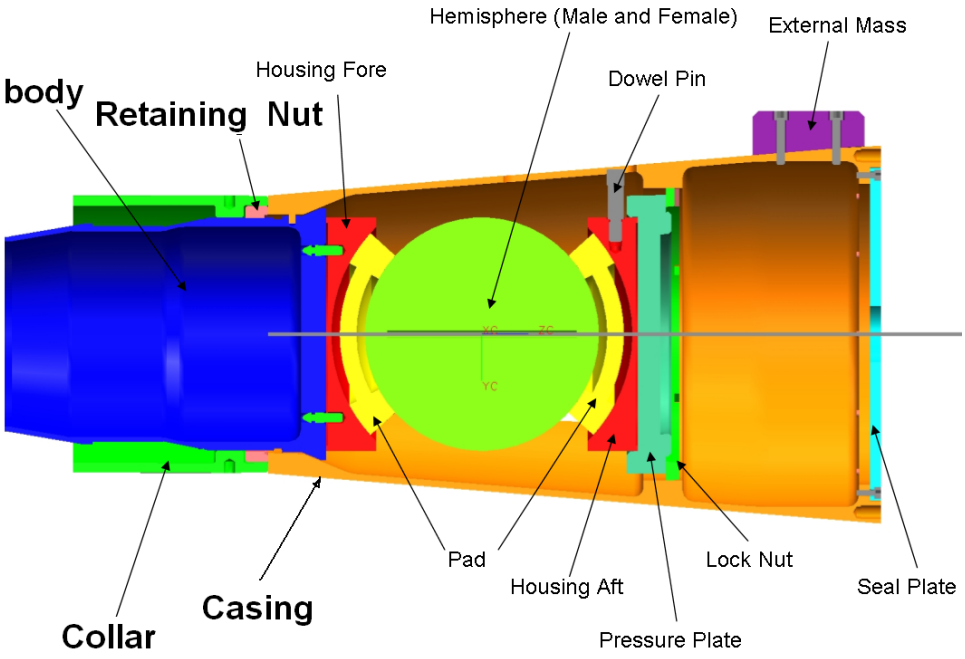

Figure 7.1 Computer-generated drawing of the MACE structure

A sub-assembly of the MACE structure, called Sub-assembly 3, is used for the current exercise. Sub-assembly 3 consists of four parts: body, collar, retaining nut and casing.

7.1.2 Description of joints in Sub-assembly 3

Sub-assembly 3 has four joints between different components. Figure 7.2 shows a schematic of Sub-assembly 3, clearly indicating the joint locations. Two of the joints are screw joints and the other two are surface-to-surface joints. Table 7.1 describes the joints in Sub-assembly 3. If the components are assembled together with the design torque of 28 Nm, all joints can be assumed to be locked under low-amplitude

excitation. At higher excitation amplitudes, the two surface-to-surface joints may exhibit non-linear behaviour due to clearance, or friction type of non-linearity.

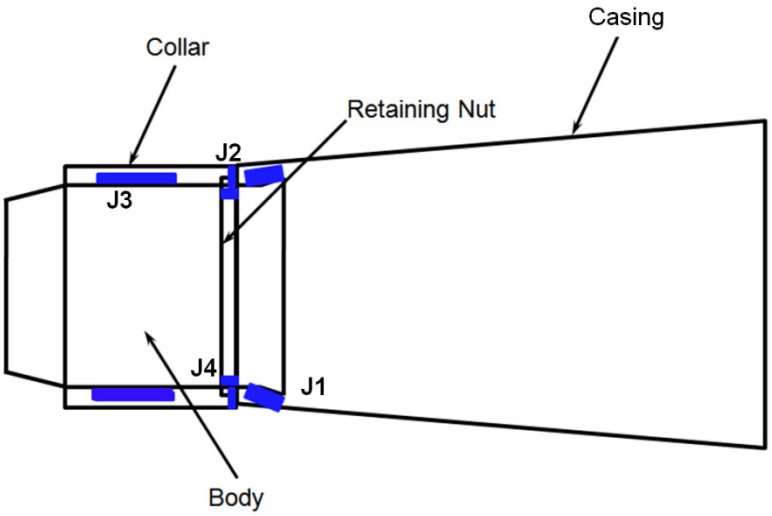

Figure 7.2 Schematic of Sub-assembly 3

Table 7.1 Description of joints in Sub-assembly 3

Joint Number	Part 1	Part 2	Description
1	Casing	Body	Conical surface to surface joint
2	Casing	Collar	Annular surface to surface joint
3	Collar	Body	Screw joint
4	Body	Retaining nut	Screw joint

7.1.3 Objectives of the exercise

Based on the aim of this study mentioned in Section 7.1, the specific objectives are identified as follows:

(i) To detect the presence of non-linear behaviour in the structure.

(ii) To collect qualitative information about any non-linear behaviour. This can be in terms of the extent of non-linearity, the effects on the resonance frequencies and resonance amplitudes, the contribution of higher harmonics etc.

(iii) To understand the challenges in non-linear vibration testing and to find the ways to perform vibration measurements on non-linear structures efficiently using the standard tools.

(iv) To attempt to locate the non-linearity, to extract the non-linear restoring force, and to estimate the non-linear parameters using the proposed methods.

7.2 Validation of the FE models

To obtain a numerical model of the underlying linear structure, the components were modelled using the FEM in ANSYS. The FE models of the three components, the casing, the collar, and the body, were meshed using 3-D, 10-noded tetrahedral elements (SOLID 187) with 3 DOFs per node. The retaining nut was not modelled separately in this analysis, as it has insignificant mass compared to the other components, and it would not add any significant stiffness to the system [63]. The mesh size for the individual components was decided after checking the convergence. Figure 7.3 shows a picture of three component meshes. The details of material properties used for the components and the mesh sizing are given in Appendix D.

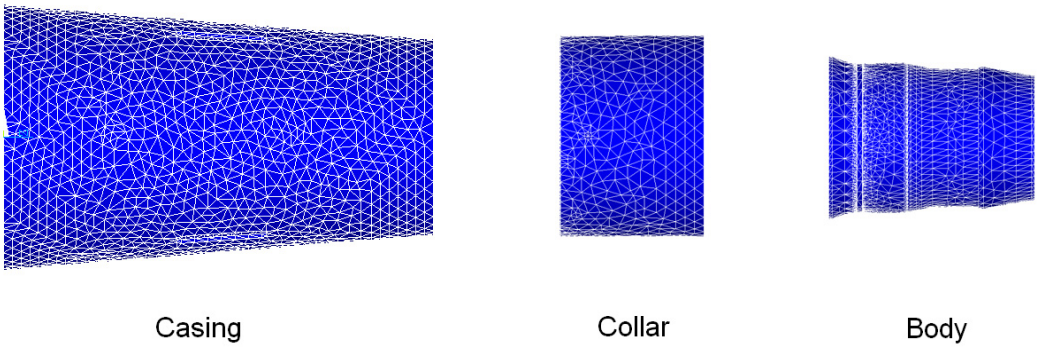

Figure 7.3 FE models of the individual components

Modal properties for the individual components, in free-free condition, were obtained by performing modal analysis on the FE models. The components were also tested experimentally to find the modal properties using experimental modal analysis (EMA). The global-M method, available in MODENT-2006 [117], was used for the EMA. Because of axial symmetry of the components, double modes were obtained at each natural frequency. Only one mode from the pair was used for the comparison. The frequency range was restricted to 0-1000 Hz for the comparison. Table 7.2 shows the results of the correlation between the FE models and the EMA.

Table 7.2 Correlation of modal properties for individual components

Component	Mode	Natural frequency (Hz)		Discrepancy (%)	MAC
		FEA	EMA		
Casing	1	584.8	585.7	0.15	0.98
	2	712.1	706.9	0.74	0.97
	3	1327.5	1328.4	0.07	0.99
Collar	1	515.4	513.1	0.45	0.96
	2	854.3	826.7	3.33	0.92
	3	1285.9	1301.0	1.16	0.87
Body	1	538.9	537.3	0.3	0.84
	2	1197.5	1174.2	1.9	0.80

It is observed from Table 7.2 that the maximum discrepancy in the prediction of natural frequencies using the FE models is around 3%. The minimum value of modal assurance criteria (MAC) is 0.8. The low MAC value for some modes can be attributed to the presence of double modes due to symmetric nature of the structure. While identifying the modes via modal analysis, only one mode at a frequency was identified. The correlation shows that the FE models of the individual components are accurate enough for dynamic response predictions.

After obtaining the accurate FE models for the individual components, the components were assembled together in ANSYS. In an ideal condition, all joints are locked with no relative motion between the components. This condition was simulated by using the option of bonded-contact, available in the ANSYS software. The modal properties of the assembly were obtained by performing modal analysis on the assembled FE model. Figure 7.4 shows the first twelve modes obtained via FEA of the assembly.

To perform EMA on the assembled structure, the structure was suspended freely using elastic cords. The FRFs were calculated by measuring the response at one location and exciting the structure at several locations using an instrumented hammer. The FRFs acquired with the excitation location on one side of the joints and the response location on the other side, were found to be noisy. Because of the poor transmissibility of force across the joints, all measurement locations were selected from the Casing-side of the joints. This put a limitation on the number of observable modes through the EMA. The modes which are local modes of the body could not be identified. The modal properties were extracted using the multi-FRF global-M method. Figure 7.5a shows the direct FRF plot along with the phase for the

assembled structure to give an idea regarding the quality of measurements. The overlaid FRF measurements obtained via hammer testing are shown in Figure 7.5b.

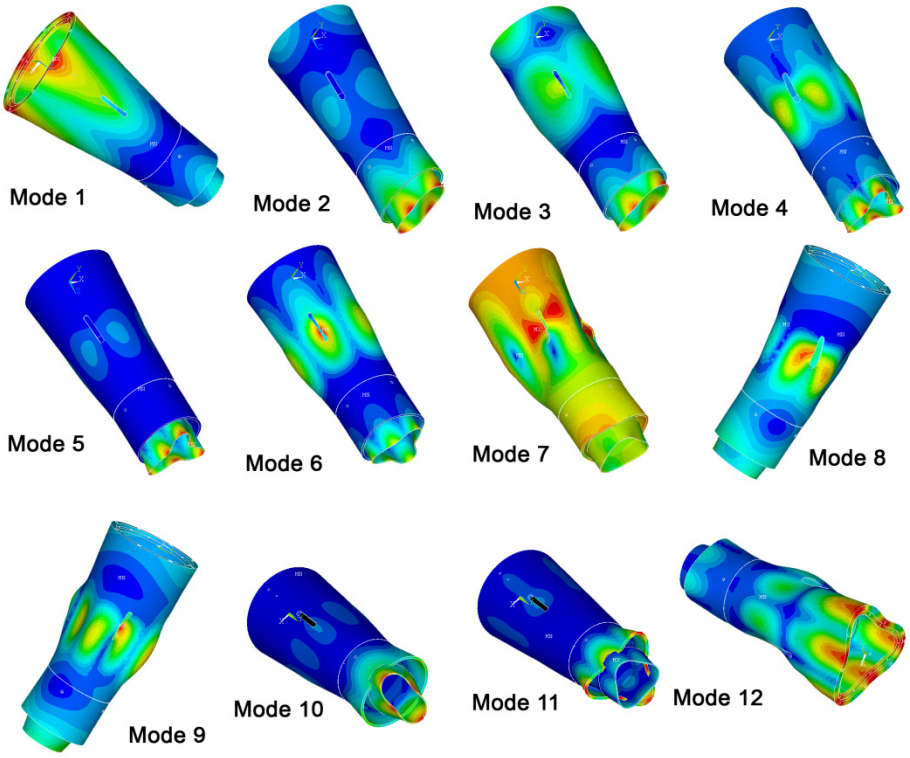

Figure 7.4 Mode shapes of the assembled structure via FEA

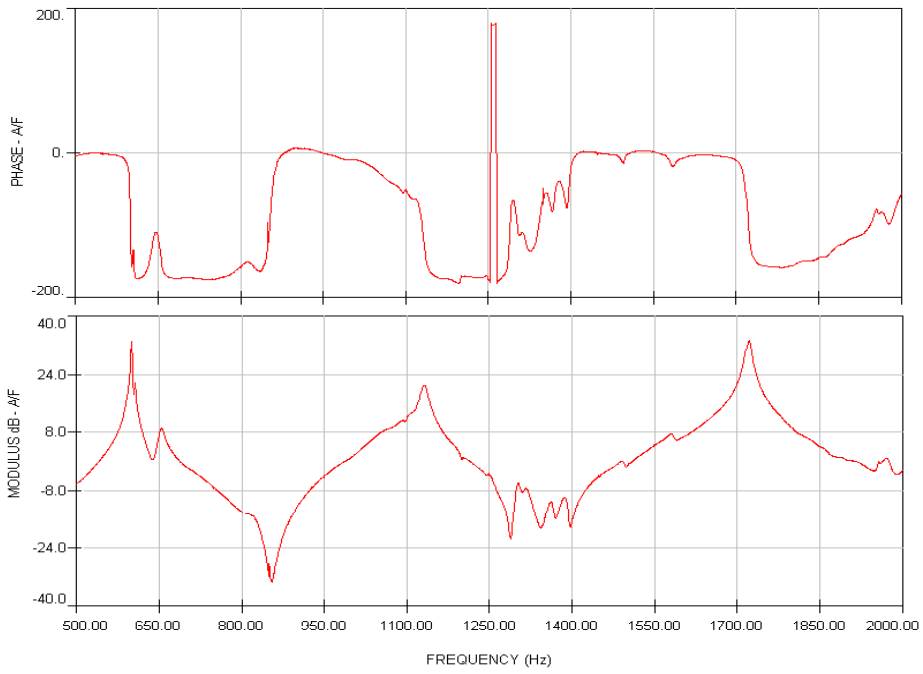

Figure 7.5a Point FRF plot for the assembled structure (hammer test)

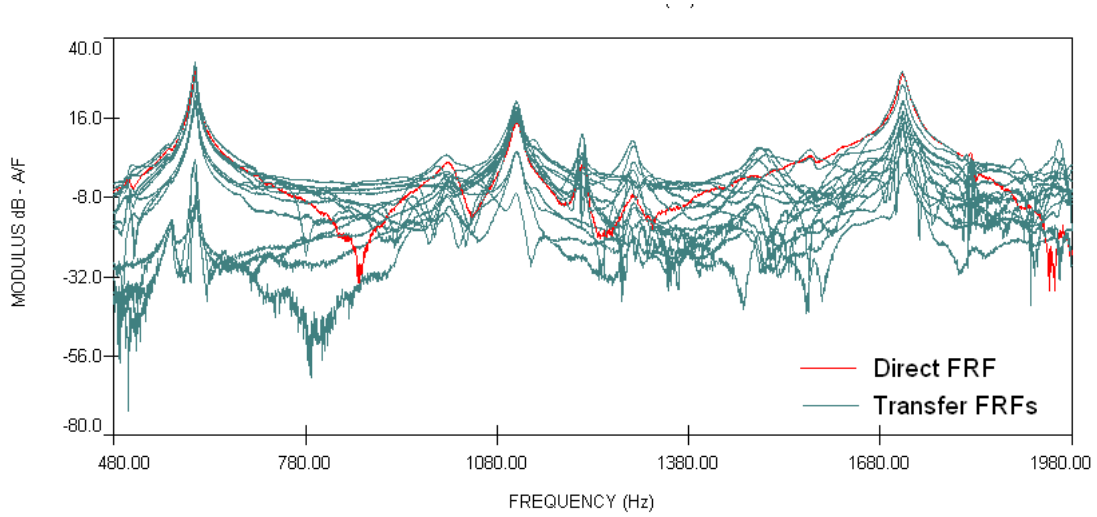

Figure 7.5b Overlaid FRFs for the EMA on the assembled structure

The modal properties of the assembled structure, extracted using the FEA and the EMA, are compared in Table 7.3. It is observed that the difference in natural frequencies is much higher than the difference observed in the correlation of individual components. The maximum difference is around 15% for Mode 7. The MAC values for the correlated modes are also lower when compared to the results with the individual components. The high discrepancy suggests that the assumption of locked joints used in the FE model may not be valid.

Table 7.3 Comparison of the modal properties of the assembled structure

Mode	**Natural frequency (Hz)**		**Discrepancy**	**MAC**
	FEA	EMA	**(%)**	
1	610.6	607.5	0.51	0.89
2	976.6	1002.5	2.58	0.67
3	1231.3	1110.4	10.89	0.75
4	1278.0	1211.3	5.51	0.69
5	1306.9	-	-	-
6	1361.8	-	-	-
7	1486.7	1292.4	15.03	0.59
8	1504.1	-	-	-
9	1578.6	-	-	-
10	1593.2	-	-	-
11	1615.5	-	-	-
12	1725.2	1715.0	0.59	0.93

The results can further be improved via model updating, or by using some interface elements at the joint locations. The interface elements can be linear as implemented in [63]. If the structure happens to be non-linear, the use of linear interface elements will result in an equivalent linear model of the assembly at a particular excitation level.

7.3 Detection of non-linear behaviour

Inherently, all assembled structures are non-linear to some extent. If the nominal operating conditions are such that the structure does not exhibit any non-linear behaviour, it is usually safe to use an equivalent linear model of the structure for response predictions. It is therefore necessary to check if the structure is behaving non-linearly in the operating range of excitations.

For linear vibration testing, impulse and random excitations are popular, because they are less time consuming. For non-linear systems, the use of impulse or random excitation tends to linearize the system about the operating point. On the other hand, stepped-sine excitation, though time-consuming, is recommended for non-linear systems [2, 120]. Most of the methods for non-linearity detection do not make use of the mode shapes of the system. Thus, responses at only a few locations are sufficient for non-linearity detection. In the current study, the responses at the excitation location under different excitation levels are used to detect non-linear behaviour.

7.3.1 Problem of force-drop near resonance

It has been stated in the literature [6, 7] that, with a constant supply of input current to the exciter, the input force may vary with the excitation frequency. A drop in the input force is usually observed when the excitation frequency is close to any of the system's resonance frequencies. For linear systems, since the ratio of response over force is of primary interest, the force-drop phenomena can be overlooked. On the other hand, for non-linear systems, if the input force is not kept constant, the non-linearities are not exhibited properly. This may lead to erroneous system identification. Figure 7.6 shows the force-drop phenomena, which was observed for the MACE structure sub-assembly.

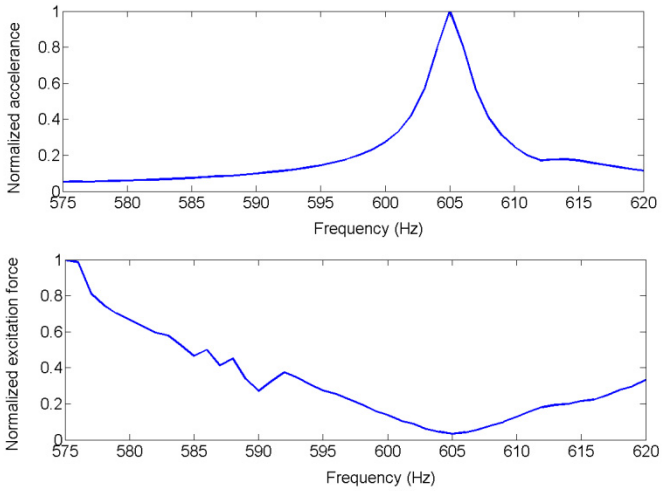

Figure 7.6 Force drop near resonance for the MACE sub-assembly

The direct FRF of the sub-assembly, around the first resonance, was measured at different excitation levels with step-sine tests without force control. Figure 7.7 shows the overlaid FRFs at different excitation levels. It can be seen from Figure 7.7 that the FRFs at different excitation levels do not overlay perfectly, indicating the presence of non-linearity. Thus, the non-linearity can be detected at a very early stage, even without maintaining a constant value of the input force. But to characterize the non-linearity type and to identify the non-linear parameters, the step-sine tests with force control are required [2, 6, 7].

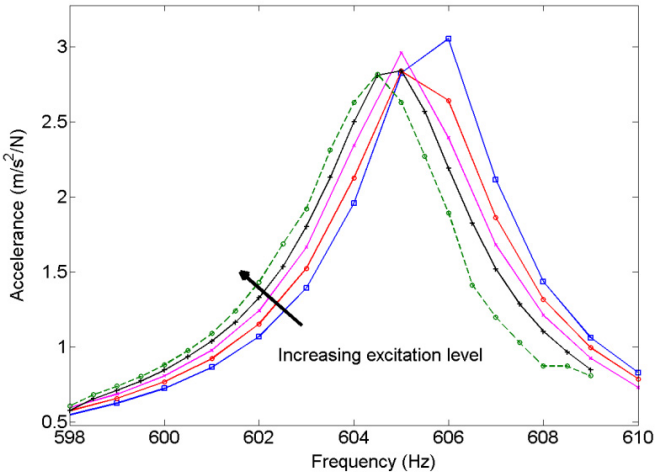

Figure 7.7 Overlaid FRFs at different excitation levels without force-control

The control algorithm used in the current research, to keep the input force constant, is an iterative algorithm using the Newton Raphson method [101, 107]. Figure 7.8 shows the flowchart for the algorithm used. An in-house control system [101],

developed in the Lab-view software which implements this algorithm, was used to carry out the force-controlled step-sine tests on the MACE sub-assembly.

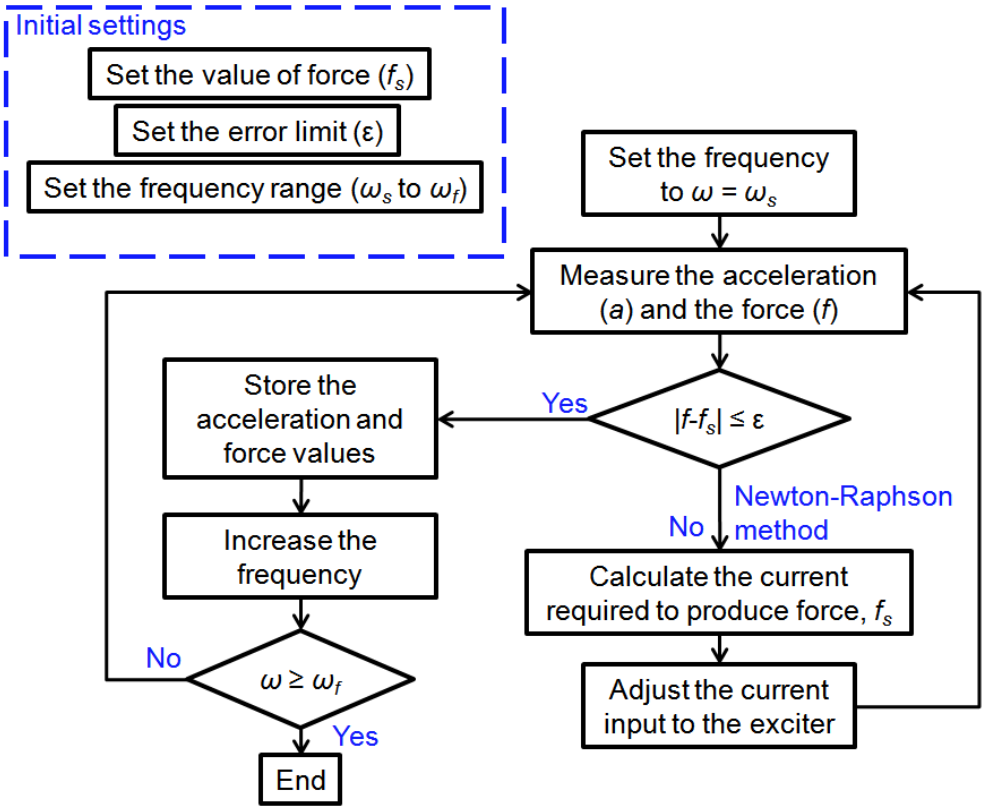

Figure 7.8 Flow chart for the force-control algorithm

7.3.2 Non-linearity detection with constant-force step-sine tests

The control algorithm discussed in Section 7.3.1 was used to perfom constant-force step sine tests on the MACE sub-assebmly. Figure 7.9 shows the experimental set-up used for the experiment.

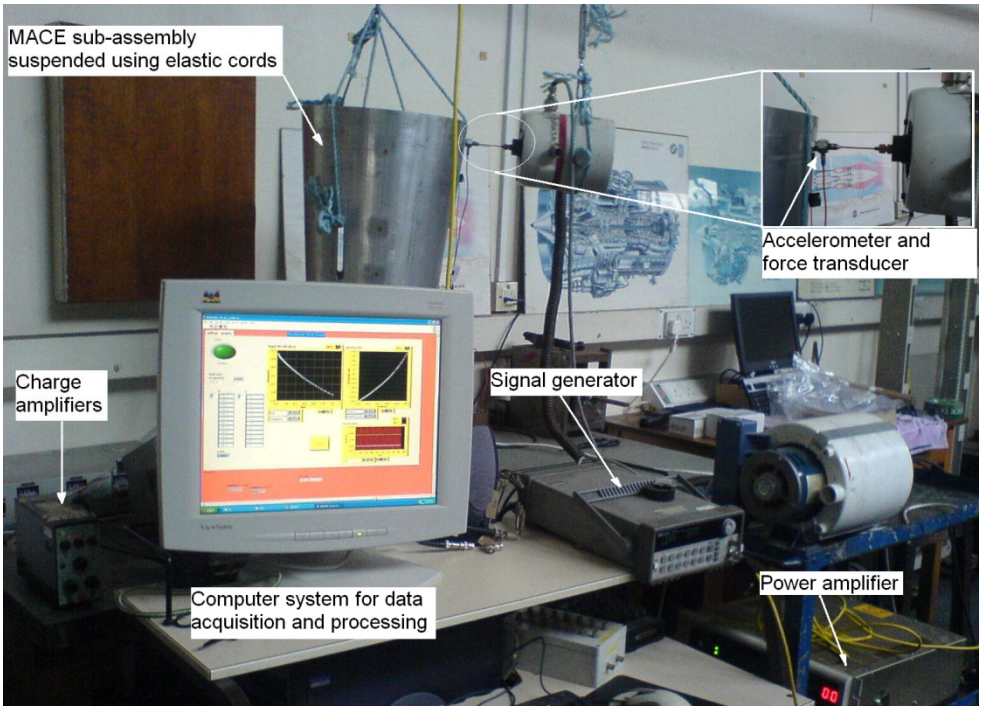

Figure 7.9 Experimental setup for non-linear step-sine testing

Since during the initial hammer testing it was observed that the first mode of the sub-assembly was the most dominant mode, the detection, characterization and parameter estimation of non-linearities were performed using the response around this mode.

For the detection of non-linear behaviour, the response at the excitation location was measured at different levels of excitation. Figure 7.10 shows the overlaid FRFs at different excitation levels. It can be seen that the value of accelerance drops continuously with increase in the force level. This suggests a non-linear behaviour with energy dissipation. The resonance frequency is observed to be reducing slightly with the increasing force level.

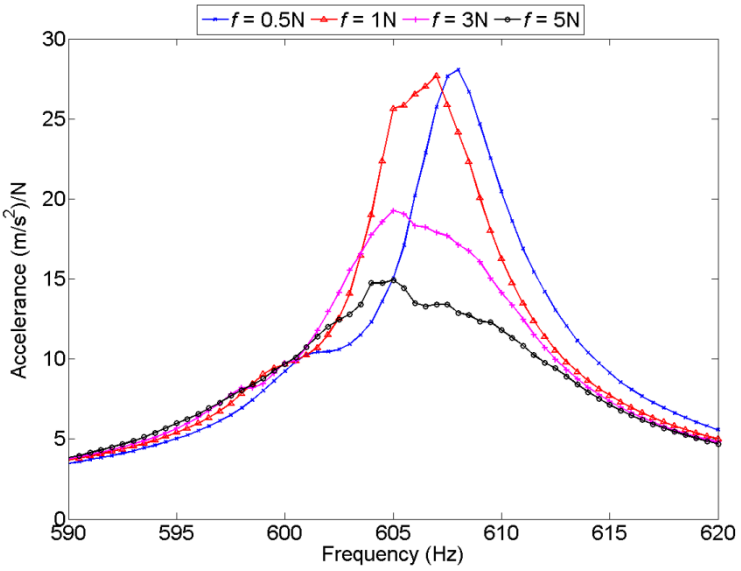

Figure 7.10 Overlaid accelerance at different excitation levels with force-control

The Nyquist plots for the same FRFs are overlaid in Figure 7.11. It can be observed from Figure 7.11 that as the excitation amplitude increases, the Nyquist plots become more elliptical. The presence of double modes, as discussed in Section 7.2 can be observed from the Nyquist plots in Figure 7.11.

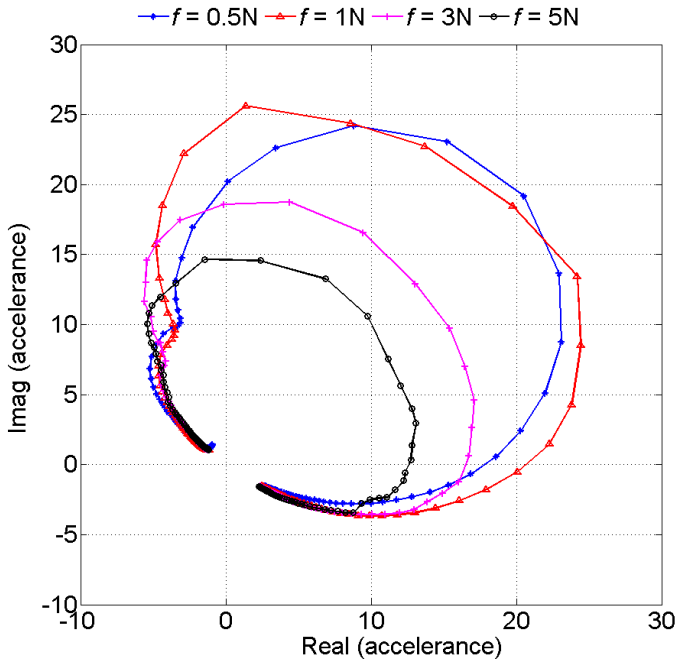

Figure 7.11 Nyquist plots for accelerance at different excitation levels

The presence of higher harmonics in response is also an indicator of non-linear behaviour of a system. In conventional vibration tests, spectral analysers calculate FRFs by considering the fundamental harmonics only in the time-domain response.

To capture higher harmonics during the tests, raw time signals of the response were acquired, and Fourier analysis was performed on the signals externally.

Figure 7.12 shows the contribution of the higher harmonics in the signal captured at the resonance frequency for the excitation force of 10N. The presence of higher harmonics is clearly visible from the figure. Figure 7.13 presents a bar chart showing the amplitudes of the second and third harmonic components, at the resonance frequency, for different values of excitation force. The amplitudes are normalized to the fundamental harmonic component at each force level. From Figure 7.13, it can be seen that, at higher excitation levels, the contribution of the 2nd and the 3rd harmonic components in the signal is significant, reaching to almost 20% of the fundamental harmonics at 10N excitation force. The higher contribution of 2nd harmonic component may suggest a symmetric nature of non-linearity.

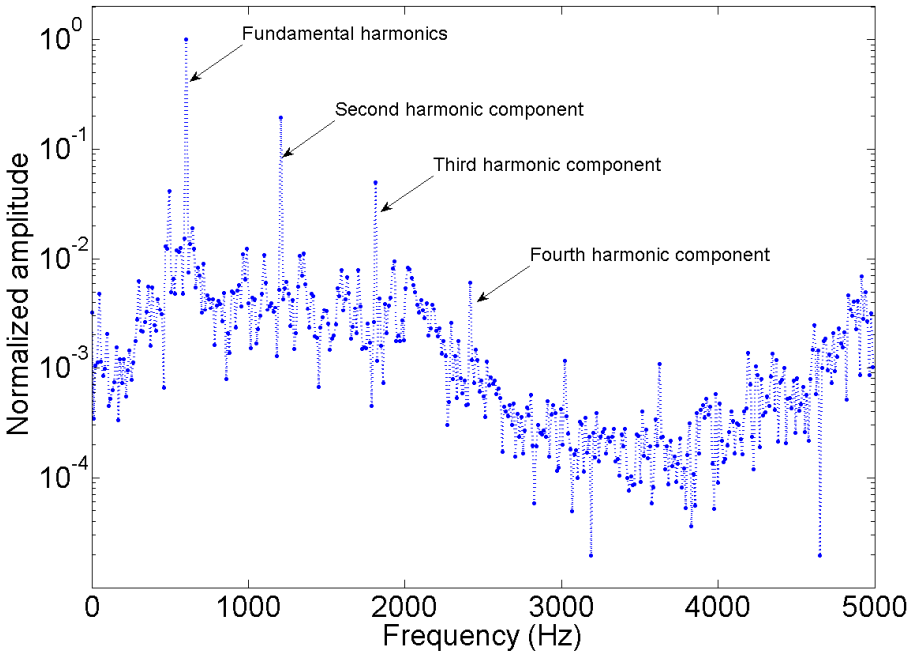

Figure 7.12 Presence of higher-harmonics in the response at 10N force level

After checking the system with different non-linearity detection techniques, it is concluded that the sub-assembly behaves non-linearity at higher excitation amplitudes.

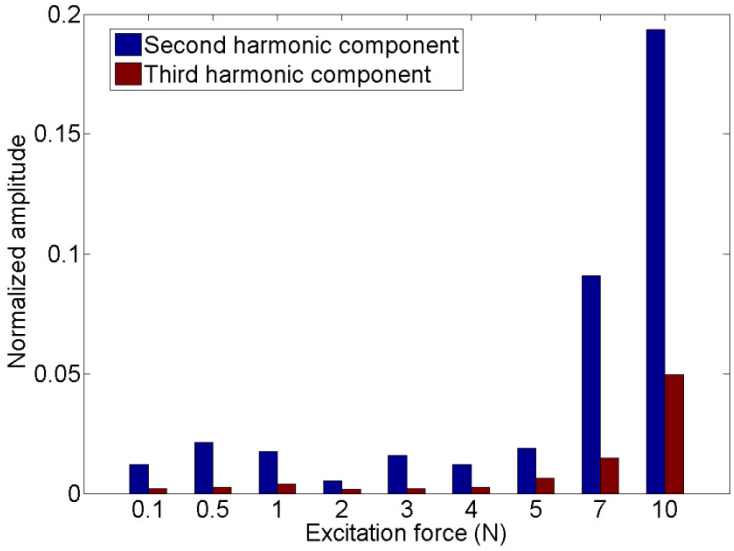

Figure 7.13 Contribution of the higher harmonics at different excitation levels

7.4 Characterization of the non-linearity

Once it is verified that the MACE sub-assembly behaves non-linearly at high excitation levels, the next stage is to find the location of non-linearity and to identify the probable type of non-linearity. These tasks traditionally come under the realm of non-linearity characterization.

At this stage of non-linear system identification, an accurate set of response measurements at several locations distributed over the structure are required. Because of the poor transmissibility of force through the connection area, as discussed in Section 7.2, the measurement locations were distributed uniformly on the casing-side of the joints. Figure 7.14 shows a schematic of the MACE sub-assembly, indicating the locations of measurements. Four locations along the length, denoted by the numbers 1 to 4, and four locations along the circumference, denoted by the letters A to D, were selected for measurements. Thus, a total of 16 measurement locations were used in the analysis.

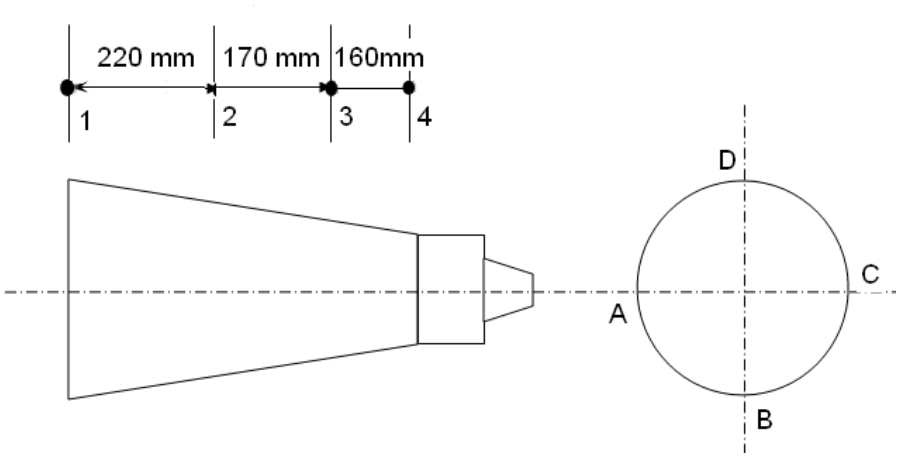

Figure 7.14 Measurement locations on the MACE sub-assembly

The transducers used for the testing were calibrated before their use. The repeatability of the measurements was checked at different excitation levels. Excellent repeatability was achieved at all excitation levels. The plots showing the repeatability of the measurements are given in Appendix D.

7.4.1 Identifying the location non-linearity

The FRF-based method, described in Chapter 5, was used to the extract the cumulative non-linear force at all 16 measurement locations. Figure 7.15 presents a bar chart showing the normalized cumulative non-linear forces at 16 locations.

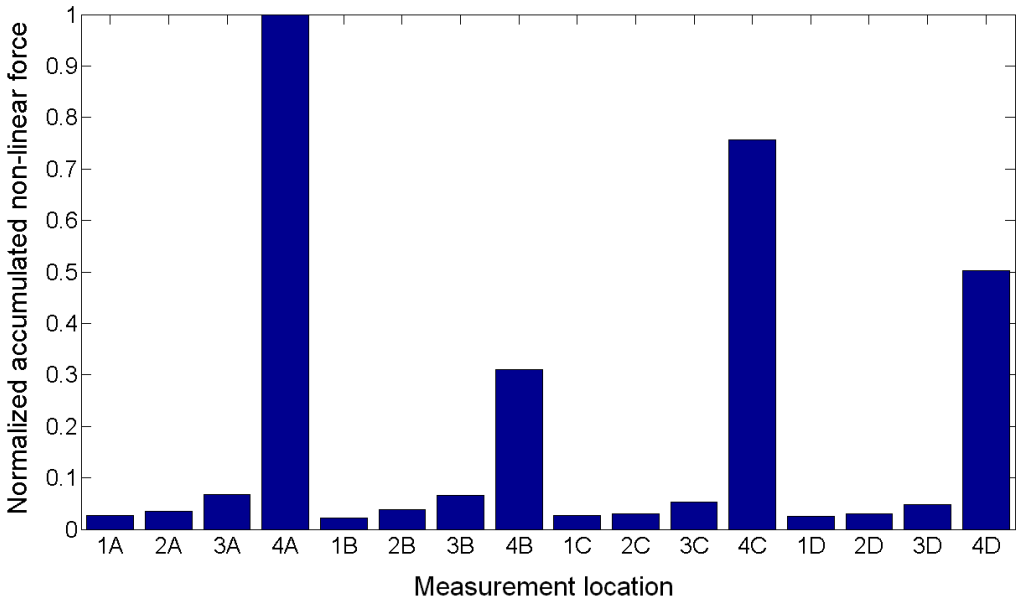

Figure 7.15 Accumulated non-linear force at the measurement locations

It can be observed from Figure 7.15 that the accumulated non-linear forces at the locations close to the joint location are significantly higher than those at other

locations. Thus, the location of non-linearity is identified to be within the vicinity of the joint.

7.4.2 Identifying the type of non-linearity

Before going to the last stage of actually estimating the non-linear parameters, it is important to gain some knowledge about non-linear behaviour trend, and the possible mathematical models which can be fitted into the observed behaviour.

The analysis of the responses obtained at different excitation levels provided initial trends in the non-linear behaviour. The variations in the resonance amplitude and in resonance frequency for the first mode of the sub-assembly were studied. Figure 7.16 shows the variation of the resonance amplitude with the excitation level.

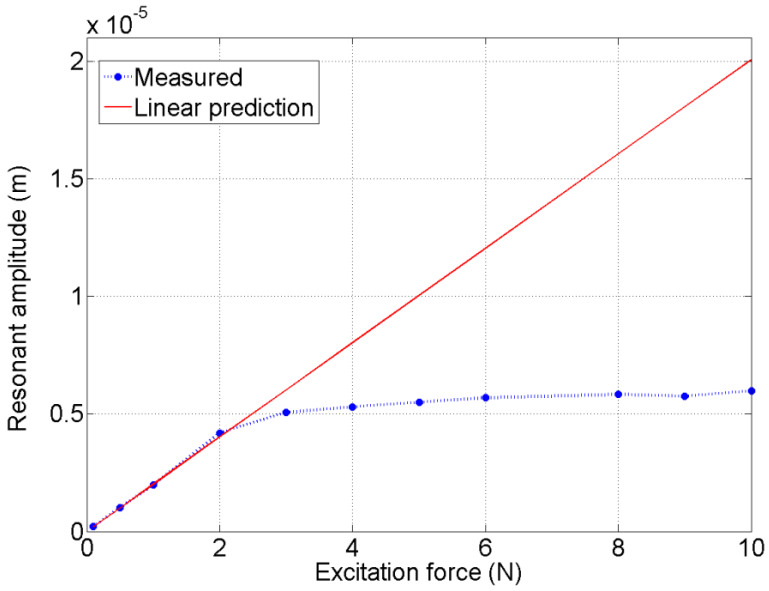

Figure 7.16 Variation of the resonance amplitude for the first mode

It is seen from Figure 7.16 that the resonance amplitude does not increase linearly with the excitation force. The curve flattens beyond the force of 3N. This suggests dissipative behaviour of non-linearity which might come from the frictional contacts between the components.

Figure 7.17 shows the variation of resonance frequency with the excitation force. It is observed that the resonance frequency drops with the excitation force, suggesting a softening-stiffness behaviour of non-linearity.

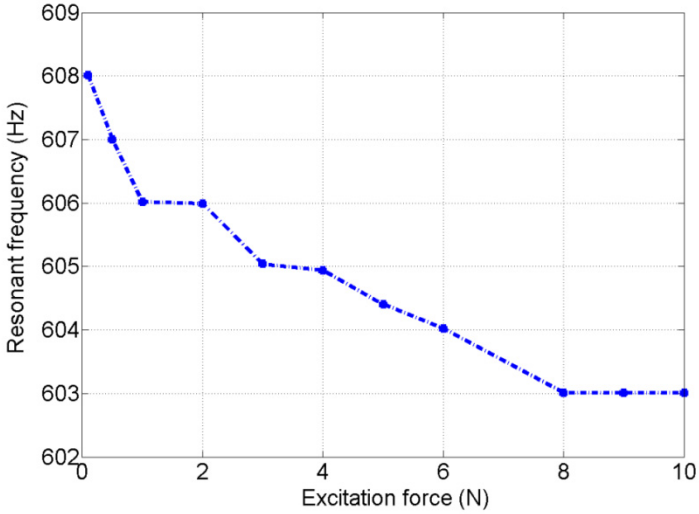

Figure 7.17 Variation of the resonance frequency of the first mode

As explained in [6], the real and imaginary parts of inverse-accelerance can be used to indicate the type of non-linearity. If the real part of an accelerance, plotted against (frequency)^2, deviates from a straight line, it indicates a stiffness type non-linearity. Similarly, if the imaginary part of an accelerance plotted against frequency deviates from a straight line, it indicates a damping type non-linearity.

The direct or point accelerance plots at different excitation levels were used to identify whether the non-linearity is of stiffness-type or damping-type. Figure 7.18 shows the inverse-accelerance plot at the excitation force level of 5N. It can be seen that both the real and imaginary parts deviate from a straight line, indicating the presence of both stiffness and damping type of non-linearity.

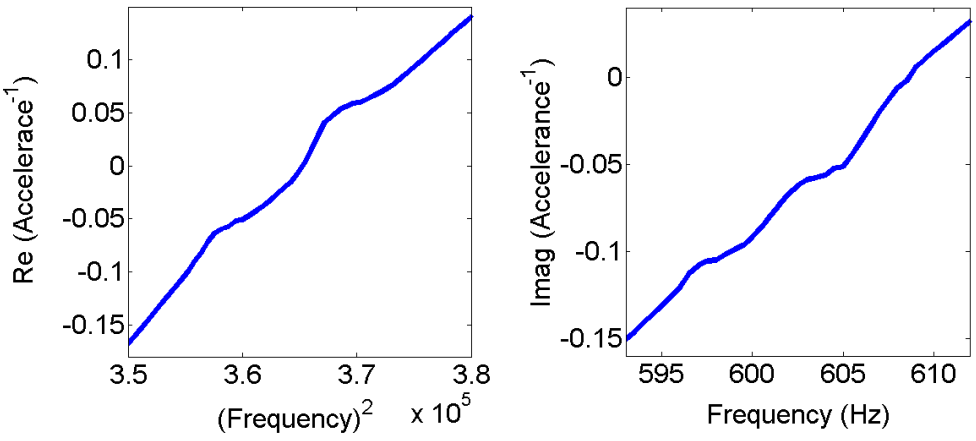

Figure 7.18 Inverse FRF plots at excitation force level = 5N

Using the different techniques as above, a general idea about the non-linear behaviour has been obtained. At this point, the reduction in peak amplitude of

vibrations and reduction in the resonance frequency as the excitation is increased, suggests either damping type non-linearity alone, or both softening stiffness and damping types of non-linearity.

Once the general characteristics of the non-linear behaviour are understood and the non-linearity location is identified, the non-linear force at the non-linear DOFs can be extracted. The FRF-based method was used to extract the non-linear force. When all 16 measurements were used to extract the non-linear force vector, the matrix became ill-conditioned giving erroneous results. Later, the measurements at only 2 locations, A1 and A4, were used to extract the non-linear force vector. Figure 7.19 show the non-linear force at these two locations plotted against frequency. It can be seen that the magnitude of non-linear force at the excitation location A1 is insignificant when compared to the magnitude of non-linear force at the location A4, which is close to the joint area.

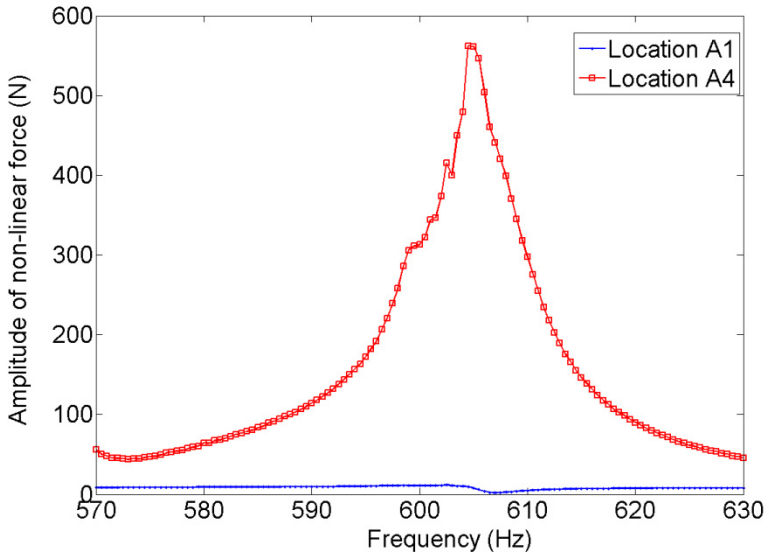

Figure 7.19 Non-linear force at locations A1 and A4

Figure 7.20 shows the non-linear force at the location A4, plotted against the amplitude of displacement at the same location. Ideally, the non-linear force should be plotted against the relative displacement between the interfacing components. In this case, since the actual contact locations were inaccessible for measurements, only the measurement on the outer side of the Casing was used.

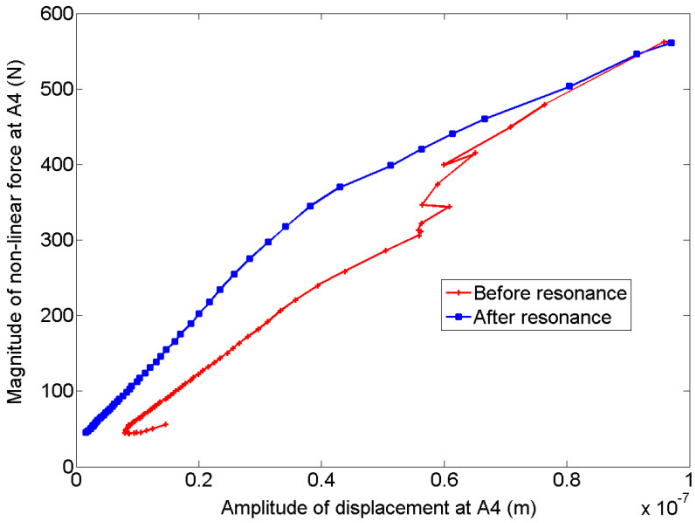

Figure 7.20 Non-linear force at A4 against displacement at A4

An interesting observation is made from Figure 7.20. Before and after the resonance, the non-linear forces trace different paths, thus forming a loop. It can be argued that the non-linear parameters as used in the conventional models, corresponding to the friction and clearance non-linearity, change as the system passes through a resonance.

The non-linear force at location A4 was extracted using two different methods, the I-HMT method and the FRF-based method. It was found that the two curves match closely. Figure 7.21 shows the comparison of non-linear force extracted using the two methods.

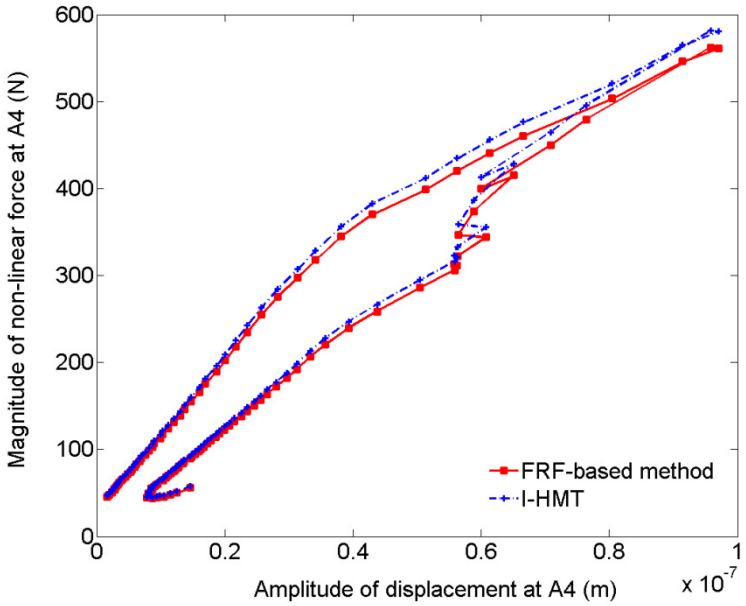

Figure 7.21 Comparison of non-linear force extracted using different methods

To identify the type of non-linearity using the footprint library presented in Chapter 3, the extracted non-linear force at A4 was compared with different footprints in the library. The shape matching algorithm was used to find SSD values for each non-linearity type. Figure 7.22 shows the comparison of the extracted non-linear force with different non-linear footprints and the corresponding SSD values. It is observed that the extracted non-linear force closely matches with (i) pure stick type friction non-linearity and (ii) combined clearance and friction non-linearity, the plots with a square border.

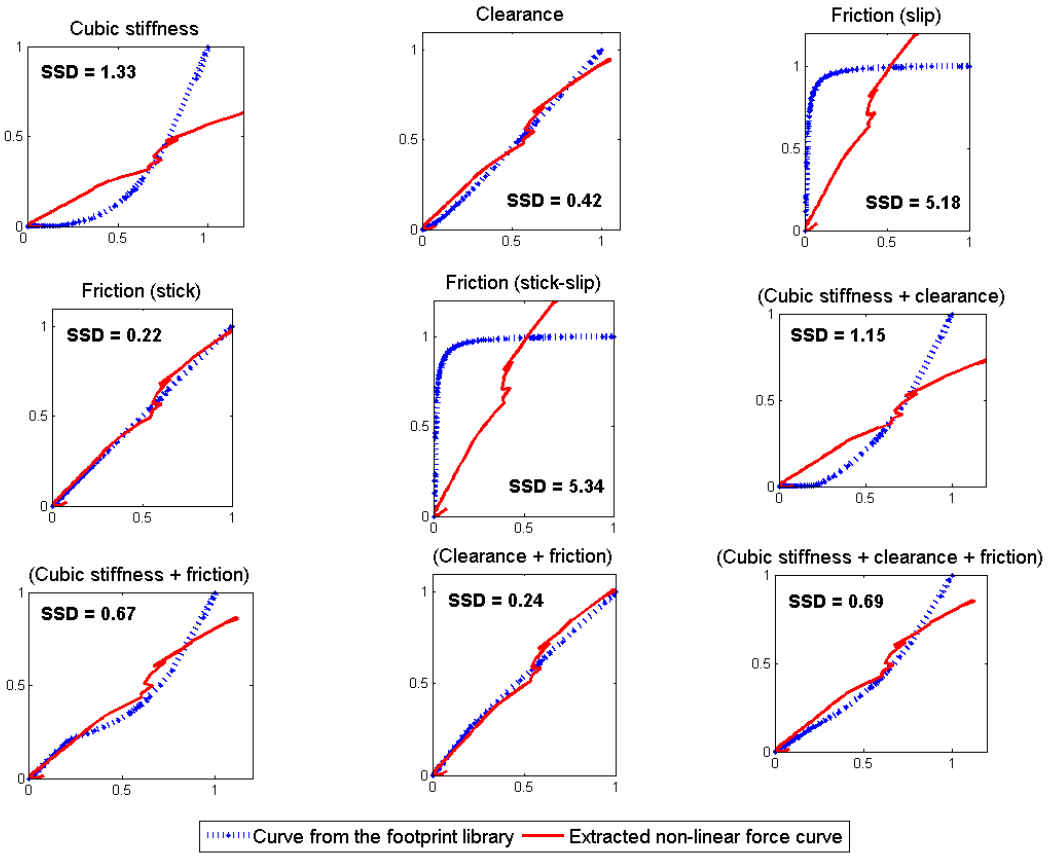

Figure 7.22 Comparison of the extracted non-linear force with footprint library

From the physics of the joints, the trend observed in the non-linear force, and the quantitative comparison with the footprints from the library, it may be concluded that the non-linearity present in the structure is of clearance and friction type.

7.4.3 Estimation of non-linear parameters

This is the last stage in non-linear system identification in which the parameters of the models which describe the non-linearities in the system are estimated. Since measurements were distributed only on the casing, the relative displacements

between any two points in contact were not measured. This puts a limitation on the parametric identification of non-linearities.

The non-linear parameters were estimated assuming that casing is in contact with a component which is grounded. The non-linear parameters were extracted using a genetic algorithm optimization with binary-multipliers. Based on the results of non-linearity characterization, high probability values (p = 0.9) were assigned for both clearance and friction non-linearities and a low probability value (p = 0.3) was assigned for cubic stiffness non-linearity. Since the extracted non-linear forces traced different paths before and after the resonance, two sets of parameters were identified corresponding to the two regions.

A non-parametric identification was also attempted on the same data. A non-parametric model was obtained by fitting a polynomial into the extracted non-linear force, using the norm-2 minimization criteria. Table 7.4 shows the estimated parameters for the parametric and non-parametric cases. The negative stiffness value identified for the clearance stiffness indicates opening of gaps.

The non-linear force at location A4 was regenerated using the estimated non-linear parameters. Figure 7.23 shows the comparison of the extracted and regenerated non-linear force for both cases.

Table 7.4 Estimated non-linear parameters with parametric and non-parametric models

Model used	**Estimated parameters**
Non-parametric of form: $a_0 + a_1 x + a_2 x^2 + a_3 x^3$	$a_0 = 0$ $a_1 = -7.5\times10^{9}$ $a_2 = 5\times10^{11}$ $a_3 = 1.65\times10^{23}$
Parametric model with (clearance + friction) non-linearity	Clearance stiffness: $K_z = -1.18\times10^{10}$ N/m (below resonance) $= -1.29\times10^{10}$ N/m (above resonance) Clearance gap, $y_c = 2\times10^{-9}$m Frictional force, μN = 5N Tangential stiffness: $K_d = 7\times10^{8}$ N/m (below resonance) $= 1.5\times10^{8}$ N/m (above resonance)

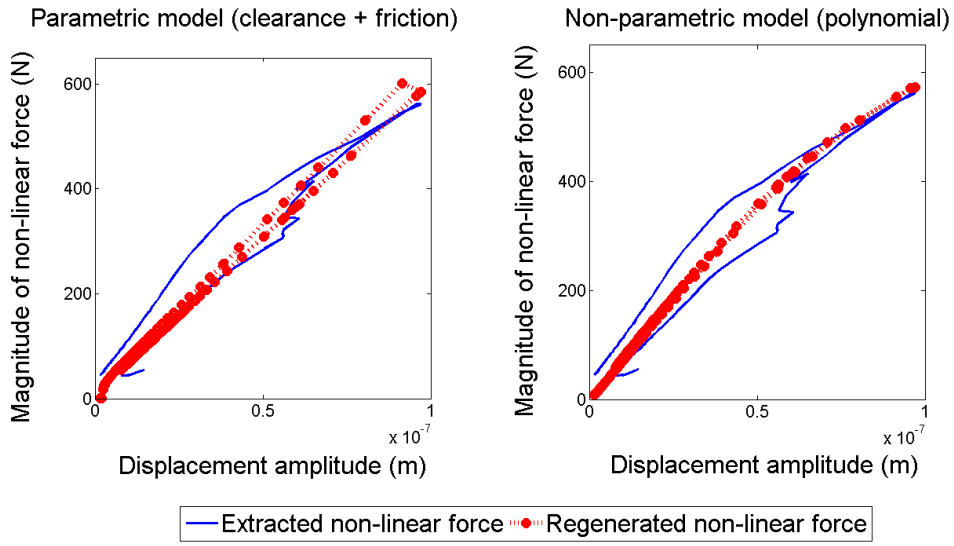

Figure 7.23 Regenerated non-linear forces with parametric and non-parametric models

The estimated non-linear parameters were substituted back into the numerical model to predict the system response at two different excitation levels. Figures 7.24 and 7.25 show the comparison of the regenerated response with the experimental response, for the parametric and non-parametric model respectively. Table 7.5 presents the summary of errors in prediction of the resonance frequency (ε_ω) and the resonance amplitude (ε_y) for the parametric and non-parametric non-linear models, and the underlying linear model

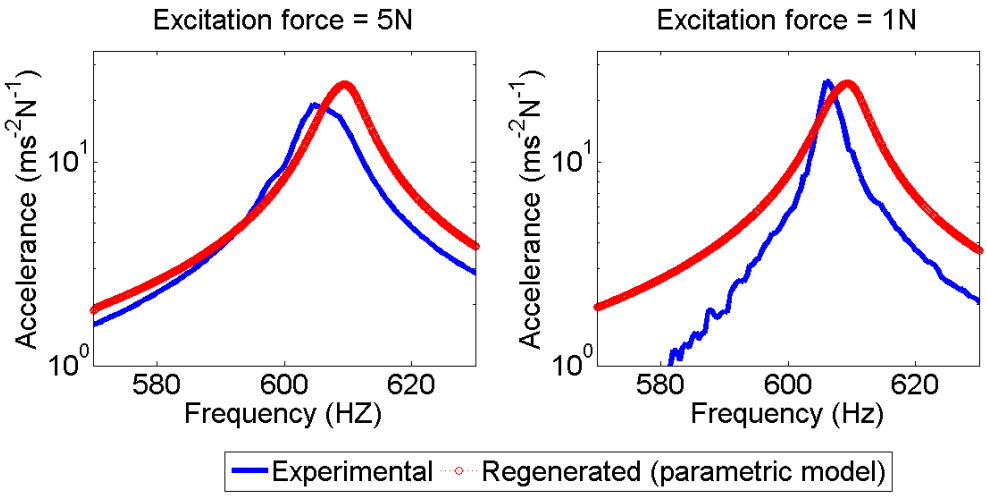

Figure 7.24 Regeneration of response using non-parametric model

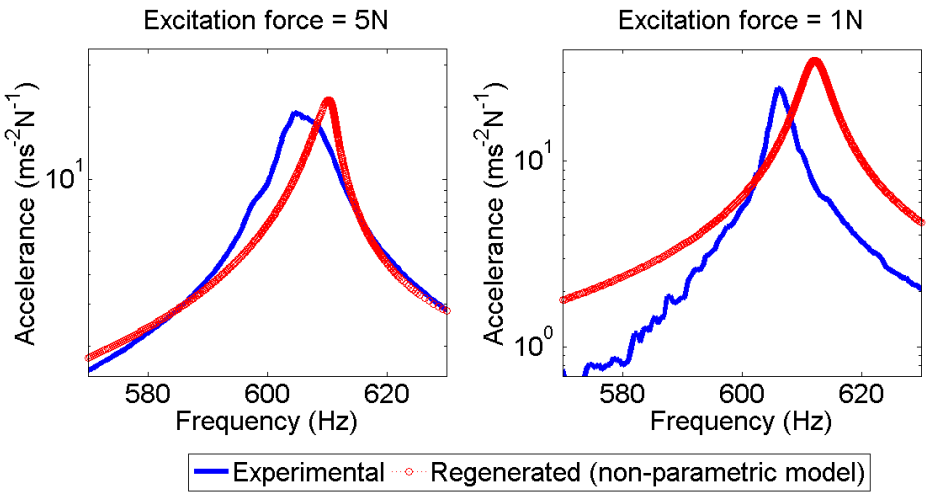

Figure 7.25 Regeneration of response using parametric model

Table 7.5 Comparison of errors in the regenerated response

Model used	**Excitation force = 5N**		**Excitation force = 1N**	
	ε_ω (%)	ε_y (%)	ε_ω (%)	ε_y (%)
Parametric	0.81	16.1	0.56	2.18
Non-parametric	0.96	12.3	1.02	40.7
Linear	0.48	76.6	0.23	3.13

From Table 7.5, it is observed that if the underlying linear model of the system is used for the prediction, the discrepancy increase with the excitation force. This is reasonable as with increase in the excitation force, the system moves into the non-linear regime.

For non-linear models, the predictions at the excitation force of 5N, at which the non-linear system identification was carried out, are fairly accurate. The maximum error in the prediction of peak response is around 16%. When these same models are used to predict the dynamic behaviour at the excitation force of 1N, out of the two models, the parametric model performs better. Still the shape of plots for predicted and observed response at 1N are different. This may be because the parametric model identified in the current study does not utilise the relative displacements between the two parts in contact. Thus, the clearance and friction models fitted are not parametric in true sense. It is necessary to investigate the effect of approximating relative displacement by the absolute displacement at one of the contributing DOF. This can be checked on a simple 3 DOF system, with non-linearity acting between any two DOFs.

Since the regeneration capability of the models is checked at only two discrete excitation levels, it cannot be concluded that the identified models are valid over a wide range of operating conditions.

7.5 Concluding remarks

This chapter presents the results of an experimental investigation of non-linearities in the MACE structure sub-assembly. It has been observed that when the accurate FE models of the individual components are assembled together with the locked-joints assumption, the predictions for the assembled structure are inaccurate. This suggests some relative motion between different parts of the joints, which may contribute towards the non-linear behaviour of the system.

The results of different non-linearity detection techniques have been presented to conclude that the structure's behaviour is significantly non-linear at higher excitation levels. The measurements at different excitation levels were used to characterize the non-linear behaviour. Softening-stiffness type behaviour along with dissipating mechanism has been observed in the structure. It has been observed that the detection of non-linear behaviour and approximate characterization of non-linearity type can be successfully performed with very limited measurement data.

The measurement data from the constant-force step-sine vibration tests, performed at relatively high force amplitude, were used to extract the non-linear force vector at the measured locations. The accumulated non-linear force plots were used to locate the non-linearity. The locations close to the joint location have been correctly identified as the non-linearity locations. The extracted non-linear force at the non-linear location was compared with the curves from the footprint library for type identification. The SSD values corresponding to the combined clearance and friction non-linearity and pure-stick friction non-linearity were found to be the lowest. This type identification is consistent with engineering judgement.

The results of both parametric and non-parametric identifications have been presented. The identified models are found to be accurate at the excitation level at which they were identified. The extrapolation capacity of the models and their universality needs to be verified.

Chapter 8

Non-linear parameter identification for base-excited structures

This chapter presents a method for non-linear system identification of base-excited structures with controlled acceleration input. The proposed method works in three stages to estimate the non-linear parameters in a system. The method is entirely based on measured data with no need for an FE model. The proposed method is illustrated on a pyramid-like structure using simulated data. The performance of the method in the presence of measurement noise is also evaluated.

8.1 Introduction

The civil engineering structures like buildings, bridges, stadia and dams are often designed to avoid the transmissibility of ground vibrations. For laboratory testing of such structures, a scaled model of the structure is mounted on a shaker table, and it is given acceleration input at the base to simulate operating conditions. Similar tests are sometimes performed for military applications, spacecrafts and aircraft structures, to evaluate their dynamic performance under base loading. In such cases, the excitation forces do not act locally, but they are distributed throughout the structure, depending on mass distribution in the structure.

The traditional non-linear parameter identification techniques described in [28, 36-38], and the methods proposed in Chapters 4 and 5 of this thesis, require force and response information at all excitation DOFs for their successful implementation. For cases where the excitation comes from acceleration input, these requirements can be met only if: (i) all DOFs are measured, and (ii) the mass distribution in the structure is known a-priori. Thus, in practical cases it may not be possible to use the available identification methods directly.

The chapter presents a three stage strategy for non-linear system identification in case of base-excited structures.

8.2 Theoretical formulation

A system with a moving-base configuration can be represented as an equivalent system with a fixed-base configuration if the displacement vector is represented as a vector relative to the base displacement [6]. Thus, the equations of motion for a non-linear MDOF system excited using acceleration input at the base can be written in the equivalent fixed base configuration as:

$$[M]\{\ddot{u}\}+([K]+i[D])\{u\}+\{g(u,\dot{u})\}=-[M]\{l\}\ddot{y}_b \tag{8.1}$$

where, $[M]$, $[K]$,and $[D]$ represent the mass, stiffness and proportional damping matrices of the system in fixed base configuration, $\{g\}$ is the non-linear restoring force vector, $\ddot{y}_b$ is the acceleration input at the base, $\{u\}$ is the vector of displacements relative to the base, and $\{l\}$ is a transformation vector (l_i = cos$\emptyset_i$, where, $\emptyset_i$ is the angle between the i^{th} DOF and the direction of base motion). The proportional damping matrix can be written as:

$$[D]=\alpha[K] \tag{8.2}$$

For the underlying linear system, the set of equations can be obtained by substituting the non-linear restoring force to zero. If the input acceleration at the base is sinusoidal, the set of equations for the underlying linear system can be written in the frequency domain as:

$$[Z]\{U\}=\omega^2[M]\{l\}Y_b \tag{8.3}$$

where, $[Z]$ is the dynamic stiffness matrix of the underlying linear system , ω is the excitation frequency, $\{U\}$ is the vector of displacement amplitudes relative to the base displacement, and Y_b is the amplitude of base displacement.

The right hand side of (8.3) represents the excitation force vector, which is dependent on the distribution of mass in the system. If a constant-acceleration is maintained, the excitation force remains constant throughout the frequency range. On the other hand, if the base displacement is constant, the excitation force will vary as a quadratic function of the excitation frequency. It should be noted that the excitation force vector remains the same for the underlying linear system and the non-linear system, if the non-linearities are not mass-dependent. If the excitation force vector from the right hand side of (8.3) is represented by $\{F^d\}$, then the

equations for the linear system can be written in terms of the FRF matrix of the system as

$$\{U\} = [\alpha]\{F^d\} \tag{8.4}$$

In practical cases, not all DOFs of the system can be measured. To deal with this, (8.4) is partitioned into the measured and un-measured DOFs:

$$\begin{Bmatrix} U_m \\ U_u \end{Bmatrix} = \begin{bmatrix} \alpha_{mm} & \alpha_{mu} \\ \alpha_{um} & \alpha_{uu} \end{bmatrix} \begin{Bmatrix} F_m^d \\ F_u^d \end{Bmatrix} \tag{8.5}$$

Considering only the measured responses from (8.5), we can write:

$$\{U_m\} = [\alpha_{mm}]\{F_m^d\} + [\alpha_{mu}]\{F_u^d\} \tag{8.6}$$

Multiplying (8.6) by $[\alpha_{mm}]^{-1}$, we get a pseudo excitation force vector at the measured DOFs as:

$$\{P^d\} = \{F_m^d\} + [\alpha_{mm}]^{-1}[\alpha_{mu}]\{F_u^d\} \tag{8.7}$$

This vector can be considered as the projection of the excitation force vector of the entire system onto the measured DOFs. It is possible to extract this vector solely from the measured data as:

$$\{P^d\} = [\alpha_{mm}]^{-1}\{U_m\} \tag{8.8}$$

Now, for a non-linear system, the equation for harmonic amplitude can be written as:

$$\{\tilde{U}\} + [\alpha]\{G\} = [\alpha]\{F^d\} \tag{8.9}$$

where, $\{\tilde{U}\}$ represents the non-linear response vector relative to the base. Partitioning (8.9) into measured and un-measured DOFs, the non-linear force vector at the measured DOFs can be extracted as:

$$\{G_m\} = \{F_m^d\} + [\alpha_{mm}]^{-1}([\alpha_{mu}]\{F_u^d\}) - [\alpha_{mm}]^{-1}([\alpha_{mu}]\{G_u\}) - [\alpha_{mm}]^{-1}\{\tilde{U}_m\} \tag{8.10}$$

If non-linearities are confined to the measured zone, $\{G_u\}$ can be set to zero and (8.10) becomes:

$$\{G_m\} = \underbrace{\{F_m^d\} + [\alpha_{mm}]^{-1}([\alpha_{mu}]\{F_u^d\})}_{P^d} - [\alpha_{mm}]^{-1}\{\tilde{U}_m\} \tag{8.11}$$

As the pseudo excitation force vector remains same for linear and non-linear systems if the non-linearities do not cause mass matrix variation, (8.10) can be written as

$$\{G_m\} = \{P^d\} - [\alpha_{mm}]^{-1}\{\tilde{U}_m\} \tag{8.12}$$

Once the non-linear force vector corresponding to the measured DOFs is extracted using (8.12), the non-linearity location can be identified by plotting the cumulative non-linear force. The non-linear force at the non-linear DOF can then be used to extract the non-linear parameters using a genetic algorithm optimization.

8.3 Implementation of the method

The proposed method is applied in 3 stages: at the first stage, the pseudo excitation force vector at the measured DOFs is extracted using (8.8). To do this, beforehand the FRF matrix of the underlying linear structure is obtained via modal analysis of the structure in fixed base configuration at low excitation levels. The vector of relative displacements for the underlying linear structure is then obtained by performing slip-table tests with low acceleration input.

The second stage consists of extracting the non-linear force vector at the measured DOFs. First the relative non-linear displacement vector is measured by subjecting the structure to high acceleration input at the base. The non-linear force is then extracted using (8.12).

In the last stage, the non-linear force at the measured DOFs is used to estimate the non-linear parameters via genetic algorithm optimization. Figure 8.1 shows the flowchart for the method.

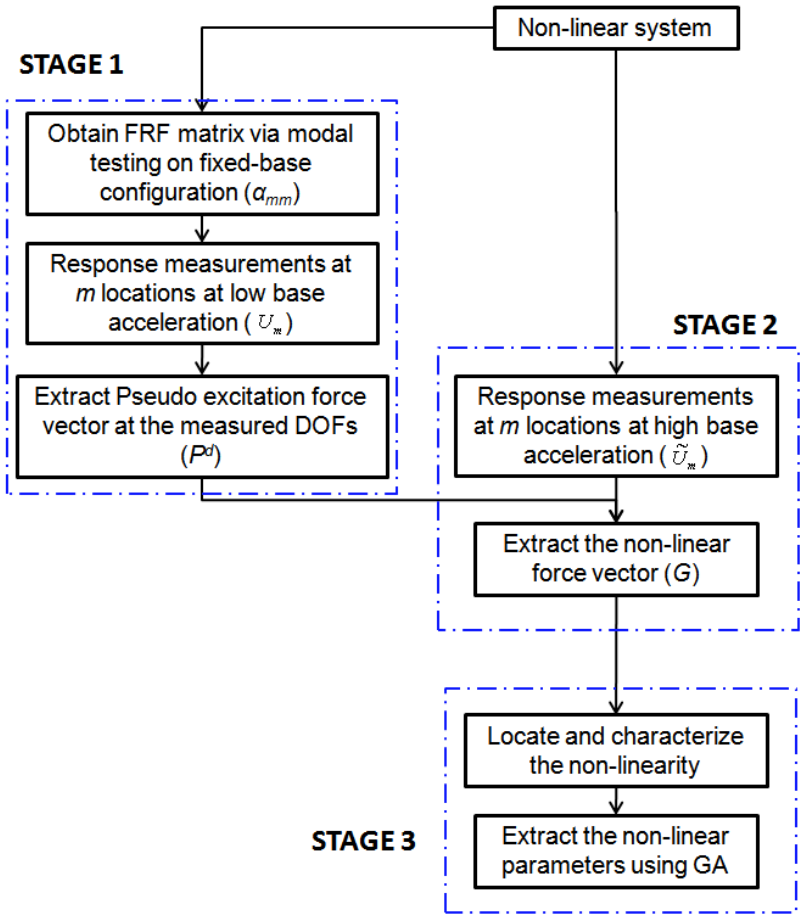

Figure 8.1 Flowchart of the proposed method

8.4 Illustration of the method

The proposed method is illustrated on Validation structure-3; a pyramid-like structure made of 4 beams and mounted on a rigid platform. The slip-table tests can be simulated by giving the platform a constant acceleration input. Figure 8.2 shows the schematic of the structure with measurement locations, non-linearity location, and the node numbers. The detailed engineering drawing of the structure and the properties of materials used are documented in Appendix B.

For the current simulation, the platform was given a constant acceleration in X direction. A grounded cubic stiffness non-linearity, acting in X direction was placed at one of the beams (Node 7). The non-linear coefficient β = 5×10^{12} Nm^{-3}, was used for the simulation. To mimic the condition of incomplete measurements, displacement responses in the X direction were measured at 5 nodes including the

non-linear DOF. A constant modal damping of 1% (η =0.01) was used in the simulation.

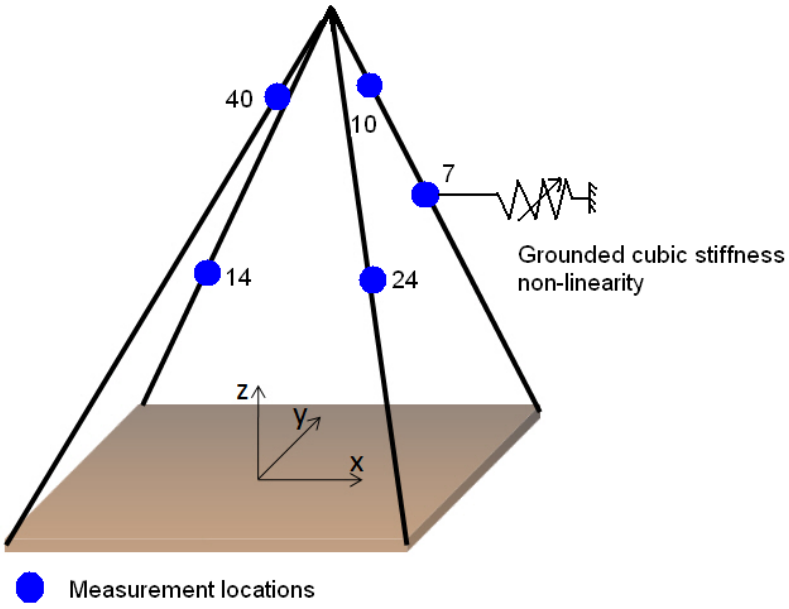

Figure 8.2 Schematic of Validation structure-3

8.4.1 Stage 1: Extraction of pseudo excitation force vector (P^d)

To extract the pseudo excitation force, the FRF matrix, and the relative displacement vector of the underlying linear structure are required. The FRF matrix of the structure, $[\alpha_{mm}]$, corresponding to the measured DOFs, in the fixed-base configuration, was obtained by performing modal analysis on the system matrices. Figure 8.3 shows the overlaid FRFs. The displacement responses at the measured DOFs were then obtained by giving a constant acceleration of 0.09 m/s^2 to the base. The low value of acceleration resulted in close-to-linear behaviour of the structure. Thus, the relative displacement vector (U), of the underlying linear structure, was calculated.

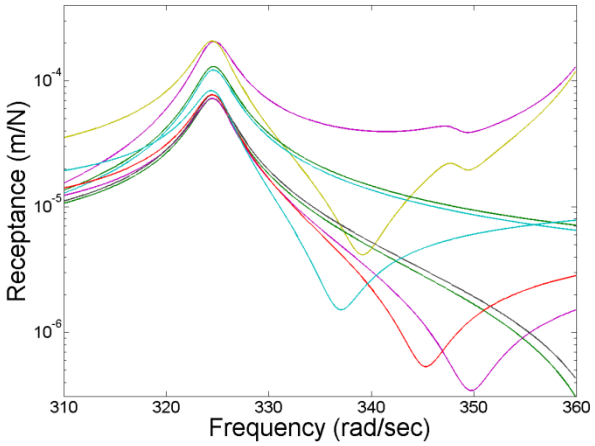

Figure 8.3 Overlaid FRFs of the underlying linear structure

With the FRF matrix, and linear relative displacement vector available, (8.8) was used to extract the pseudo excitation force at the measured DOFs. Figure 8.4 shows the pseudo excitation forces at the measured DOFs plotted against frequency, in the vicinity of the first resonance. The actual excitation force should remain constant throughout the frequency range, because of the constant acceleration input. The variation in the pseudo excitation force, seen in Figure 8.4, is caused by the second term in (8.7) which projects the force at un-measured DOFs onto the measured DOFs.

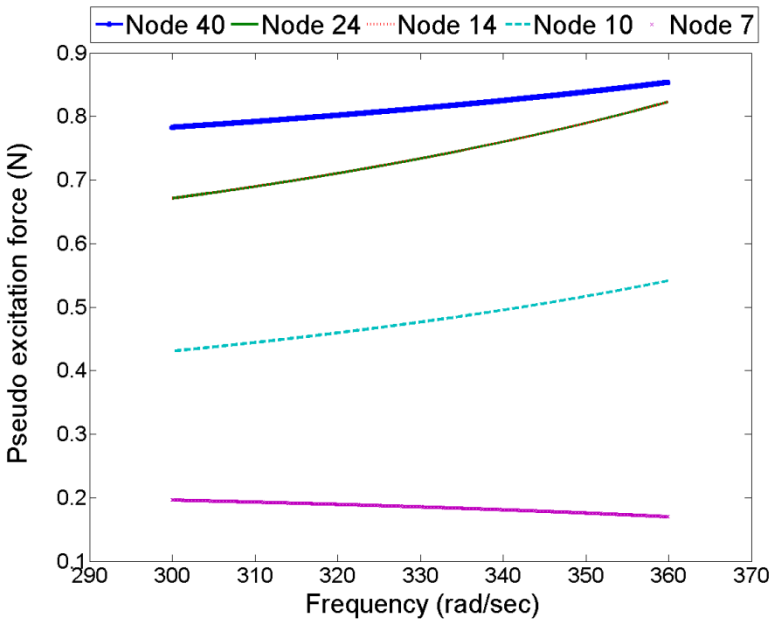

Figure 8.4 Pseudo excitation force at measured DOFs

8.4.2 Stage 2: Obtaining the non-linear restoring force

The non-linear displacement responses, relative to the base displacement were obtained by subjecting the structure to a constant acceleration of 0.9 m/s^2. At this high acceleration level, the structure exhibited non-linear behaviour in the presence of the cubic stiffness non-linearity. Figure 8.5 shows the comparison of relative displacement at Node 7 for low (a = 0.09 m/s^2) and high acceleration levels (a = 0.9 m/s^2). The non-linear restoring force vector corresponding to the measured DOFs was later extracted using (8.12).

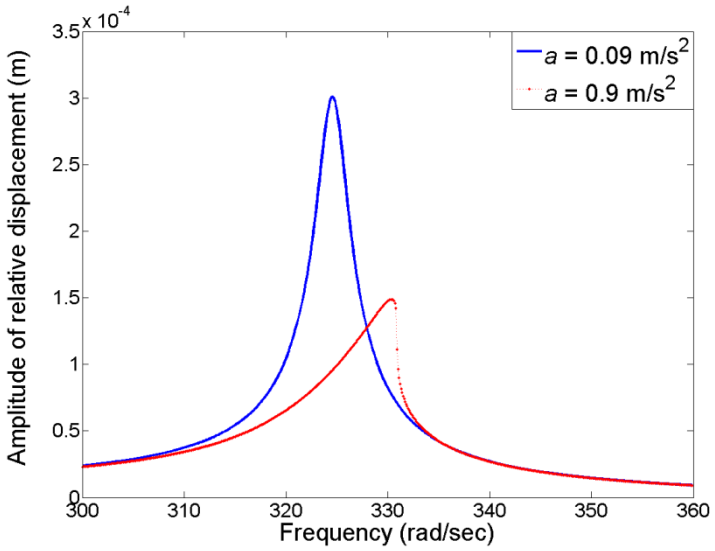

Figure 8.5 Comparison of linear and non-linear responses at low and high acceleration input

8.4.3 Stage 3: Estimation of the non-linear parameters

Once the non-linear force at the measured DOF was extracted, the location of non-linearity was identified by plotting the cumulative non-linear force. Figure 8.6 shows the bar chart of cumulative non-linear force at the measured DOFs.

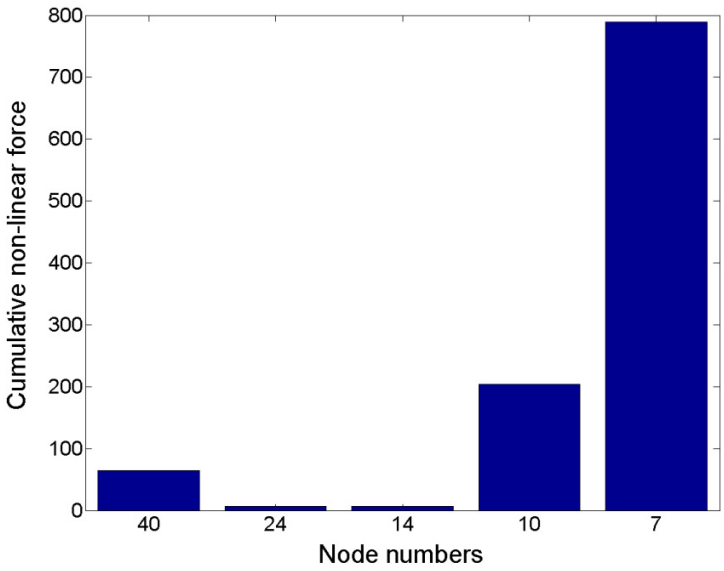

Figure 8.6 Identification of non-linearity location

It can be seen from Figure 8.6 that the cumulative non-linear force is maximum at Node 7, and its magnitude is significantly higher than the magnitude of forces at other nodes. This correctly identifies the location of non-linearity. Figure 8.7 shows the plot of non-linear restoring force at the identified non-linear DOF.

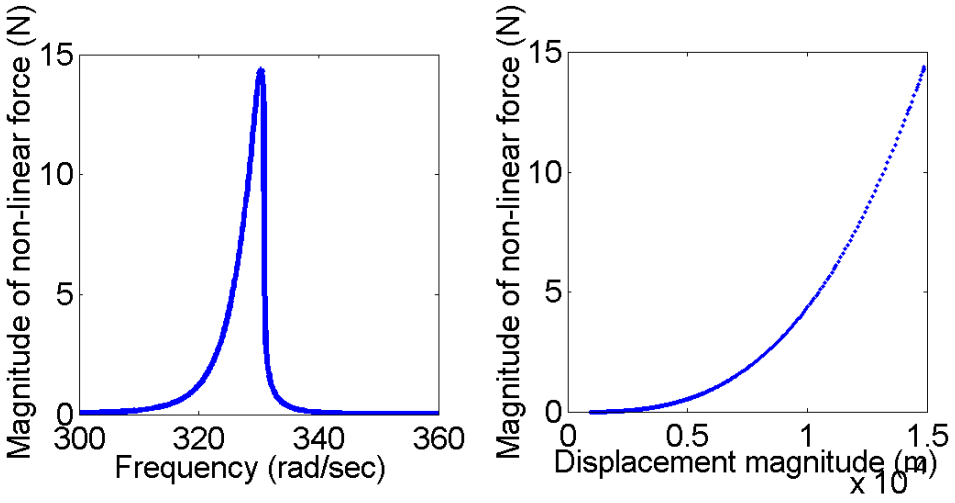

Figure 8.7 Non-linear force at the non-linear DOF

The non-linear force at the non-linear DOF was then used to extract the non-linear parameters using the genetic algorithms. The initial range for the parameter in the GA was kept from 0 to 5×14 Nm^{-3}. The range was narrowed in subsequent civilizations to gain accuracy. The value of identified parameter and the corresponding error is recorded in Table 8.1.

8.4.4 Performance in the presence of experimental noise

Since the method relies completely on measured data, it is important to check the sensitivity of the method to measurement noise. There are three quantities which are obtained from experimental measurements: the FRF matrix, the response at low excitation level, and the response at high excitation level. Each of these can act as a source of measurement noise. Thus, four different cases were considered in order to analyse the effects of noise in each measured quantity independently, and the combined effect noise in all three.

In the first case, only the FRF matrix, $[\alpha_{mm}]$, was polluted with artificial noise of 3% using equation (6.1) from Chapter 6. In the second and the third case, the response vectors, $\{U_m\}$ and $\{\tilde{U}_m\}$ were polluted with 3% noise respectively, using (4.15). Table 4.1 summarizes the results for all these cases.

Table 8.1 Estimated parameters with and without noise

Case	Noise level (%)	Estimated value of β ×10^{12} (Nm^{-3})	Error in estimation (%)
No-noise	0	5.06	1.2
Noise in the FRFs	3	5.09	1.8
Noise in linear responses	3	5.84	16.8
Noise in non-linear responses	3	6.37	27.4
Noise in all three	3	7.10	42

It can be seen from Table 8.1 that the non-linear parameter is identified accurately with noise-free measurement data. For the cases with noise, the error is highest when all three measured data contain noise, which was expected. The effect of noise in FRF matrix is observed to be the least. Overall, it is observed that the method is sensitive to measurement noise, and the error of the order of 40%, which is reported in this study, may not be acceptable in many cases.

8.5 Concluding remarks

A method for the parametric identification of non-linearities for base-excited structures has been proposed. The formulation of the method can be used for any direction of base motion. The method is applicable in case of constant base

displacement or constant base acceleration configuration. The method uses only raw measurement data, eliminating the need for the FE model of a structure.

The method has been illustrated on a pyramid-like structure with simulated data. The method was found to be accurate in the absence of experimental noise. There are three different sources of experimental noise in this method. In the case where noise from all three sources is considered, the method estimated parameters with around 40% error, which may be un-acceptable in many cases. Thus, the method demands clean measurement data to identify the non-linear parameters accurately.

Though the method is presented for base-excited structures, it is generic, and can be extended for any case in which the excitation force is not measured. The extension of this method to the output-only non-linear tests can be beneficial.

Chapter 9

Conclusions and future work

This chapter concludes the thesis by presenting a summary of the research findings, contributions by the author, details of published research papers from this work, and finally the author's view, on the scope of further research in this area.

9.1 Conclusions of the research work

Non-linear structural dynamics is an important research topic, relevant to different industries. It encompasses various sub-areas like non-linear system identification, stability studies for non-linear systems and the prediction of dynamic response for a non-linear system. The work in this thesis is restricted to *parametric identification of non-linear systems in the frequency-domain*. Different strategies for non-linear system identification are proposed, and they are illustrated with the use of simulated non-linear response data. During the research, the focus is always kept on the practicality of the proposed strategies, and their integration with the established tools like finite element analysis, modal testing and modal analysis. The detailed conclusions on different topics are presented below.

9.1.1 Type characterization using footprints

Identifying the type of non-linearity is an important step in the parametric identification of non-linear systems. Once the type of non-linearity is identified correctly, a mathematical function can be chosen to fit the identified non-linearity. It has been previously reported in the literature that the shape of non-linear restoring force in a system is unique to the type of non-linearity. Taking this observation further, a library of non-linear force footprints for different non-linearities, plotted in different formats like Bode plots and Nyquist plots, has been generated. This library can be used as a look-up chart for subjective identification of non-linearity type.

It has been observed that, if the non-linear force for a system is plotted against the relative displacement amplitude at the non-linear DOFs, the shape of the curve is independent of the underlying linear system. Thus, the footprint library which is generated using a 2 DOF system can be used for identifying non-linearity types for any practical non-linear system.

The type of non-linearity in a system can be identified by visual comparison of the extracted non-linear force with the forces from the footprint library. To avoid subjectivity in the visual comparison, a shape-matching algorithm has been proposed for numerical comparison of non-linear forces.

For individual non-linearities, the algorithm proved to be accurate, correctly identifying the non-linearity type. For the case of combined non-linearities, it has been observed that the shape of non-linear force plot is dependent on the contribution of each non-linearity type in the non-linear force. As this contribution may vary from case to case, the correct identification of non-linearity type was found difficult to achieve with the current footprint library. If the library is extended to include footprints of combined non-linearities with unequal contributions, it may be possible to identify the type of non-linearity, and even the contribution of each non-linearity type.

9.1.2 Genetic algorithm optimization

In the current research, the last stage in the parametric identification, that of estimating the non-linear parameters, has been formulated as an optimization problem. The optimization problem, with non-linear parameters as design variables, has been solved via a genetic algorithm. The method has been found to successfully estimate the non-linear parameters, even if the non-linearity type is not known a-priori. This feature is important in practical cases where the type of non-linearity may not be identified.

A novel concept of ‘binary-multipliers’ has been proposed to efficiently estimate the non-linear parameters if a user has some idea about the type of non-linearity in a system. A significant improvement in the computational efficiency has been achieved with the use of the binary multipliers.

9.1.3 On the choice of the model for the underlying linear system

The basic formulation proposed in the thesis requires a numerical model of the underlying linear system. Three methods, each using different form of model for the underlying linear system, has been investigated and compared.

It has been observed that the FRF-based method, which uses a response model of the underlying linear system, performs better in the weighted comparison against the other two methods. This method uses data directly from vibration measurements, thus eliminating the need for analysis tools like FEA and modal analysis. On the downside, the use of raw measurement data makes the method susceptible to random noise in measurements.

The spatial method which uses an updated FE model of the underlying linear system has been found to be sensitive to errors in the FE model. Moreover, for practical structures with large system matrices, the method becomes computationally expensive. As it may be difficult to obtain an accurate FE model of a complex structure, this method may have a limited use in practice.

The I-HMT method, which uses a modal model of the underlying linear system, has been found to be less accurate than the other two methods, but the fastest of all three. This method also possesses an important feature of quantifying the level of non-linearity in each mode, thus enabling users to select the modes which are to be considered in further non-linear analysis.

Since the basic methodology for all three methods assumes frequency-independent non-linear parameters, the number of equations available to solve the optimization problem is usually much higher than the number of design variables. Thus, a few measurements are sufficient to identify the non-linear parameters. For all three methods, it has been observed that if measurements at all non-linear DOFs and excitation DOFs are available, the non-linear parameters can be estimated accurately. Moreover, it has been observed that the effect of measurement noise increases with the number of measurements used in the analysis. Thus, it may be best to use only the minimum required number of measurements.

For a successful application of all three proposed methods, measurements must be taken very close to the non-linearity locations. This may put limitations on the use of these methods in the case when the non-linearities are at several un-accessible locations.

9.1.4 Experimental investigation of non-linear behaviour

To understand the difficulties faced by an engineer when dealing with experimentally measured vibration data on a real-life engineering structure, a study was undertaken on the MACE structure sub-assembly, which employs different joints. The structure was found to behave non-linearity under high excitation amplitudes.

It has been observed that the methods available in the literature, and those proposed in this thesis allow detection, and approximate type characterization of non-linearities at early stage of analysis with only a few measurements. Since non-linearities in real-life engineering structures may not behave as per their idealized mathematical form, a universal non-linearity identification method may not be readily applicable in such cases.

From the results of the experimental study conducted in this research, the author would suggest that the methods proposed in this thesis, and those available in the literature may be used at initial stages of the analysis to get an idea about the non-linear behaviour of a structure. Later on, the non-linearities may be identified within relevant frequency and excitation ranges based on the operating conditions. A universal model of a non-linear system may be difficult to identify for practical engineering systems. A non-parametric identification may prove easier in such cases, but again the model obtained via non-parametric identification may not be accurate over a wide frequency and amplitude ranges of the input excitation.

It has also been observed that the contribution of higher harmonics was significant in the response captured near the resonance frequency of the structure. Thus, it may be best to check the contribution of higher-order harmonics in the response before employing non-linear identification methods which are based on the first order describing functions.

9.1.5 Identification method for base-excited structures

In the tests, in which the excitation comes from an acceleration input at the base, the excitation force is distributed over the entire structure, and is usually not measured. Thus, the conventional non-linear system identification methods may not be directly applicable in such cases. To overcome this difficulty, a three-stage method for non-linear system identification has been proposed. The method works for both, acceleration controlled and displacement controlled tests. The method has been found to be applicable for any oblique excitation direction. Though the method is presented for base-excited structures, the same formulation can be extended to the case of output-only tests which are performed in an actual operating environment.

9.3 Contributions and publications of the thesis

The summary of the author's contribution to the research field is presented below:

- A novel idea of a footprint library containing non-linear force for different individual and combined non-linearities.
- A shape-matching algorithm to numerically compare the extracted non-linear force with the curves from the footprint library.
- A genetic algorithm based optimization methodology to estimate the non-linear parameters from the non-linear force.
- A concept of binary multipliers to improve the computational efficiency of the genetic algorithm by making use of partial information known to a user regarding the type of non-linearity in the system.
- Validation and comparison of the proposed non-linear identification methods on a MDOF representative engineering structure.
- The development of non-linear system identification method for base-excited structures.

A part of the work presented in this thesis is published in the following conference and journal articles:

(1) Gondhalekar A. C., Petrov E. P., Imregun M., *"Identification of MDOF nonlinear system using genetic algorithm optimization",* International modal analysis conference (IMAC)- XXVII, Florida-2008.

(2) Gondhalekar A., C., Petrov E. P., Imregun M, *"Parameters identification for nonlinear dynamic systems via genetic algorithm optimization"*, Journal of computational and nonlinear dynamics, Vol-4(4), pp 1-9, 2009.

9.4 Suggestions for future work

The research presented in this thesis started with the aim of developing strategies for parametric non-linear system identification, which can be used for practical engineering structures. Still at the end of this research certain questions remain

unanswered. The research in the area of non-linear system identification can be taken further in the direction of topics presented below:

- The formulation in the thesis uses the first-order describing functions to model the non-linear elements. The experimental investigation on the MACE structure showed a significant presence of higher order harmonics in the response near the resonance frequency. It would highly valuable to extend the current methods to use higher order describing functions and compare the accuracy with the methods presented here.

- The footprint library presented in this thesis has footprints of combined non-linearities, which are prepared based on an equal contribution assumption. In practice, different non-linearities may not always contribute equally in the non-linear force. This makes it difficult to identify the combined non-linearities with the current footprint library. The idea of banded-footprints, which is mentioned in Chapter 3, can be pursued further to create an extended footprint library with different contributions of non-linearities.

- The methods presented in the thesis are applicable for structures with localized non-linearities. Moreover, the response very close to the non-linearity location must be measured for their successful application. It would be valuable to propose methods which are applicable for structures with distributed non-linearities.

- The quantification of non-linear behaviour is still an area of research. There haven't been many methods described in the literature to quantify the level of non-linearity in a system. It would be a nice piece of research to propose certain criteria to quantify the level of non-linearity in a structure.

- From practical point of view, non-linear system identification is only an intermediate task, in the bigger aim of predicting the system response. Some systems are more sensitive to the errors in non-linear parameters than others. Thus, it is necessary to calculate the sensitivity of a system to errors in the non-linear parameters, and evaluate the performance of any identification method by keeping the sensitivity in perspective. A tool which integrates these two would be worth researching.

References

1. Imregun M.. Special issue on non-linear structural dynamics. Mechanical Systems and Signal Processing 23[1], 5-7. 2009.
2. Tomlinson G.R. and Worden K.. Nonlinearity in structural dynamics- Detection, identification and modelling. 2000. Bristol, Institute of Physics Publishing.
3. Golinval J.C., Kerschen G., Lenaerts V., Thouverez F., and Argoul P.. European COST action F3: Identification of nonlinear systems. Activities and results. Proceedings of ISMA 2002 III, 1177-1182. 2002.
4. Petrov E. and Ewins D.J.. State-of-the-art dynamic analysis for nonlinear gas turbine structures. Journal of Aerospace Engineering, Proc.of the IMech E 218[G3], 199-211. 2004.
5. Goege D.. Fast identification and characterization of nonlinearities in experimental modal analysis of large aircraft. Journal of Aircraft 44[2], 399-409. 2007.
6. Ewins D.J.. Modal testing: Theory and practice. 1984. Research Studies Press.
7. Maia N.M.M. and Silva J.M.M.. Theoretical and experimental modal analysis. 1997. Taunton, Somerset, England, Research Studies Press Ltd.
8. Gelb A. and Vander Velde W.E.. Multiple-input describing functions and nonlinear system design. 1968. New York, McGraw-Hill book company.
9. Goge D., Sinapius M., Fullekrug U., and Link M.. Detection and description of non-linear phenomena in experimental modal analysis via linearity plots. International Journal of Non-linear Mechanics 40, 27-48. 2005.
10. Imregun M.. Survey of non-linear analysis tools for structural systems. The Shock and Vibration Digest 30[5], 363-369. 1998.
11. Kerschen G, Worden K., Vakasis A.F., and Golinval J.C.. Past present and future of nonlinear identification in structural dynamics. Mechanical Systems and Signal Processing 20, 505-592. 2006.
12. Vanhoenacker K., Schoukens J., Swevers J., and Vaes D.. Summary and comparing overview of techniques for the detection of nonlinear distortions. Proceedings of ISMA 2002 III, 1241-1256. 2002.
13. Natke H., Jaung J.N., and Gawronski W.. A brief review on the identification of non-linear mechanical systems. Proceedings of IMAC-VI , 1569-1574. 1988.
14. Nayfeh A.H. and Mook D.T.. Nonlinear oscillations. 1979. Virginia, USA, John Wiley & Sons, Inc.
15. Ewins D.J.(Editor). Dynamic testing agency handbook on guidelines to best practice: Modal testing V.3. 1996.
16. Sjoberg J., Zang Q., Ljung L., Benveniste A., Delyon B., Glorennec P., Hjalmarsson H., and Juditsky H.. Nonlinear blackbox modelling in system identification- A unified overview. Automatica 31[12], 1691-1724. 1995.
17. Sjoberg J., Zang Q., Ljung L., Benveniste A., Juditsky H., Delyon B., Glorennec P., and Hjalmarsson H.. Nonlinear blackbox modelling in system identification: The mathematical foundation. Automatica 31[12], 1725-1750. 1995.
18. Vanlanduit S., Guillaume P., Schoukens J., and Vanhoenacker K.. Detection and localization of nonlinearities using a scanning laser vibrometer. Proceedings of ISMA-25 1, 473-482. 2000.
19. Schoukens J., Pintelon R., Rolain Y., and Dobrowiecki T.. Frequency response function measurements in the presence of nonlinear distortions. Automatica 37[6], 939-946. 2001.

20. Ewins D.J. and He J.. A simple method of interpretation of the modal analysis of nonlinear systems. Proceedings of IMAC V , 626-634. 1987. London, England.
21. Mertens M., Auweraer H.V., Vanherck P., and Snoeys R.. The complex stiffness method to detect and identify non-linear dynamic behaviour of SDOF systems. Mechanical Systems and Signal Processing 3[1], 37-54. 1989.
22. Tomlinson G.R.. Developments in the use of the hilbert transform for detecting and quantifying non-linearity associated with frequency response functions. Mechanical Systems and Signal Processing 1, 151-171. 1987.
23. Wyckaert K.. Development and evaluation of detection and evaluation schemes for the nonlinear dynamical behaviour of mechanical structures. PhD Thesis . 1992. Department of Mechanical Engineering, Division PMA, Katholieke Universiteit Leuven.
24. Chong Y.H. and Imregun M.. Use of reciprocal modal vectors for nonlinearity detection. Archive of Applied Mechanics 70, 453-462. 2000.
25. Kim W.J. and Park Y.S.. Non-linearity identification and quantification using an inverse fourier transform. Mechanical Systems and Signal Processing 3, 239-255. 1993.
26. Elizalde H.. Non-linear modal analysis methods for engineering structures. PhD Thesis . 2004. London, Imperial College, London.
27. Al-Hadid M.A. and Wright J.R.. Developments in the force-state mapping technique for non-linear systems and the extension to the location of non-linear elements in a lumped-parameter system. Mechanical Systems and Signal Processing 3[3], 269-290. 1989.
28. Ozer M.B., Ozguven H.N., and Royston T.J.. Identification of structural non-linearities using describing functions and Sherman-Morrison method. Mechanical Systems and Signal Processing 23[1], 30-44. 2009.
29. Masri S.F. and Caughy A.. A non parametric identification technique for nonlinear dynamic problems. Journal of Applied Mechanics 46, 433-447. 1979.
30. Adams D.E. and Allemang R.J.. Characterization of nonlinear vibrating systems using internal feedback and frequency response modulation. Journal of Vibration and Acoustics 121, 495-500. 1999.
31. Tanrikulu O. and Ozguven H.N.. A new method for the identification of non-linearities in vibrating structures. Structural dynamics: Recent advances, Proceedings of the 4th International Conference , 483-492. 1991. University of Southampton, U.K.
32. Billings S.A. and Leontaritis I.J.. Input-output parametric models for nonlinear systems Part I- Deterministic nonlinear systems. International Journal of Control 41[2], 303-328. 1985.
33. Park B.H. and Kim K.J.. Vector ARMAX modelling approach in multi-input modal analysis. Mechanical Systems and Signal Processing 3[4], 373-387. 1989.
34. Mickens R.E.. Comments on the method of harmonic balance. Journal of Sound and Vibrations 94, 456-460. 1984.
35. MacDonald N.. Choices in the harmonic balance technique. Journal of Physics A: Mathematical and General 26, 6367-6377. 1993.
36. Elizalde H. and Imregun M.. An explicit frequency response function formulation for multi-degree-of-freedom non-linear systems. Mechanical Systems and Signal Processing 20, 1867-1882. 2006.
37. Richards C.M. and Singh R.. Identification of multi degree of freedom nonlinear systems under random excitations by the reverse path spectral method. Journal of Sound and Vibrations 213, 673-708. 1998.

38. Adams D.E and Allemang R.J.. A frequency domain method for estimating parameters for nonlinear structural dynamic model through feedback. Mechanical Systems and Signal Processing 14, 637-656. 2000.
39. Rosenberg R.M.. The normal modes of nonlinear n-degree-of-freedom systems. Journal of Applied Mechanics 30[1], 7-14. 1962.
40. Vakasis A.F.. Analysis and identification of linear and nonlinear normal modes in vibrating systems. PhD Thesis . 2009. California Institute of Technology, Pasadena, California.
41. Vakasis A.F.. Non-linear normal modes (NNMs) and their applications in vibration theory:An overview. Mechanical Systems and Signal Processing 11[1], 3-22. 1996.
42. Shaw S.W.. An invariant manifold approach to nonlinear normal modes of oscillation. Journal of Nonlinear Science 4, 419-448. 1994.
43. Shaw S.W. and Pierre C.. Non-linear normal modes and invariant manifolds. Journal of Sound and Vibration 150[1], 170-173. 1991.
44. Gilbert C.. Fitting measured frequency response using non-linear modes. Mechanical Systems and Signal Processing 17[1], 211-218. 2003.
45. Kerschen G., Peeters M., Golinval J.C., and Vakasis A.F.. Nonlinear normal modes, Part I: A useful framework for the structural dynamicist. Mechanical Systems and Signal Processing 23, 170-194. 2009.
46. Peeters M., Viguie R., Serandour G., Kerschen G., and Golinval J.C.. Nonlinear normal modes, Part II: Toward a practical computation using numerical continuation techniques. Mechanical Systems and Signal Processing 23, 195-216. 2009.
47. He J.. Identification of structural dynamic characteristics. PhD Thesis . 1987. Imperial College London.
48. Feldman M.. Non-linear system vibration analysis using Hilbert transform-I. Free vibration analysis method 'Freevib'. Mechanical Systems and Signal Processing 8[2], 119-127. 1994.
49. Feldman M.. Non-linear system vibration analysis using the hilbert transform-II - Forced vibration analysis method 'Forcevib'. Mechanical Systems and Signal Processing 8[3], 309-318. 1994.
50. Setio S., Setio H.D., and Jezequel L.. A method of non-linear modal identification from frequency response tests. Journal of Sound and Vibration 158[3], 497-515. 1992.
51. Chong Y.H. and Imregun M.. Variable modal parameter identification for nonlinear MDOF systems part I: Formulation and numerical validation. Shock and Vibration 7[4], 217-227. 2000.
52. Chong Y.H. and Imregun M.. Variable modal parameter identification for nonlinear MDOF systems part II: Experimental validation and advanced case study. Shock and Vibration 7[4], 229-240. 2000.
53. Platten M.F., Wright J.R., Cooper J.E., and Sarmast M.. Identification of multi-degree of freedom non-linear simulated and experimental systems. Proceedings of ISMA 2002 3, 1195-1202. 2002.
54. Platten M.F., Wright J.R., and Cooper J.E.. Identification of a continuous structure with discrete non-linear components using an extended modal model. Proceedings of ISMA 2004 , 2155-2168. 2004.
55. Arslan O. and Ozguven H.N.. Modal identification of non-linear structures and the use of modal model in structural dynamic analysis. International Modal Analysis Conference (IMAC-XXVI) . 2008.
56. Elizalde H., Imregun M., and Ramirez-Mendoza R.A.. Semi-analytical derivation of approximate non-linear eigenvalues and eigenvectors for general non-linear MDOF systems. Mechanical Systems and Signal Processing 23[1], 87-103. 2009.

57. Imregun M. and Visser W.J.. A review of model updating techniques. Shock and Vibration Digest 23[1], 9-20. 1991.
58. Mottershead J. and Friswell M.. Model updating in structural dynamics: A survey. Journal of Sound and Vibration 167[2], 347-375. 1993.
59. Friswell M. and Mottershead J.. Finite element model updating in structural dynamics. 1995. Dordrecht, Netherlands, Kluwer Academic Publishers.
60. Mottershead J., Friswell M., Ng G.H.T., and Brandon J.A.. Geometric parameters for finite element model updating of joints and constraints. Mechanical Systems and Signal Processing 10[2], 171-182. 1996.
61. Moon Y.M., Jee T.H., and Park Y.P.. Developement of an automobile joint model using an analytically based formulation. Journal of Sound and Vibrations 220[4], 625-640. 1999.
62. Ratcliffe M.J. and Lieven A.J.. A generic element-based method for joint identification. Mechanical Systems and Signal Processing 14[1], 3-28. 2000.
63. Ahmadian H., Mottershead J., Friswell M., James S., and Reece C.A.. Modelling and updating of large surface to surface joints in the AWE-MACE structure. Mechanical Systems and Signal Processing 20, 869-880. 5-1-2005.
64. Palmonella M., Friswell M., Mottershead J., and Lees A.W.. Finite element models of spot welds in structural dynamics: Review and updating. Computers and Structures 83, 648-661. 2005.
65. Schmidt R.. Updating non-linear components. Mechanical Systems and Signal Processing 8[6], 679-690. 1994.
66. Hemez F.M. and Doebling S.W.. Review and assesment of model updating for nonlinear transient dynamics. Mechanical Systems and Signal Processing 15[1], 45-74. 2001.
67. Schultze J.F., Hemez F.M., Doebling S.W., and Sohn H.. Statistical based non-linear model updating using feature extraction. Proceedings of IMAC-XIX . 2001. Kissimmee, Florida.
68. Lenaerts V., Kerschen G., and Golinval J.C.. Proper orthogonal decomposition for model updating of non-linear mechanical systems. Mechanical Systems and Signal Processing 15[1], 31-43. 2001.
69. Lenaerts V., Kerschen G., and Golinval J.C.. Identification of a continuous structure with a geometrical non-linearity. Part II: Proper orthogonal decomposition. Journal of Sound and Vibration 262, 907-919. 2003.
70. Petrov E.. Analysis of sensitivity and robustness of forced response for nonlinear dynamic structures. Mechanical Systems and Signal Processing 23, 68-86. 2009.
71. Ibrahim R.A. and Pettit C.L.. Uncertainties and dynamic problems of bolted joints and other fastners. Journal of Sound and Vibrations 279, 857-936. 2005.
72. Zienkiewicz O.C. and Taylor R.L.. The finite element method, Volume 2:Solid mechanics. [5th Edition]. 2000. Butterworth-Heinemann.
73. Berger E.J.. Friction modelling for dynamic system simulation. Applied Mechanics review 55[6], 535-577. 2002.
74. Iwan W.D.. On a class of models for the yielding behaviour of continuous and composite systems. Journal of Applied Mechanics , 612-617. 1967.
75. Menq C.H. and Griffin J.H., "A comparison of transient and steady state finite element analyses of the forced response of a frictionally damped beam," *Journal of vibration, acoustics, stress, and reliability in design*, Vol. 107, 1985, pp. 19-25.
76. Menq C.H., Chidamparam P., and Griffin J.H.. Friction damping of two-dimensional motion and its application in vibration control. Journal of Sound and Vibrations 144[3], 427-447. 1991.

77. Sanliturk K.Y. and Ewins D.J.. Modelling two dimensional frictional contact and its application using harmonic balance method. Journal of Sound and Vibrations 193[2], 511-523. 1996.
78. Sanliturk K.Y., Ewins D.J., and Imregun M., "Harmonic balance vibration analysis of turbine blades with friction dampers," *Journal of vibration, acoustics, stress, and reliability in design*, Vol. 119, No. 1, 1997, pp. 96.
79. Petrov E. and Ewins D.J.. Analytical formulation of friction interface elements for analysis of nonlinear multi-harmonic vibrations of bladed disks. Journal of Turbomachinary 125, 364-371. 2003.
80. Petrov E. and Ewins D.J.. Analysis of nonlinear multiharmonic vibrations of bladed discs with friction and impact dampers. National Turbine Engine High fatigue Conference [7]. 5-14-2002. Florida.
81. Petrov E. and Ewins D.J.. Generic friction models for time-domain vibration analysis of bladed disks. Journal of Turbomachinary 126, 184-192. 2004.
82. Gaul L. and Lenz J.. Nonlinear dynamics of structures assembled by bolted joints. Acta Mechanica 125, 169-181. 1997.
83. Mottershead J., Oldfield M., and Ouyang H.. Simplified models for bolted joints under harmonic loading. Computers and Structures 84, 25-33. 2005.
84. Genzo A., Sextro W., and Popp K.. Analysis of forced vibration of two bolted half-pipes with extended friction contacts. Proceedings in Applied Mathematics and Mechanics (PAMM) 5[1], 91-92. 2005.
85. Petrov E. and Ewins D.J.. Method for analysis of nonlinear multiharmonic vibrations of mistuned bladed disks with scatter of contact interface characteristics. Journal of Turbomachinary 127, 128-136. 2005.
86. Petrov E.. A method for use of cyclic symmetry properties in analysis of nonlinear multiharmonic vibrations of bladed disks. Journal of Turbomachinary 126, 175-183. 2004.
87. Budak E. and Ozguven H.N.. Interative receptance method for determining harmonic response of structures with symmetrical non-linearities. Mechanical Systems and Signal Processing 7[1], 75-87. 1993.
88. Budak E. and Ozguven H.N.. A modal superposition method for non-linear structures. Journal of Sound and Vibration 189[3], 315-339. 1996.
89. Comparin R.J. and Singh R.. Frequency response characteristics of a multi-degree-of-freedom system with clearances. Journal of Sound and Vibration 142[1], 101-124. 1990.
90. Kim T.C., Rook T.E., and Singh R.. Super- and sub-harmonic response calculations for a torsional system with clearance nonlinearity using the harmonic balance method. Journal of Sound and Vibration 281, 965-993. 2005.
91. Guyan R.J.. Reduction of stiffness and mass matrices. American Institute of Aeronautics and Astronautics Journal 3[2], 380. 1965.
92. Friswell M., Garvey S.D., and Penny J.E.T.. Model reduction using dynamic and iterated IRS techniques. Journal of Sound and Vibrations 186[2], 311-323. 1995.
93. O'Callahan J.. A procedure for an improved reduced system (IRS) model. Proceedings of IMAC VII , 17-21. 1989. Las Vegas.
94. Kerschen G., Golinval J.C., Vakasis A.F., and Bergman L.A.. The method of proper orthogonal decomposition for dynamical characterization and order reduction of mechanical systems: An overview. Nonlinear Dynamics 41, 147-169. 2005.
95. Segalman D.J.. Model reduction of systems with localized nonlinearities. Journal of Computational and Nonlinear Dynamics 2[3], 249-266. 2007.
96. Avitabile P. and O'Callahan J.. Efficient techniques for forced response involving linear modal components interconnected by discrete nonlinear

connection elements. Mechanical Systems and Signal Processing 23[1], 45-69. 2009.
97. Reece C.A.. Model correlation applied to mechanical couplings and interfaces- An empirical approach. International Modal Analysis Conference (IMAC-VXIII) , 992-998. 2000.
98. Kerschen G., Lenaerts V., Marchesiello S., and Fasana A.. A frequency domain versus a time domain identification technique for nonlinear parameters applied to wire rope isolators. Journal of Dynamic systems, Measurement, and Control 123, 645-650. 2002.
99. Dohner J.L.. On the development of methodologies for constructing predictive models of structures with joints and interfaces. Sandia National Laboratories Report . 4-26-2000.
100. Segalman D.J., Paez T., Smallwood D., Sumali A., and Urbina A.. Status and integrated road-map for joint modelling research. Sandia National Laboratories Report . 2003.
101. Ferreira J.V.. Dynamic response analysis of structures with nonlinear components. PhD Thesis . 1998. Imperial College,London.
102. Chong Y.H. and Imregun M.. Coupling of non-linear substructures using variable modal parameters. Mechanical Systems and Signal Processing 14[5], 731-746. 2000.
103. McGee C.G., Haroon M, Adams D.E, and Luk Y.W.. A frequency domain technique for characterizing nonlinearities in a tire-vehicle suspension system. Journal of Vibration and Acoustics 127, 61-76. 2005.
104. Muhammad Haroon, Adams D.E, and Luk Y.W.. A technique for estimating linear parameters using nonlinear restoring force extraction in the absence of an input measurement. Journal of Vibration and Acoustics 127, 483-492. 2005.
105. Worden K., Hickey D., Haroon M., and Adams D.E.. Nonlinear system identification of automotive dampers: A time and frequency domain analysis. Mechanical Systems and Signal Processing 23[1], 104-126. 2009.
106. Garibaldi L., Giorcelli E., and Marchesiello S.. Experimental identification of non-linear parameters over a scaled multi-storey building. Proceedings of ISMA 2006 , 2723-2734. 2006.
107. Perinpanayagam S., Robb D., Ewins D.J., and Barragan J.M.. Non-linearities in an aero-engine structure: From test to design. Proceedings of ISMA 2004 , 3167-3181. 2004.
108. Gloth G. and Sinapius M.. Influence and characterisation of weak non-linearities in swept-sine modal testing. Aerospace Science and Technology 8, 111-120. 2004.
109. Kerschen G. and Golinval J.C.. Generation of accurate finite element models of nonlinear systems- Application to an aeroplane like structure. Nonlinear Dynamics 39, 129-142. 2005.
110. Da Silva D.G. and Varoto P.S.. Identification and characterization of the non-linear dynamic behaviour of a laboratory aircraft structure. Proceedings of ISMA 2006 , 2821-2833. 2008.
111. Tomlinson G.R. and Simon M.. Use of hilbert transform in modal analysis of linear and non-linear structures. Journal of Sound and Vibrations 96[4], 421-436. 1984.
112. Rodriguez-Vazquez K. and Fleming P.J.. Multi-objective genetic programming for nonlinear system identification. Electronics Letters 34[9], 930-931. 1998.
113. Kyprianou A., Worden K., and Panet M.. Identification of hysteretic systems using the differential evolution algorithm. Journal of Sound and Vibration 248[2], 289-314. 2001.

114. Charalampakis A.E. and Koumousis V.K.. Identification of Bouc-Wen hysteretic systems by a hybrid evolutionary algorithm. Journal of Sound and Vibration 314[3-5], 571-585. 2008.
115. Haupt R.L. and Haupt S.E.. Practical genetic algorithms. 1. 1999. John Wiley & Sons, Inc.
116. Goldberg D.E.. Genetic algorithms in search, optimization and machine learning, 1st edition. 1989. Addison-Wesley Longman publishing company, Inc.
117. ICATS-2006, MODENT User's Guide. Imperial College London . 2009.
118. Petrov E.P.. Analysis of sensitivity and robustness of forced response for non-linear dynamic structures. Mechanical Systems and Signal Processing 23[1], 68-86. 2009.
119. Sen H.. Dynamic analysis of assembled structures with nonlinearity. PhD Thesis . 2007. Imperial College London, Imperial College London.
120. Ewins D.J.(Editor). Dynamic testing agency handbook on guidelines to best practice: Modal testing Version 3. 1996.

Appendix A

System used for the generation of footprint library

The figure for the 2-DOF system used to generate the footprint library is shown below. The underlying linear system remains the same and the non-linear element is changed each time to generate the footprint for the corresponding non-linearity.

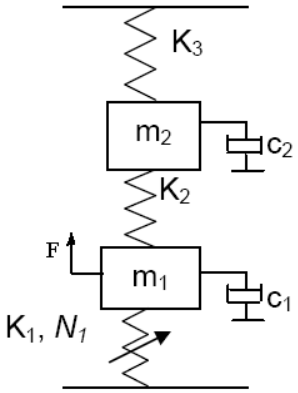

Figure A1 2DOF system used to generate the footprint library

The parameters used for the underlying linear system are listed below:

$K_1 = K_2 = 40$ N/m; $K_3 = 80$ N/m; $m_1 = m_2 = 1$ Kg; $C_1 = C_2 = 0.01$ N-sec/m;

F = 0.002 N; N_1 is the non-linear element attached between the DOF-1 and the ground. The non-linear parameters used for different non-linearities are listed in the Table A1.

Table A1 Non-linear parameters for different non-linearities

Non-linearity type	Non-linear parameters used
Cubic stiffness (hardening)	$\beta = 5e6$ Nm^{-3}
Cubic stiffness (softening)	$\beta = -5e6$ Nm^{-3}
Clearance	$K_z = 80$ N/m; $y_c = 0.5$mm
Friction (slip only)	$K_d = 120$ N/m; $\mu N = 6e\text{-}3$ N
Friction (stick only)	$K_d = 120$ N/m; $\mu N = 6$N
Friction (stick-slip)	$K_d = 120$ N/m; $\mu N = 0.06$N
Cubic stiffness + clearance	$\beta = 5e6$ Nm^{-3}; $K_z = 80$ N/m; $y_c = 5e^{-4}$m
Cubic stiffness + friction	$\beta = 5e6$ Nm^{-3}; $K_d = 120$ N/m; $\mu N = 0.06$N
Clearance + friction	$K_z = 80$ N/m; $y_c = 0.5$mm; $K_d = 120$ N/m; $\mu N = 0.06$N
Cubic stiffness + clearance + friction	$\beta = 5e8$ Nm^{-3}; $K_z = 120$ N/m; $y_c = 5e^{-4}$m; $K_d = 120$ N/m; $\mu N = 0.06$N

Appendix B

Structures used for the validation

Validation Structure-1: Cantilever beam

A cantilever beam is used as the validation structure-1 for the validation purpose. A detailed drawing of the structure is shown in the Figure B1.

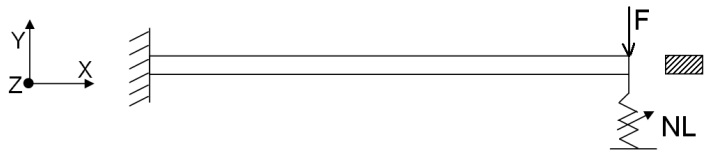

length = 0.6m, width = 0.015m, thickness = 2×10^{-3}m
E = 2.1×10^{11} N/m^2 , ρ = 7800 kg/m^3 , Poisson's ratio = 0.3
Modal damping factor = 0.5% for all modes

Figure B1 Validation structure-1: Cantilever beam

The cantilever beam is modelled using FE method with beam elements processing 2 DOFs per node: a translational DOF along Y axis and a rotational DOF about the Z axis. The excitation force of sinusoidal nature with amplitude 0.001N is applied at the free end of the beam. The non-linear element is placed at the free end of the beam.

Validation Structure-2 Cantilever plate

A cantilever plate is used as validation structure-2 for the validation of the algorithms in the thesis. Figure B2 shows the detail drawing of the structure. The plate is modelled in FEM using Kirchhoff's plate elements with 3 DOF per node: a translational DOF along Z axis and rotations about X and Y axes. The excitation force of 0.05N is applied to the edge of the plate as shown. The non-linear element is placed at the corner of the plate. The type of non-linearity is varied during the validation of different algorithms.

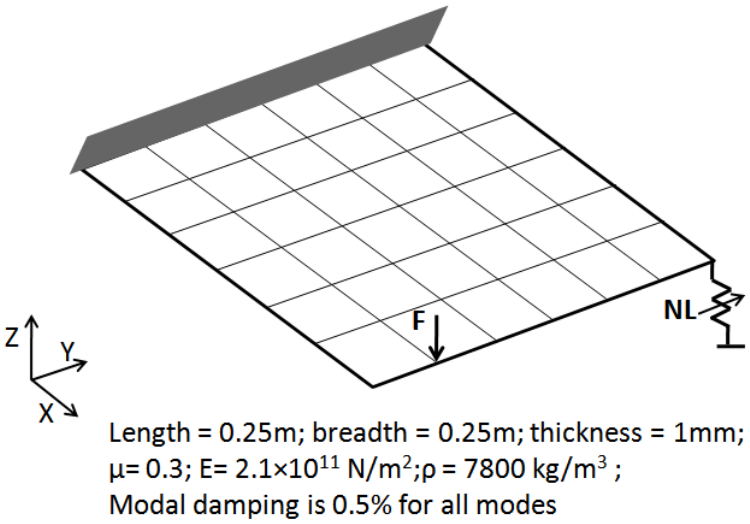

Figure B2 Validation structure-2: cantilever plate

The plate is meshed with 36 elements. After imposing the boundary conditions, the total number of nodes in the model equals 42, with 3 DOFs per node. Table B1 lists the linear natural frequencies for the first 9 modes.

Table B1 Linear natural frequencies for validation structure-2

Mode Number	Natural frequency (rad/sec)
1	87.2
2	213.8
3	537.8
4	680.9
5	777.8
6	1345.9
7	1548.7
8	1613.9
9	1782.1

Figure B3 shows the mode shapes of the first 9 modes of the structure.

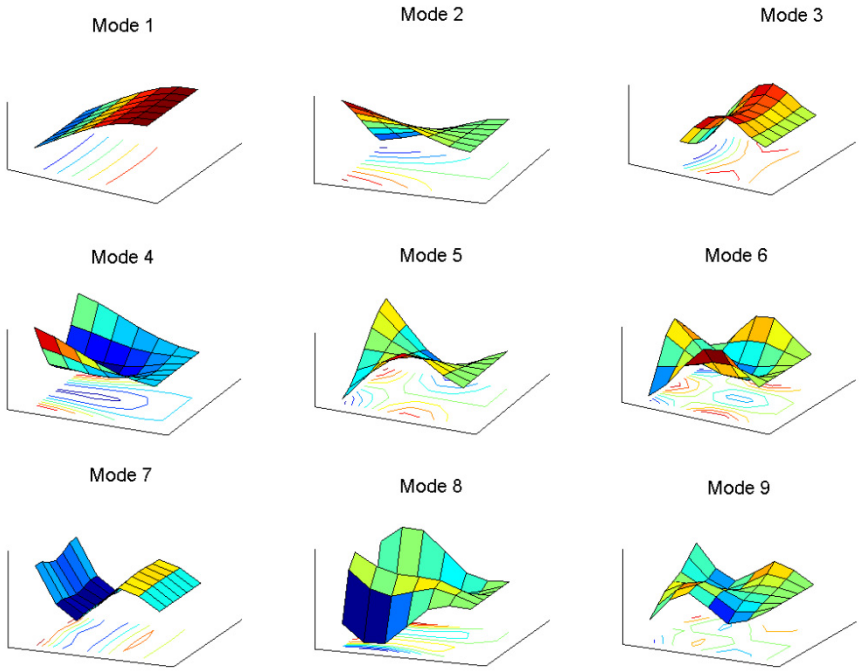

Figure B3 Mode shapes of validation structure-2

Validation Structure-3 Pyramid

A pyramid-like structure is used as Validation structure-3 for the validation of the identification method proposed for base-excited structure in Chapter 8. It consists of 4 beams joined at the top to form a tower. The beams are grounded at the base on a rigid platform. Figure B4 shows the engineering drawing of the structure. The material properties for the beams in the structure are listed in Table B2.

Table B2 Material properties for the beams in Validation Structure-3

Material property	**Value**
Density (ρ)	7800 kg/m^3
Poisson's ratio (v)	0.28
Young's modulus of elasticity (E)	2.1×10^{11} N/m^2

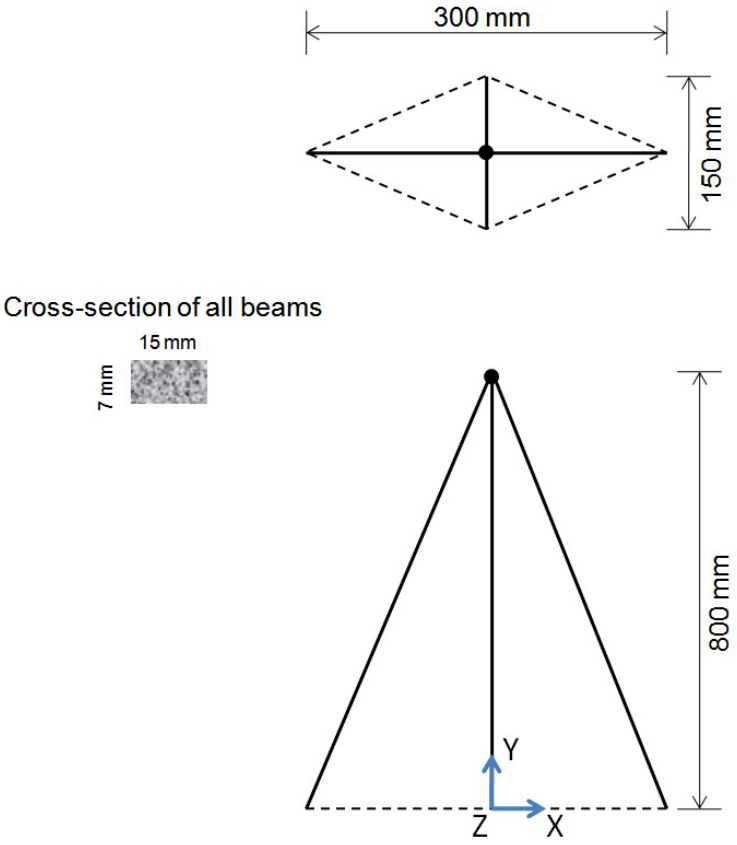

Figure B4 Engineering drawing of Validation structure-3

The structure was modelled using the FEM in ANSYS with 3-D beam elements. Each of the beams in the structure was meshed with 10 beam elements making a total of 222 DOFs after applying the boundary conditions.

Appendix C

Details of '1203 structure'

The engineering drawings of '1203 structure' are shown below in Figure C1. The properties of Aluminum alloy used in the simulation are as follow:

Young's modulus of elasticity, E = 71×10^9 N/m^2

Density of the material, ρ = 2800 Kg/m3

Poisson's ratio, v = 0.3

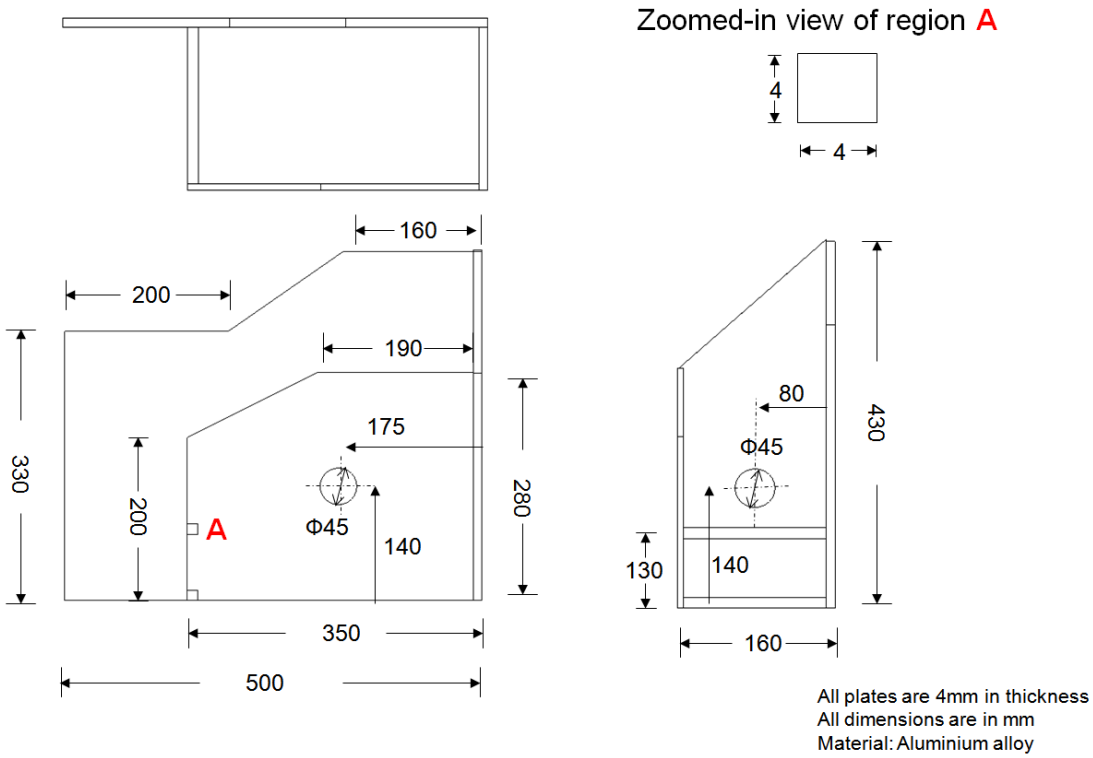

Figure C1 Engineering drawing of 1203 structure

The natural frequencies for the underlying linear structure are presented in Table C1.

Table C1 Natural frequencies of the underlying linear structure

Mode No	Natural frequency (Hz)	Mode No	Natural frequency (Hz)
1	8.905	8	137.94
2	10.711	9	166.34
3	38.166	10	187.12
4	41.236	11	188.71
5	62.209	12	198.33
6	119.10	13	210.06
7	131.70	14	249.41

Appendix D

MACE structure details and repeatability test results

D.1. Material properties and the FE model mesh information

The following table gives the details of the material properties for different components of the MACE sub-assembly and the mesh-sizes used in the FE models of the sub-assembly.

Table D1 Details of the material properties and FE model mesh

Component	Material	Material properties			Maximum element edge length (mm)
		E (N/m^2)	ρ (Kg/m^3)	v	
Case	Aluminum alloy	7×10^{10}	2724.7	0.33	40
Collar	Aluminum alloy	7×10^{10}	2800	0.33	20
Body	Aluminum alloy	7×10^{10}	2747.3	0.33	40
Retaining nut	Stainless steel	1.95×10^{11}	7272.1	0.29	3

D.2. Repeatability tests for non-linear measurements

For non-linear systems, sometimes it is difficult to get repeatable measurements. In order to perform proper system identification, it is necessary to have measurement data which is consistent and repeatable. For the data used in thesis, repeatability tests were performed to check the consistency of the experimental setup. The repeatability tests were performed at three excitation levels. At each level, the measurements were taken by disassembling the structure completely and again assembling it with the designated torque. Figure D1, D2 and D3 show the results of the repeatability tests performed at 0.5N, 3N, and 5N excitation force respectively.

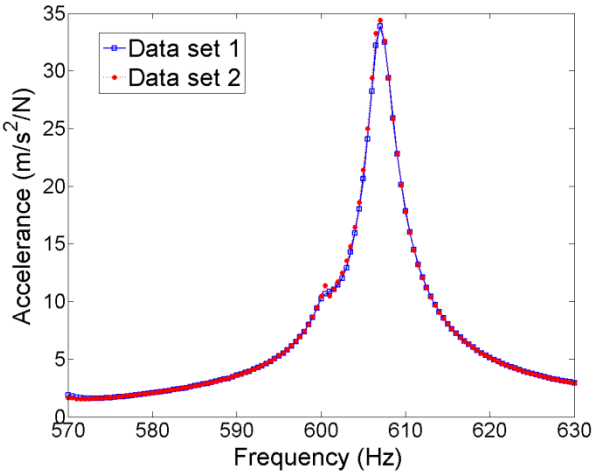

Figure D1 Repeatability test results at force level 0.5N

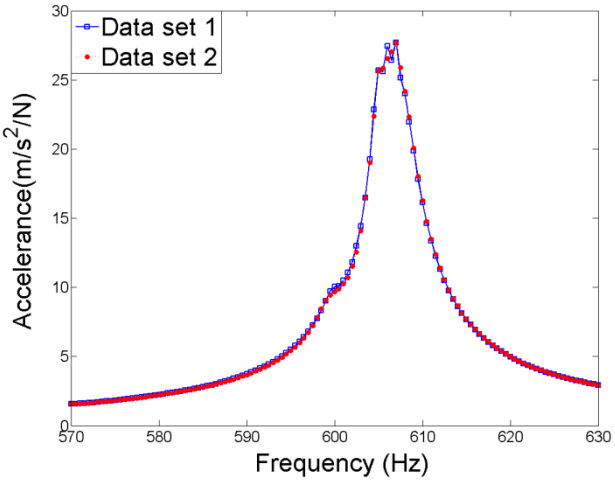

Figure D2 Repeatability test results at force level of 3N

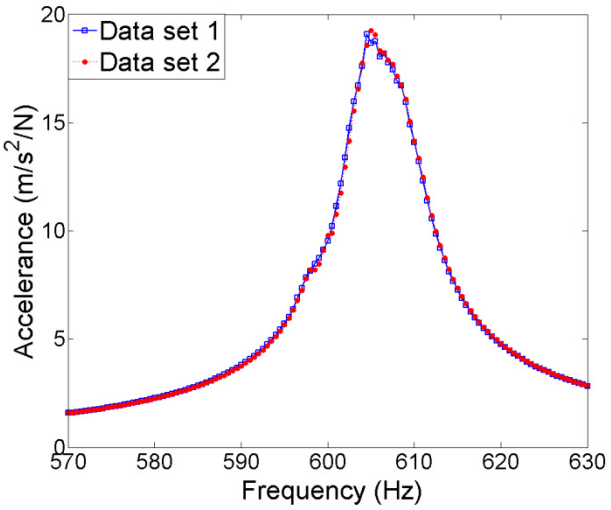

Figure D3 repeatability test results at force level of 5N